



DIPLOMARBEIT

**Hygrothermal Performance of Selected Wall Systems  
in Central Europe**

unter der Leitung von

Univ.-Prof. Dipl.-Ing. Dr. techn. Ardeshir Mahdavi

E 259-3 Abteilung für Bauphysik und Bauökologie

Institut für Architekturwissenschaften

eingereicht an der

Technischen Universität Wien

Fakultät für Architektur und Raumplanung

von

Jakub Rozumek

1426325

## KURZFASSUNG

---

Baumaterialien, deren Herstellung und Einbau als energieintensiv betrachtet werden können, erfreuen sich in den letzten Jahren steigender Beliebtheit. Dies trifft speziell auf jüngere Personen sowohl bei PlanerInnen, wie auch bei der Bauherrenschaft, zu. Es ist wesentlich, dass der Wissensstand hinsichtlich dieser Materialien erweitert und strukturiert verfügbar gemacht wird.

Die Zielsetzung dieser Master-These war eine vertiefte Analyse der hygro-thermischen Performance einer Reihe von Wandsystemen, in welchen zum Teil solche „Low-embodied-energy“-Materialien verwendet wurden. Diese Analyse wurde anhand typischer mitteleuropäischer Klimabedingungen durchgeführt (verschiedene Locations unterschiedlicher Mikroklimata) und die Ergebnisse mit denen von konventionellen Wandsystemen verglichen.

Neun Wandsysteme wurden hinsichtlich Feuchtediffusion und Effusion untersucht, und zwar zunächst analytisch und dann unter Verwendung von State-of-the-Art Computersimulationen getestet. Dabei wurden sowohl extreme, wie auch typische Annahmen betreffend der klimatischen Randbedingungen angesetzt.

Darüber hinaus wurden, aufbauend auf verschiedenen Vorstudien drei unterschiedliche Szenarien entwickelt, welche aus Sicht der hygro-thermalen Performance der Bauteile bedeutsam sind:

Im ersten Szenario wurden die Bauteile einem rapiden thermischen Temperaturabfall (Emulation des nächtlichen Temperaturabfalls) ausgesetzt. Im zweiten Szenario wurden die Bauteile vordefinierten thermischen Zyklen ausgesetzt, welche auf den üblichen transienten Bedingungen in der Realität basieren. Im dritten Szenario wurden die verschiedenen Konstruktionen zyklischen Feuchteanfällen ausgesetzt, um zu untersuchen, wie sich die MBV (Moisture-Buffer-Values) der unterschiedlichen Materialien auswirken bzw. darstellen. Dieses letzte Szenario ist insofern wichtig, weil davon abhängt, wie gut die Materialien eingesetzt werden können um die relative Luftfeuchtigkeit im Gebäudeinneren zu regulieren.

Reale Klimadaten der Standorte Prag, Wien und Serak (dabei handelt es sich um den unwirtlichsten Ort in der Tschechischen Republik betreffend niedrigen Außentemperaturen und starken Niederschlägen bzw. hohen Außenluftfeuchtigkeiten). Der Wärmetransport durch die Wandkomponenten wurde sowohl kurzfristig, wie auch über lange Zeitspannen evaluiert um auf die thermische Performance der Konstruktionen schließen zu können. Hierbei wurde die Reaktion der Materialien auf die Luftfeuchtigkeitswerte im Innenraum berücksichtigt und mit den zuvor erwähnten MBV-Werten verglichen. Der TOW-Wert (Time of Wetness) wurde ermittelt und diente als Hinweis auf die potentielle Lebensspanne der untersuchten Komponenten (an den unterschiedlichen Orten).

Die Ergebnisse der Untersuchungen zeigen, dass Langzeitbetrachtungen von Komponenten mit ähnlichen U-Werten auch in dieser detaillierteren Betrachtungsweise nur insignifikante

Unterschiede in den Ergebnissen aufweisen. Dies trifft allerdings auf zwei der untersuchten Systeme nicht zu, nämlich das Leichtbausystem, das auf Mineralwolle und AAC (Autoclaved Aerated Concrete) basiert und kaum thermische Masse aufweist, sowie ein Ziegelsystem mit perforierten Ziegeln, deren thermische Performance stark von den Feuchtigkeitströmen darin abhängt. Diese beiden Systeme zeigten in einigen Anwendungsfällen erhöhte Heizwärmebedarfswerte und erhöhten Wärmestrom.

Hinsichtlich der zeitlich kurzfristigen Betrachtungen kann gesagt werden, dass der Wärmestrom vor allem vom Aufbau der Wand abhängt: Hier zeigen Bauteile, bei denen Lastabtragung und Wärmedämmung in unterschiedlichen Materialien aufgelöst sind, tendenziell bessere Werte betreffend thermischer Performance (Wärmestrom und Innenraumkomfort), als Bauteile, die diese Funktionen in einer Schicht vereinen.

Die hygrischen Simulationen weisen auf Schwächen im Feuchte-Puffer-Verhalten von lehm-basierten Materialien (Oberflächen) hin, speziell im Vergleich mit Silikat-basierten. Dies kann doch als einigermaßen überraschend bezeichnet werden. Die TOW-Analyse zeigte, dass viele der „Natur“-Materialien, vor allem strohbasierte Materialien, relativ empfindlich gegen langandauernde Feuchtigkeitsbelastungen sind. Hier zeigt sich, dass es noch wesentliche Forschungs- und Entwicklungsarbeit im Bezug auf solche Naturbaustoffe für einen zeitgemäßen Einsatz in der gebauten Umwelt bedarf.

**Schlüsselwörter:**

Natur-Baustoffe, Hygro-thermische Simulation, Time of Wetness, Moisture-Buffering Value, zentraleuropäische Klimate

## ABSTRACT

---

Low embodied energy building materials are gaining popularity especially among younger generation and therefore their understanding from different points of view should be encouraged. The goal of this thesis was deeper analysis of hygrothermal performance of selected low embodied energy wall systems in the climate of central Europe and comparison of these with conventional wall systems of tested locations.

Nine selected wall systems were firstly assessed analytically using concept of hygrothermal diffusivity and effusivity following by computer-aided 1D hygrothermal simulations under theoretical and real climatic conditions.

Three different theoretical scenarios were proposed based on previous research in order to determine parameters relevant for transient hygrothermal environment. The studied components were exposed firstly to sudden thermal shock, which intended to simulate outside temperature drop during night-time and secondly to predefined thermal cycles in outside environment representing daily thermal cycles. Based on these scenarios were generated parameters characterising thermal behaviour of studied components in transient thermal environment. In the third scenario were individual wall components subjected to inside humidity cycles, which generated moisture-buffer value (MBV), parameter, which determines components' potential to regulate indoor RH level.

The real climate simulations were performed under reference years of Prague, Vienna and Serak (coldest and wettest region in the Czech Republic). Both short-term and long-term heat transfers through the wall components were analysed to benchmark their overall thermal performance. Reaction of components to indoor RH fluctuations was also determined and compared with previously defined MBV. Standard damage function TOW (time-of-wetness) was ultimately applied to simulation results in order to assess potential lifespan of the wall components in selected locations.

Long-term simulations showed that when analysing wall components with the same U-value the difference in annual heat transfer between individual components is mostly insignificant. The exception to this was mineral wool lightweight wall system with no thermal mass layer together with AAC (autoclaved aerated concrete) and perforated brick wall systems with high liquid transfer coefficients combined with high dependency of thermal conductivity upon moisture content. These systems transferred in certain cases considerably higher amounts of heat than the other studied wall systems.

Regarding the short-term simulations, it was found out that the heat flux through inside surface of components is mainly dependent on the wall layer composition. Wall systems composed of high thermal mass layer and separate insulation layer were found to provide more stable indoor temperature conditions than wall systems composed of one main layer having both thermal insulation and thermal mass.

The main finding of hygric simulations was poor indoor moisture buffering potential of loam-based products in comparison with other simulated finishing materials. The conventional silicate-based renders were simulated to have considerably higher MBV than loam render, which was in contradiction with expected results.

The TOW analysis showed that wall systems based on raw natural building materials (especially straw bale wall system) suffer from longer periods with unfavourable outside conditions. This was caused mainly due to their incapability of withstanding higher levels of RH without significant deteriorating action.

**Keywords:**

Raw natural building materials, Numeric hygrothermal simulation, Moisture-Buffering Value, Time of Wetness, Central Europe

## ACKNOWLEDGEMENTS

---

First and foremost I would like to thank to Ing. Václav Kočí, Ph.D., who kindly agreed to externally supervise this thesis, for his valuable support, professional guidance and provision of fundamental simulation input data. Also, I would like to acknowledge Univ.-Prof. Dipl.-Ing. Dr. techn. Ardeshir Mahdavi, who made my cooperation with Ing. Václav Kočí, Ph.D. possible and gave me necessary professional perspective upon my work. Further I want to thank Univ.Ass. Dipl.-Ing. Dr.techn. Ulrich Pont for his time and feedback during finalization of this thesis.

My deepest thanks go to my family for their endless support, encouragement and patience during the last years of my studies, which made this work possible.

Finally, I would like to thank to my dearest Nadia for her emotional encouragement, love and positive spirit, which kept me going throughout the entire time I was working on this thesis.

# Table of contents

<b>Acronyms</b> . . . . .	<b>1</b>
1 INTRODUCTION . . . . .	2
1.1 Introduction . . . . .	2
1.2 Motivation . . . . .	3
2 BACKGROUND . . . . .	5
2.1 Hygrothermal processes in building envelope . . . . .	5
2.1.1 Heat transfer . . . . .	6
2.1.1.1 Transfer mechanisms . . . . .	6
2.1.1.2 Steady state temperature scenario . . . . .	11
2.1.1.3 Transient thermal conditions . . . . .	14
2.1.2 Mass transfer . . . . .	17
2.1.2.1 Psychometrics . . . . .	17
2.1.2.2 Porous materials . . . . .	18
2.1.2.3 Phase change / Latent heat effect . . . . .	21
2.1.2.4 Transfer mechanisms . . . . .	22
2.1.2.5 Steady state humidity scenario . . . . .	26
2.1.2.6 Transient hygric conditions . . . . .	28
2.1.3 Partial conclusion . . . . .	32
2.2 Raw natural building materials (RNBM) . . . . .	33
2.2.1 Unfired earth . . . . .	33
2.2.1.1 Material . . . . .	34
2.2.1.2 Material variations . . . . .	35
2.2.1.3 Hygrothermal performance . . . . .	36
2.2.2 Natural stalk fibre materials . . . . .	37
2.2.2.1 Variables affecting hygrothermal properties . . . . .	38
2.2.3 Wood . . . . .	39
2.2.3.1 Hygrothermal performance . . . . .	41
2.2.4 Straw . . . . .	42
2.2.4.1 Hygrothermal performance . . . . .	43
2.2.5 Hemp . . . . .	44
2.2.5.1 Material variations . . . . .	46
2.2.5.2 Hygrothermal performance . . . . .	47
3 AIMS AND OBJECTIVES . . . . .	49
3.1 Aims of the work . . . . .	49
3.2 Objectives . . . . .	49
4 METHODOLOGY . . . . .	50
4.1 Analytical assessment of individual materials . . . . .	50
4.1.1 Thermal parameters . . . . .	50
4.1.2 Hygric parameters . . . . .	51

4.2	Definition of the wall systems . . . . .	51
4.3	Computer aided hygrothermal simulation . . . . .	54
4.3.1	Simulation tools and procedure . . . . .	54
4.3.2	Simulation input data . . . . .	56
4.3.2.1	Hygrothermal material parameters . . . . .	56
4.3.2.2	Boundary conditions and other input data . . . . .	59
4.3.3	Simulation tools comparative and sensitivity analysis . . . . .	62
4.4	Hygrothermal simulation under theoretical conditions . . . . .	64
4.4.1	Sudden change in outside temperature . . . . .	65
4.4.2	Thermal cycles in outside environment . . . . .	65
4.4.3	Inside moisture buffering . . . . .	66
4.5	Hygrothermal simulation under reference years . . . . .	67
4.5.1	Analysed parameters . . . . .	69
4.5.1.1	Thermal parameters . . . . .	69
4.5.1.2	Hygric parameters . . . . .	70
5	RESULTS AND DISCUSSION . . . . .	74
5.1	Analytical assessment of individual materials . . . . .	74
5.1.1	Thermal parameters . . . . .	74
5.1.2	Hygric parameters . . . . .	75
5.2	Comparative and sensitivity analysis . . . . .	78
5.2.1	Comparative analysis . . . . .	78
5.2.2	Sensitivity analysis . . . . .	81
5.3	Hygrothermal performance of wall systems under theoretical conditions . . . . .	85
5.3.1	Sudden change in outside temperature . . . . .	85
5.3.2	Thermal cycles in outside environment . . . . .	89
5.3.3	Inside moisture buffering . . . . .	91
5.3.4	Summary of results (theoretical simulations) . . . . .	95
5.4	Hygrothermal performance of wall systems under reference year . . . . .	96
5.4.1	Thermal performance . . . . .	96
5.4.2	Hygric performance . . . . .	104
5.4.2.1	Existence of annual moisture accumulation phenomenon inside walls . . . . .	104
5.4.2.2	Moisture-buffering effect (MBE) . . . . .	104
5.4.2.3	Time-of-wetness (TOW) . . . . .	108
6	CONCLUSION . . . . .	112
	<b>List of Figures . . . . .</b>	<b>115</b>
	<b>List of Tables . . . . .</b>	<b>120</b>
	<b>List of Equations . . . . .</b>	<b>121</b>
	<b>References . . . . .</b>	<b>123</b>
	<b>Appendix . . . . .</b>	<b>133</b>

# Acronyms

$\mu$ -factor . . . . .	Water vapour diffusion resistance factor
A-value . . . . .	Water absorption coefficient
AAC . . . . .	Autoclaved Aerated Concrete
ASHRAE . . . . .	American Society of Heating, Refrigerating and Air Conditioning
BE . . . . .	Building Envelope
CTU . . . . .	Czech Technical University
DTU . . . . .	Technical University of Denmark
EPS . . . . .	Expanded Polystyrene
HAM . . . . .	Heat, Air and Moisture storage and transfer
HVAC . . . . .	Heating, Ventilation and Air Conditioning
MBE . . . . .	Moisture-Buffering Effect
MBV . . . . .	Moisture Buffer Value
MW . . . . .	Mineral Wool
NHL . . . . .	Natural Hydraulic Lime
OSB . . . . .	Oriented Strand Board
RH . . . . .	Relative Humidity
RNBM . . . . .	Raw Natural Building Materials
sd-value . . . . .	Equivalent air layer thickness
SRE . . . . .	Stabilized Rammed Earth
TOW . . . . .	Time-Of-Wetness
U-value . . . . .	Thermal transmittance

# 1 INTRODUCTION

---

## 1.1 Introduction

World is nowadays home to almost 7.5 billion people of different culture, race, religion, tradition, people with different life style, education, economical background or possibilities. The current trend is that majority of those people is trying to achieve wealth, prosperity and living standard of people of the so-called western society. It is therefore our responsibility to set a good example to these people and ensure we use as much energy and produce as much carbon dioxide as could be sustained by our planet. Unfortunately, current situation is far from this ideal when the living standard and economy of 12 most resource demanding countries (being mostly representatives of the western world) require resources equivalent to two or more planets when adopted by entire world's population (Fig. 1).



**Fig. 1:** Amount of necessary resources for top world's economies (when recomputed to entire world's population) expressed in planet Earth equivalent (Global Footprint Network, 2016)

Building activity has been linked with mankind since the beginning of its existence as necessity of having shelter is the second most important basic need of human being (after access to food and water). It is therefore not surprising that with the rising population and living standards has building sector become one of the main environmental polluter and consumer of global resources. This issue has been already addressed by many (Huovila *et al.*, 2009, Asif *et al.*, 2007) and because it is rather naive to expect decrease of building standard demand, new "green" technologies are being constantly developed to reduce the environmental impact of buildings.

It is currently believed that the most effective way to reduce the environmental impact of buildings is to reduce operational energy consumption with no regard for production and disposal stage of building life cycle. This is being done mostly through installation of highly insulated building envelopes and energy saving building systems. Although it is certainly true that the operational energy accounts for major share of the overall (cradle-to-grave) energy consumed by buildings and is thus the most important component to reduce, the

problem should be viewed more holistically and the choice of particular building materials for achieving the energy reduction should be addressed.

First of all, during the chase for the best insulating and economically viable material, we settled for many materials whose effects on human health and local environment are yet unknown. Modern history of man is interspersed with cases like asbestos or DDT, which illustrate dangerous potential of some of the modern insulating materials. The latest example would be use of hexabromocyclododecane (flame retardant) in polystyrene, which had been used as building insulation for past decades to be eventually found to have highly toxic and carcinogen character (Rani *et al.*, 2014).

Secondly, there are some doubts about prioritising only operational energy reduction over embodied energy reduction presented by Nordby and Shea (2013). They stated that, when respecting the current EU energy directives, immediate saving of energy and carbon emission by building houses with significantly lower embodied energy may be more important step in final energy scenario than focusing on further savings of future energy supplies. It is important to understand that the life style and needs of modern man alter quite fast and so future changes caused by new user or user needs may occur earlier than expected in energy calculation, which might cause the investments into energy efficient building envelopes and equipment not reaching their energy payback time. Also, it is a well-known issue that the energy consumption of newly designed buildings often differs significantly from the assumptions based on predictive thermal models. Gram-Hanssen (2010) supports this claim when concluding that user behaviour is highly likely to undermine the technical performance estimated in energy balance calculation. On the other hand choosing low embodied energy materials for the building construction is not influenced by any estimation factors. The energy and environmental savings are immediate, which is considered more valuable than possible later energy reductions (Nordby and Shea, 2013).

Minimising the embodied energy of new constructions is therefore a very important environmental issue, which should not be overlooked. The possibilities of low embodied material choices range from raw natural building materials (RNBM), like earth, straw or wood, to lowly processed materials like sheep wool, cellulose and natural fibre insulation or hemp-lime bio-composites. Their use should be encouraged also because houses build of these materials have potential (when designed and built properly) to compete with thermal performance of houses built of conventional synthetic building materials.

## 1.2 Motivation

This work intends to analyse hygrothermal behaviour of the most used RNBM wall systems and compare these with conventional wall systems of current time both on theoretical and real environment level (Central Europe). It is thus a case study summarizing suitability of the selected wall systems for considered regions.

As it was mentioned above, use of RNBM in building industry has various positives for human life on both local and global scale. Those materials are the closest materials to human beings, as the humanity was progressing with them for its entire existence. The nature of man is to be attracted by these materials, as their beneficial effects on both our physical and mental health are indisputable. Over the time were their benefits, however, disregarded, and the materials were substituted by synthetic, energetically demanding materials with allegedly better material characteristics.

It is only the matter of last years, when the properties of raw natural materials are gaining the lost attention. Many researchers understood that future of sustainable construction might lie in past techniques altered with help of present science and that the low-energy or passive houses do not have to be always built of conventional cementitious elements and polystyrene or rock wool panels. This thesis intends to continue this effort by summarizing findings of others and applying them for benchmarking of hygrothermal behavior of selected RNBM wall systems between each other and with other nowadays common building materials and wall systems.

It is believed that the outcome of the thesis will provide a straightforward answer on how well the selected wall systems will perform in the Central European climate by focusing on differences in heat and moisture transfer behaviour of the different wall systems as well as on their capability to regulate inside relative humidity level. Although the materials have already been tested numerous times, it has mostly been done in different climatic region (e.g. Yates, 2002). The set of the materials and wall systems have never been tested under the same climatic conditions neither. The outcome could thus confirm or rebutter some of the claims of previous researches and material producers with regards to the considered climate. It is also believed that such document could provide better understanding for non-professionals, who could be interested in building with RNMB.

## 2 BACKGROUND

---

### 2.1 Hygrothermal processes in building envelope

The primary function of building envelope (BE) is to separate human beings from influences of outer environment such as rain, wind and extensive heat or cold. As result of this are elements of BE constantly exposed to hygrothermal disequilibrium due to different boundary conditions caused by the two environments they separate. None of the known materials can resist forces driven by this disequilibrium and thus constant hygrothermal fluxes through BE can be observed.

Fig. 2 shows the hygrothermal fluxes in BE element as described in ASHRAE standard (American Society of Heating, Refrigerating and Air Conditioning) (ASHRAE, 2009). It is evident that the number of outside influences acting upon BE makes understanding and predicting its final hygrothermal behaviour a very complex discipline. It requires detailed knowledge of individual hygrothermal processes occurring within BE as well as understanding the effect of material characteristics upon these.

This section intends to discuss the principal hygrothermal processes in porous BE materials and their relation to different material properties.

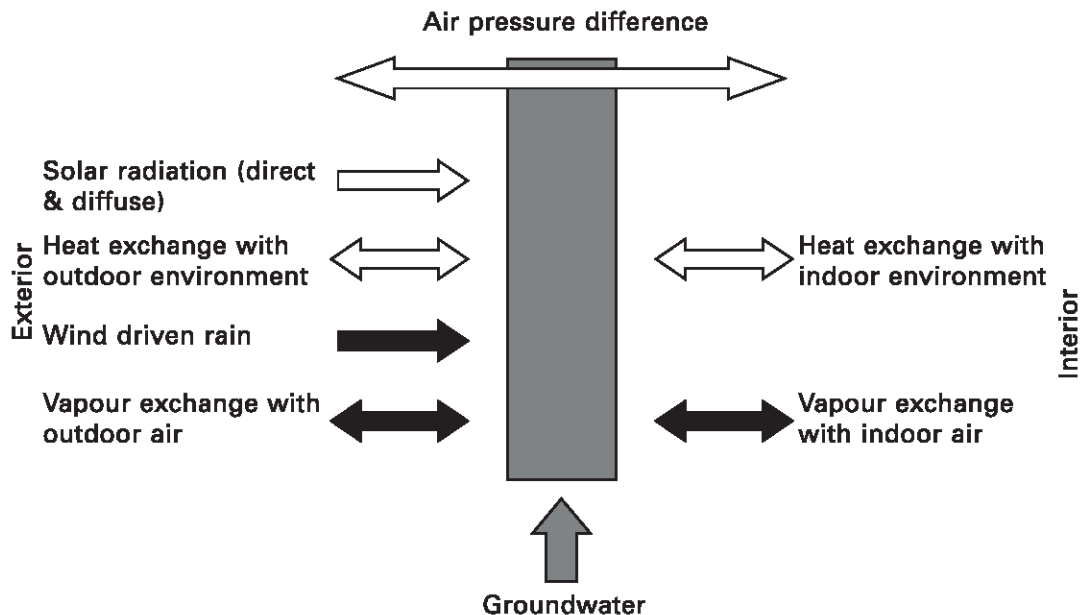


*Fig. 2: Hygrothermal fluxes and their alternating diurnal or seasonal directions acting upon building envelope according to ASHRAE (2009)*

### 2.1.1 Heat transfer

Heat is a type of energy, which propagates in an arbitrary environment, provided there exist spaces or bodies with unequal temperatures within this environment. Due to the effect of conservation energy law is heat transferred from higher temperature areas to lower temperature areas.

#### 2.1.1.1 Transfer mechanisms

Depending on environment in which is heat transferred and physical laws by which is this transfer governed, there exist three different mechanisms of heat transfer:

- Conduction
- Convection
- Radiation

**Conduction** results from energy exchange between microparticles, e.g. molecules of substance. The warmer and faster oscillating molecules with higher kinetic energy transfer their energy to adjacent, slower oscillating molecules. The heat exchange occurs between immediately neighbouring particles of a body, when there is an induced temperature difference within the body, or between neighbouring particles of two touching bodies with different temperatures. Conduction thus occurs usually in solids, although it can also occur in liquid and gaseous substances, provided they are in idle condition.

The principal material property describing ability of material to conduct heat is called *thermal conductivity*  $\lambda$  [W/(m K)]. It is defined as heat flux transmitted through 1 m<sup>2</sup> of 1 m thick material assuming 1 K temperature difference between two surfaces of the material. Materials with low thermal conductivity (below 0.1 W/(m K)) are considered as thermal insulators, whilst high thermal conductivity is characteristic for thermal conductors.

Thermal conductivity is often evaluated in terms of first Fourier's law, which is the fundamental physical law describing thermal conduction through matter. It defines dependency of heat flux density on temperature gradient in stationary temperature field (condition where temperature distribution in a given body does not change with time). Assuming homogeneity and isotropy of a given body the first Fourier's law is defined for one dimensional heat conduction as:

$$q = -\lambda \cdot \text{grad}\theta = -\lambda \frac{\partial\theta}{\partial x} \quad (1)$$

and for three dimensional heat conduction as:

$$q = -\lambda \nabla \theta = - \left( \lambda \frac{\partial \theta}{\partial x}, \lambda \frac{\partial \theta}{\partial y}, \lambda \frac{\partial \theta}{\partial z} \right) \quad (2)$$

where  $q$  is local heat flux density in  $\text{W}/\text{m}^2$ ,  
 $\lambda$  thermal conductivity in  $\text{W}/(\text{mK})$ ,  
 $\partial \theta / \partial x$  temperature gradient in  $^{\circ}\text{C}/\text{m}$ .

The one dimensional temperature gradient  $\theta$  and the heat flux  $q$ , which it induces is schematized in Fig. 3. It can be observed that direction of the heat flux is opposite to direction of the gradient, thus the minus sign in equations (1) and (2).

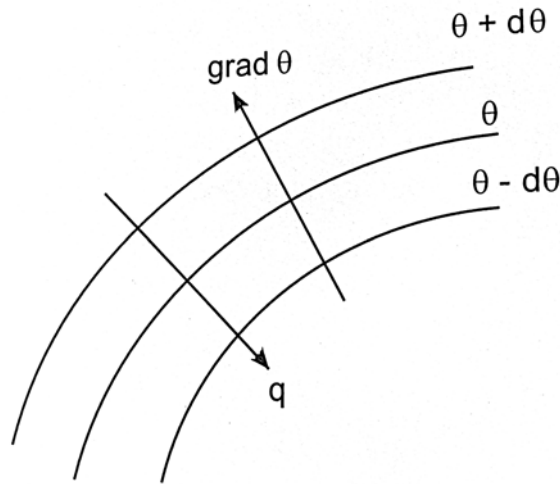


**Fig. 3:** Relationship of thermal gradient caused by different potentials to direction of induced heat flux (Bošová and Kulháněk, 2014)

The second, often called general, Fourier's law describes not only relationship between spatial temperature gradient, but also its dependency on time (non-stationary temperature field where temperature distribution in a given body changes with time). Assuming homogeneity and isotropy of a given body the second Fourier's law is defined for one dimensional heat conduction as:

$$\frac{\partial \theta}{\partial t} = \alpha \frac{\partial^2 \theta}{\partial x^2} \quad (3)$$

and for three dimensional heat conduction as:

$$\frac{\partial \theta}{\partial t} = \alpha \left( \frac{\partial^2 \theta}{\partial x^2} + \frac{\partial^2 \theta}{\partial y^2} + \frac{\partial^2 \theta}{\partial z^2} \right) \quad (4)$$

where  $t$  is time in s,  
 $\theta$  temperature in °C.

The stated  $\alpha$  parameter is called *thermal diffusivity*, which is defined as:

$$\alpha = \frac{\lambda}{\rho \cdot c} \quad (5)$$

where  $\rho$  is bulk density in kg/m<sup>3</sup>,  
 $c$  specific heat capacity in J/(kg K).

From the two Fourier's laws is evident that *thermal conductivity*, as a material characteristic defining heat flux through a body, is only sufficient when assuming steady state (time independent) temperature distribution throughout the body. When assuming transient regime of temperature distribution, also *bulk density* and *specific heat capacity* influence the final heat flux through the body.

**Convection** is a mechanism, which occurs only in liquid and gaseous substances. It is a motion of fluid particles caused by differences in density or pressure potentials, which results in heat transfer.

When we locally heat or cool any fluid, its density changes, which induces fluid particle displacement. The higher density (less oscillating) particles fall down and replace the particles of lower density (more oscillating). This process is called natural convection and it is governed by temperature and/or concentration gradients.

Intensity of heat exchange of the natural convection process is rather low and it is rarely sufficient for the purposes of modern building constructions. In order to increase heat exchange intensity in buildings the so-called forced convection, which can be induced by means of various technical devices (HVAC, pump, fan blower, . . .), needs to be introduced. Driving force of this process is an imposed pressure difference, which forces the fluid particles from spaces of higher pressure to spaces of lower pressure regardless of their temperature or concentration. The forced convection also occurs naturally in form of wind caused by difference in atmospheric pressure.

BE elements are mainly affected by convection (both natural and forced) due to heat transfer between surfaces of the elements and adjacent air. Relationship describing this phenomenon is defined by Newton's law of cooling:

$$q_c = h_c(\theta_{fl} - \theta_s) \quad (6)$$

where  $q_c$  is heat flux density due to convection in  $\text{W}/\text{m}^2$ ,  
 $h_c$  convective heat transfer coefficient in  $\text{W}/(\text{m}^2 \text{K})$ ,  
 $\theta_{fl}$  fluid temperature in  $^\circ\text{C}$ ,  
 $\theta_s$  surface temperature in  $^\circ\text{C}$ ,

The convective heat transfer coefficient depends on velocity of fluid induced by forced convection or on magnitude of temperature gradient, which drives the natural convection. It applies that  $h_c$  is much greater for forced convection, which confirms the low intensity of heat exchange in case of natural convection.

Heat transfer by **Radiation** fundamentally differs from the two above described mechanisms. Unlike conduction or convection, radiation does not need any medium for its propagation. Due to its character of electromagnetic wave, radiation transfers heat between two bodies of different temperature also in vacuum.

Every surface, which is warmer than 0 K, emits electromagnetic radiation. This radiation is eventually absorbed by other surfaces and causes thermal excitement of atoms and electrons of the absorbent matter and consequent local temperature rise. We talk about *radiant heat flux*  $\phi$  [W] or *radiant heat flux density*  $q$  [ $\text{W}/\text{m}^2$ ].

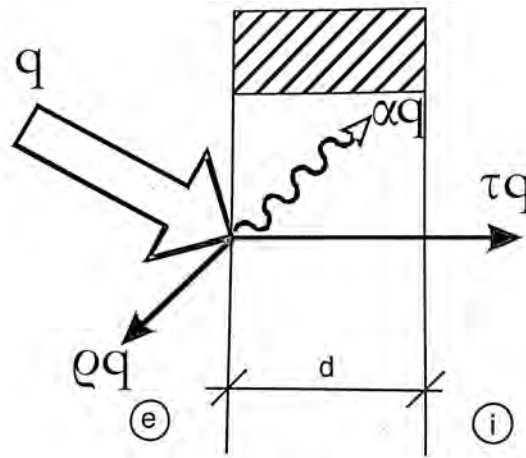


**Fig. 4:** Scheme of distribution of radiation incident on a surface of a wall (Bošová and Kulhánek, 2014)

In reality, every surface emits radiation and at the same time absorbs radiation from surrounding surfaces. The amount of absorbed radiation depends on nature of the receiving surface. Fig. 4 shows a typical distribution of radiation incident on a surface of semi-transparent wall. The radiant *heat flux density*  $q$  is after the incidence of radiation on the surface divided in three components. Part of the radiation is absorbed by the material, other part is reflected back (following laws of optic) and the last part is transmitted through the material. We talk about *surface absorptivity*  $\alpha$ , *reflectivity*  $\rho$  and *transmissivity*  $\tau$  and (as it can be observed in Fig. 4) the relationship between these material qualities writes as:

$$\alpha + \rho + \tau = 1 \quad (7)$$

While the amount of absorbed radiation depends purely on absorption properties of the receiving surface, the amount of emitted radiation depends also on temperature of this surface. To define the relationship between these two, the so-called black body needs to be defined.

Black body is a theoretical "ideal" body with absorptivity  $\alpha = 1$  (consequently  $\rho = \tau = 0$ ). Radiation energy incident on surface of the body is thus fully absorbed. The relationship between temperature of the black body and its *emittance*  $M_b$  [W/m<sup>2</sup>] (radiant heat flux emitted by m<sup>2</sup> of surface of the body) is defined by Stefan-Boltzmann law as:

$$M_b = \sigma T^4 \quad (8)$$

where  $\sigma$  is Stefan-Boltzmann constant ( $5.67 \cdot 10^{-8}$  W/(m<sup>2</sup> K<sup>4</sup>)),  
 $T$  temperature of the body in K.

In practice is normally used emittance of "grey" (real) body  $M$  [W/m<sup>2</sup>], which is defined using another material characteristic - *emissivity*  $\epsilon$  [-]. It is calculated as:

$$M = \epsilon M_b \quad (9)$$

Following the conservation energy law, it can be stated that emissivity of a surface equals to its absorptivity,  $\epsilon = \alpha$  (Kirchoff's law) (Hall and Allinson, 2010). This is confirmed on an example of black body. The surface of black body has an absolute absorptivity 1 from the nature of its definition. The value of absolute emissivity of black body 1 results from equation (9).

Given the information stated above and the general building physics knowledge, surface radiation properties ( $\alpha, \rho, \tau, \epsilon$ ) of surface materials of BE element are determining factors influencing heat transfer of the entire assembly of BE.

In reality conduction, convection and radiation happen always simultaneously, which is shown on an example of external wall in Fig. 5.

As regards heat transfer through a material on microscale level, the same set of heat transfer mechanisms can be observed. Provided we deal with porous material, the entrapped air within the material acts as a medium for convective and radiant heat transfer. On macroscale level is this, however, understood as pure conduction (as depicted in Fig. 5), as thermal conductivity, which is measured in real conditions, accounts also for convection and radiation within the material. Heat transfer mechanisms inside of porous material are illustrated in Fig. 6, on an example of granular material.

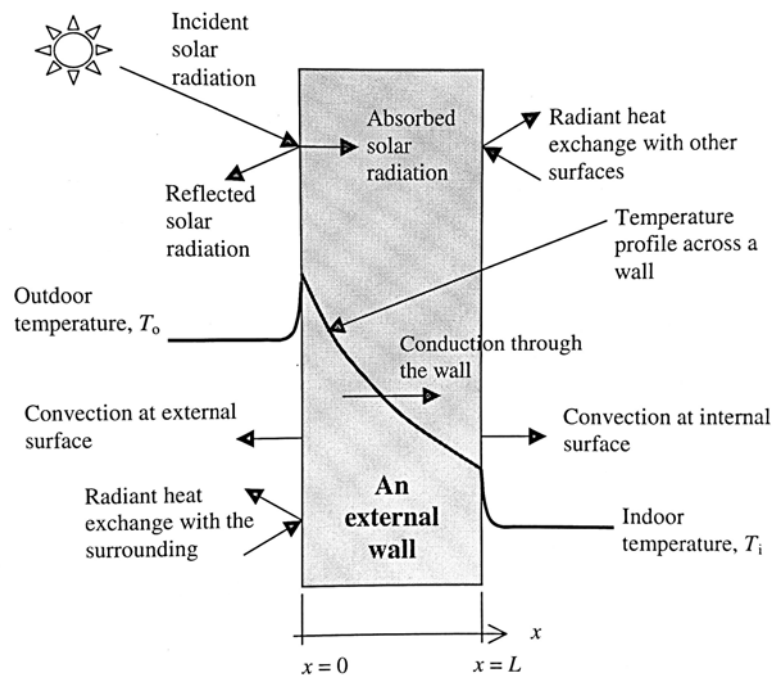


**Fig. 5:** Combination of all heat transfer mechanisms on an example of external wall (Moss, 2007)

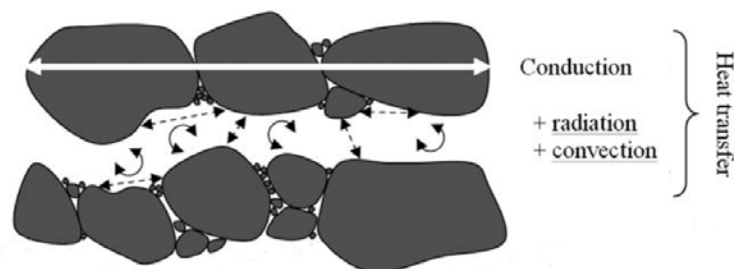


**Fig. 6:** Heat transfer mechanisms within granular material – microscale (Hall and Allinson, 2009)

### 2.1.1.2 Steady state temperature scenario

As it was explained in section about thermal conductivity, there are two ways of approaching the heat flow through solid matter problematics; steady state temperature scenario (distribution of temperature within the considered thermal system does not change with time) and transient state temperature scenario (distribution of temperature within the considered thermal system does change with time).

The steady state method was developed primarily due to high complexity of transient method, which used to be, especially during the pre-computer era, very hard to solve and interpret. Although the time has changed and computer technology nowadays allows thorough transient hygrothermal simulations, the simplified steady state method is still more common for analysis of BE thermal behaviour. There are several reasons for this:

- It is easier for architects and other non-building physicists involved in the construction design to deal with.
- The analysis of buildings using this method are easier to conduct and therefore faster and cheaper.
- It is the main tool for the energy certification of buildings, which is nowadays required by law in most of the developed countries.
- It provides benchmarking of different building components, regardless the climatic conditions they are set in.

Steady state heat transfer theory should be therefore considered as fundamental knowledge of building physics, which is adapted by individuals from other building design disciplines (mainly architects) during the primary design of the construction.

Two fundamental parameters of this theory are *thermal resistance*  $R$  and *thermal transmittance*  $U$  of building components, which are defined in European standard EN ISO 6946:2007 (ISO, 2007c) and its national variations.

*Thermal resistance*  $R$ , as the name suggests, is a property of building component, which indicates how resistant is the component towards conductive heat flux from interior to exterior. Assuming homogeneous layers of the component and 1D heat flux through it, total thermal resistance of the component  $R_T$  [(m<sup>2</sup>K)/W] writes as:

$$R_T = \sum R_j + R_{si} + R_{se} \quad (10)$$

where  $R_j$  is thermal resistance of  $j^{th}$  layer defined as:

$$R_j = \frac{d_j}{\lambda_j} \quad (11)$$

$d_j$  - thickness of the  $j^{th}$  layer in m,  
 $\lambda_j$  - thermal conductivity of the  $j^{th}$  layer in W/(mK),

and  $R_{si,se}$  thermal resistances of interior and exterior stagnant air layers adjacent to the wall surfaces (see temperature drop close to outer surfaces in Fig. 7) usually taken as tabulated value from standards (e.g. EN ISO 6946:2007 (ISO, 2007c)).

$R_{si,se}$  are defined using coefficients of convective heat transmission  $h_{i,e}$  [W/(m<sup>2</sup> K)] as:

$$R_{si,se} = \frac{1}{h_{i,e}} \quad (12)$$

where  $h_{i,e}$  are combination of convective heat transfer coefficient  $h_c$  (see equation (6)) and its radiation equivalent  $h_r$  (radiation and convection influence of ambient environment upon the considered component).

Distribution of temperature through a multi-layer composite wall in steady state temperature gradient environment can be analysed by graphical method (see Fig. 7). Knowing the wall geometry, thermal conductivities of individual layers and temperature boundary conditions, the graphical method can be conducted using equation:

$$\frac{\Delta T}{T_T} = \frac{R}{R_T} \quad (13)$$

where  $T_T$  is total temperature difference across the wall component in  $^{\circ}\text{C}$ ,  
 $\Delta T$  temperature difference across a layer in  $^{\circ}\text{C}$ ,  
 $R_T$  total thermal resistance of the wall component in  $(\text{m}^2\text{K})/\text{W}$ ,  
 $R$  thermal resistance of the considered layer in  $(\text{m}^2\text{K})/\text{W}$ .

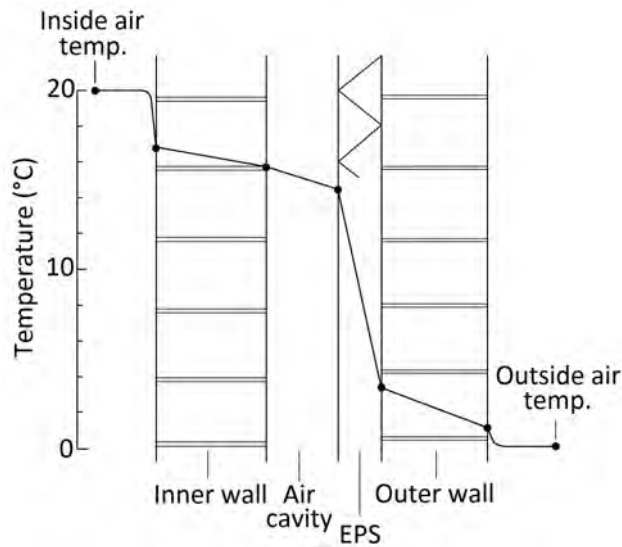


**Fig. 7:** Distribution of temperature through a multi-layered composite wall in steady state temperature environment (Hall and Allinson, 2010)

More common method of assessing the building components' thermal quality is nowadays *thermal transmittance*  $U$ , also known as U-value. *Thermal transmittance*  $U$   $[\text{W}/(\text{m}^2 \text{K})]$  determines heat flux passing through  $1 \text{ m}^2$  of building component given  $1 \text{ K}$  temperature difference between interior and exterior. Mathematically is thermal transmittance of a building component expressed as inverse value of its total thermal resistance  $R_T$   $[(\text{m}^2\text{K})/\text{W}]$ :

$$U = \frac{1}{R_T} \quad (14)$$

The overall steady state 1D heat flux density through building components [ $\text{W}/\text{m}^2$ ] is thereafter defined as a function of temperature gradient between interior and exterior ( $\theta_i - \theta_e$ ) [ $^{\circ}\text{C}$ ] and total U-value [ $\text{W}/(\text{m}^2 \text{K})$ ] of the considered building component:

$$q = U(\theta_i - \theta_e) \quad (15)$$

### 2.1.1.3 Transient thermal conditions

In reality are components of BE exposed to continual temperature fluctuation, which dramatically influence the overall character of heat transfer through these components. Thermal performance of materials in such environment depends on three previously described material parameters: *thermal conductivity*  $\lambda$ , *specific heat capacity*  $c_p$  and *bulk density*  $\rho$  (see equation (4); second Fourier's law).

The ability of material to conduct heat (represented by *thermal conductivity*  $\lambda$ ) is no longer sufficient for complete thermal behaviour analysis as the ability of material to store heat (represented by combination of *specific heat capacity*  $c_p$  and *bulk density*  $\rho$ ) plays also its undeniable role. We talk about thermal mass of a material.

**Thermal mass**, as a term predominantly used in construction terminology, defines amount of heat energy, which can a building component hold, when its temperature rises by 1 K. Scientifically is thermal mass equivalent to *heat capacity*  $C_{th}$  [ $\text{J}/\text{K}$ ], which is (for homogeneous building component) derived as product of component's mass  $m$  [ $\text{kg}$ ] and its specific heat capacity  $c_p$  [ $\text{J}/(\text{kg K})$ ]:

$$C_{th} = mc_p \quad (16)$$

Whilst heat transfer pattern through materials with low thermal mass in dynamic conditions does not differ much from that of the steady state conditions, thermal behaviour of material with high thermal mass is significantly different. Such materials act as a thermal sink. This means that heat energy, which would be normally conducted through the material, is used for increase of temperature of the material. In other words, heat transfer through the material is delayed, due to its high thermal inertia. In the environment of cyclic temperature change between day and night can this material quality crucially affect the final thermal behaviour of building components and the overall building (Gregory *et al.*, 2008).

Fig. 8 shows the effect of high thermal mass building component on indoor temperature distribution in transient temperature model researched by Hall and Allinson (2008). In this model is the outside temperature represented by sin curve, which is projected inside as sin curve with different amplitude and phase shift. It is evident that the large external outside fluctuations are moderated to more stable indoor temperature situation (thermal

dampening represented by difference between amplitude  $A_{eo}$  and  $A_{ei}$ ) and that the outside temperature peak is shifted in time (phase shift  $\phi$ ). This is especially important in climates with high temperature difference between day and night, where building components with high thermal mass reduce heating or cooling demand of a building as well as increase thermal comfort of inhabitants.

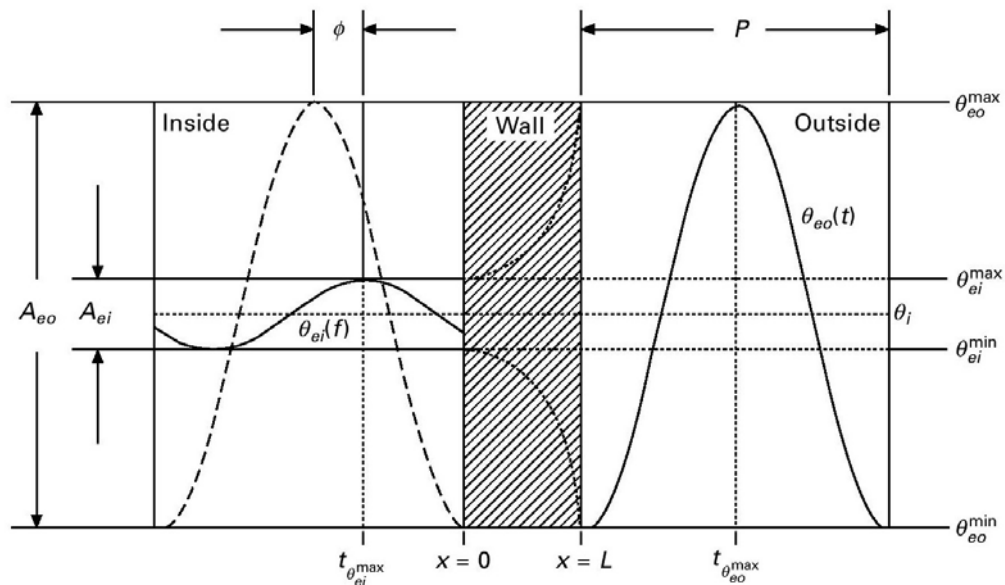


**Fig. 8:** Visual explanation of effect of high thermal mass wall on moderation of external temperature fluctuations (Hall and Allinson, 2008)

The combined effect of thermal mass and thermal conductivity is represented by two parameters, which characterise materials behaviour in dynamic environment: *thermal diffusivity*  $\alpha$  and *thermal effusivity*  $b$ .

**Thermal diffusivity**  $\alpha$  [ $\text{m}^2/\text{s}$ ] is defined as rate at which the temperature of a material can vary (Evrard, 2008). It determines speed of heat diffusion into the material and depth of a component, which is affected by daily temperature fluctuation. It is calculated as:

$$\alpha = \frac{\lambda}{\rho \cdot c} \quad (17)$$

where

- $\lambda$  is material's thermal conductivity in  $\text{W}/(\text{m K})$ ,
- $\rho$  bulk density in  $\text{kg}/\text{m}^3$ ,
- $c$  specific heat capacity in  $\text{J}/(\text{kg K})$ .

The higher thermal diffusivity of a material, the faster the material reaches its thermal equilibrium. Fig. 9 shows difference between materials with high and low thermal diffusivity (in combination with thermal effusivity). It can be observed that heat flows through the

material with higher thermal diffusivity much more rapidly than through the one with lower thermal diffusivity.

**Thermal effusivity**  $b$  [ $(\text{Ws}^{1/2})/(\text{m}^2\text{K})$ ], also known as thermal inertia, represents quantity of energy given to (or taken out from) a material when it is subjected to heating or cooling during a given time laps (Evrard, 2008). Mathematically is thermal effusivity expressed as:

$$b = (\rho \cdot c \cdot \lambda)^{1/2} \quad (18)$$

The higher the thermal effusivity of a material the more energy exchanges material with its ambient environment. It is the quality, which defines how material is perceived by human body. Materials with high thermal effusivity are perceived as cool, whilst the ones with low thermal effusivity are perceived as warm. On the other hand, materials with high thermal effusivity regulate indoor environment temperature more effectively, due to their faster reaction on temperature variations (Stahl, 2009).

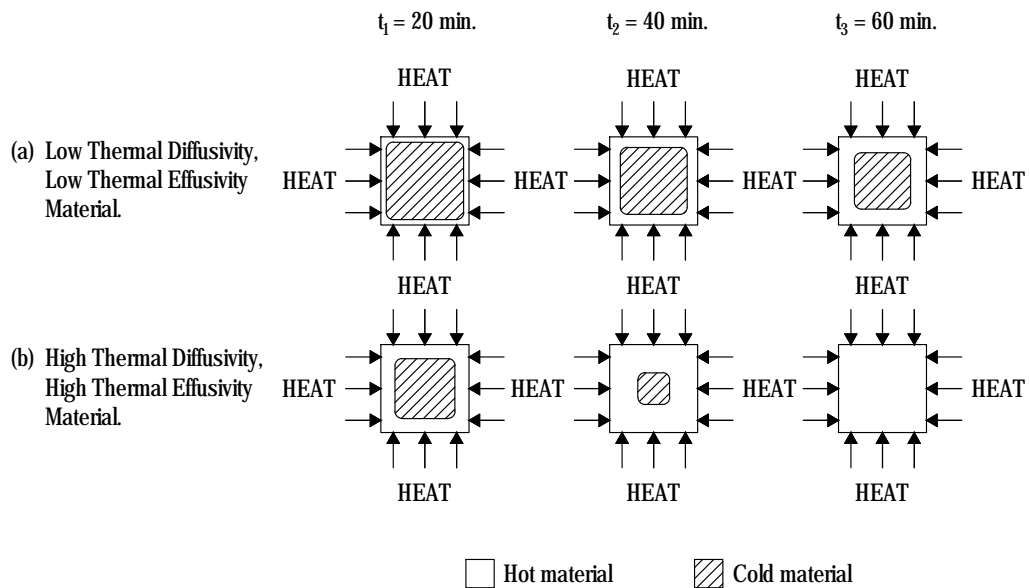


**Fig. 9:** Blocks of high thermal diffusivity (effusivity) material (a) and low thermal diffusivity (effusivity) material (b) heated at the same rate ((Ahmed and Sturges, 2014)).

Whilst thermal diffusivity and effusivity are ideal indicators to compare thermal performance of single-layered building components in dynamic thermal environment, they fail to assess the difference between multi-layered components. As an example of this drawback would be two wall components of the same dimensions differing in the position of thermal insulation. The two components will have the same sets of thermal diffusivities and effusivities, but very different thermal performance.

### 2.1.2 Mass transfer

The term 'mass transfer' designates propagation of air, water, water vapour, dissolved solids and other fluids in a solid material. The ability of those fluids to diffuse through construction elements is analogical to the heat flux theory. While the heat flux is driven by temperature gradient between boundary environments, the so-called moisture flux needs gradient in partial water vapour pressures (Mrlík, 1985).

#### 2.1.2.1 Psychometrics

Out of the above named potential mass flows, air and moisture (water in both gaseous and liquid state) have the most important effect on final hygrothermal performance of building elements.

Air carries water vapour and energy, which is often expressed as enthalpy (amount of energy stored in a thermodynamic system). Depending on its temperature and atmospheric pressure, air can carry different amount of water molecules. This is again related to kinetic energy of molecules in air. The faster moving (oscillating) water vapour molecules in the air are more likely to keep themselves from clustering into small liquid drops. This means that the higher kinetic energy of water molecules in the air, the closer to each other they can exist without condensing into liquid state. Atmospheric pressure, on the other hand, represents force with which are air molecules forced one to another. The higher the atmospheric pressure the more are the molecules pushed closer to each other and the lower is the maximum amount of water molecules carried in air.

The maximal possible water vapour concentration in air is therefore a function of air temperature and atmospheric pressure, which is usually presented in tabulated form (see Appendix A). The amount of water molecules in air is expressed in absolute humidity and it is usually measured in  $\text{g}/\text{m}^3$  or  $\text{kg}/\text{kg}$  (mass of water molecules in volume/mass of air-vapour mixture).

Dalton's law states that when two gases are mixed, the total pressure they impose on a surface is equal to sum of pressures of the individual gases. Those pressures are then called partial pressures (Dutton, 1961). Knowing the maximal (saturated) concentration of water molecules in air, saturation partial water pressure (usually referred to as saturation pressure) can be determined. Relative humidity (RH)  $\varphi$  [-] of air-vapour mixture of given temperature and absolute humidity is thereafter defined as ratio between partial (actual) water vapour pressure  $p_v$  [Pa] and saturation water vapour pressure  $p_{v,s}$  [Pa]:

$$\varphi = 100 \frac{p_v}{p_{v,s}} \quad (19)$$

It is evident that air-vapour mixture can exist in many different states, depending on the amount of water molecules, temperature and atmospheric pressure. Fig. 10 shows psychrometric chart, which covers those states graphically (for typical atmospheric pressure of 101 kPa). Individual lines represent different indicators (absolute/relative humidity, dry/wet bulb temperature and enthalpy) of air in given state. The saturation line separates stable state air conditions from air conditions (temperature vs. absolute humidity), which are not physically possible. The boundary air condition between fully saturated state and vapour condensing state is called dew point. When the air temperature drops below the dew point (saturation line), condensation inevitably occurs.

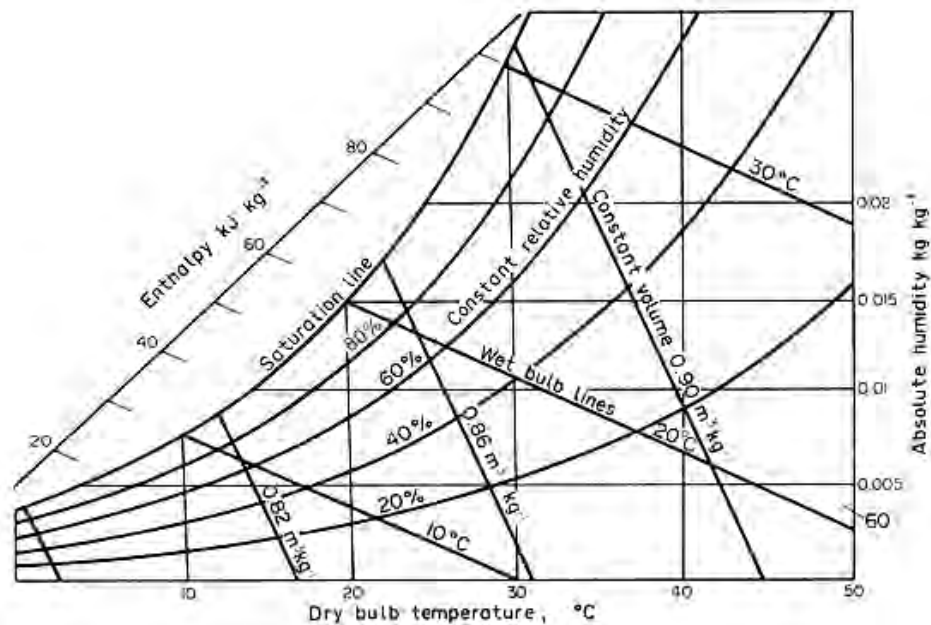


**Fig. 10:** An example of psychrometric chart (Earle, 1983)

#### 2.1.2.2 Porous materials

Mass transfer through a solid material occurs through its open pores. The fundamental condition of this process is minimal intermolecular space of a material larger than the mean trajectory of water vapour molecules ( $2.78 \times 10^{-10}$  m) (Vaverka *et al.*, 2000). In case of materials common in building industry, is the intermolecular space usually referred to as capillary system or pore network in materials. These systems are commonly divided into:

- microcapillaries (micropores)
- macrocapillaries (macropores)

The prevalent mass transfer through microcapillaries ( $< 5 \times 10^{-7}$  m) is called effusion. Collision of water molecules and surfaces of the pores is more frequent during the transfer and the so-called capillary condensation often occurs. The process is independent of ambient pressure and it is driven by capillary and van der Waals forces (forces caused by permanent

or instantaneously induced electric dipole between electrically neutral molecules). Effusion is commonly described by Graham's law of effusion (Pickover, 2008).

In macrocapillaries ( $> 5 \times 10^{-7}$  m) is the mass transfer governed by ambient pressures and it is referred to as diffusion (see section 2.1.2.4). Water vapour diffusion mechanism in macropores is practically identical to water vapour diffusion through air. Two material characteristics defining water vapour permeability of a material can be therefore introduced:

- *Water vapour diffusion permeability*  $\delta$  [kg/(m s Pa)] - defines how much water vapour is transferred through 1 m of material per 1 s, when considering pressure gradient of 1 Pa and depends mainly on pore structure of the material (Hall and Allinson, 2010).
- *Water vapour diffusion resistance factor*  $\mu$  [-] (commonly called  $\mu$ -factor) - determines ratio between  $\delta_a$  of air and  $\delta$  of the considered material ( $\delta_a/\delta$ ), where  $\delta_a$  depends on thermodynamic temperature  $T$  [K] and ambient pressure  $P_a$  [Pa] and equals to  $2 \cdot 10^{-7} \cdot T^{0.81}/P_a$  (ISO, 2001).

When water molecules are being diffused through a porous material, they can be adsorbed to internal surfaces of voids by van der Waals forces. Due to their dipolarity, the molecules bonds also one to another and with increasing RH of ambient air, multi-layered formations can occur. With higher RH values can this process result in capillary condensation, which is a condition, when metastable groups of adsorbed water vapour molecules spontaneously nucleate into a liquid water meniscus (Hall and Allinson, 2009). Due to increased number of van der Waals interaction between water molecules, the phase change phenomenon (condensation) occurs below saturation pressure (Hall and Allinson, 2010). Schematic representation of this process is shown in Fig. 11.

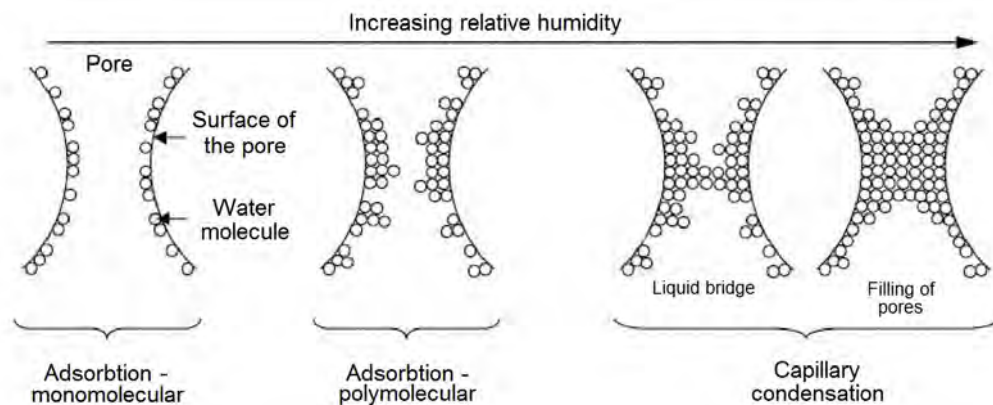


**Fig. 11:** Schematic representation of physical adsorption phenomena in a pore (Moevus et al., 2013)

Each material has ability to absorb and hold different amount of moisture, depending on its microscopic structure and hygroscopy (ability of material to attract and hold water molecules from surrounding environment). The actual amount of absorbed water in material depends on ambient RH and marginally on temperature (Samuel *et al.*, 2016). A curve

called sorption isotherm (see Fig. 12) describes the relationship between water content of a porous material and RH of ambient air (for given temperature).

As it can be seen from the curve shape in Fig. 12, water absorption in materials happens in three stages. First, are the water molecules adsorbed to surfaces of the pores (monomolecular adsorption), which is characterised by initial steeper part of the isotherm. Second, the diffusion through material happens and water content increases less rapidly (polymolecular adsorption). And eventually capillary condensation and liquid water suction characterise the last stage, when large amount of moisture is absorbed within considerably little increase of RH.

In addition, three different regions of sorption process can be observed (see the right part of Fig. 12). Depending on phase in which is water absorbed in a material and extent to which it is attracted to surfaces of voids, there exists:

- **hygroscopic region**, which represents state when water is absorbed by material from surrounding air in vapour phase. It is represented by hygroscopic range, which is defined by RH between 0 and 98 %
- **capillary region**, which is reached when material is in direct contact with liquid water (RH 100 %). The capillary forces are prevalent in this region. Maximal water content in this region is represented by  $w_c$  line in Fig. 12.
- and **gravitational region** ( $w_s$  line in Fig. 12), which defines state, in which the electrostatic attraction between water molecules and surfaces of pores is not sufficient to act against gravity force any more (no capillary potential in pores).

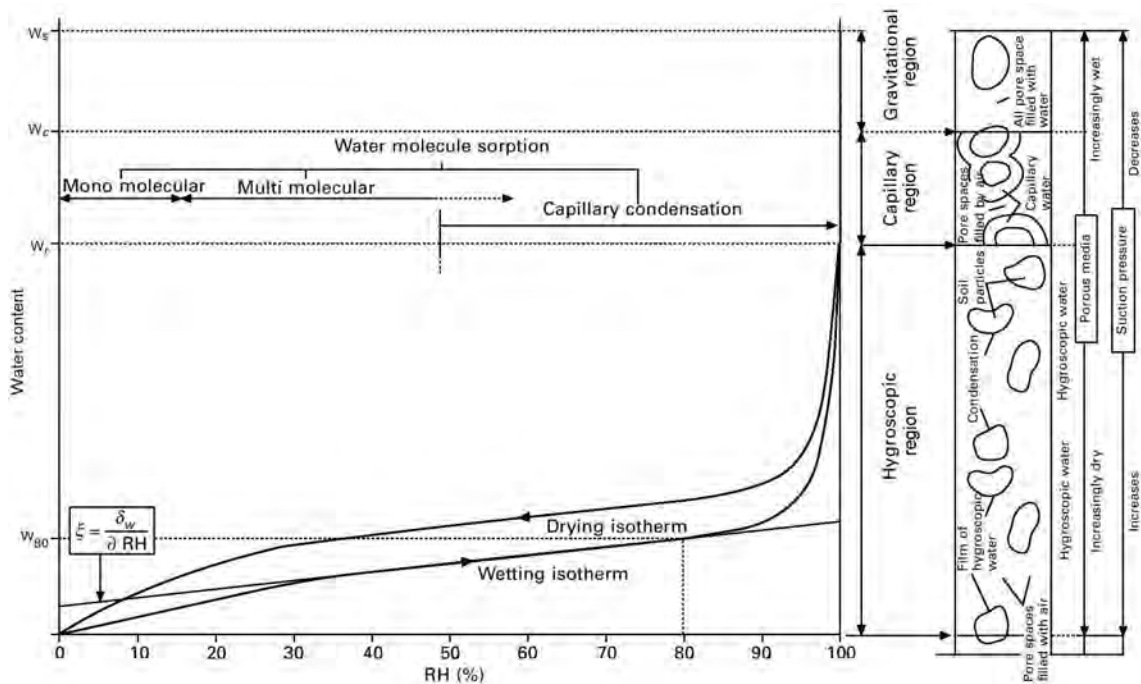


**Fig. 12:** A typical sorption isotherm of porous material (wetting and drying curves) with corresponding moisture storage regions (Hall and Allinson, 2009)

Due to its apparent complexity is sorption isotherm often characterised by *specific hygric capacity*  $\xi$  [kg/m<sup>3</sup>]. As can be seen in Fig. 12, specific hygric capacity represents slope of gradient of the isotherm curve at given RH and is defined as:

$$\xi = \frac{\partial w}{\partial \varphi} \quad (20)$$

where  $w$  is water content of a material in kg/m<sup>3</sup>,  
 $\varphi$  relative humidity of ambient air in [-].

In heat transfer analogy would be the sorption isotherm (represented by specific hygric capacity) equivalent to thermal mass. The term 'hygric mass' is often used in literature (Allinson and Hall, 2010).

Yet, unlike in heat transfer analogy, sorption behaviour of materials shows hysteresis effect between adsorption and desorption process (drying and wetting isotherm in Fig. 12). One reason causing this phenomenon is capillary condensation within the micropores - water molecules, which condensed below saturation pressure do not evaporate at the same enthalpy, at which they have condensed. The other reason is existence of surface adsorption van der Waals forces, which also raise the enthalpy at which are water molecules vaporized (Hall and Allinson, 2009).

### 2.1.2.3 Phase change / Latent heat effect

An important phenomenon, which has been long neglected by many building physicists is latent heat effect, which occurs as a result of phase change of moisture within materials or during adsorption and desorption of water molecules by pore surfaces of a material.

As it was already discussed, water molecules in vapour state are fast moving (oscillating) and thus have higher kinetic energy than slower moving (oscillating) molecules in liquid state. What was not discussed is that vapour molecules have also higher potential energy, stored in weaker inter-molecular forces. Therefore, when molecules in vapour state change their phase into liquid state, new stronger inter-molecular forces are formed, and part of the potential energy of molecules is lost (Joule, 2011). This energy is consequently released into the surrounding environment in form of heat. The same situation can be observed during adsorption of molecules by pore surfaces (van der Waals force binding the vapour molecules to pore surfaces also reduce their molecular potential energy). Latent heat is thus defined as amount of energy that is required to break the inter-molecular forces or gained by their creation (Babbitt, 1942).

As the above described processes are reversible, we can talk about latent heat of vaporisation, condensation, adsorption and desorption.

In real environment causes latent heat effect (which is higher for materials with high hygric mass) mitigation of heat flow through BE by contribution to thermal inertia of the material (Bevan *et al.*, 2008). To address this phenomenon the so-called practical thermal inertia was defined as combination of sensible and latent heat storage potentials of materials (Nordby and Shea, 2013). The actual thermal dampening effect of building component therefore depends on both thermal and hygric mass.

When compared to overall energy consumption of buildings, latent heat effect plays usually minor role. Evrard *et al.* (2006) reported the effect of latent heat for hemp-lime composite wall (with considerably high hygric mass) to be small, but not negligible complement of thermal load of the wall element.

The main benefit of latent heat effect was reported by some authors (Evrard, 2008, Winkler *et al.*, 2014) as potential contribution to higher comfort feeling of occupants due to offsetting of daily thermal peaks. Dubois *et al.* (2013) conducted experiment, which confirms this potential by addressing the effect of latent heat on surface temperature of hemp-lime composite wall.

They subjected this wall to RH cycles (8 hrs of RH 75 % followed by 16 hrs of RH 33 %) with no temperature variation (according to Nordtest protocol; see section 2.1.2.6) and observed the impact of those cycles upon development of surface temperature. Fig. 13 shows the final results, which, in spite of constant ambient temperature, display clear surface temperature rise (about 0.8 °C) during the absorption (shorter) phase.

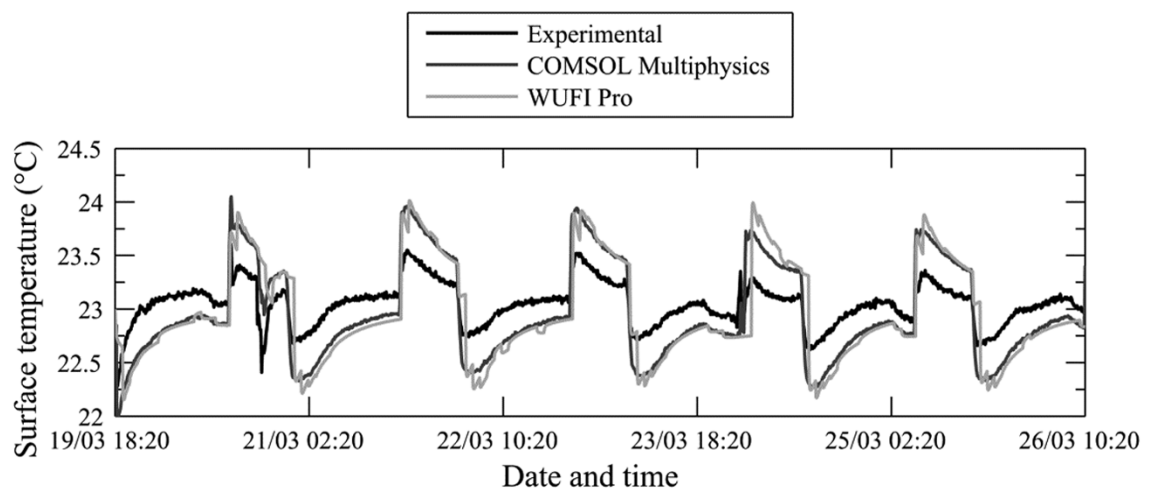


**Fig. 13:** Surface temperature of hemp-lime composite samples subjected to RH variation cycles (determined by real measurement and two simulation software tools) (Dubois *et al.*, 2013)

#### 2.1.2.4 Transfer mechanisms

Depending on the phase, in which water molecules propagate through building element, two moisture transfer mechanisms can be observed:

- Water vapour transfer
- Liquid water transfer

**Water vapour transfer** can be either convective or diffusive. The convective water vapour transfer is directly linked to airflow through building component (infiltration), which is driven by total pressure gradient. It is a well-known fact that movement of air through poorly sealed construction can transfer large amounts of moisture, which can cause significant damage of the building element (Newport Partners, 2004). The air tightness of construction can be, however, achieved in majority of building components, when built thoroughly (Christian *et al.*, 1998) and since the air infiltration is not an objective of this paper, the convective part of water vapour transfer will be further not considered.

The diffusive water vapour transfer is described by kinetic gas theory of molecules in multi-component gas mixture as sum of three different diffusion potential gradients; partial pressure, temperature and total pressure (Bear, 2013). In building physics applications is, however, water vapour diffusion caused by temperature and total pressure gradients negligible when compared to the so-called Fick's diffusion (Auracher, 1974).

Fick's diffusion is a process when water molecules travel (diffuse) through a substance from places of high concentration to places of low concentration. As discussed above, partial water vapour pressure (water vapour molecule concentration) is the driving force of the process. In heat transfer analogy is Fick's diffusion equivalent to heat conduction and it is evaluated in terms of first Fick's law of diffusion. Assuming homogeneity and isotropy of a given body, the first Fick's law of diffusion is defined as:

$$g = -D \cdot \text{grad}v = -D \frac{\partial v}{\partial x} \quad (21)$$

where  $g$  is water vapour diffusive flux density in  $\text{kg}/(\text{m}^2 \text{s})$ ,  
 $\partial v/\partial x$  absolute humidity gradient in  $\text{kg}/\text{m}^3$ ,  
 $D$  water vapour diffusion coefficient (vapour diffusivity) in  $\text{m}^2/\text{s}$   
 defined as:

$$D = \frac{\delta \cdot R \cdot T}{M} \quad (22)$$

$\delta$  - water vapour diffusion permeability in  $\text{kg}/(\text{m s Pa})$   
 (described in section 2.1.2.2),  
 $R$  - universal gas constant in  $\text{J}/(\text{mol K})$ ,  
 $T$  - absolute temperature in K,  
 $M$  - molar mass of water in  $\text{kg}/\text{mol}$ .

For practical purposes is Fick's law often reformulated using *water vapour partial pressure gradient*  $p_v$  [Pa/m] as:

$$g = -\delta \cdot \text{grad}p_v = -\delta \frac{\partial p_v}{\partial x} \quad (23)$$

Water vapour diffusion permeability of materials is mostly determined by dry cup/wet cup method according to EN ISO 12572 (ISO, 2001). This method measures the absolute amount of water, which passes through the material in temperature and humidity controlled environment. Due to this fact, not only Fick's diffusion is taken into account when applying Fick's law using lab obtained coefficients, but also the other two known vapour diffusion mechanisms are considered; effusion (see section 2.1.2.2) and surface diffusion (diffusion of water molecules adsorbed to the walls of pores) (see Fig. 14).

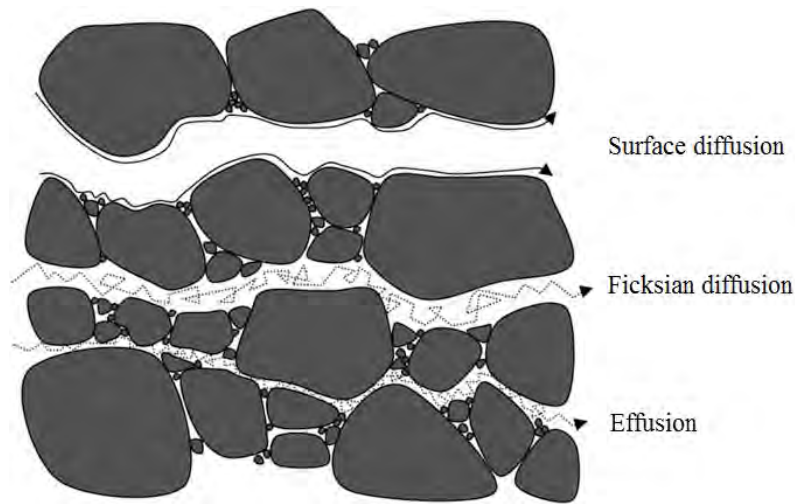


**Fig. 14:** Mechanisms of vapour diffusion in porous materials (Hall and Allinson, 2009)

**Liquid water transfer** through porous materials can be (based on above discussed saturation regions) divided into two moisture intervals:

1. When water content of a material is within hygroscopic and capillary region (unsaturated state), the driving force governing liquid transport in pores is capillary potential (suction)  $\Psi$  [Pa]. This potential results from capillarity phenomenon, which causes flow of liquids in narrow (capillary) spaces without assistance of (or even against to) external forces (e.g. gravity). It is caused by surface tension (which results from cohesion within the liquid) and adhesive forces between liquid and surrounding surfaces (Hens, 2008).

*Capillary liquid water flux density*  $q_l$  [kg/(m<sup>2</sup>s)] through a pore can be therefore expressed as:

$$q_l = -k_w(\Psi) \cdot \text{grad}\Psi = -k_w(\Psi) \frac{\partial \Psi}{\partial x} \quad (24)$$

where  $k_w$  is liquid water permeability (capillary potential dependent) in  $\text{kg}/(\text{m s Pa})$ ,  
 $\partial\Psi/\partial x$  capillary suction gradient in  $\text{Pa}/\text{m}$ .

- When the capillary potential becomes less prevalent (in case of pores with wider diameter or when water content rises towards capillary saturation), gravity force based liquid transfer dominates in the material. The governing force of this transfer is hydrostatic pressure differential  $P_w$  (water head) and it is defined by Darcy's law of fluid flow through porous media as:

$$q_s = -k_{w,s} \cdot \text{grad}P_w = -k_{w,s} \frac{\partial P_w}{\partial x} \quad (25)$$

where  $q_s$  is liquid water flux density (non-capillary) in  $\text{kg}/(\text{m}^2 \text{s})$ ,  
 $k_{w,s}$  liquid water permeability at saturation in  $\text{kg}/(\text{m s Pa})$ ,  
 $\partial P_w/\partial x$  water head pressure gradient in  $\text{Pa}/\text{m}$ .

*Liquid water permeability*  $k_{w(s)}$ , similarly like water vapour diffusion permeability, is (for both cases) a material characteristics depending mainly on pore structure of material (cross-section of pore), properties of the floating liquid (viscosity, surface tension) and material type (Hall and Allinson, 2010).

Due to rather irregular system of pores and difficult measurement of liquid water permeability material characteristics, a simplified model of combined liquid transfer (capillary and gravitational) was developed. *Moisture content*  $w$  [ $\text{kg}/\text{m}^3$ ] in material was introduced as an 'improper' driving force of this model (its value changes between individual material layers) (Hens, 2008). A simplified *liquid water flux density*  $q_w$  [ $\text{kg}/(\text{m}^2 \text{s})$ ] is then written as:

$$q_w = -D_w \cdot \text{grad}w = -D_w \frac{\partial w}{\partial x} \quad (26)$$

where  $D_w$  is liquid transfer coefficient (liquid diffusivity) of a material in  $\text{m}^2/\text{s}$  (analogous to vapour diffusivity in equation (21)),  
 $\partial w/\partial x$  moisture content gradient (varying with material layers) in  $\text{kg}/\text{m}^4$ .

Liquid transfer coefficient is commonly determined for two different scenarios. When a material is in direct contact with liquid water, we talk about surface diffusion and *liquid transfer coefficient of suction*  $D_{ws}$ , whilst when the material has no direct contact with liquid water and the moisture within the material is not in equilibrium, we talk about capillary conduction and *liquid transfer coefficient of redistribution*  $D_{ww}$  (Künzel, 1995).

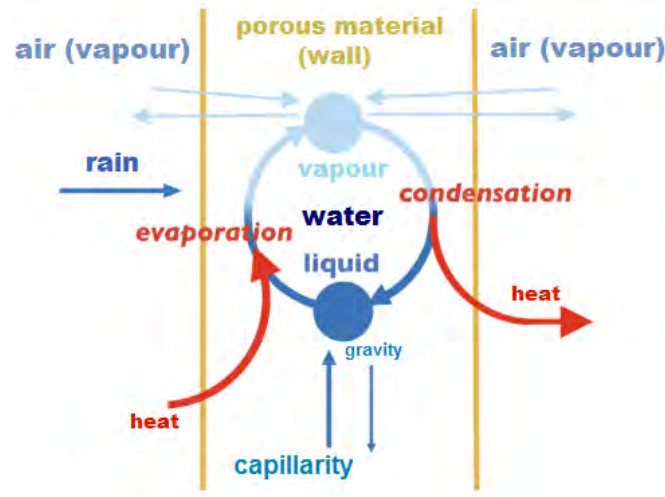


**Fig. 15:** Moisture transfer in porous BE wall element and the phenomena resulting from it (Heitz et al., 2015)

Similarly like in the heat transfer theory, moisture transfer mechanisms happen always simultaneously. Fig. 15 shows those mechanisms, their interaction and link to heat transfer, which results from it in schematized manner.

#### 2.1.2.5 Steady state humidity scenario

When distribution of RH throughout considered hygric system does not change in time, the same set of parameters describing behaviour of building component in steady state heat transfer scenario can be applied.

We talk about water vapour resistance (or permeance) of building components (in detail described in EN ISO 9346:2007 (ISO, 2007d)), which are defined either with regard to absolute humidity or to partial vapour pressure. Assuming homogeneous layers of a component and 1D water vapour diffusive flux through it, total *water vapour resistance* of the component  $Z_{pT}$  [(m<sup>2</sup>sPa)/kg] (with regard to partial pressure) writes as:

$$Z_{pT} = \sum Z_{pj} + Z_{pi} + Z_{pe} \quad (27)$$

where  $Z_{pj}$  is water vapour resistance of  $j^{th}$  layer defined as:

$$Z_{pj} = \frac{d_j}{\delta_j} \quad (28)$$

$d_j$  - thickness of the  $j^{th}$  layer in m,

$\delta_j$  - water vapour diffusion permeability of the  $j^{th}$  layer in kg/(m s Pa),

and  $Z_{pi,pe}$  water vapour diffusion resistances of interior and exterior stagnant air layers adjacent to wall surfaces defined as:

$$Z_{pi,pe} = \frac{1}{\beta_{pi,pe}} \quad (29)$$

$\beta_{pi,pe}$  - convective water vapour transfer coefficient in  $\text{kg}/(\text{m}^2 \text{s Pa})$ , which can be computed from convective heat transfer coefficient  $h_{ci,ce}$  as:

$$\beta_{pi,pe} = 7 \times 10^{-9} \cdot h_{ci,ce} \quad (30)$$

The overall steady state 1D *water vapour diffusive flux density*  $g$  [ $\text{kg}/(\text{m}^2 \text{s})$ ] through a building component is defined as function of partial water vapour pressure gradient between interior ( $p_{vi}$  [Pa]) and exterior ( $p_{ve}$  [Pa]) and total water vapour resistance of the considered building component  $Z_{pT}$  [ $(\text{m}^2 \text{s Pa})/\text{kg}$ ]:

$$g = \frac{p_{vi} - p_{ve}}{Z_{pT}} \quad (31)$$

In case of mass transfer is, however, not as important how much vapour flows through the construction, but rather whether this vapour condensates on its way out. The so-called interstitial condensation occurs, when the actual water vapour partial pressure  $p_v$  [Pa] reaches the value of saturation pressure  $p_{v,sat}$  [Pa] in any part of the building component's cross-section:

$$p_v \geq p_{v,sat} \quad (32)$$

Assessment of occurrence of interstitial condensation can be done either by numerical-graphical method (e.g. Glaser method, see Appendix A) or by use of computer software. The Glaser tangent method (described in EN ISO 13788 (ISO, 2012)) is based on graphical representation of *equivalent air layer thickness*  $s_d$  [m] (sd-value) of individual component layers, saturation pressure given by temperature distribution through the layers and partial water vapour pressure given by the boundary conditions (outside/inside RH and temperature).

sd-value of a construction layer represents theoretical thickness of an air layer with equivalent water vapour resistance and can be computed as:

$$s_d = \mu \cdot d \quad (33)$$

where  $\mu$  is vapour diffusion resistance factor of the considered layer [-]  
 (see section 2.1.2.2),  
 $d$  thickness of the layer [m].

Wihan (2007), however, points out that Glaser method provides only approximate estimation of interstitial condensation occurrence, as it does not consider capillary condensation. It simply expects that porous materials remain completely dry until the dew point condition is reached somewhere within the material.

#### 2.1.2.6 Transient hygric conditions

Just as thermal conditions in real environment vary through day and season, hygric conditions (both outside and inside) also follow dynamic, unpredictable pattern. It is therefore important to define material characteristics, which address material behaviour in such conditions.

As it was already discussed in section 2.1.2.2, the response mechanism of porous materials to ambient RH variation mostly depends on their hygroscopy and microscopic structure and it is characterised by sorption isotherm curve (Fig. 12). In building physics very important potential of material to buffer the RH fluctuations of ambient environment is given by slope of gradients of sorption isotherm. Depending on magnitude of the slope we talk about high or low hygric mass (capacity) of a material.

**Hygric mass (capacity)** is term, which was defined based on analogy with thermal mass. It characterises how a building component deals with ambient moisture in terms of its absorption and storing ability. Materials with high hygric mass can absorb, store and release significant amount of moisture, which helps to maintain stable indoor air RH. They act as a moisture sink.

Yet, unlike in the thermal mass case, the cumulative function of moisture uptake (sorption isotherm) is not linear and therefore hygric mass of a material cannot be defined by single value. From Fig. 12 can be seen that the moisture uptake follows different trend in different RH intervals. This means that materials absorb different amount of moisture at different stage of saturation. To address this non-linearity, *specific hygric capacity*  $\xi$  [kg/m<sup>3</sup>] (see equation 20) can be defined at any point of the sorption isotherm. This allows to assess hygric behaviour of materials in arbitrary hygric conditions with arbitrary hygric change (shock)  $\Delta\varphi$ .

Having the specific hygric capacity defined, Rode *et al.* (2005) give an expression of hygric diffusivity and effusivity, which are theoretical parameters based on heat transfer analogy, which characterise materials behaviour in dynamic environment.

**Hygic diffusivity**  $\alpha_h$  [ $\text{m}^2/\text{s}$ ] is defined as rate at which water content of a material can vary due to vapour flow (Evrard, 2008). The higher the hygic diffusivity of a material, the faster the material reaches its hygic equilibrium. It is calculated as:

$$\alpha_h = \frac{\delta \cdot P_{sat}}{\xi} \quad (34)$$

where  $\delta$  is water vapour diffusion permeability in  $\text{kg}/(\text{m s Pa})$  (defined in 2.1.2.2),

$\xi$  specific hygic capacity in  $\text{kg}/\text{m}^3$  (see equation 20),

$P_{sat}$  saturation pressure of air of considered temperature in Pa.

**Hygic effusivity**  $b_h$  [ $\text{kg}/(\text{m}^2 \text{s}^{1/2} \text{Pa})$ ] represents quantity of moisture uptake/release of a material subjected to vapour flow during a given time laps (Evrard 2008). The higher hygic effusivity of a material the more moisture the material exchanges with its ambient environment. It is calculated as:

$$b_h = \left( \frac{\delta \cdot \xi}{P_{sat}} \right)^{1/2} \quad (35)$$

It is important to note that time to reach hygic equilibrium after hygic shock (characterised by hygic diffusivity) is usually much longer than time to reach thermal equilibrium after thermal shock (characterised by thermal diffusivity). While majority of known materials reach permanent heat flow in order of hours or days after thermal shock, in case of moisture transfer, it can be in order of months after hygic shock. Evrard (2008) reports transient moisture evolution during drying of a hemp-lime wall component to be more than 6 months. For comparison of thermal and hygic transient evolution of Evrard's hemp-lime wall component, see Fig. 16.

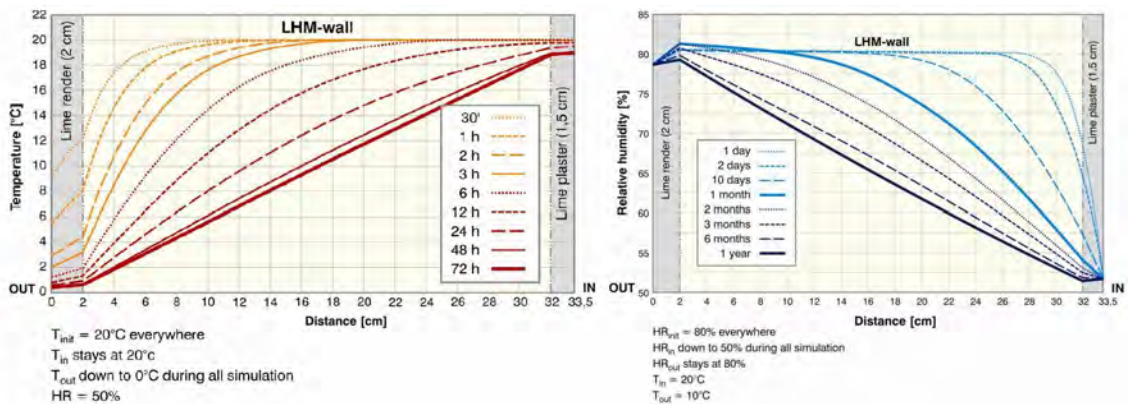


**Fig. 16:** Thermal (left) and hygic (right) transient evolution of hemp-lime wall component after thermal and hygic shock respectively (simulated in WUFI<sup>®</sup> Pro computer simulation tool) (Evrard, 2008)

It is therefore evident that the ability of material to buffer RH fluctuations of ambient (indoor) environment does not depend only on character of sorption isotherm, but also on material's time response to changes in RH. E.g. some materials can be good moisture absorbers (high hygric capacity), but react very slowly to change in RH and reversely others can have fast reaction to changes in RH, but low hygric capacity.

For the purpose of clear assessment of materials' moisture buffering qualities a concept of moisture buffer value (MBV) was developed at DTU (Technical University of Denmark) (Rode *et al.*, 2005).

**Moisture buffer value (MBV)** is a material parameter, which addresses moisture buffer performance of materials in direct contact with indoor air during diurnal RH variations. The so-called practical moisture buffer value ( $MBV_{practical}$  [kg/(m<sup>2</sup> %RH)]) is an experimentally determined value, which is defined as: "the amount of water that is transported in or out of a material per open surface area, during a certain period of time, when it is subjected to variations in relative humidity of the surrounding air" (Rode *et al.*, 2005).

The experimental setup is described in Nordtest protocol (Rode *et al.*, 2005). According to this protocol are material samples sealed from their sides and bottom so only one surface area is exposed to test conditions. These samples are then subjected to cyclic step changes in RH at constant air temperature of 23 °C and weighted continuously. A single cycle composes of moisture uptake during 8 hrs at RH of 75 % followed by moisture release during 16 hrs at RH of 33 % and it is repeated until constant mass variation between three consecutive cycles is reached (see Fig. 17).  $\Delta m$  [kg] is than given as ( $m_{8hrs} - m_{16hrs}$ ) and the  $MBV_{practical}$  is calculated as:

$$MBV_{practical} = \frac{\Delta m}{S \cdot \Delta RH} \quad (36)$$

where  $S$  is unsealed surface area of the tested sample in m<sup>2</sup>,  
 $\Delta RH$   $RH_{8hrs} - RH_{16hrs}$  in % (42 % in case of Nordtest protocol).

Unlike the previously discussed transient hygric parameters,  $MBV_{practical}$  does not depend only on material properties (active thickness of the material, its water vapour permeability and moisture storage capacity) but also on convective water vapour transfer coefficient  $\beta_p$  (see section 2.1.2.5).

When ideal situation of no surface layer resistance is assumed ( $\beta_p$  tending to infinity) the so-called ideal moisture buffer value ( $MBV_{ideal}$ ) can be defined.  $MBV_{ideal}$  is a theoretical maximal value, which can be analytically computed only on basis of materials characteristics and the same 8/16 hrs 75/33 % RH scenario (represented by signal function) as:

$$MBV_{ideal} = 0.00568 \cdot p_{sat} \cdot b_h \cdot \sqrt{t_p} \quad (37)$$

where  $p_{sat}$  is saturation water vapour pressure in Pa (air of temp. 23 °C),  
 $b_h$  hygric effusivity in  $\text{kg}/(\text{m}^2 \text{s}^{1/2} \text{Pa})$ ,  
 $t_p$  time period of one cycle in s ( $24 \times 3600$  s for diurnal variations and Nordtest protocol scenario).

There is always a difference between measured and analytically calculated MVB due to dynamic nature of the experimental protocol and hygric resistance of tested exchange surface (Dubois *et al.*, 2014). However, McGregor *et al.* (2014) showed that ideal and practical MBV can be in agreement when reducing surface resistance in the dynamic test and improving precision of the steady state measured properties.

Both values have therefore good potential for moisture regulation assessment and comparison of different building materials, which would be hardly achievable when using only the previously listed transient hygric measures (sorption isotherm, hygric diffusivity and effusivity).

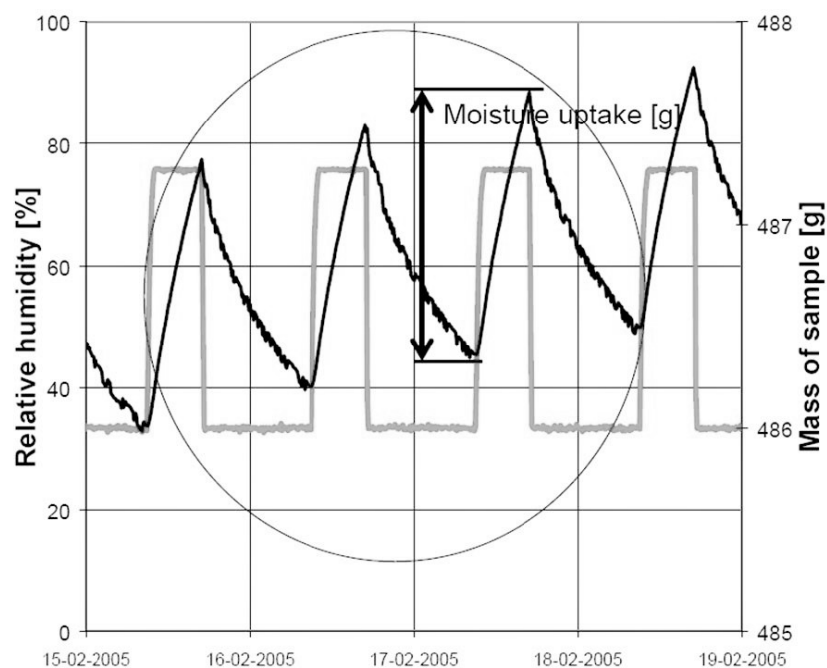


**Fig. 17:** Course of the RH step cycles during Nordtest experiment and their relation to mass of the tested samples together with graphical representation of moisture uptake  $\Delta m$  during one RH cycle (Rode *et al.*, 2007)

**Effects of moisture buffering materials** upon indoor environment and the construction itself were studied by many authors. Evrard (2008) reports that position of material within a multi-layered component affects the final MBV crucially. Due to limited penetration depth of building component (thickness of component, which actively affects the indoor moisture regulation), only finishing material layers can potentially buffer the indoor RH.

Research shows that use of excellent moisture buffering materials as finishing layers contributes to reduction of structural degradation caused by moisture ingress (Lucas *et al.*, 2002), reduction of energy use for humidification/dehumidification (Antretter *et al.*, 2012) and to higher perceived thermal and hygric comfort in buildings (Winkler *et al.*, 2014). Furthermore, Hall (2010) concludes that due to humidity and temperature buffering of air, acceptable air quality may be achieved at reduced ventilation rates, which might lower heating demand in winter and cooling demand in summer.

Due to more stable indoor RH, high MBV finishing materials also contribute to improvement of indoor air quality. E.g. Cunningham (1996) reports reduction of dust mite populations and mould growth. Fig. 18 shows the influence of RH on health and indoor air quality presented by Simonson *et al.* (2001). As can be seen, keeping the indoor RH on optimal level ensures higher probability of healthy indoor environment.

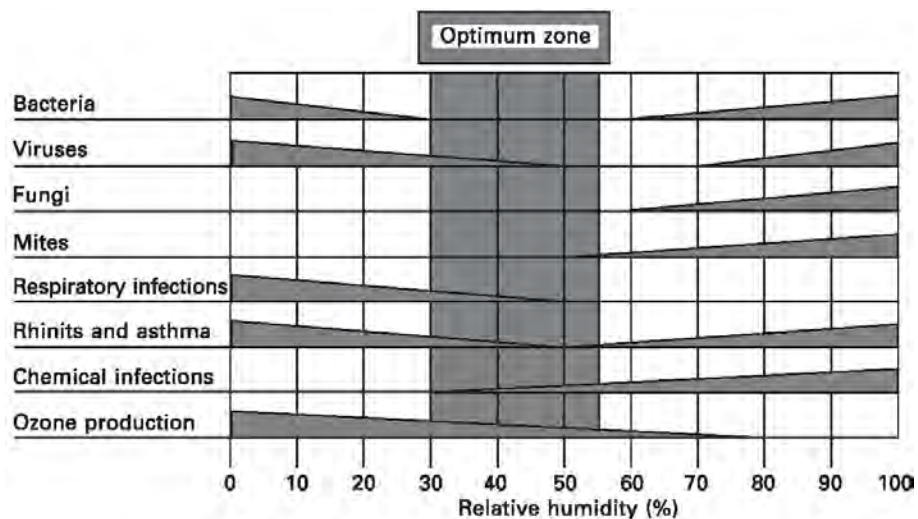


*Fig. 18: RH related effects on health and indoor air quality (Simonson et al., 2001)*

### 2.1.3 Partial conclusion

It was shown that analysis of hygrothermal processes in building elements is a very complex discipline, which needs to be always addressed with respect to dynamic climates (both inside and outside) representing boundary conditions for the analysed case.

The steady state scenarios represent only rough estimation of real situation and should be only used for preliminary analysis; not for determination of actual heat losses and fluxes through elements. For the actual analysis of hygrothermal response of building elements to real environment are nowadays commonly used advanced computer simulation software tools such as WUFI<sup>®</sup> (WUFI, 2016), Energy-plus (EnergyPlus, 2017) or Delphin (Grunewald *et al.*, 2015), which are able to address variations of ambient climate instantaneously (see section 4.3).

## 2.2 Raw natural building materials (RNBM)

Hofer (2014) defines raw natural materials as low processed materials that are close to their original natural state, use little primary energy and produce less waste during manufacturing phase. Such materials have consequently lower embodied energy, cause less pollution, are easily recyclable and generally are considered as more sustainable.

This section provides a brief overview of RNBM selected for purposes of this paper (unfired loam-based building components, straw, hemp-based building components and wood; Fig. 19) together with discussion of their hygrothermal properties.



**Fig. 19:** Four raw building materials analysed in this paper; earth (loam) (Stockscape, n.d.), straw (Flamingo, n.d.), hemp (Gettyimages, n.d.) and wood (Wrrnetwork, n.d.)

### 2.2.1 Unfired earth

Earth, in all its variations, is one of the oldest and most wide spread building material, which has been used for building purpose for more than 9000 years (Pumpelly, 1908). It is estimated that more than one third of today's world population still lives in earthen houses (Minke, 2012). It is therefore surprising how little information about employment of this material in building industry do we currently have in comparison with materials known to human kind for at most several decades. One reason for this is natural variation in composition of this material, which makes it impossible to unify its properties and behaviour, another one is its general perception of "a primitive material", which has no place among the modern high performance building materials of these days.

It is mostly effort of a narrow minority of professionals working with this material, who have often shown that the traditional earthen building techniques can be adapted and modernized by means of today's construction industry. Such approach can ensure building within the constraints of current demand and standards or initiation of creation of new ones, where missing. Martin Rauch is one of such pioneers, who has been using earth for construction of modern, functional and healthy building for more than 25 years (see Fig. 20, right).



*Fig. 20: Examples of use of earth for building purposes; City of Shibam in Yemen (Günter, n.d.), Martin Rauch's personal house in Austria (Rauch, n.d.)*

#### 2.2.1.1 Material

Earth or loam, as it is referred to scientifically, is a mixture of clay, silt and sand, with eventual content of gravel and pebbles. No organic substances (humus) are acceptable for the construction purposes. Each of those particle types has its own role in the final loam mix just like have cement and aggregates in conventional concrete mix.

**Clay** is the smallest component of the loam mix ( $<0.002$  mm). It acts as binding agent of the other coarser elements. Clay is a product of erosion of feldspar rich rocks and other minerals. Feldspar contains e.g. aluminium oxide, potassium oxide or silicon oxide, which are main chemical compounds of clay minerals. Among the most common clay minerals count kaolinite ( $Al_2O_3 \cdot 2SiO_2 \cdot 2H_2O$ ) and montmorillonite ( $Al_2O_2 \cdot 4SiO_2$ ), the more rare ones would be illite, bentonite or smectite.

Influence of clay mineral type on final hygrothermal properties of building material was reported by Cagnon *et al.* (2014), who did not observe significant effect of clay type variation on those properties. The only exception was water vapour absorption capability of material, which was much higher for mixes with montmorillonite clay type. Influence of clay type variation on non-hygrothermal properties was reported by Minke (2012), who claims clay type to influence final material shrinkage, cracking and even tensile strength.

The nature of clay bonding is not chemical like for most other aggregate composite building materials, but electromagnetic. The flat non-spherical shape of clay particle (see Fig. 21, left) has different charge along edges and along flat parts. Clay particles can then bond to each other and to other loam particles due to these charges. When water gets in contact with clay particle, it penetrates its crystalline structure and causes swelling. Loam mix with sufficient amount of water becomes workable allowing its formation into different shapes. After evaporation of the water, clay particles again form the electromagnetic bond with surrounding aggregates. The nature of this bond is the reason, why are clay-based materials vulnerable to high amounts of liquid water.

**Silt, sand and gravel** are spherical particles of same character, but different size, which differ from clay particles very much (see Fig. 21, right). They are also produced by erosion of different types of rocks, but there is no electrical activity on their surfaces. They function as filler for clay binding elements. Their presence in loam makes the final mix stronger, more durable and lowers shrinkage and swelling dynamic of the mix (prevention of cracking during drying construction phase).

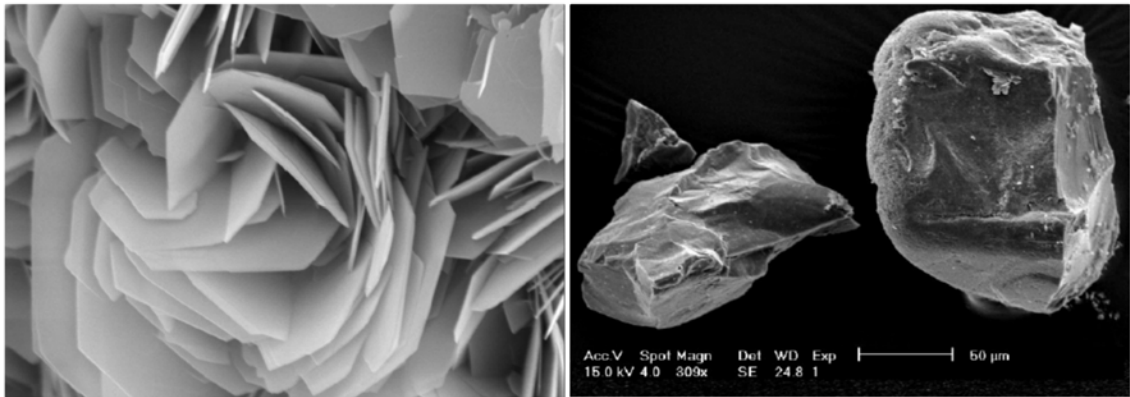


*Fig. 21: Electroskan microscope image of flat kaolinite clay vs. granular silt (Couvreur, 2015)*

#### 2.2.1.2 Material variations

Depending on loam mix, used admixtures and building technology there has been developed many different construction techniques and different types of uses. Among the most well-known ones count rammed earth, cob, adobe bricks or loam plastering (Fig. 22).

Each of these techniques requires very different composition of loam mix. The most important factor is relative gravimetric clay content in the mix, as it determines cohesiveness of the mix as well as shrinkage potential of final element. The ideal clay content for different techniques is hard to claim due to diverse character of clays from different clay-pits. Minke (2012), however, suggests the gravimetric clay content of around 15 % for adobe bricks around 10 % for rammed earth and as little as 12-5 % for loam plaster mixes.



*Fig. 22: Different loam construction techniques: a) rammed earth (left) b) adobe bricks and cob (Rieger-Jandl, 2015)*

### 2.2.1.3 Hygrothermal performance

Thermal conductivity of loam ranges from about 0.2 W/(m K) (lightweight expanded clay loam with density of about 750 kg/m<sup>3</sup>) to approximately 1.2 W/(m K) (solid loam with density of about 2000 kg/m<sup>3</sup>) (Minke, 2012). This classifies loam as a non-insulating material, which (when used as part of BE) requires coupling with thermal insulation to attain higher thermal resistance. The actual thermal quality of loam material was reported by many (Cagnon *et al.*, 2014, Stone and Katunsky, 2015, Fix and Richman, 2009) as high thermal mass and thermal effusivity (especially in case of solid loams), which results in high thermal inertia of loam (thermal buffering potential). This gives the material ability to provide superior levels of indoor thermal comfort as well as ability to self-regulate indoor temperature with only relatively small intervention of mechanical devices (Karlsson *et al.*, 2013). Taylor and Luther (2004) confirms this by reporting good indoor environmental performance of a two storey stabilized rammed earth (SRE) office in New South Wales (Australia) due to passive cooling and dehumidification of SRE.

While thermal properties of loam depend mostly on its porosity and bulk density, hygric properties are influenced primarily by amount (and type) of clay in the loam mix. As mentioned, clay minerals have (due to their chemical composition) electrostatic charge, which makes them highly hygroscopic (electric attraction of dipolarly charged water molecules). The amount of adsorbed water depends both on clay particle size (specific surface area) and its surface potential, i.e. magnitude of the net electrical charge (relative to clay particle size) (Hall, 2010). Fig. 23 shows the difference in size and surface potential (thickness of adsorbed water layer relative to clay particle size) between montmorillonite and kaolinite clay particles. It can be observed that clays with smaller particle sizes adsorb higher amount of water molecules, which confirms previously discussed high water adsorption potential of montmorillonite clays. It is therefore evident that content of montmorillonite and the overall clay content determine the hygric dynamic of the final loam mix.

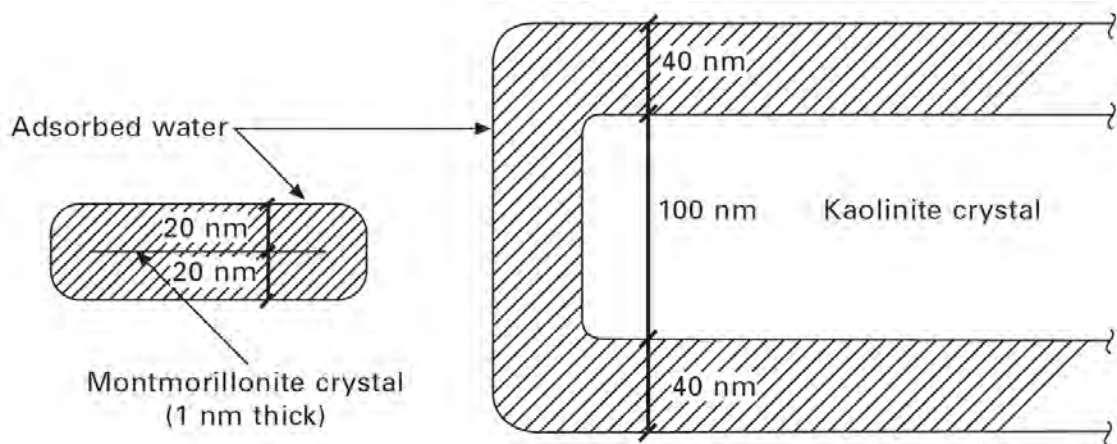


**Fig. 23:** Relative sizes of adsorbed water layers (surface potential) of montmorillonite and kaolinite clay particles (Holtz and Kovacs, 1981)

In general is loam considered as material with high moisture buffering potential. Its ability to regulate RH of indoor environment and thus improve occupants comfort, has been confirmed over the time by many (Cagnon *et al.*, 2014, Allinson and Hall, 2010, Hall and Allinson, 2009 , Liuzzi *et al.*, 2013). As an example would be a test house (adobe brick plastered with loam plaster) designed to passively regulate indoor RH between 40 % and 60 %. The performed tests confirmed that RH in bathroom after shower was the same regardless the operation of mechanical ventilation (Morton *et al.*, 2005).

As it is usual practise to have the loam materials exposed to interior of a house, both thermal and hygric buffering potential of loam (i.e. passive air conditioning) can reduce need for active air conditioning measures (heating, air conditioning and dehumidification) (Allinson and Hall, 2010).

### 2.2.2 Natural stalk fibre materials

The following group of RNBM is based on the so-called stalk fibre materials, which is a subcategory of plant fibres with wood-like structure (including the tree wood). The cellular composition and its hygric performance is more or less similar for all the plants and will be therefore discussed beforehand the actual RNBM.

The main structural feature of plant cell is the presence of rigid cell wall, which cannot be found in animal cells. This cell wall provides both structural rigidity (mechanical support) and natural protection of lumen (inner cell cavity with content of the cell). Depending on the plant type, cell wall is composed of primary cell wall and optionally one to three secondary cell walls (see Fig. 24, right) (Gibson, 2012). While the primary cell wall is very similar for all plants, the presence and nature of the secondary cell wall defines final rigidity and properties of the plant body. E.g. wooden fibre cells have considerably thick set of secondary cell walls to be able to support the weight of the tree and withstand ambient natural forces.

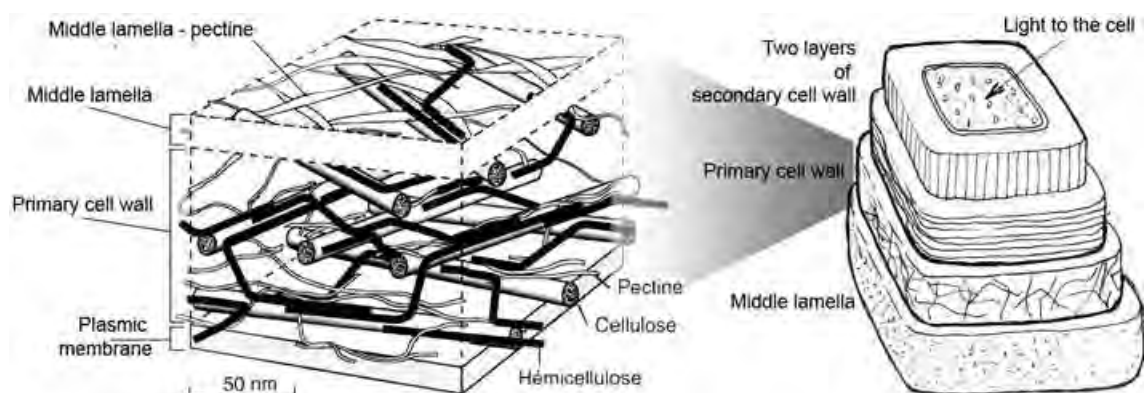


**Fig. 24:** Illustration of single fibre cell (cell walls surrounding the lumen; right) together with complex structure of the cell wall (left). Note the difference in cellulose micro fibre orientation in the primary and secondary cell walls (Hopkins *et al.*, 1999)

Detailed view on the fibre cell wall structure is depicted in Fig. 24 (left). It can be observed that the cell wall neighbours with inner cell (plasmic) membrane on one side and middle lamella, which fills the intercellular space, on the other side. The actual body of the cell wall is primarily composed of four basic building blocks (chemical constituents):

- cellulose
- hemicellulose
- lignin
- pectin

Additional constituents present in cell walls are water extractives (resins, waxes, ...) and minerals (mainly K, Ca and Mg in form of carbonates and silicates) (Kettunen, 2006).

Cellulose, which is almost crystalline natural polymer is a main structural fibre in the plant kingdom. It is organised in long chains of irregular orientation, which stretch over multiple cell walls usually arranged in longitudinal direction (plant fibres). It acts as reinforcing microfibre and ensures tensile strength of the cell wall.

The matrix of cell wall body is composed mainly of semi-amorphous hemicellulose and amorphous pectin, which (together with lignin) ensure compressive strength of the cell wall. The amount of amorphous lignin (complex phenolic compound) in cell wall changes over the life span of cell. As the cell matures, lignin penetrates the cell wall all the way through. Microfibrils of cellulose then become embedded in lignin just the way steel reinforcement is embedded in concrete. This cell wall structure ensures high resistance and structural impeccability of the cell (Wihan, 2007).

When the lignification process is completed or when the plant body is cut off the nutrient source, the cell dies. Such cell then loses water in its lumen (the so-called free water) and, depending on the ambient humidity, keeps the so-called bounded water dissolved in the cell wall.

For understanding of hygrothermal properties of individual natural fibre materials is important to note that any plant based building material is nothing but a complex system of dead cell walls arranged in fibrous structures mostly oriented along the direction of plant growth.

#### 2.2.2.1 Variables affecting hygrothermal properties

The main factor affecting hygrothermal behaviour of stalk fibre materials is arrangement and share of plant fibres in overall volume of the plant body. Slowly growing plants with dense microstructure and low porosity will provide less air pockets for thermal insulation benefits and less room for water vapour diffusion. In addition, the shape of pores is also important (smaller pores in higher count provide less free space for thermal convection and

larger surface area for water absorption). An example of difference in cellular composition is depicted in Fig. 25.

Second factor affecting primarily hygric behaviour of plant-based materials is the amount of constituents with high ability of establishing hydrogen bonds with water molecules. Berthold *et al.* (1998) determine the constituents with polar groups and thus ability of water absorption to be cellulose, hemicellulose, lignin and pectin. Céline *et al.* (2013), however, claim the amorphous polymers (primarily hemicellulose and lignin) to have more significant ability to bond water molecules, when reporting significant decrease of saturated weight gain of hemp fibres after removal of hemicellulose and lignin.

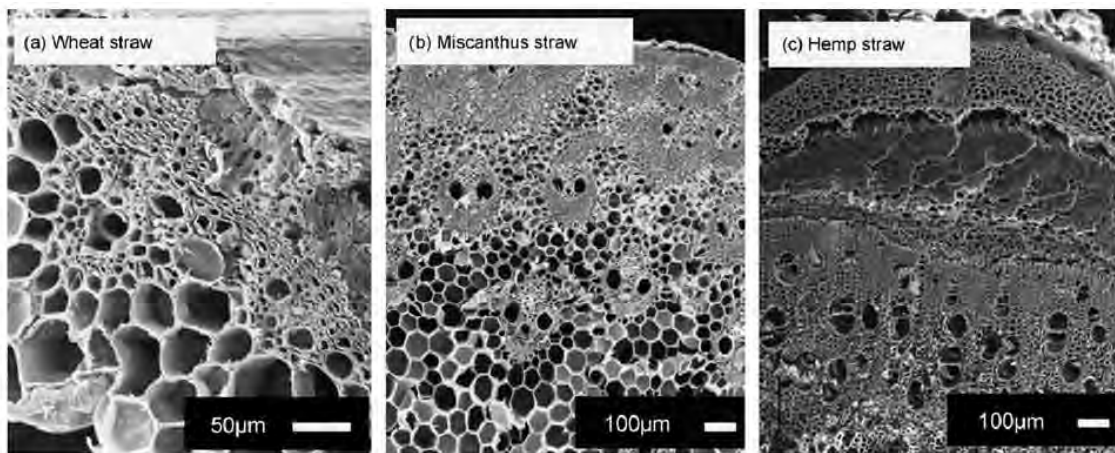


**Fig. 25:** Cross-section of cellular composition of wheat straw (a) miscanthus straw (b) and hemp straw (c) scanned by electron microscope (Wihan, 2007). The dense cellular structure with higher pore surface area and higher lignification level of hemp makes it considerably better moisture buffering material.

### 2.2.3 Wood

Wood is one of the oldest building materials (most likely predating even stone constructions) used by mankind. It is also the only traditional building material, which managed to remain in building sector (in considerable amount) through the industrial era of fabricated materials (silicate-based materials, metal, plastics etc.). Its success lies mostly in its availability, versatility, workability and strength-to weight ratio, which are (together with its competitive price) still very interesting for today's constructors. Another quality, which gained in past decades a great deal of attention, is its renewability and carbon dioxide sequestration capability. Wood entraps during its life huge amount of carbon dioxide (approximately half of its weight), which, when incorporated in a building, remains locked in the construction rather than being given back to atmosphere. Building with wood thus (temporarily) spares the environment from  $CO_2$  load rather than burdening it with it (Mayo, 2015).

Detailed microstructure of wood is shown in Fig. 26. Image (e) clearly shows the geometry of cell walls which are organised into vertical fibres (c, d) by overlapping of wood cells (ensuring continuous lumen for transport of nutrients). Image (b) shows the presence of

horizontal fibres, the so-called rays, and images (f-h) present structure of cell wall with chemical designation of lignin and cellulose. Details on wood microstructure are summarized by Kettunen in his work *Wood structure and properties* (Kettunen, 2006).

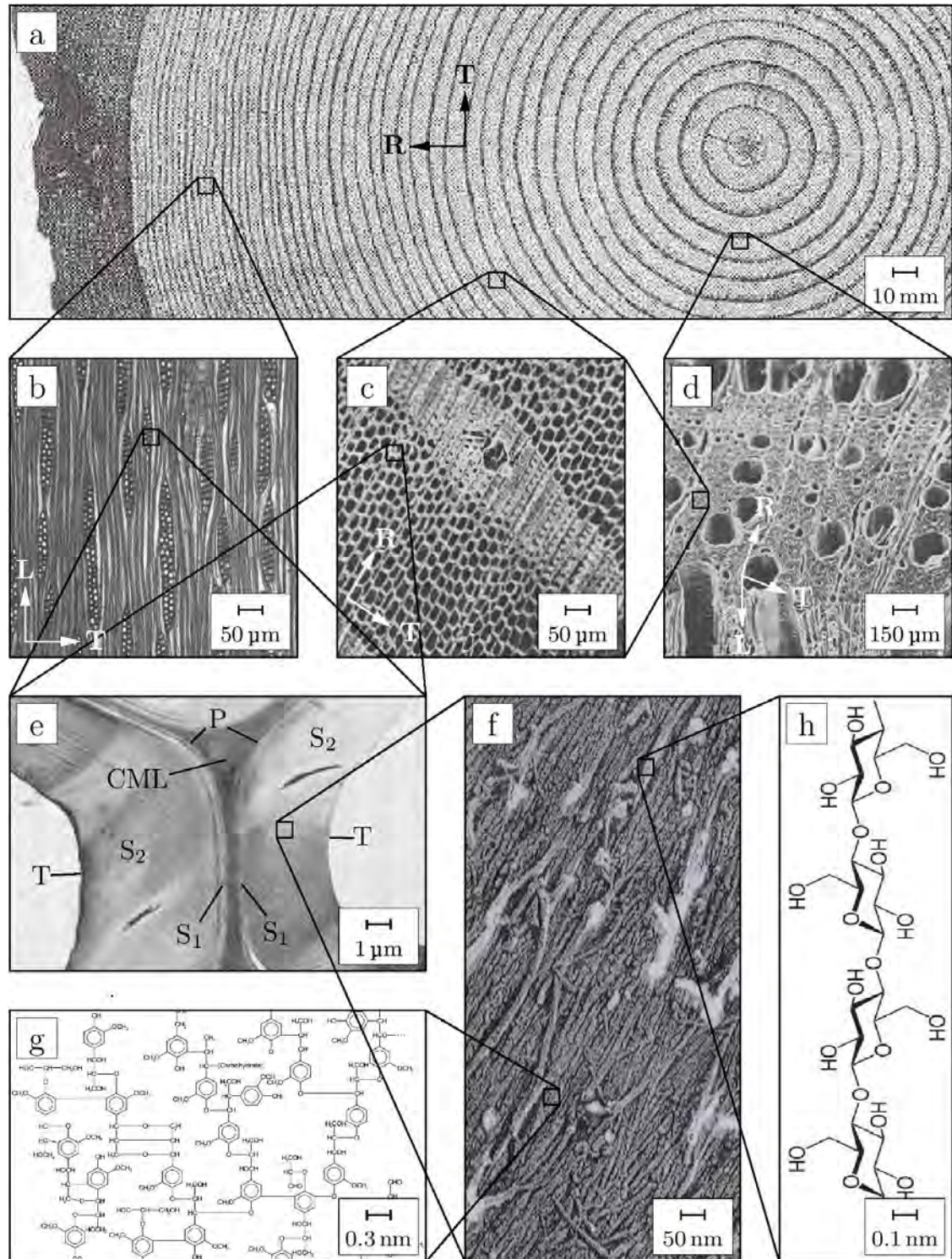


**Fig. 26:** Hierarchical organization of wood: (a) cross-section of a log, (b) longitudinal section showing horizontal fibres (rays) going through vertical ones, (c) transverse section through softwood, (d) transverse section through hardwood, (e) section of cell wall showing the cell wall layers ( $S_1$ ,  $S_2$ ), (f) fibrous structure of the cell wall, (g) chemical structure of lignin, (h) chemical structure of cellulose (Eitelberger, 2011).

### 2.2.3.1 Hygrothermal performance

To address hygrothermal properties of wood, it is important to distinguish between two general types of wood. Hardwood, which is normally from broad-leaved deciduous trees like ash, elm, beech or oak is wood with dense close-grained cellular structure resulting from very slow grow of these trees. Softwood is, on the other hand, lower density fast growing wood with open-grained cellular structure (mostly coniferous trees like pine, spruce or douglas fir).

Thermal conductivity of wood is determined partly by thermal conductivity of cell wall material ( $\sim 0.35 \text{ W}/(\text{m K})$ ) and partly by porosity and geometry of inner cell structure of wood material (varying between different tree types). Orientation of cellular fibres plays also its important role as heat is transferred two to three times more rapidly in longitudinal direction than in transversal one. The actual thermal conductivity of wood varies from about  $0.09 \text{ W}/(\text{m K})$  (red cedar) to  $0.2 \text{ W}/(\text{m K})$  (maple) across the wood fibres and can reach values of  $0.3 - 0.35 \text{ W}/(\text{m K})$  along the fibres (Eitelberger, 2011).

Specific heat capacity of wood is due to its definition independent on material density (porosity) and its value therefore does not vary considerably between different wood types. It depends only on cell wall material, temperature and moisture content. Specific heat capacity of oven-dry wood is approximately  $1360 \text{ J}/(\text{kg K})$  (Desch *et al.*, 1996).

As regards the hygric properties of wood cell wall matrix, it is a highly hygroscopic material. This gives it high indoor RH regulation potential and ability to influence indoor thermal environment when applied as finishing material. Gaur and Bansal (2002) demonstrated this when applying simplistic model of a spruce panelled room. They found out that neglecting the hygroscopic effect of wood resulted into temperature errors of  $2 - 3 \text{ }^\circ\text{C}$  (for climatic region of Delhi, India).

Unisotropy of the material gives wood, however, very different moisture performance in different directions. This is apparent especially in case of water vapour permeability of wood. While in longitudinal direction is moisture transferred through hollow lumens filled with moist air of low moisture capacity, in transversal direction must moisture overcome cell walls with high sorption capacity. We can therefore state that vapour transport occurs much faster in longitudinal than in transversal direction. Also, it is evident that the closer to saturation state the cell wall is the more water molecules pass by it deeper into the material (the absorption process of cell walls is not as intensive). Vapour permeability is thus direction, moisture and location dependant.  $\mu$ -factor of wood can therefore vary between units in longitudinal direction and humid state and hundreds in transversal direction and dry state (Zillig, 2009).

## 2.2.4 Straw

The term straw denotes dry stalks of particularly cereal grasses such as oats, wheat, barley and rye, but also other plants like flax, hemp or rice. The most suitable straw bales for construction purposes were, however, reported to be made of wheat or rye (Minke and Mahlke, 2005).

Cellular composition of wheat straw is shown in Fig. 25 (a) and the average chemical composition of cell walls of different kinds of straw can be found in Appendix A.

the first use of straw bales for construction purposes correlates with invention of straw baler in the second half of 19<sup>th</sup> century in prairie region of Nebraska in USA. The oldest known inhabited (some of them up to now) straw bale houses can be found also in this region and date back to 1900-1914 (Minke and Mahlke, 2005) (see Fig. 28, left). Since that time, two main structural systems were developed for building with straw bales:

- **Load bearing straw bale structural system (also called Nebraska style)** is a system, where horizontal building components and roof are supported only by structural strength of straw bale walls (see Fig. 27, left). The function of straw bales is both structural and insulating in this case.
- **Timber frame structural system** is a system, where straw bales serve only as an infill of structural timber frame wall (see Fig. 27, right). In this case, straw bales secure only the insulating function.

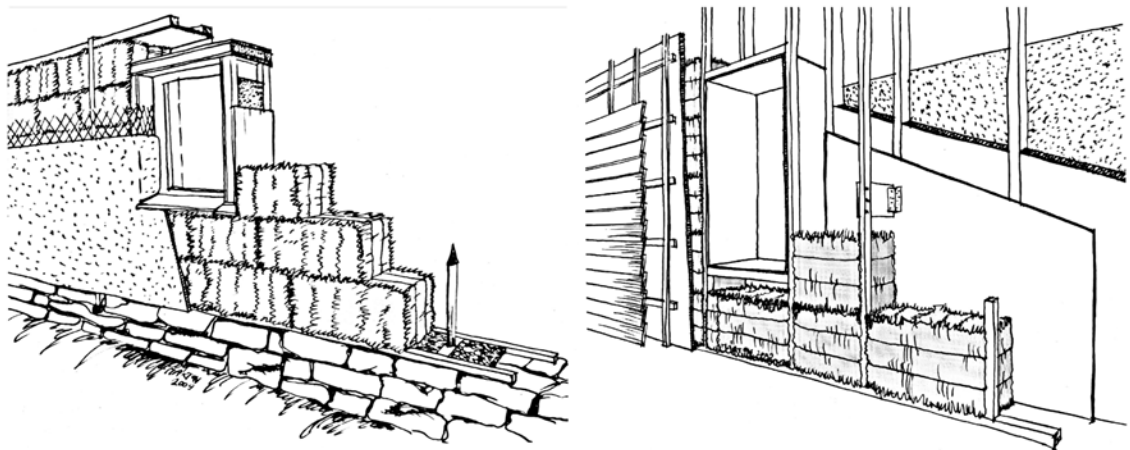


*Fig. 27: Structural systems of straw bale construction: Nebraska style system (left) and timber frame system (right) (Márton, 2014)*

Similarly like the earth material, straw bales stand on the periphery of builders' interest, as it does not have as many references as conventional materials and building with this material has its specifics. One of the most well-known straw bale builder is Barbara Jones, who built one of the first legally authorized and first double storey Nebraska type straw bale house in Europe (see Fig. 28, right).



**Fig. 28:** *The Burke house in Nebraska built in 1903 (left) (Márton, 2014) and spiral house built by Barbara Jones in Ireland in 2003 (right) (Jones, n.d.)*

#### 2.2.4.1 Hygrothermal performance

Thermal conductivity of straw bale depends on two factors; bulk density of the bale and orientation of straw stalks within the bale (type of straw has only marginal influence).

Bulk density varies for the classical agricultural bales approximately between 70 and 130 kg/m<sup>3</sup> and it applies that the lower bulk density of bale the lower thermal conductivity. Lighter bales, however, contain high amount of air gaps, which induces convection process and thus energy losses through bales. Márton (2014) states the optimum bulk density of a construction straw bale to be around 100 kg/m<sup>3</sup>. This reduces hygrothermal convection rates while still keeping relatively low thermal conductivity.

The orientation of straw stalks influences final thermal conductivity also through different convection rates. While stalks placed laterally to direction of heat flow tend to prevent air within the bale from natural movement caused by temperature gradient between outside and inside environment, parallelly placed stalks present lower resistance to this phenomenon (convective flow through hollow stalks).

It is therefore evident that the actual thermal conductivity measured by researchers around the globe varies significantly. Minke and Mahlke (2005) summarise the outcomes of different researches to vary between 0.034 and 0.086 W/(mK) (in dry state), when stressing the importance of safety factor of 1.2 for thermal conductivity design value. Two respected European research institutes (Forschungsinstitut für Wärmeschutz in München and Versuchs-und Forschungsanstalt der MA 39 in Wien) agreed on implementation of dry thermal conductivity design value of 0.045 W/(mK) in German/Austrian national standards, which classifies straw as a well insulating material (Minke and Mahlke, 2005).

Disadvantage of most insulation materials is, however, their poor contribution to thermal inertia effect. Straw is not an exception to this as it has rather low thermal mass and thus thermal accumulation capabilities. To counterbalance this drawback, straw bales are normally plastered with several layers of loam plaster to gain some extra thermal mass.

As regards hygric properties of straw bales, it depends again on bulk density and orientation of straw stalks in the bale. Generally, straw bales perform very high vapour permeability, which is projected into low  $\mu$ -factor (around 2.5). All the stalk fibre types perform high hygroscopicity, which is given by the nature of the stalk fibre material (see section 2.2.2). This is not as interesting from the inside humidity regulation perspective (straw bales always need to be covered by additional construction layers to ensure air tightness and prevent convection heat losses) as it is from thermal comfort point of view. Due to latent heat effect and high dynamics of sorption process has been straw reported to positively influence thermal indoor environment especially during summer months (cooling effect of latent heat of desorption/evaporation) (Szász, 2013).

### 2.2.5 Hemp

Hemp (*Cannabis Sativa*) has been used by man for more than three thousand years and since then were developed numerous ways for its utilization. Nowadays we can find beside well-known hemp oils, food supplements, drugs, cosmetics or textiles also less-known use for this versatile plant, like hemp plastics or organic concrete often called hempcrete (Allin, 2012).

**Hempcrete** is a bio-composite material composed of three constituents: hemp shiv, lime-based binder and water.

The term hemp shiv refers to small chips made of woody core of the hemp plant, which had been long considered as waste material (Fig. 29, right). The idea of mixing shiv with cementitious material for construction purposes came from France in about 1980s and since then it has spread mostly through Western Europe, North America and Australia. In comparison with the other presented materials is thus hempcrete far the newest low embodied energy building material. It cannot be classified as RNBM due to necessity for binding material, which needs to be processed before its final use. For its biological character, high  $CO_2$  sequestration capabilities and potential for local production belongs, however, hempcrete indisputably among highly sustainable building materials (Stanwix and Sparrow, 2014).

The term lime-based binder suggests that there exist more types of binder, which could be used for mixing of hempcrete. There have been numerous discussions about suitability of particular commercially available products for attaining ideal hempcrete hygrothermal and durability properties, which have never been settled entirely. In general, we can say that there are two main desired requirements for binder to be suitable for hempcrete mix:

- The binder should not compromise high vapour permeability of hemp shiv in order to maintain high hygroscopicity of the material and prevent water from being trapped within the material.

- The binder should set fast enough so the material does not collapse after drying out of initial water, which helps to hold material together during the initial setting phase (after demoulding of formwork).

The first quality is best achieved with pure air lime nowadays sold in form of hydrated lime. This binder has much higher specific surface area than other easily accessible binding materials (Portland or natural cements, hydraulic lime), which contributes to higher permeability and hygroscopicity of the material (larger specific surface of inner pores for adsorption of water molecules).

Air lime sets, however, through carbonation, which is a very slow process often lasting for many years. Hempcrete mixed only with air lime can therefore never withstand self-weight of the construction element during initial stage of setting process. To prevent this, a mix of hydraulic and pozzolanic additives like natural hydraulic lime (NHL), trasses or pozzolans needs to be added to speed up the initial setting process.

Fig. 29 (left) shows three officially recognised binders for hempcrete mix application. Those are; Tradical<sup>®</sup> in its variations, Batichanvre<sup>®</sup> and prompt natural cement sold under name VICAT.



**Fig. 29:** Most common binders for hempcrete mix, Tradical<sup>®</sup>, VICAT and Batichanvre<sup>®</sup> (left) and loose hemp shiv (right) (Stanwix and Sparrow, 2014)

Out of the four discussed building materials has hempcrete (together with wood) the highest potential for penetration the conventional construction market. It is due to similarity of its building process with concrete casting, prescribed mixing processes and character of the final construction elements. As carbonation process goes on and air lime turns back into limestone, hemp shiv, which is wrapped in the lime, changes its biological character into mineral state; in other words, it petrifies (Allin, 2012). Houses built of such material (when plastered) cannot be distinguished from houses build of conventional materials (see Fig. 30).



**Fig. 30:** Examples of houses constructed of hempcrete; classical (left) and modern (right) design (Stanwix and Sparrow, 2014)

#### 2.2.5.1 Material variations

Hempcrete is normally mixed on construction site in a pan mixer. The material is afterwards tamped into erected formwork with light pressure to maintain high porosity and thus high insulation potential of the material. Examples of partially erected and finished unplastered hempcrete walls are shown in Fig. 31.



**Fig. 31:** Example of one level of wall formwork filled with hempcrete (left) and cast hempcrete variations of construction elements; roof, wall and floor (right) (Stanwix and Sparrow, 2014)

The undertaken studies (de Bruijn *et al.*, 2009, Elfordy *et al.*, 2008, Nguyen *et al.*, 2009) indicated that mixtures, which are manufactured from the raw materials in various propor-

tions, can cover wide range of performances (when adjusting for a suitable ratio between insulating and structural properties). The general rule is that the more lime binder we put into the mixture the stronger, more rigid, but less insulating, material we get. Due to high flexibility and low compressive strength of hemp shiv can, however, hempcrete never satisfy requirements for load-bearing material. All the structures built using hempcrete technology are therefore constructed only in association with load bearing timber frame.

The three commonly used hempcrete mixes are:

- **Lightweight hempcrete**, which is used primarily for its insulating qualities (both acoustic and thermal). Structural properties are less important as hempcrete is only applied to areas where it is only required to stay in place, with no imposed load upon it. The mixture contains minimum amount of lime, just enough to coat all hemp particles and fix them to each other, so that the whole becomes a weak mass. The approximate amount of binder is 10 % of the volume of shiv. Typical example for use of such mixture would be insulation of roof spaces or spaces in between floors.
- **Wall hempcrete** is already capable of withstanding forces of outer impacts, such as wind load. The amount of binder added to the mixture increases to around 25 % of the volume of shiv in order to get more rigid bond of hemp particles, together with retaining as much of insulation qualities as possible.
- **Floor hempcrete** is used as insulating material beneath solid floor at ground level where greater compressive strength is needed to transmit load between gravel (beneath) and tiles and mortar (above). For this use increases lime portion in the mix to around 50 % of the volume of shiv.

Example of building built using all three mixes is shown in Fig. 31 (right).

#### 2.2.5.2 Hygrothermal performance

Cellular composition of hemp shiv is shown in Fig. 25 (c) and average chemical composition of cell walls of shiv from different kinds of hemp plants can be found in Appendix A. As it was mentioned above, hemp shiv (when used in hempcrete) petrifies over time so its hygroscopicity differs from its natural state. Its pores structure, however, remains the same through the petrification process. Both carbonated lime and hemp shiv represent highly porous materials with large specific surface of inner pores (Fig. 25 (c)), which causes high hygroscopicity of hempcrete. Evrard (2008) classifies hempcrete as material with surprisingly high hygroscopicity lying between cellular concrete or clay brick (for their fast change in moisture content) and wood (for its high quantity of transferred moisture). The material has therefore, similarly like clay, high moisture buffering potential resulting in significant indoor humidity regulation ability (Hall, 2010). High open porosity is also linked with high vapour permeability, which is projected into low  $\mu$ -factor (around 5 for wall mix).

As regards the thermal performance of hempcrete, the wall mixture cannot be classified as typical building insulant. Its thermal conductivity varies from about 0.1 to 0.13 W/(mK) (Evrard and De Herde, 2005, Evrard *et al.*, 2014, Rozumek, 2013) depending on bulk density and orientation of hemp shiv in construction element (similarly like in case of straw). Hempcrete has, however, non-negligible thermal mass and rather low thermal diffusivity, which gives it high thermal inertia. Hempcrete therefore combines properties of thermal insulants and capacitors, which is believed to give it a distinctive thermal performance. Shea *et al.* (2012) concluded that thermal conductivity (U-value) alone is not a suitable parameter for assessing thermal performance of hempcrete houses, as it does not reflect low thermal diffusivity of the material. Yates (2002) confirms this in his study *The Haverhill Hemp Houses*, when comparing energy consumption of experimental hempcrete construction with conventional brick-built homes in Haverhill (UK). He found that heating fuel consumed by the hemp homes was no greater than that used in traditionally constructed houses, despite SAP (The Standard Assessment Procedure) ratings and U-values calculations prediction that the hempcrete houses should have been using significantly more energy than the brick houses.

## 3 AIMS AND OBJECTIVES

---

### 3.1 Aims of the work

The aim of this work is investigation of transient hygrothermal behaviour of small-scale construction wall systems composed of RNBM and compare this with hygrothermal behaviour of conventionally used wall systems.

The hygrothermal analysis is performed in three steps:

- Analytical assessment of hygrothermal parameters of main wall layers materials
- Computer aided hygrothermal simulation under theoretical environment
- Computer aided hygrothermal simulation under real outside conditions (reference years)

This work aims to provide mainly relative benchmarking of the selected materials and wall systems with use of computer aided simulation software tools. The absolute benchmarking would be (at this scale) task for long-term high budget research with access to modern measuring devices and extensive laboratory facilities.

### 3.2 Objectives

- Two independent one-dimensional hygrothermal simulation tools (WUFI<sup>®</sup> Pro 6.0 and HeMoT) will be used for analysis of the selected wall systems.
- All necessary data needed for conduction of the simulations will be gathered from official research institutes and universities.
- Outputs from the two simulation tools will be compared in order to determine reliability of individual simulation outputs.
- Sensitivity analysis will be conducted.
- Hygrothermal performance of the wall systems will be compared between each other both from long-term and short-term perspectives. Differences between individual locations and seasons will be addressed.

## 4 METHODOLOGY

---

### 4.1 Analytical assessment of individual materials

As it was discussed in section 2.1, there are several parameters addressing hygrothermal performance of building materials in transient environment, which can be assessed analytically. Those parameters were calculated and analysed for selected materials of examined wall systems to attain basic understanding of their transient hygrothermal behaviour. All the parameters were calculated based on material characteristics, which are later used for the hygrothermal simulation (see section 4.3.2.1).

#### 4.1.1 Thermal parameters

*Thermal diffusivity*  $\alpha$  [ $\text{m}^2/\text{s}$ ] and *thermal effusivity*  $b$  [ $(\text{Ws}^{1/2})/(\text{m}^2\text{K})$ ] defined in section 2.1.1.3 were calculated according to equations (17) and (18) respectively. Since we assume dynamic hygrothermal environment, dependency of the parameters on ambient RH was addressed through:

- *Moisture dependent thermal conductivity*  $\lambda^*$

$$\lambda^*(w) = \lambda_0 \left( 1 + \frac{b_t \cdot w}{\rho_0} \right) \quad (38)$$

where  $\lambda_0$  is thermal conductivity in dry state in  $\text{W}/(\text{m K})$ ,  
 $\rho_0$  bulk density in dry state in  $\text{kg}/\text{m}^3$ ,  
 $b_t$  moisture-induced thermal conductivity supplement [%/%<sub>mass</sub>]  
- defining increase of thermal conductivity of material in %  
(with regards to dry  $\lambda$ ) when moisture content rises by 1 %  
(with regards to dry mass).

- *Moisture dependent specific heat capacity*  $c^*$

$$c^*(w) = \frac{\rho_0 c_0 + c_w w}{\rho_0 + w} \quad (39)$$

where  $c_0$  is specific heat capacity in dry state in  $\text{J}/(\text{kg K})$ ,  
 $c_w$  specific heat capacity of water in  $\text{J}/(\text{kg K})$ .

- *Moisture dependent bulk density*  $\rho^*$

$$\rho^*(w) = \rho_0 + w \quad (40)$$

4.1.2 Hygric parameters

*Hygric diffusivity*  $\alpha_h$  [ $\text{m}^2/\text{s}$ ] and *hygric effusivity*  $b_h$  [ $\text{kg}/(\text{m}^2 \text{s}^{1/2} \text{Pa})$ ] defined in section 2.1.2.6 were calculated according to equations (34) and (35) respectively. Their dependency on ambient RH is given through the nature of *specific hygric capacity*  $\xi$ , which represents derivation of sorption isotherm curve. Unlike their thermal equivalents, hygric diffusivity and effusivity also depend on non-hygrothermal parameter, *saturation pressure*  $P_{sat}$ , which was assumed to be  $P_{sat} = 2338 \text{ Pa}$  (air temp. of  $20 \text{ }^\circ\text{C}$ ).

Ideal moisture buffer value ( $MBV_{ideal}$ ) was also calculated for the considered materials according to equation (37).  $MBV_{ideal}$  was calculated following Nordtest protocol described in section 2.1.2.6.

4.2 Definition of the wall systems

Five low embodied energy wall systems, which are mainly based on RNBM, were selected for purposes of this work. Their design was based on wall composition typical for such materials (see Fig. 32).

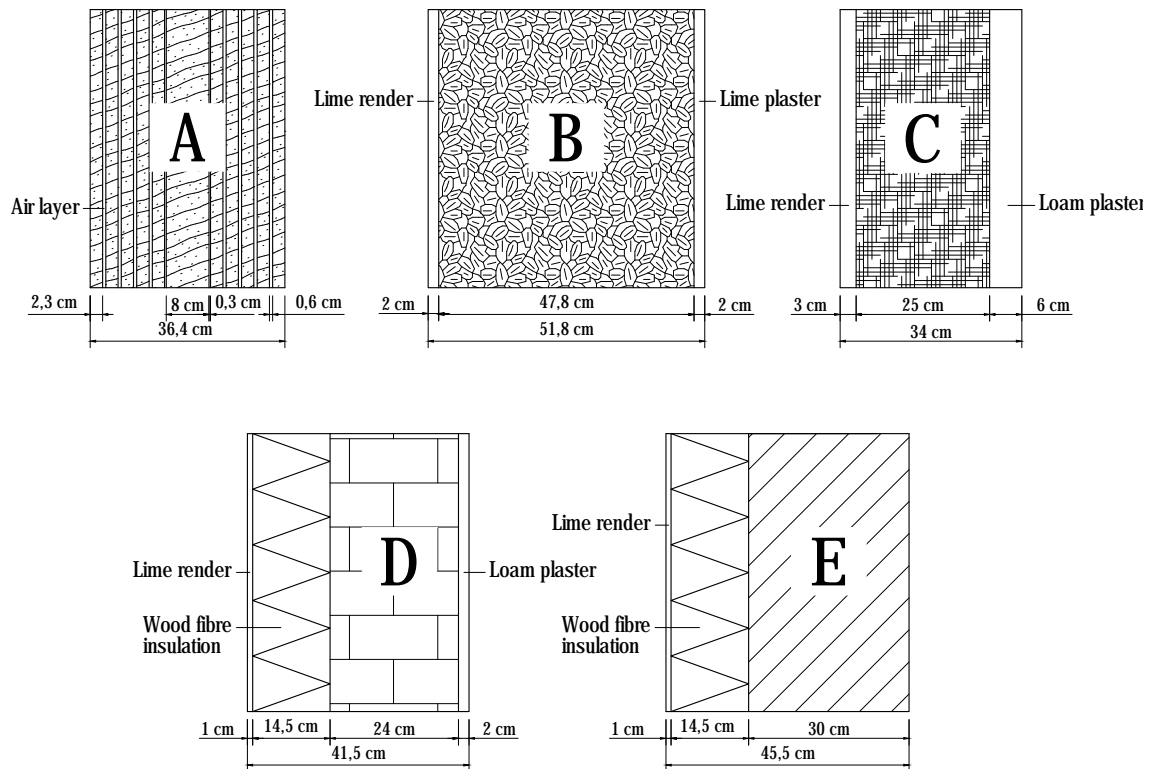


**Fig. 32:** Low embodied energy wall systems (based on RNBM) considered in this work; (A) spruce panel Holz100, (B) hempcrete wall component, (C) straw bale wall component, (D) insulated adobe brick wall component, (E) insulated SRE wall component

It is an insulating wooden panel 'Holz100' (A), which was developed by Ing. Dr. Erwin Thoma and is produced by Thoma Holz GmbH. This panel was selected as it does not contain any synthetic substances, so it fulfils the definition of RNBM and can be simulated using hygrothermal characteristics of plain wood (spruce). Next is hempcrete wall system (B) covered on both sides with lime render and lime plaster respectively. Thickness of the render/plaster was (based on Lime Technology Ltd. technical lists) designed to be 2 cm on both sides. See Appendix B for composition of hempcrete mix used in the simulations. Another wall system is straw bale wall (C), which was designed based on Wihan's, (2007) work. To prevent speculations about usability of loam render for outside applications, lime render was used as outside finishing material. Thickness of outside lime render was designed to be 3 cm, while thickness of inside loam plaster was 6 cm. The final two low embodied energy wall systems are based on loam material. It is 24 cm thick unfired loam brick - adobe brick (D) and 30 cm thick SRE wall (E) (for the SRE mix composition, see Appendix B). Both walls are insulated with wood fibre insulation boards, which are rendered with 1 cm thick lime render. Adobe brick wall is additionally plastered with 2 cm thick loam plaster, while SRE remains exposed to interior as it is done in general praxis. Thicknesses of adobe bricks and SRE were determined based on CLAYTEC e.K. technical lists.

As referencing conventional wall systems were selected four construction systems typical for the region of Central Europe in the 21<sup>st</sup> century (see Fig. 33).

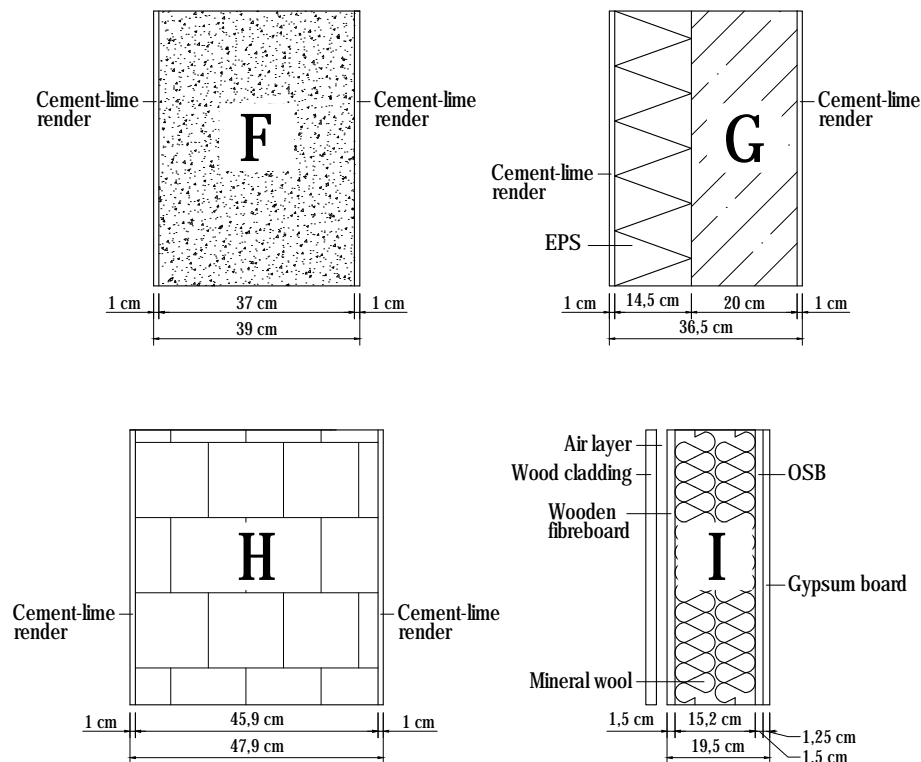


**Fig. 33:** Conventional wall systems considered in this work; (F) AAC wall component, (G) insulated concrete wall component, (H) perforated brick wall component, (I) lightweight wall component

It is autoclaved aerated concrete (AAC) wall system (F) together with regular concrete wall system (G), which is insulated with expanded polystyrene insulation (EPS), and perforated brick wall system (H). Due to assumption of considerably low compressive strength requirement (assumed small-scale construction), minimal reasonable thickness of concrete wall was considered (20 cm). As finishing layer (components F-H) was selected cement-lime render/plaster of thickness 1 cm. Cement-lime render/plaster was recognised to be the most common render/plaster type, universally used throughout different conventional construction systems. Adhering glue between concrete and EPS was not considered due to its small thickness and low  $\mu$ -factor.

Finally, a lightweight timber-framed wall system (I) was selected to complete the pallet of different construction techniques. It was designed based on EGGER Ltd technical list as layered construction composed of ventilated wooden cladding, vapour diffusion-open wooden fibreboard (1.5 cm), mineral wool insulation, vapour diffusion-closed oriented strand board (OSB) (1.5 cm) and gypsum board (1.25 cm).

*Note: All the wall systems that are built in association with load-bearing timber frame are considered without this frame due to character of 1D hygrothermal simulation.*

The most widespread indicator of thermal quality of any wall system in Europe is concept of U-value (see section 2.1.1.2). Following this convention, U-value was decided to be taken as benchmarking factor of the individual wall systems.

In order to compute the overall U-value of a wall system, it is, however, needed the so-called *design thermal conductivity*  $\lambda_d$ , which differs from thermal conductivity of materials in dry state due to non-zero moisture content of materials in real climate conditions. Following European standard EN ISO 10456 (ISO, 2007a), it was decided to use *design thermal conductivities*  $\lambda_d$ , which correspond to moisture content equivalent to 70 % RH of ambient air. 70 % RH is averaged conservative estimation of mean outside RHs of considered locations and average to above-average RH in simulated indoor environment.  $\lambda_d$  was computed according to equation (38) or extrapolated from thermal conductivity vs. moisture function, when available. The overall U-value of wall systems was computed according to equations (10) and (14).

As a reference wall component was taken the thickest commonly produced 'Holz100' panel (A) with computed U-value of 0.237 W/(m<sup>2</sup> K). This value meets both the Austrian (0.35 W/(m<sup>2</sup> K)) and the Czech (0.30 W/(m<sup>2</sup> K)) U-value requirements and complies even with Czech recommended U-value for heavy wall systems (0.25 W/(m<sup>2</sup> K)). The rest of the wall systems had the thickness of insulating layers designed to meet the overall U-value of 0.237 W/(m<sup>2</sup> K).

All the wall systems were also checked for interstitial condensation under Prague design winter conditions (exterior: -13.0 °C, 84.0 % RH and interior: 21.0 °C, 55.0 % RH) according to EN ISO 13788 (ISO, 2012) using building physic software tool developed at Czech Technical University (CTU) in Prague; Teplo 2015 (Svoboda, 2015). The same set of  $\lambda_d$  as

for U-value computation was used for the analysis. Except the straw bale wall are all the considered wall systems condensation free. In case of straw bale is condensation in extreme cases expected, due to very low  $\mu$ -factor. Wihan (2007), however, states that straw bale can withstand the repetitive moisture load due to interstitial condensation without any damage.

It is important to note that the selected wall systems are theoretical assemblies (dimensionwise), which would not be used in practical construction. E.g. the smallest straw bale produced is 32 cm, while component (C) is only 25 cm thick. Also, insulation boards and blocks have atypical dimensions serving the benchmarking strategy. For the purposes of relative comparison of individual systems is design based on U-value, however, considered as the most appropriate one.

### 4.3 Computer aided hygrothermal simulation

Over the last decades, numerous Heat, Air and Moisture storage and transfer (HAM) mathematical models were developed to predict dynamic hygrothermal behaviour in porous building materials. With the advancement of computer technology, could be those models adapted and used in hygrothermal simulation software to provide powerful dynamic simulation tools.

Due to high cost and time consuming character of experimental methods is nowadays hygrothermal simulation research taking over classical physical experiments. Although measurements and laboratory experiments are still needed to obtain input material characteristics and to validate the models specific conditions, the use of computer simulation software tools cuts the necessary time and expenses significantly.

This work uses the instant character and low cost potential of computer aided simulation to assess hygrothermal performance of previously defined wall systems in different locations of Central Europe. In the following sections are described used simulation software tools, input data needed for the simulations and limitation of the software together with conducted comparative and sensitivity analysis.

#### 4.3.1 Simulation tools and procedure

Two computer programs developed for dynamical simulation of moisture and heat transport in multi-component porous building material systems were selected for the purposes of this work. It is WUFI<sup>®</sup> Pro 6.0 (Künzel *et al.*, 2006); extensively validated software tool developed by Fraunhofer Institute for Building Physics in Germany, and HeMoT (Heat and Moisture Transport) (Kočí *et al.*, 2010b); developed by department of Materials Engineering and Chemistry at CTU in Prague.

Both of the computer programs are based on Künzel's mathematical model (Künzel and Karagiozis, 2010), which assumes mass transfer in form of diffusion without its convective

component. The model is in principal based on fluid dynamics and diffusion laws - Fick, Darcy (mass) and Fourier (heat) (see section 2.1).

User interface of both selected simulation tools are displayed respectively in Figs. 34 and 35.

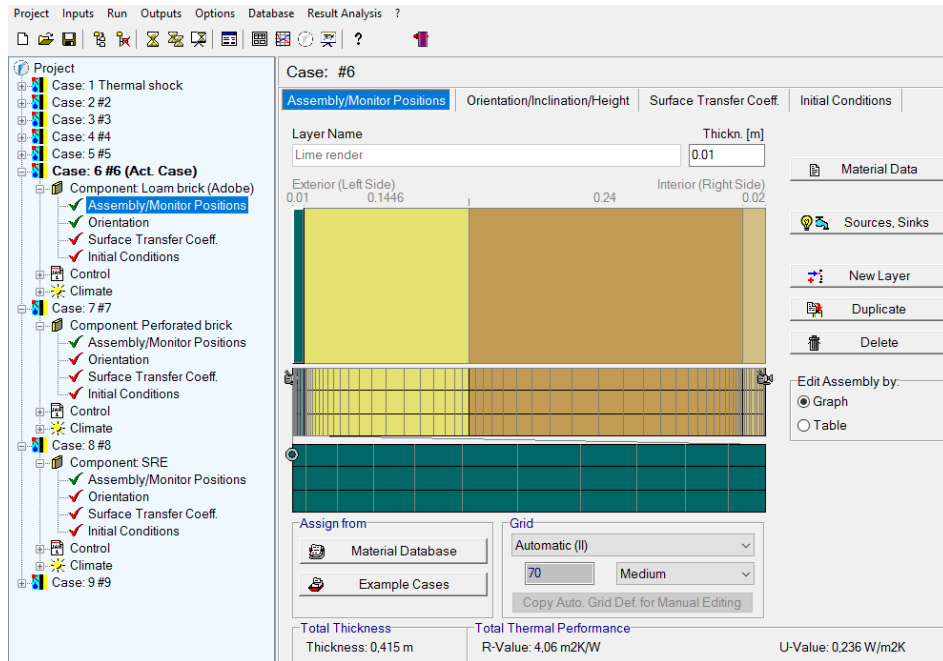


Fig. 34: User interface of WUFI<sup>®</sup> Pro 6.0 simulation tool

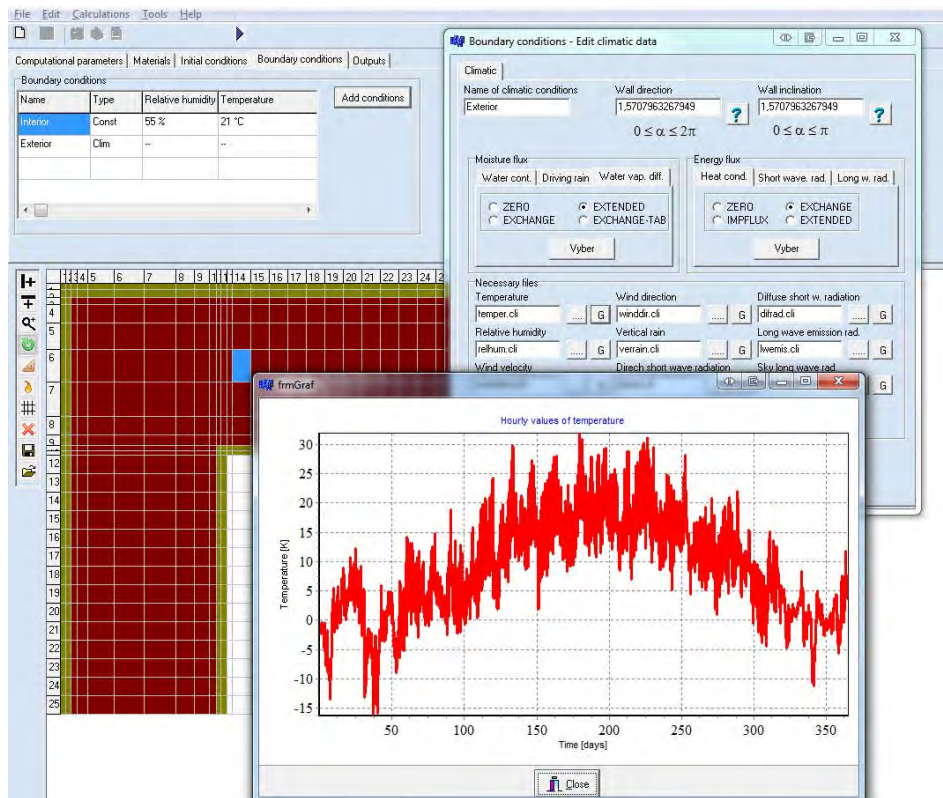
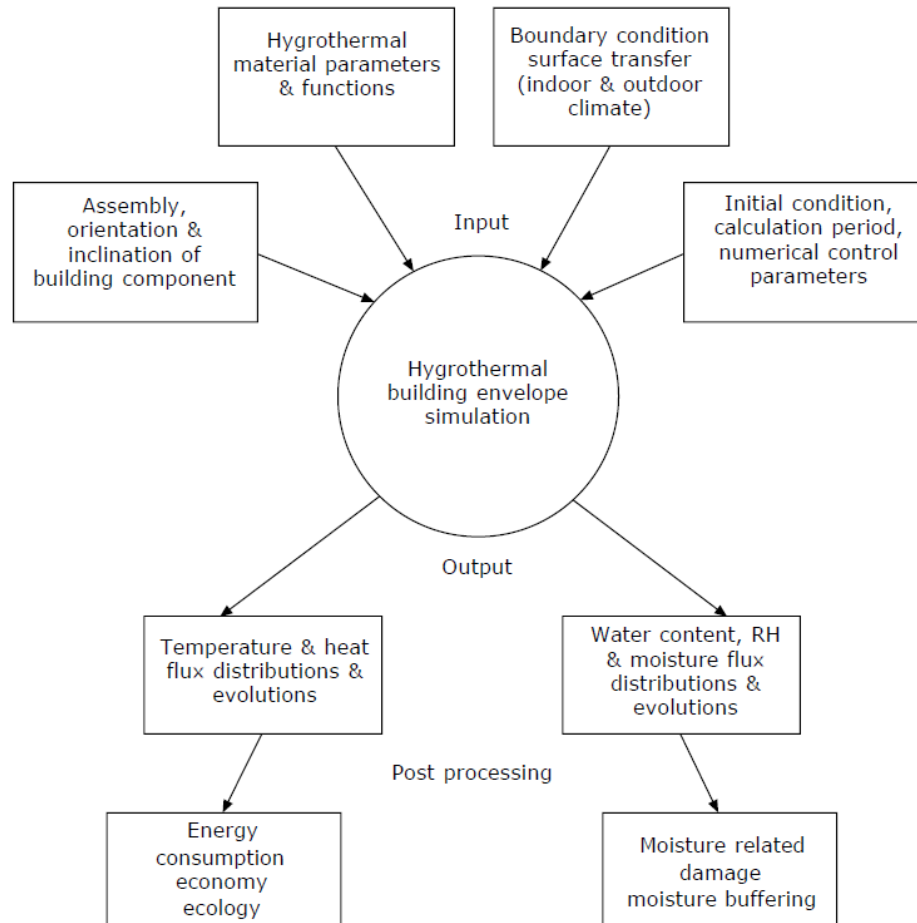


Fig. 35: User interface of HeMoT simulation tool

The procedure used for simulations is illustrated in Fig. 36. It can be seen that there are four types of input parameters, based on which are calculated hygrothermal outputs. Those outputs are then interpreted using post processing software tools (e.g. MATLAB (MATLAB, 2010)).



**Fig. 36:** Flow chart for hygrothermal simulations from former version of EN 15026 (2004) (Künzel and Karagiozis, 2010)

### 4.3.2 Simulation input data

#### 4.3.2.1 Hygrothermal material parameters

To be able to perform simulations both in WUFI<sup>®</sup> Pro and HeMoT, set of basic material parameters related to materials in dry state, needs to be known. It is:

- *bulk density*  $\rho$  [kg/m<sup>3</sup>]
- *total open porosity*  $\Psi$  [m<sup>3</sup>/m<sup>3</sup>]
- *specific heat capacity*  $c$  [J/(kg K)]
- *thermal conductivity*  $\lambda$  [W/(m K)]

- *water vapour diffusion resistance factor*  $\mu$  [-]

Those parameters allow the mathematical model to perform simulations, however, results obtained based on these inputs are rather informational. To be able to describe dynamic hygrothermal behaviour of building components accurately, additional material information, the so-called 'hygrothermal extensions', are needed. It is a set of functions, which describe behaviour of materials in transient hygrothermal environment:

- moisture storage function (sorption isotherm)  $w(\varphi)$  [kg/m<sup>3</sup>]
- moisture-dependant water vapour diffusion resistance factor  $\mu(\varphi)$  [-]
- moisture-dependent liquid transfer coefficient for suction  $D_{ws}(w)$  [m<sup>2</sup>/s] (situation when material is in direct contact with liquid water)
  - either measured or generated from water absorption coefficient (A-value) [kg/(m<sup>2</sup> s<sup>1/2</sup>)]
- moisture-dependent thermal conductivity  $\lambda(w)$  [W/(m K)]
  - either as table or generated from moisture-induced thermal conductivity supplement  $b_t$  [-]
- temperature-dependent thermal conductivity  $\lambda(\theta)$  [W/(m K)]
  - usually taken as constant or from temperature-induced thermal conductivity supplement [W/(m K<sup>2</sup>)]

In case of WUFI<sup>®</sup> Pro can be further defined

- moisture-dependent liquid transfer coefficient for redistribution  $D_{ww}(w)$  [m<sup>2</sup>/s] (situation when material has been in direct contact with liquid water, but it is not any longer)
  - either measured or generated from water absorption coefficient (A-value) [kg/(m<sup>2</sup> s<sup>1/2</sup>)]

The hysteresis of sorption isotherm is usually not accounted for in hygrothermal simulation tools. It is either excluded from mathematical model of simulation tool or it requires detailed desorption input data, which are not available for vast majority of building materials. However, according to Rode and Clorius (2004) and Künzeli (1995) is the hysteresis phenomenon not very distinct for most building materials and have therefore insignificant influence on hygrothermal behaviour of materials.

Basic material parameters used in simulations of the selected wall systems (see 4.2) are summarized in Tab. 1. The main data source was Fraunhofer-IBP database, which comes with WUFI<sup>®</sup> Pro software. Input data for the RNBM and some other materials needed to be retrieved from different sources, due to their specificity or incomplete data sets in Fraunhofer-IBP database. All data sources are included in the table.

Majority of the simulated materials are generic materials of no specific type and producer. The aim of this work is to examine differences between selected wall systems independently of the producer. However, some of the materials could not be addressed generically and therefore specific products were selected. It is namely:

- AAC block *YTONG P2-350* manufactured by Xella CZ, Ltd
- Wood fibre insulation *HOMATHERM Energie Plus massive*
- Cement-lime render/plaster *MVR Uni* produced by Baunit, Ltd, designed both for outdoor and indoor use
- EPS insulation board *Isover EPS 70F*, produced by Saint-Gobain Isover CZ, Ltd

The input data of RNBM are, on the other hand, data, which were agreed on by researchers (straw bale, loam plaster) or which were measured for specific cases (Hempcrete, SRE, wood) and can vary due to the nature of the RNBM.

**Tab. 1:** Basic parameters of materials used in this work (together with their sources)

	Bulk density $\rho$ [ $kg/m^3$ ]	Total open porosity $\psi$ [ $m^3/m^3$ ]	Specific heat capacity $c$ [ $J/(kgK)$ ]	Thermal conductivity $\lambda$ [ $W/(mK)$ ]	Diffusion resistance factor $\mu$ [-]
Hempcrete <sup>c</sup>	440	0.73	1560	0.115	4.9
Spruce (radial to grain)	455	0.73	1400	0.09	130
Straw bale <sup>d</sup>	100	0.9	2000	0.045	1.3
Loam mortar (Adobe) <sup>b</sup>	1568	0.408	880	0.582	11.4
SRE <sup>e</sup>	1900	0.295	868	0.643	14.34
AAC; YTONG P2-350 <sup>af</sup>	363	0.828	1160	0.081	12
Concrete (w/c=0.5)	2300	0.18	850	1.6	180
Perforated brick <sup>b</sup>	600	0.77	850	0.105	16
Mineral wool (soft)	60	0.95	850	0.04	1.3
Lime render (historical) <sup>ag</sup>	1650	0.367	910	0.763	9
Loam plaster <sup>d</sup>	1514	0.42	1000	0.59	11
Wood fibre insul.; HOMATHERM	135	0.9	2100	0.038	2.1
Cem.-lime rend.; Baunit MVR Uni <sup>ah</sup>	1402	0.444	1276	0.473	12
EPS; Isover EPS 70F <sup>ai</sup>	16.5	0.984	1570	0.037	58
Gypsum board	850	0.65	850	0.2	8.3
OSB (formaldehyde free)	615	0.9	1400	0.13	175
Wooden fibreboard	508	0.667	1400	0.12	15

Base source: Fraunhofer IBP database.

<sup>a</sup>Database of Department of Materials Engineering and Chemistry at CTU in Prague.

<sup>b</sup>Data provided by Institute of Building Climatology, TU Dresden. MASEA database.

<sup>c</sup>Evrard (2008).

<sup>d</sup>Danielewicz *et al.* (2008).

<sup>e</sup>Allinson and Hall (2010).

<sup>f</sup>Jerman *et al.* (2013).

<sup>g</sup>Kočí *et al.* (2009).

<sup>h</sup>Jerman *et al.* (2010).

<sup>i</sup>Jerman and Černý (2012).

In case of adobe bricks were data taken from material called 'historical loam mortar' provided by Institute of Building Climatology at TU Dresden. This is considered to be

reliable substitute as Minke (2012) claims the loam/sand ratio used for adobe bricks to be not much different from that of loam mortar.

The nature of RNBM, which are not processed into commercial building products is something we need to take into consideration, but it should not discourage us from trying to advance their understanding and widen their use in construction sector.

When looking at Tab. 1, all the simulated materials can be considered as homogeneous, but one - perforated brick. This is, however, one of the most widespread components used for BE wall systems in both the Czech Republic and Austria and should be therefore not excluded from this work.

In case of non-homogeneous components, the so-called homogenization method (Korecký *et al.*, 2013) is used to generate theoretical homogeneous material with identical hygrothermal behaviour as the original component. A series of mixing equation is used in order to combine moisture-dependent properties of materials, out of which is the building component composed (brick body and air in case of perforated brick). The perforated brick component can then be handled as if it was a homogenous material.

#### 4.3.2.2 Boundary conditions and other input data

In case of real climate simulation, boundary conditions should be as realistic as possible to capture the actual conditions, to which are analysed building components exposed. Climatic data representing the so-called reference year for considered locations were applied to exterior side of the analysed wall systems. Those data consist of average hourly climatic parameters obtained from historical data for past 30 years. It is temperature, relative humidity, wind velocity/direction, different kinds of solar radiation and rain load (see Tab. 2).

Indoor situation is much simpler when it comes to number of needed parameters (temperature and relative humidity). However, the prediction of occupants' behaviour makes it not trivial. European standard EN 15026 (ISO, 2007b) solves this issue by defining indoor temperature and RH as function of outside temperature and assumed indoor moisture load. This work normally assumes medium moisture load (see Tab. 2), function of which is included in WUFI<sup>®</sup> Pro simulation tool (see Fig. 37).

Tab. 2 also contains surface coefficients and wall geometry, which need to be defined prior the simulation. As regards surface coefficients, it is the previously mentioned heat and water vapour transfer coefficients (sections 2.1.1.2 and 2.1.2.5) and some other coefficients defining interaction of wall surfaces with surrounding environment. In case of wall geometry, the overall height of simulated wall, its orientation and inclination should be defined.

**Tab. 2:** Remaining main input data required for successful simulation

Input data	[Unit]	Actual value
<b>Time step</b>	[h]	1
<b>Climate data</b>		
<i>exterior</i>		
temperature	[°C]	reference year data
relative humidity	[%]	reference year data
horizontal solar radiation (diffused)	[W/m <sup>2</sup> ]	reference year data
horizontal solar radiation (direct)	[W/m <sup>2</sup> ]	reference year data
rain load	[Ltr/(m <sup>2</sup> h)]	reference year data
wind direction	[°]	reference year data
wind speed	[m/s]	reference year data
<i>interior</i>		
temperature	[°C]	EN 15026
relative humidity	[%]	EN 15026 (medium load)
<b>Surface transfer coefficients</b>		
<i>exterior</i>		
heat transfer coefficient	[W/(m <sup>2</sup> K)]	25
water vapour transfer coefficient	[kg/(m <sup>2</sup> sPa)]	13 × 10 <sup>-8</sup>
vapour diffusion thickned (sd-value)	[m]	0 (no additional coating)
short wave radiation absorptivity	[-]	0.4 (bright stucco surface)
long wave radiation emissivity	[-]	0
ground short-wave reflectivity	[-]	0.2
adhering fraction of rain	[-]	0.7
<i>interior</i>		
heat transfer coefficient	[W/(m <sup>2</sup> K)]	8
water vapour transfer coefficient	[kg/(m <sup>2</sup> sPa)]	2.5 × 10 <sup>-8</sup>
<b>Wall component</b>		
numerical grid	-	optimised
orientation	-	main weather side
inclination	[°]	90
height of the component	[m]	<10

An important parameter is numerical grid (see Fig. 38). It defines points through wall profile, which serve to discretise continuous heat and moisture fields (normally described by differential equations). By discretisation of the fields the differential equations are reduced to a system of algebraic equations describing interdependence of the points, which can be treated numerically. The denser the numerical grid is, the more precise the final results are and the more demanding is the simulation task for computer processor.

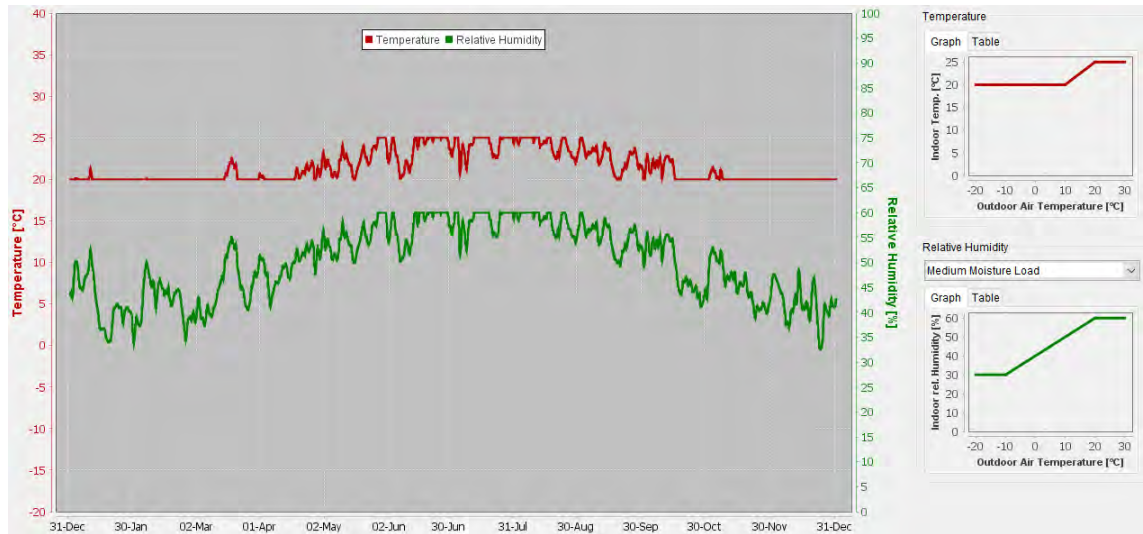


**Fig. 37:** Reference indoor climate in Prague together with its defining functions (medium moisture load according to EN 15026)

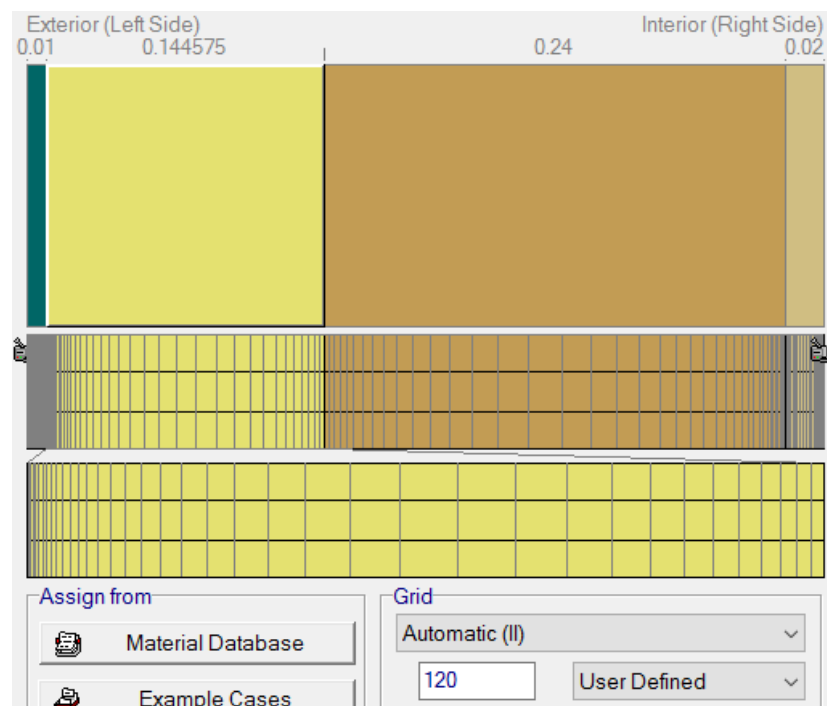


**Fig. 38:** Graphical representation of numerical grid through wall element in WUFI® Pro

Finally, the time of simulation should be long enough to achieve stabilized hygrothermal conditions of the simulated BE wall system. This depends very much on initial conditions (water content and temperature of wall component layers), which can, when set close to the real situation, shorten the simulation time significantly. According to up to now gained experience, minimal simulation time of 3 years is needed for simulation of real climate situation.

### 4.3.3 Simulation tools comparative and sensitivity analysis

Both of the selected simulation tools are recognised by scientific community and have been used for numerous official researches. HeMoT is being extensively developed and used for scientific purposes at CTU in Prague (e.g. (Kočí *et al.*, 2010b, Kočí *et al.*, 2014b, Kočí *et al.*, 2016)), while WUFI<sup>®</sup> Pro is one of the most scientifically and commercially used hygrothermal simulation tool worldwide (e.g. (Nytsch-Geusen *et al.*, 2005, Le *et al.*, 2010, Evrard *et al.*, 2012)). Both tools have been also successfully validated by comparison of simulation results with real measurements. In case of HeMoT, it was its predecessor TRANSMAT 6.2 (Kočí *et al.*, 2010a) and in case of WUFI<sup>®</sup> Pro, its previous version WUFI<sup>®</sup> Pro 5.0 (Mundt Petersen and Harderup, 2013).

However, like any other real situation simulation tool, these two programs will never be able to simulate all hygrothermal processes absolutely. There will always be simplifications of real processes, which are usually approximated by applied mathematical models. In general, there are two main limitations of hygrothermal simulation tools:

- Limitations of HAM mathematical models
- Uncertainty of input material data

Limitations and simplifications of Künzels's mathematical model are discussed by Künzels (1995) in his dissertation thesis. The previously mentioned absence of sorption hysteresis phenomenon in the model is one of those simplifications. The most noticeable limitation of this model is disregard of convective heat and mass transfer by airflows. As Künzels states, it is difficult to quantify and it has rarely 1-D character. All the constructions are therefore considered airtight.

**Comparative analysis** is one of the mechanisms to address potential weak spots of simulation tools and mathematical models behind them. Scientists in CTU have developed HeMoT with its mathematical model independently from Fraunhofer Institute, which presents opportunity to compare two different adaptations of hygrothermal simulation process.

The analysis was performed as simulation of identical input values and boundary conditions by the above mentioned simulation tools. The final comparison of obtained simulation outputs provided the necessary perspective on simulation results and their consistency. Based on this analysis was also determined the main simulation tool for this work (see section 5.2.1).

Considering the amount of simulations done in this study, it was rather unreal to perform the comparative analysis for all simulated cases. It was therefore decided to select representative case, based on which were the other results interpreted. Wall system G (AAC) was selected for this purpose as it had been simulated and tested by researchers from CTU in Prague, with whom was this work consulted.

The selected wall system was oriented to the north and simulated under Prague reference year outside conditions. The inside conditions were set to be constant 21 °C and 55 % of RH. All the rest input values were set according to Tab. 2. Simulation time was set to 10 years and the results were evaluated based on data from 10<sup>th</sup> year of simulation.

Both simulation tools provide output data in form of temperature and relative humidity fields, which are generated based on simulated time step and numerical grid. All the additionally available results (moisture/heat flux and water content) are computed based on these fields. To simplify the process of analysis, it was decided to compare simulated temperature and RH fields in form of cross-sectional profiles at selected times (24.2. (10:00), 16.4. (16:00), 31.7. (15:00), 16.10. (7:00)) and time courses of selected monitoring points in wall (mid-outside render 0.005 m, mid-AAC 0.195 m) throughout 10<sup>th</sup> year of simulation.

The effect of uncertainty of input material data is commonly addressed by **sensitivity analysis**, which determines influence of variations (uncertainties) of individual material input values on final simulation results. It may be that some material input values affect the studied result marginally, while other rather significantly. For relevant interpretation of results is therefore necessary to know, which input values affect which type of results.

Sensitivity analysis in this paper was performed in WUFI<sup>®</sup> Pro software (see section 5.2.1 for reasoning of the choice) using standard deviation  $\sigma$  values from Tab. 3. These values were adapted from Holm's and Künzl's (2002) work and represent uncertainties of input material hygrothermal properties obtained by standard testing procedures (EN standards).

**Tab. 3:** Simulation input material properties and their uncertainties (Holm and Künzl, 2002)

Hygrothermal material properties	[Unit]	Standard deviation $\sigma$ [%]
<i>Basic parameters</i>		
Bulk density	[kg/m <sup>3</sup> ]	5
Specific heat capacity	[J/(kgK)]	5
Thermal conductivity	[W/(mK)]	5
Moisture-induced thermal conductivity supplement	[[%/mass]	5
Total open porosity	[m <sup>3</sup> /m <sup>3</sup> ]	5
Diffusion resistance factor	[-]	15
<i>Hygrothermal functions (RH dependant)</i>		
Moisture storage function	[kg/m <sup>3</sup> ]	10
Liquid transfer coefficient for suction $D_{ws}$	[m <sup>2</sup> /s]	10
Liquid transfer coefficient for redistribution $D_{ww}$	[m <sup>2</sup> /s]	10
A-value	[kg/(m <sup>2</sup> s <sup>1/2</sup> )]	20

The analysis was done in two steps.

- First were the material input parameters varied individually and always for all the component layers at a time, which showed degree of dependence of simulation results upon individual material parameters and their uncertainties.
- Second, the extreme values (reference value  $\pm \sigma$ ) of four most influencing parameters were varied and simulated in all possible combinations.

*Note: Liquid transfer coefficients ( $D_{ws}$ ,  $D_{ww}$ ) were, for purposes of sensitivity analysis, generated from A-value to address uncertainty of materials without measured liquid transfer coefficients to cover most uncertain simulation scenario. Generation of liquid transfer coefficients using A-value is considered to be less accurate variant when compared with precisely measured  $D_{ws}$  and  $D_{ww}$  coefficients.*

The outcome of sensitivity analysis is combination of 16 simulations results graphically presented as a field of potential results, which was numerically interpreted as standard deviation of possible errors caused by uncertainty of input material data for each analysed simulation profile.

The set of data for determination of standard deviation of possible errors for individual profiles was obtained from the field of potential results as a difference of extreme values measured at interval of 1 centimetre throughout the entire cross-section of the simulated wall. In case of time courses was considered only 10<sup>th</sup> year of simulation and interval of 1 hour.

Following the probability theory and assuming normal (Gaussian) data distribution, standard deviation was calculated for each profile as:

$$\sigma = \frac{Q_{0.683}}{2} \quad (41)$$

where  $Q_{0.683}$  is 68.3<sup>th</sup> percentile of all errors obtained in sensitivity analysis for one profile or time course.

#### 4.4 Hygrothermal simulation under theoretical conditions

After the conduction of comparative analysis was WUFI<sup>®</sup> Pro software selected as main simulation tool for this work (see section 5.2.1). An indisputable advantage of most hygrothermal simulation tools is possibility of conduction of various theoretical simulation experiments. WUFI<sup>®</sup> Pro allows to generate theoretical boundary conditions files containing development of RH and temperature (optionally other climate parameters) in time, which can be applied both to interior and exterior surfaces of analysed components and

which can be used for deeper understanding of studied BE systems under specific sets of situations.

Following sections describe three theoretical scenarios, which were simulated in order to obtain hygrothermal parameters relevant for transient environment, to which are BE components normally exposed. To eliminate influence of wall orientation on results, neither of the following scenarios (4.4.1 – 4.4.3) took the vector climatic data (sun radiation, wind and rain) into consideration.

#### 4.4.1 Sudden change in outside temperature

This theoretical simulation experiment is inspired by Evrard (2008), who suggested two parameters describing transient thermal behaviour of BE component under sudden change in outside temperature ( $t_{s-s}$  [h] and  $Q_{24h}$  [%]) as an addition to steady state based U-value.

The wall components defined in section 4.2 were subjected to theoretical thermal shock, which intends to simulate temperature drop during night-time. The simulation setting was as follows:

Initial temperature of both outside and inside environment was set to 20 °C. Temperature throughout the components was set to 20 °C, whilst moisture content of each layer was set to the amount, which corresponds to 70 % RH of ambient air. Boundary conditions were set to 20 °C (50 % RH) throughout the simulation for indoor climate and (starting with first hour of the simulation) to 0 °C (50 % RH) for outdoor climate (sudden cooling). Moisture transfer was excluded from WUFI<sup>®</sup> Pro calculation, as  $t_{s-s}$  and  $Q_{24h}$  are intended to be parameters addressing solely thermal behaviour of BE components.

After the simulation, function of heat flux through inside surface of each component was analysed as well as cumulative quantity of heat transferred through the inside surface during first 24 hours of the simulation (integral of the heat flux function).

$t_{s-s}$  was then determined as time, which is needed to reach permanent heat transfer (95 % of the final heat flux) through inside surface and  $Q_{24h}$  as a ratio of heat transferred through inside surface during first 24 hrs of simulation to heat transferred when permanent (steady-state) transfer is assumed.

#### 4.4.2 Thermal cycles in outside environment

To address response of building components to cyclic changes in outdoor temperature Evrard (2008) also suggested theoretical simulation experiment, in which BE components are exposed to outdoor thermal cycles following a sin curve with period of 24 hrs and amplitude of 10 °C (between 0 °C and 20 °C representing daily thermal cycles).

Indoor temperature for this simulation was set to 10 °C, which eliminates heat flow caused by difference between outdoor and indoor environment (average heat flux is null) and thus

allows to focus only on the effects of transient heat transfer. Moisture content of each layer was set to amount, which corresponds to 70 % of RH of ambient air and RH of outside and inside environment was set to 50 %. Moisture transfer was not taken into consideration in WUFI® Pro calculation.

Function of heat flux through inside surface of components was used to analyse thermal behaviour of the components under transient thermal conditions. Two more parameters were defined following Evrard's (2008) research,  $phs$  [h] and  $dmp$  [%]. *The phase shift ( $phs$ )* expresses delay, with which temperature peak of outdoor temperature reaches inside surface of components. In other words  $phs$  expresses time shift between simulated heat flux through inside surface and heat flux through inside surface, when permanent (steady-state) heat transfer  $P.transf.$  (computed based on equation (15)) is considered. *The thermal damping ( $dmp$ )*, on the other hand, represents proportion of theoretical permanent (steady-state) heat transfer through inside surface, which did not occur due to the transient (buffering) effect (share of theoretical  $P.transf.$ , which was actually not transferred).

#### 4.4.3 Inside moisture buffering

Nordtest protocol (Rode *et al.*, 2005) defines procedure to obtain  $MVB_{practical}$  (see section 2.1.2.6). Following this protocol, simulation setup to obtain  $MVB_{simul}$ , which substitutes the experimentally measured  $MVB_{practical}$ , was suggested.

Components were subjected to inside humidity cycles at constant air temperature of 20 °C. Individual cycles were composed of moisture uptake during 8 hrs at RH 75 % followed by moisture release during 16 hrs at RH 33 %. This could for instance represent a small bedroom during wintertime, when indoor environment tends to be rather dry. It is normally inhabited only during 8 hrs of night time (RH increase) and left empty for the rest of the day (RH decrease).

Outside environment and initial conditions through the components were set to 20 °C and 47 % RH (representing average RH value of indoor environment, which results in zero moisture flux through the components). Water vapour transfer coefficients  $\beta_{pi,pe}$  were defined according to Tab. 2.

After the simulation, function of cumulative quantity of moisture transferred through inside surface of each element was analysed and used to compute  $MVB_{simul}$  according to equation (36). Apart from wall components defined in section 4.2, two additional components were considered for this simulation; (B-) and (D-). This was to address moisture buffering potential of unplastered hempcrete and adobe brick wall systems.

As it was mentioned in section 2.1.2.3, adsorption and desorption process generates and consumes latent heat within material. Heat release to indoor environment during humid period of the RH cycle (8 hrs of night) derived from function of cumulative quantity of heat transferred through inside surface was used to analyse this phenomenon.

Finally, fluctuation of inside surface temperature, which is linked with the latent heat phenomenon, was addressed as temperature difference of inside surface between individual phases of the RH cycle.

#### 4.5 Hygrothermal simulation under reference years

The final step of this work was subjection of defined wall systems to action of real climate of Central Europe. As described in section 4.3.2.2, climatic data for hygrothermal simulation need to be provided in form of reference year files. WUFI<sup>®</sup> Pro has a worldwide database of reference years data, which can be used for real climate simulation purposes. Those data cannot, however, be accessed for post-processing purposes, which limits post-processing options considerably. It was therefore decided to use primarily local database of reference years for locations in the Czech Republic, which was created for scientific purposes at CTU in Prague.

Three different locations (climates) were ultimately selected as representatives of Central European climate. *Prague* and *Vienna*, being two main Central European metropolises with similar mean outside temperatures and RH (but different amount of incident solar radiation and annual sum of rainfall), were compared with one of the wettest and coldest locations in the Czech Republic - *Serak* in Jeseniky mountains (north-east of the Czech Republic). Detailed characteristic of the selected climates is provided in Fig. 39.

Indoor climatic files (indoor temperature and RH) were generated using outside air temperature data based on functions defined in Eurocode EN 15026 (ISO, 2007b), which are embedded in WUFI<sup>®</sup> Pro software (see section 4.3.2.2). Medium moisture load (30 - 60 % RH) was assumed for majority of simulation scenarios, although high moisture load (40 - 70 % RH) was also simulated to analyse its effect upon hygric behaviour of the wall systems. Tab. 4 summarises input climatic data considered in the real climate hygrothermal simulation performed in this work together with their sources.

**Tab. 4:** *Boundary condition data considered for real climate simulations*

Input climatic data	Source
<i>Outdoor</i>	
Prague (the Czech Republic)	CTU database
Vienna (Austria)	WUFI <sup>®</sup> Pro database
Serak (the Czech Republic)	CTU database
<i>Indoor</i>	
Medium moisture load (30 - 60 % RH)	En 15026
High moisture load (40 - 70 % RH)	En 15026

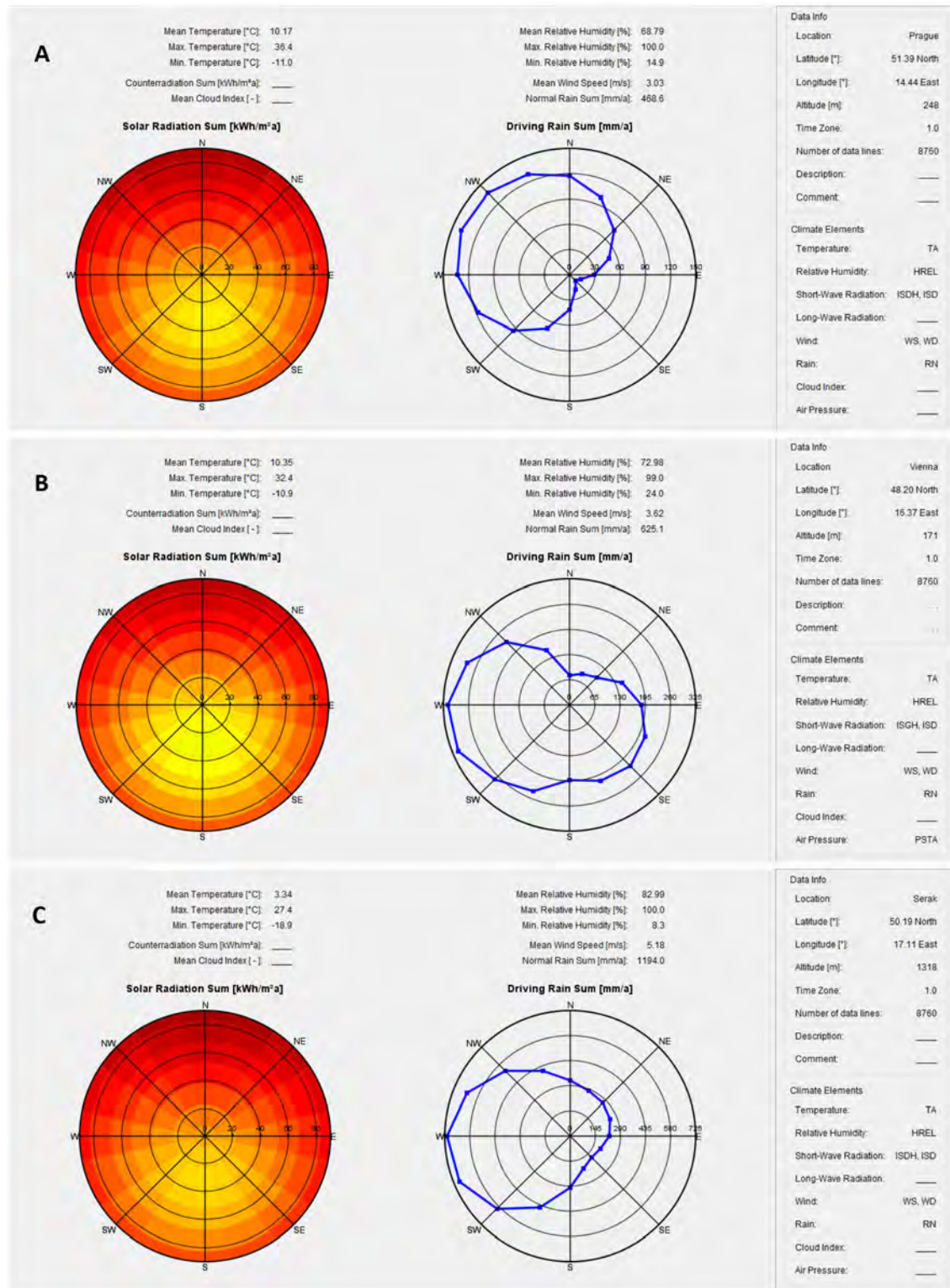


*Fig. 39: Analysis of climates used in this work: (A) Prague (B) Vienna (C) Serak*

As can be seen in Fig. 39, walls oriented in different direction receive substantially different amount of incident solar radiation and wind driven rain. To investigate effect of those phenomena, each simulation was performed with walls orientated both to main sunward and main windward (humid) side (see Tab. 5).

**Tab. 5:** *Simulated orientations for different locations*

Location	Sunward side	Windward side
Prague	South	North-west
Vienna	South	West
Serak	South	West

Simulation time was set to 10 years for all cases as wall systems (A and G) needed long time for stabilisation of water content in individual wall layers. Results were evaluated based on data from 10<sup>th</sup> year of simulation.

The considered wall systems were primarily simulated with input values set according to Tab. 2. The only exception was wall system (I), which is protected against rain and solar radiation by wooden cladding. *Short wave radiation absorptivity* and *adhering fraction of rain* surface coefficients were thus set for wall system (I) to zero value.

#### 4.5.1 Analysed parameters

MATLAB R2010a (MATLAB, 2010) was used as a post-processing tool for evaluation of hygrothermal behaviour of the studied wall systems. The following sections describe analysed hygrothermal parameters, which were used for benchmarking of individual wall systems.

##### 4.5.1.1 Thermal parameters

The main benchmarking thermal parameter of the conducted hygrothermal performance comparison was respectively annual, winter and summer heat losses/gains through one square meter of wall component. These were computed as integral of heat flux through inside surfaces of components during the considered reference year (heating/cooling season). Heating and cooling seasons were defined by function based on outside temperature. Heating season was considered when outside temperature dropped below 16 °C, cooling season when outside temperature rose above 25 °C.

The simulated heat losses/gains were subsequently compared between individual components and to heat losses/gains obtained from steady-state calculations (i.e. integral of heat flux through a component of U-value equal to 0.237 W/(m<sup>2</sup> K), which was computed based on immediate temperature differences between indoor and outdoor environment according to equation (15)). Influence of different climates as well as different component orientation upon heat transfer through individual components was assessed by comparison of relevant charts. Influence of driving rain and direct sun radiation was analysed by excluding of those phenomena (change of surface transport coefficients) from simulations and subsequent comparison of heat losses/gains before and after the exclusion action.

Finally, short-term dynamics of heat flux was analysed by plotting heat flux through inside surface of individual components together with indoor and outdoor air temperature during three selected two-week periods of reference year - winter, summer and spring period.

#### 4.5.1.2 Hygric parameters

Assessment of hygric behaviour of BE cannot be done through quantitative analysis like in case of thermal behaviour assessment (amount of transferred water through wall component is not an indicator of component's quality). For hygric assessment of individual wall components were therefore used three theoretical concepts, which characterise different aspects of hygric behaviour of general interest. Those are:

- Existence of annual moisture accumulation phenomenon inside wall systems
- Moisture-buffering effect (MBE)
- Time-of-wetness (TOW)

Although the wall systems considered in this work were checked for interstitial condensation according to EN ISO 13788 (ISO, 2012), accumulation of moisture throughout reference year could not be ruled out as calculation check was done for steady state hygrothermal conditions and only for Prague location. It was therefore reasonable to evaluate the **annual moisture accumulation phenomenon inside wall systems**, before any further hygric analysis. This was done by comparison of water content inside of wall at the end of 9<sup>th</sup> and 10<sup>th</sup> year of simulation.

Second, the **moisture-buffering effect (MBE)** was analysed. Wall systems B- and D- were again simulated as part of this analysis to address MBE of hempcrete and adobe brick finishes (see section 4.4.3).

As moisture flux through inside surfaces of components follow unpredictable patterns, no concept such as MBV could be used when evaluating MBE of real climate simulations. It was therefore decided to analyse MBE by computing annual sum of moisture transferred through inside surface (integral of moisture flux) in both directions (in/out). Each wall system has principal direction, in which moisture flux occurs. This is the direction of moisture flux, which results in higher value of computed annual sum of transferred moisture. The other direction subsequently characterises temporary reactions of wall surfaces to sudden changes of indoor RH, which represent ability of those surfaces to buffer fluctuations of indoor RH. It was therefore decided to use the lesser value of computed moisture transfer sum as principal indicator of MBE.

MBE was also assessed by analysis of short-term dynamics of moisture flux through inside surface of components during selected winter and summer period, which was compared with dynamics of indoor RH.

The last concept to benchmark hygric performance of the wall systems was standard damage function called **time-of-wetness (TOW)**. This function is defined by ISO 9223 (ISO, 1992) and is primarily used for evaluation of atmospheric corrosion of metals and alloys. Its appropriateness for building materials assessment has been acknowledged e.g. by Van den Bulcke *et al.* (2009), who used this concept for evaluation of effect of outdoor climate upon plywood boards. Kočí *et al.* (2014a) further claim its suitability for conventional building materials such as bricks, stone, or renders.

TOW describes how many hours per year [hrs/year] it is building component exposed to hydrothermal conditions exceeding prescribed RH and temperature critical levels  $RH_0$  and  $T_0$  (both conditions need to be met at the same time). Its value thus ranges from 0 to 8760 hrs/year. The threshold values are usually taken as  $RH_0 = 80\%$  and  $T_0 = 0\text{ °C}$ , which has been recognised as values, below which is the environment corrosion and mould free (CSN, 2005).

Bronsema (2010), however, claims limit of 80 % RH to be overly conservative, as it requires long time and relatively high temperatures before germination of mould spores occurs in such RH. Straube (2006) confirms this in his study about moisture management of straw bale walls, where he states that fungal growth in local RH of over 80 % begins on most surfaces after many months. He also states that atmospheric corrosion and decay require levels of RH well over 90 % to proceed at dangerous rates.

In dynamic hygric environment was thus threshold value of 80 % RH considered as non-sufficient as it does not represent dangerous conditions even for straw bale wall (potentially the most vulnerable wall system). Also, when assessing the studied wall systems, it was decided to focus on more destructive phenomena such as risk of biodegradation or moisture/frost straining, which are all characteristic for higher RH levels of over-hygroscopic region. Kočí *et al.* (2014a) writes that RH values close to maximum hygroscopic moisture content (98 %) are difficult to measure as most RH sensors have lower accuracy in high RH regions and suggests TOW threshold values  $RH_0 = 95\%$  and  $T_0 = 0\text{ °C}$ . Künzel (1995) supports this suggestion, when he considers 95 % RH as upper limit of hygroscopic region in his mathematical model. The critical values of TOW function for conventional materials were thus taken as suggested by Kočí *et al.* ( $RH_0 = 95\%$ ,  $T_0 = 0\text{ °C}$ ).

In case of RNBM were considered different critical RH as they are vulnerable to decomposition (decay) by various microorganisms (bio-based RNBM) or they lose part of their load-bearing capacity (loam-based RNBM). Limiting moisture contents (RH), which correspond to these phenomena, are shown in Tab. 6.

As stated above, microbial growth, which causes daily rate of straw decay of 0.009 % is considered negligible (Summers *et al.*, 2003). Similarly, colonisation by fungi at 81 % RH is considered marginal threat for wooden material (long time of germination). The critical level of RH for straw and wood-based materials (spruce, wooden fibreboard, wood fibre insulation) was thus considered  $RH_0 = 90\%$ , which already represents conditions in which can certain types of fungi decay wood. Decay of straw is also considered to reach rates

of more than 1 ‰ a day (see Fig. 40), which can already have certain damaging effect. Critical level of temperature ( $T_0$ ) remained 0 °C.

**Tab. 6:** Limiting amounts of moisture (RH) for RNBM for different types of damages

Minimum moisture content $u$	[M. – %]	[kg/m <sup>3</sup> ]	Corresponding RH [%]
<i>Wood<sup>a</sup></i>			
Colonization by fungi	18	82	81
Decay by fungi	22	100	90
<i>Straw bale<sup>b</sup></i>			
Decay of 0.009% a day	13	13	84
Decay of 1.8% a day	68	68	98
<i>Adobe brick<sup>c</sup></i>			
Decrease of compressive strength under 1.5 MPa	6	94	98
<i>Rammed earth<sup>c</sup></i>			
Decrease of compressive strength under 1.5 MPa	6	114	95

<sup>a</sup>Schmidt (2007).

<sup>b</sup>Wihan (2007).

<sup>c</sup>Bui *et al.* (2014).

In case of loam-based materials was found out that RH up to 95 % does not affect compressive strength of unfired clay (Fernández-Cabo, 2009, Bui *et al.*, 2014). Minke (2012) also states that when building with appropriate loam, risk of biodegradation is eliminated.

As regards hempcrete material, findings of Ghrici *et al.* (2007) suggest that hempcrete does not have sufficient available nutrients to support microbial growth (due to the petrification process becomes hempcrete over the time practically inorganic material). Critical values for TOW function of loam-based RNBM and hempcrete were thus taken as for the conventional materials ( $RH_0 = 95 \%$ ,  $T_0 = 0 \text{ °C}$ ).

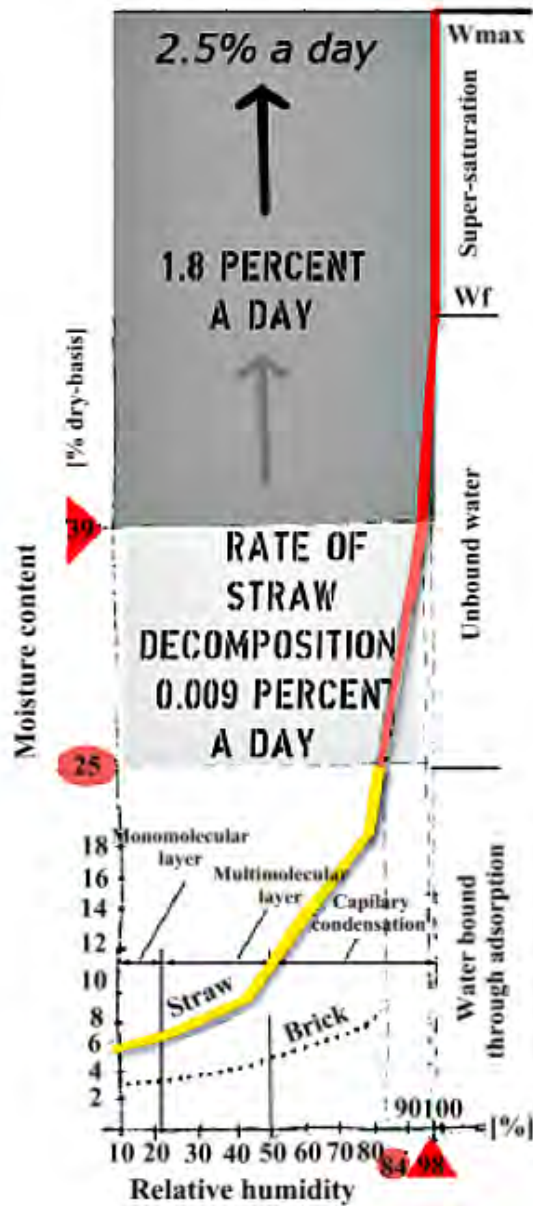


**Fig. 40:** Sorption isotherm of straw together with regions of different rates of decomposition (84 % RH - start of decomposition process at marginal rates, 98 % RH - critical boundary (high rate of decomposition)) (Wihan, 2007)

## 5 RESULTS AND DISCUSSION

### 5.1 Analytical assessment of individual materials

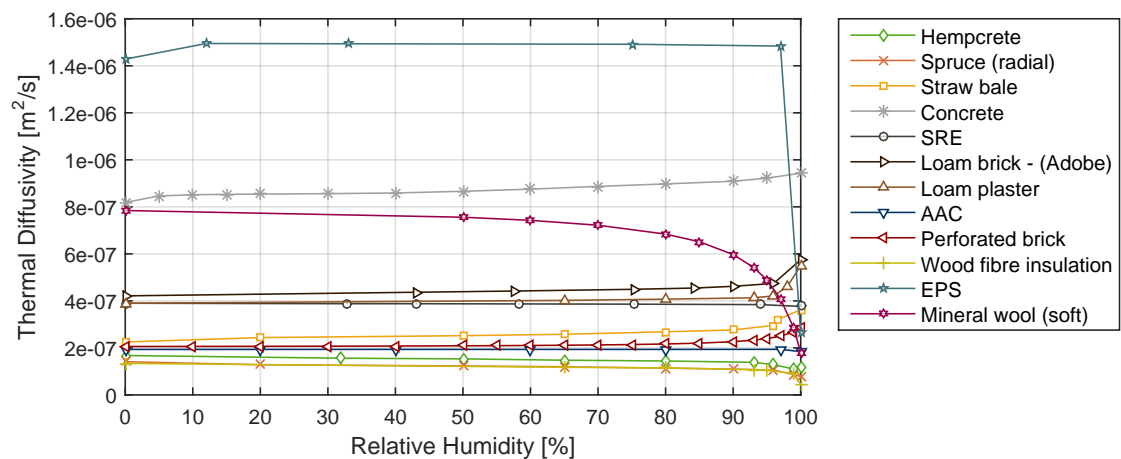
#### 5.1.1 Thermal parameters

Fig. 41 shows course of thermal diffusivity in RH for principal wall materials considered in this work. As it was already stated, the lower the thermal diffusivity of a material the slower it reaches its thermal equilibrium after exposure to thermal shock.

Wood and wood fibre insulation show the lowest thermal diffusivity out of the studied materials, confirming that solid wood is a very good thermal retardant in transient thermal environment. The other natural stalk fibre materials also present low thermal diffusivity, as well as AAC and perforated brick material. All these materials can be considered as materials with long response to outside temperature change. Conventional insulation materials (MW and EPS) and concrete, on the other hand, adjust to outside temperature situation much more willingly, when EPS, which shows by far the highest thermal diffusivity values, overtops wood fibre insulation's thermal diffusivity by one order. This represents a huge difference when considering the same intended function of those materials in BE.

Loam-based materials have about half-thermal diffusivity, when compared to other heavy structural material (concrete). When compared to previously discussed lightweight wall materials, their thermal diffusivity is about twice as high.

The course of thermal diffusivity in different RH levels is almost constant for all the materials. An exception is EPS and MW, thermal diffusivity of which dramatically decreases when approaching free saturation. For numerical thermal diffusivity of other materials (in dry state), see Tab. 7.



*Fig. 41: Thermal diffusivity of principal wall materials considered in this work*

Course of thermal effusivity in RH for discussed materials is illustrated in Fig. 42. The higher the thermal effusivity the more heat is exchanged between material and its thermally inequivalent ambient environment during a given time laps (higher short-term thermal buffering potential and lower subjectively perceived temperature).

Insulation materials (especially the conventional ones) show the lowest thermal effusivity throughout the RH scale. Lightweight wall materials (AAC, perforated brick, hempcrete and solid wood) present five to ten times higher thermal effusivity than insulation materials, with conventional materials having again lower values than natural stalk fibre materials. When comparing heavyweight materials, thermal effusivity of loam materials is approximately half of that presented by concrete. SRE, which contains cementitious substances, has higher thermal effusivity than loam brick or plaster. For numerical thermal effusivity of other materials (in dry state), see Tab. 7.

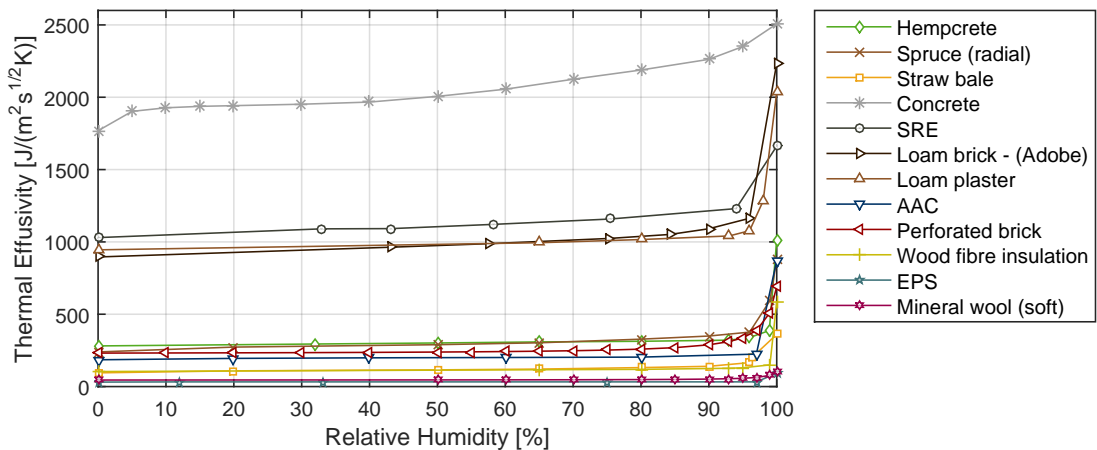


**Fig. 42:** Thermal effusivity of principal wall materials considered in this work

### 5.1.2 Hygic parameters

Hygic diffusivity represents rate of variation of water content in material due to vapour flow (in dynamic hygic environment). The higher hygic diffusivity of material the faster it reaches its hygic equilibrium after exposure to hygic shock.

Fig. 43 shows course of hygic diffusivity in RH for principal wall and potential finishing materials considered in this work. It can be seen that hygic diffusivity values depend more significantly on RH than values of its thermal equivalent. It is due to natural character of *specific hygic capacity*  $\xi$ , which changes with slope of moisture storage function of materials. For practical reasons is RH range between 30 - 70 % considered as decisive interval for further hygic parameters evaluation.

The highest values of hygic diffusivity are presented by insulating materials (especially the conventional ones) followed by lightweight wall construction materials (with the exception of solid wood). The highest hygic diffusivity of potential surface materials can be observed

in case of gypsum board followed by hempcrete, loam plaster, wooden fibre, loam brick, lime render, cement-lime render and SRE (depending on level of RH). Concrete OSB and spruce wood in its radial direction perform the lowest hygric diffusivity.

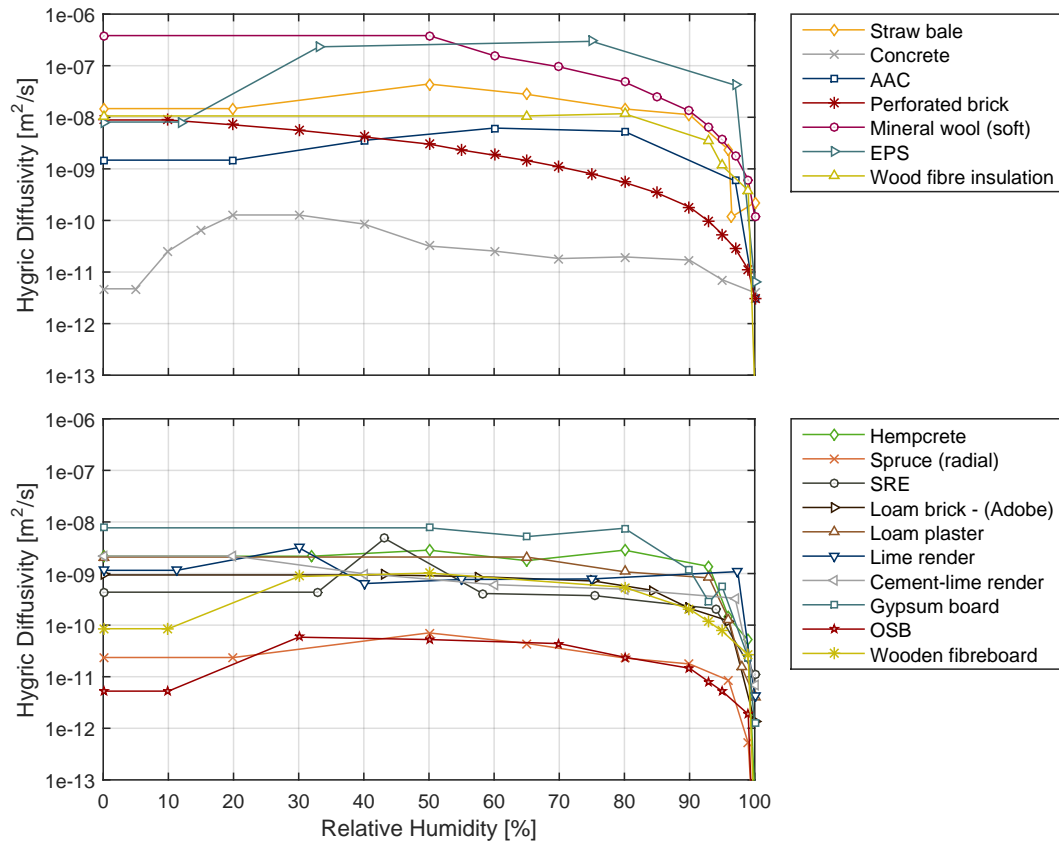


**Fig. 43:** Hygric diffusivity of principal wall materials (above) and potential finishing materials (below)

Course of hygric effusivity in RH for the studied materials is depicted in Fig. 44. It is a parameter, which determines amount of moisture uptake or release, when material is subjected to dynamical hygric environment during a given time laps. Hygric effusivity directly influences moisture buffering potential of materials and it thus for this work important parameter to assess.

It can be observed that natural stalk materials show the highest hygric effusivity within interval of 30 – 70 % RH. The exception is spruce wood in radial direction with its high  $\mu$ -factor. Among finishing materials further show high values of hygric effusivity lime render, loam brick, cement-lime render and partly SRE. Gypsum board, OSB, radial spruce, concrete, AAC and especially EPS can be considered as materials with low hygric effusivity. MW and perforated brick increase their hygric diffusivity with RH considerably, which prevents their comparisons with the other materials. Numerical values of both hygric diffusivity and effusivity (in dry state) are presented in Tab. 7.

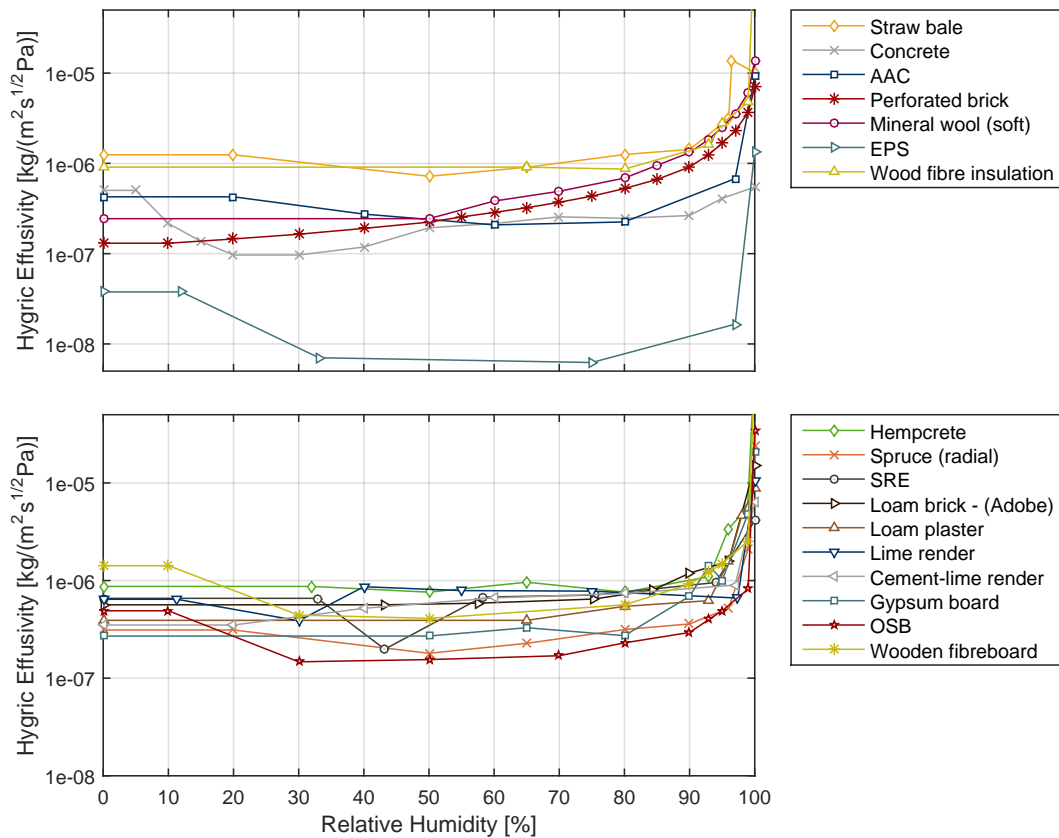


**Fig. 44:** Hygric effusivity of principal wall materials (above) and potential finishing materials (below)

Tab. 7 also shows ideal moisture buffer value of individual materials. It is computed with *specific hygric capacity*  $\xi$ , which represents slope of theoretical line connecting points of 33 % and 75 % RH of moisture storage function for each material. Materials with best  $MBV_{ideal}$  are therefore not necessarily listed as materials with highest hygric effusivity, which is computed for materials in dry state based on *specific hygric capacity*  $\xi$  of initial slope of materials' moisture storage function.

As it was discussed in section 2.2, RNBM show higher potential for inside moisture buffering. However, lime and cement-lime render (MVR Uni) are listed very high in this list and when compared with RNBM finishing material (loam plaster), they even outperform it. In case of lime is this well-known fact. Lime is in general considered as highly hygroscopic material, which is for its hygrscopicity used as finishing material in majority of historical restoration projects. As regards MVR Uni, it was found out that the render was designed to have increased moisture buffering capability, hence its high  $MBV_{ideal}$ . Another reason for loam plaster being outperformed by conventional plasters is its natural composition. When compared to loam bricks or SRE, loam plaster is composed of greater share of sand with almost no moisture buffering potential (see section 2.2.1.2).

Conventional building materials and spruce in its radial direction seem to have very low inside moisture buffering potential.

**Tab. 7:** Analytically determined parameters describing material properties in transient hygrothermal environment from most favourable (light background) to least favourable values (dark background) (values of thermal and hygric diffusivity and effusivity are displayed for materials in dry state)

	$MBV_{ideal}$ [g/(m <sup>2</sup> %RH)]	Therm. Diff [m <sup>2</sup> /s]	Therm. Eff [J/(m <sup>2</sup> s <sup>1/2</sup> K)]	Hygric Diff [m <sup>2</sup> /s]	Hygric Eff [kg/(m <sup>2</sup> s <sup>1/2</sup> Pa)]
Straw bale	4.02	2.25e-07	9.49e+01	1.47e-08	1.25e-06
Wood fibre insulation	3.86	1.34e-07	1.04e+02	1.06e-08	9.09e-07
Hempcrete	3.60	1.68e-07	2.81e+02	2.17e-09	8.71e-07
Lime render	3.43	5.08e-07	1.07e+03	1.15e-09	6.43e-07
Cement-lime render	2.88	2.64e-07	9.20e+02	2.19e-09	3.50e-07
SRE	2.63	3.90e-07	1.03e+03	4.35e-10	6.57e-07
Loam brick - (Adobe)	2.61	4.21e-07	8.96e+02	9.39e-10	5.64e-07
Wooden fibreboard	2.18	1.69e-07	2.92e+02	8.51e-11	1.42e-06
Loam plaster	1.86	3.90e-07	9.45e+02	2.09e-09	3.91e-07
Mineral wool (soft)	1.79	7.84e-07	4.52e+01	3.84e-07	2.44e-07
Perforated brick	1.26	2.06e-07	2.31e+02	8.87e-09	1.31e-07
Gypsum board	1.26	2.77e-07	3.80e+02	7.69e-09	2.70e-07
Spruce (radial)	1.01	1.41e-07	2.39e+02	2.36e-11	3.12e-07
AAC	0.97	1.93e-07	1.85e+02	1.48e-09	4.26e-07
Concrete	0.91	8.18e-07	1.77e+03	4.73e-12	5.02e-07
OSB	0.74	1.51e-07	3.35e+02	5.25e-12	4.90e-07
EPS	0.03	1.43e-06	3.10e+01	8.09e-09	3.77e-08

## 5.2 Comparative and sensitivity analysis

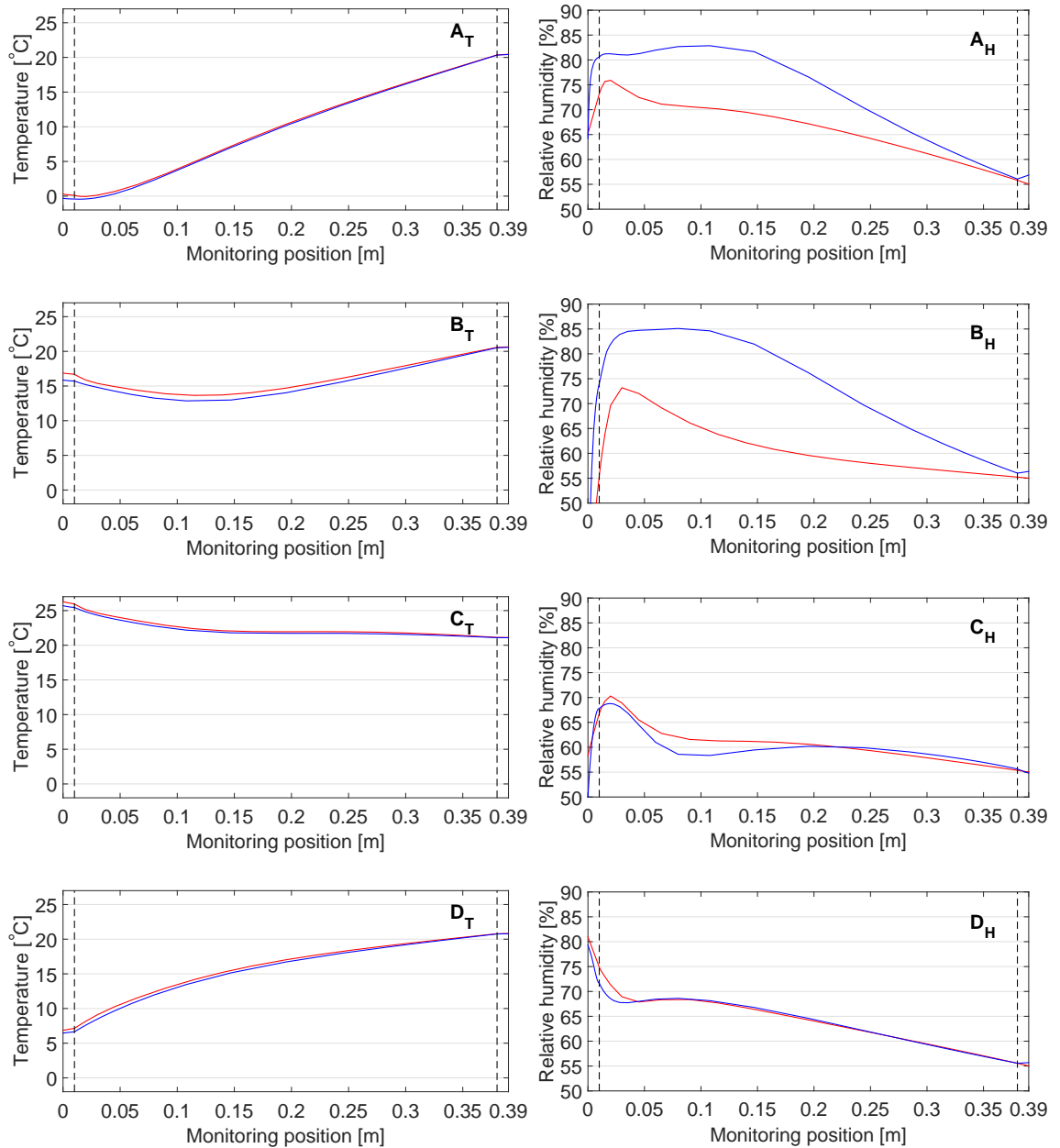
### 5.2.1 Comparative analysis

Fig. 45 shows temperature and RH profiles of wall system (G) (AAC) in different seasons (winter - autumn) simulated both in WUFI<sup>®</sup> Pro and HeMoT simulation tools. It can be observed that temperature profiles independently calculated by the two simulation tools are in very good agreement, when the greatest observed deviation between the two results does not exceed 1 °C. The relative humidity profiles show, on the other hand, much higher deviation between the two tools (up to 20 % in certain cases).

It is evident that simulations performed by WUFI<sup>®</sup> Pro exhibit higher RH throughout the entire cross-section of wall component (Fig. 45  $A_H$  and  $B_H$ ). This phenomenon is, however, present only in winter and spring simulation profile, and vanishes during summer and early autumn time (Fig. 45  $C_H$  and  $D_H$ ). It was found out that the two simulation tools provide RH results in acceptable agreement approx. between May and October, while during the rest of year (November to April) is the agreement of simulated RH profiles very poor.

WUFI<sup>®</sup> Pro calculation method for determination of moisture flux through wall systems thus clearly varies from the one used by HeMoT. Interestingly, the problematic time span

(November to April) correlates with heating season in the Czech Republic, which suggests that the deviation of RH results depends on amount of moisture within simulated wall and principal direction and magnitude of moisture flux through the wall (both tend to be greater during heating season).



**Fig. 45:** Comparison of temperature ( $X_T$ ) and relative humidity ( $X_H$ ) fields of profiles at selected times simulated by HeMoT (red line) and WUFI<sup>®</sup> Pro (blue line) software. A - 24.2. (10:00), B - 16.4. (16:00), C - 31.7. (15:00), D -16.10. (7:00)

As it was discussed in section 4.3.2.1, WUFI<sup>®</sup> Pro uses an extra material input parameter, when compared with HeMoT. It is *liquid transfer coefficient for redistribution*  $D_{ww}$ , which represents situations, when material has been in direct contact with water, but it is not any more (water redistributes itself through pores of the material). HeMoT uses only *liquid transfer coefficient for suction*  $D_{ws}$  (approx. one order greater than  $D_{ww}$ ), which is measured only for materials in direct contact with water and might not be representative for moisture redistribution situation (e.g. escape of moisture from wall after termination of rain). It is therefore likely that WUFI<sup>®</sup> Pro releases moisture, which gets build up in the wall during wintertime, into surrounding environment more slowly than HeMoT, which assumes only fast liquid transfer ( $D_{ws}$ ). The resulting RH output profiles obtained by WUFI<sup>®</sup> Pro simulation are then significantly higher than RH profiles obtained by simulation in HeMoT. During summertime, on the other hand, there is not much moisture presented in the wall and so the difference between  $D_{ws}$  and  $D_{ww}$  does not play a big role. Figs. 46 and 47 confirm this when showing RH time course of two selected monitoring positions during selected winter (January) and summer (July) months. It can be observed that RH course of monitoring position within outside render simulated by HeMoT in January follows much more dynamical pattern than the one simulated by WUFI<sup>®</sup> Pro (Fig. 46  $A_H$ ). While HeMoT simulation reacts quickly to outside environment dynamics, WUFI<sup>®</sup> Pro assumes slower moisture transfer and thus generates time course, which has slower reaction to outside environment dynamics. This is again likely to be caused by difference in liquid transfer coefficients. Deeper analysis and comparison of mathematical models behind the simulation tools is considered outside of the scope of this work.

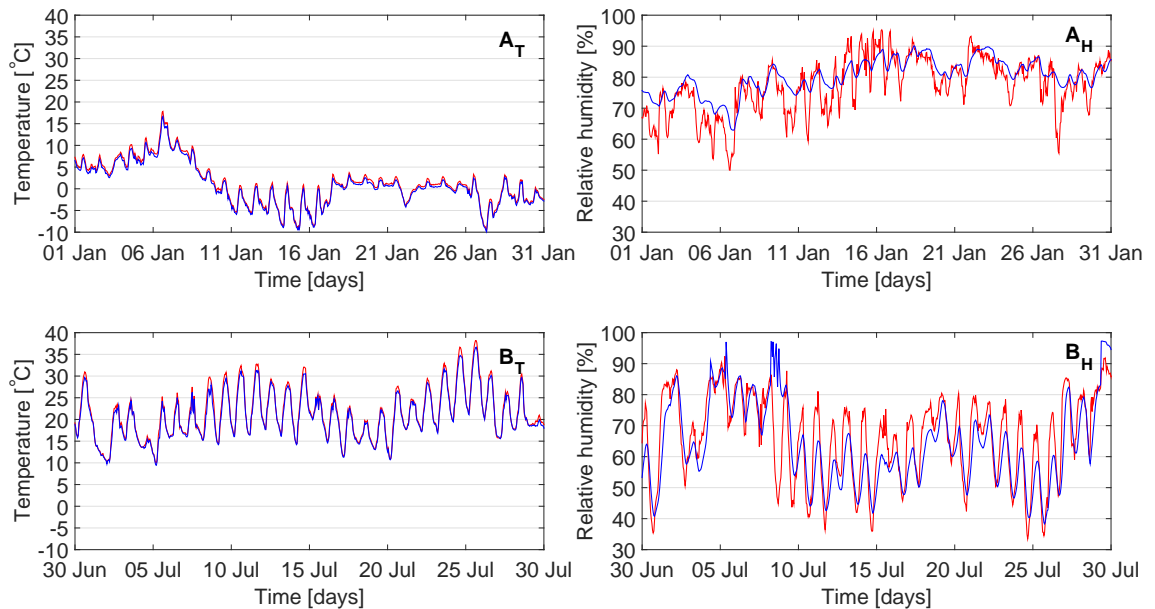


**Fig. 46:** Comparison of temperature ( $X_T$ ) and relative humidity ( $X_H$ ) time courses at monitoring position within the outside render (0.005 m) during selected winter month - A (January) and summer month - B (July) - HeMoT (red line), WUFI<sup>®</sup> Pro (blue line)

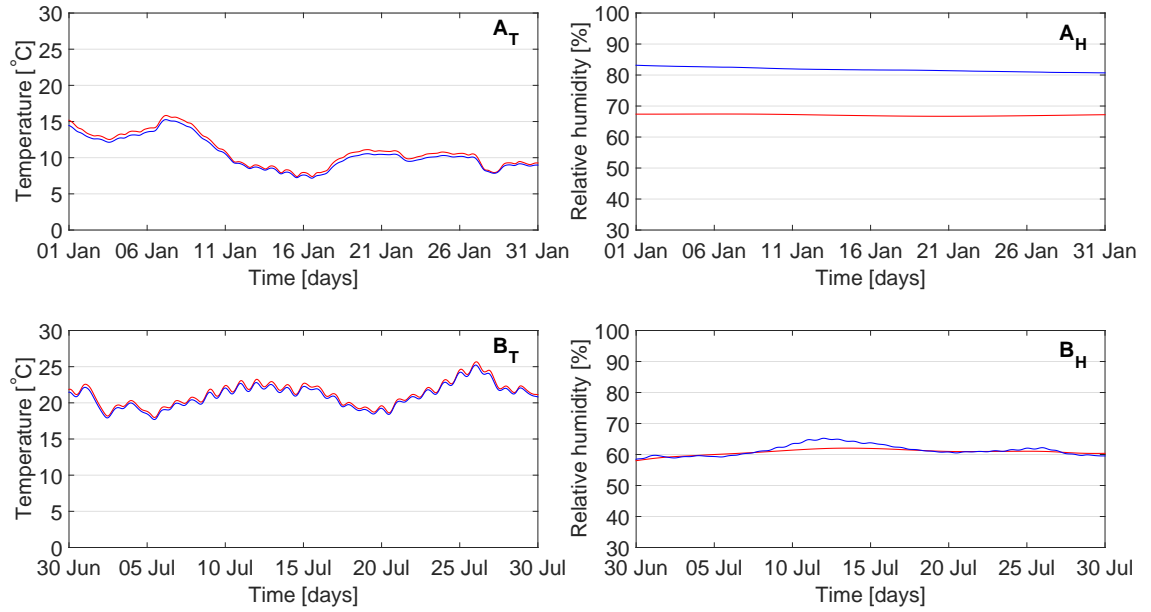


**Fig. 47:** Comparison of temperature ( $X_T$ ) and relative humidity ( $X_H$ ) time courses at monitoring position within AAC wall (0.195 m) during selected winter month - A (January) and summer month - B (July) - HeMoT (red line), WUFI<sup>®</sup> Pro (blue line)

To conclude the comparative analysis, we can give thermal simulation outputs presented further in this work higher relevance as the results are verified by two independent simulation software tools. Relevancy of hygric simulation outputs was on the other hand not supported as RH outputs of the selected simulation tools differed during wintertime significantly.

It is believed that distinguishing between the two types of liquid transfer coefficients provides more precise simulation results. The speed of suction and redistribution process indeed varies as it is described e.g. by Künzle (1995). It was already mentioned that *liquid transfer coefficient for suction*  $D_{ws}$  is approximately 10 times greater than *liquid transfer coefficient for redistribution*  $D_{ws}$ , which most likely affects the actual simulation outcome.

WUFI<sup>®</sup> Pro was therefore decided to be the main hygrothermal simulation tool for the remaining part of this work. Besides its higher relevancy has WUFI<sup>®</sup> Pro software also more user-friendly working environment, which provides better way for handling of input and output simulation data. Its higher prestige and recognition among international building physics society is also believed to give this work higher relevancy.

### 5.2.2 Sensitivity analysis

Tab. 8 shows degree of influence of individual input material uncertainties (from Tab. 3) upon thermal and hygric WUFI<sup>®</sup> Pro simulation outputs obtained from initial step of sensitivity analysis (variation of individual material input parameters). Boundaries of sensitivity classification were determined as follows:

- Low sensitivity - deviation of simulation output of less than 0.1 °C or 0.5 % RH
- Medium sensitivity - deviation of simulation output between 0.1 °C and 0.2 °C or 0.5 % and 2 % RH
- High sensitivity - deviation of simulation output of more than 0.2 °C or 2 % RH

**Tab. 8:** Classification of sensitivity of WUFI<sup>®</sup> Pro mathematical model to uncertainties of input material parameters

Sensitivity	Parameter	
	Temperature	Relative humidity
Low	$A, \rho, \mu, \psi, w(\varphi)$	$\rho, \psi, c$
Medium	$\lambda, c$	$\lambda$
High	-	$A, \mu, w(\varphi)$

It was found out that temperature profiles outputs remained rather stable during variation of individual material parameters, while outputs of RH profiles showed higher sensitivity especially to uncertainty of *A-value*,  *$\mu$ -factor*, and *moisture storage function*  $w(\varphi)$ . Those parameters were therefore considered as decisive parameters for further sensitivity analysis. *Thermal conductivity*  $\lambda$  was the only parameter, which (partially) influenced both thermal and hygric output and was thus included among decisive parameters as well.

Final sensitivity analysis was conducted by performing set of simulations of all possible combinations of variations of the four decisive input parameters and its graphical output is presented in Figs. 48 - 50. Blue line shows the original simulation output, while two dashed lines indicate potential deviation of simulated output data caused by uncertainties of experimentally measured material input data. Area between the two dashed lines therefore represents field of potential simulation outputs.

As can be seen, especially in Fig. 48, results of sensitivity analysis show similar character as results of comparative analysis. While simulated fields of potential temperatures are almost negligible and mostly copy the original simulation output, RH profiles show higher variation projected into substantial fields of potential RH simulation outputs. This phenomenon is again more distinct during periods with higher moisture content within the simulated wall – wintertime (see Fig. 48  $A_H$  and  $B_H$ ).

We can therefore assume that Künzel's mathematical model gets sensitive in situations with high moisture content and moisture flux within simulated walls, which provides also partial explanation for deviation of simulation outputs between WUFI<sup>®</sup> Pro and HeMot (see 5.2.1) in these situations.

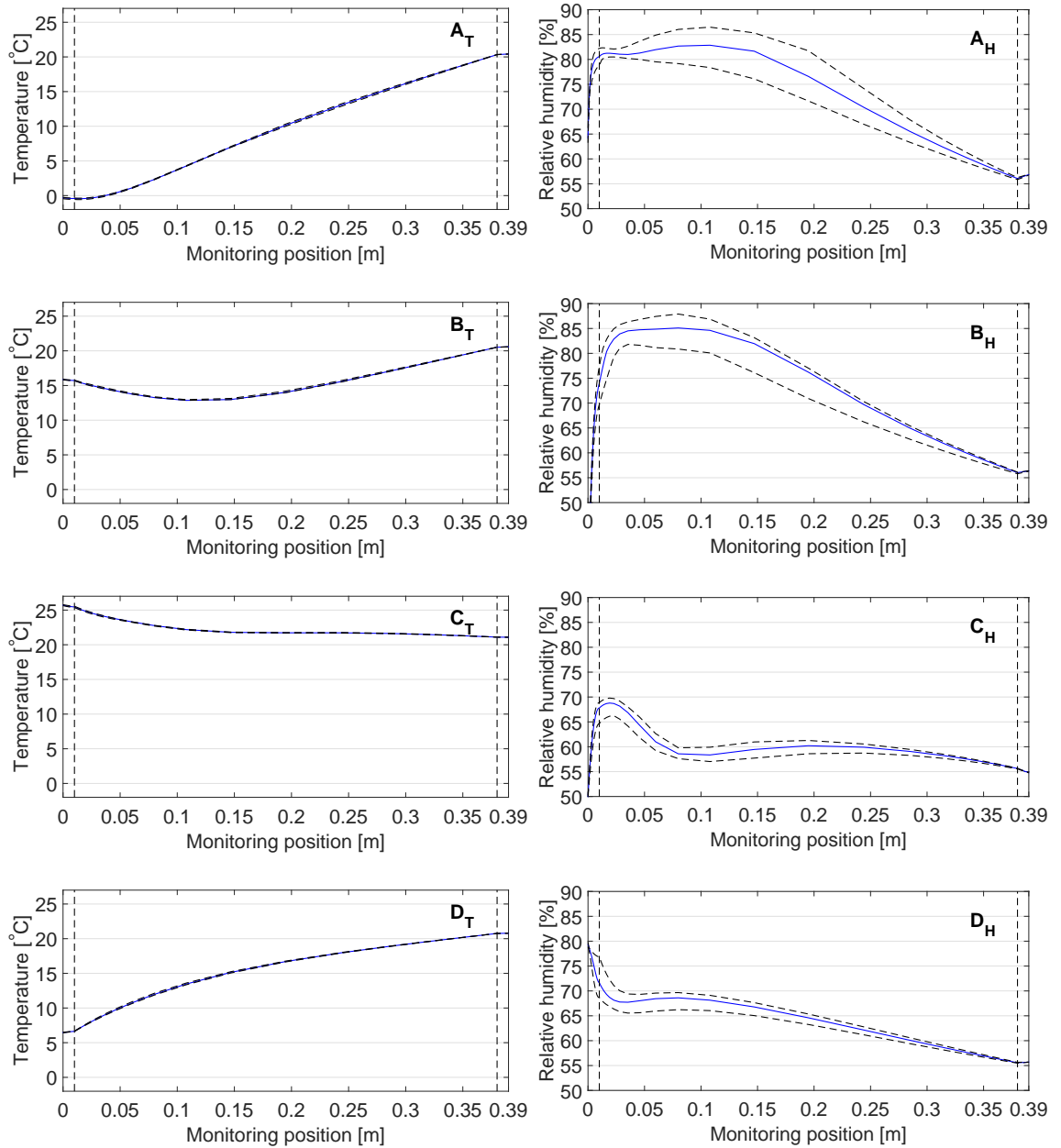


**Fig. 48:** Graphical result of sensitivity analysis in form of temperature ( $X_T$ ) and relative humidity ( $X_H$ ) fields of potential simulation outputs of profiles at selected times simulated by WUFI<sup>®</sup> Pro software (blue line). A - 24.2. (10:00), B - 16.4. (16:00), C - 31.7. (15:00), D - 16.10. (7:00)

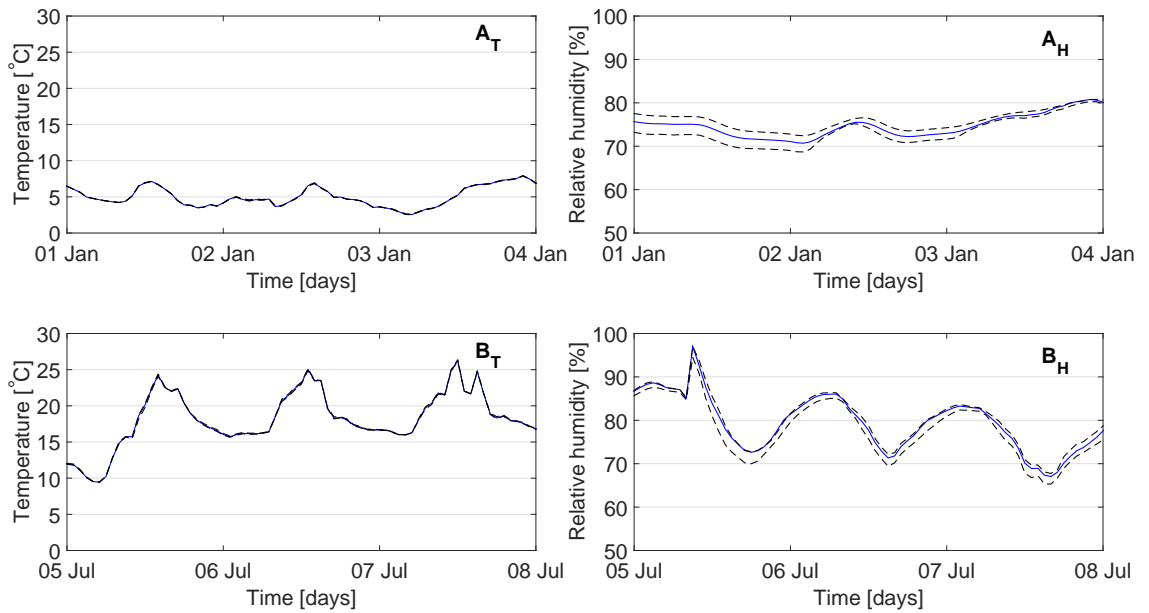


**Fig. 49:** Graphical result of sensitivity analysis in form of temperature ( $X_T$ ) and relative humidity ( $X_H$ ) fields of potential simulation outputs of time courses at monitoring position within the outside render (0.005 m) during winter time - A (January) and summer time - B (July) simulated by WUFI<sup>®</sup> Pro software (blue line)

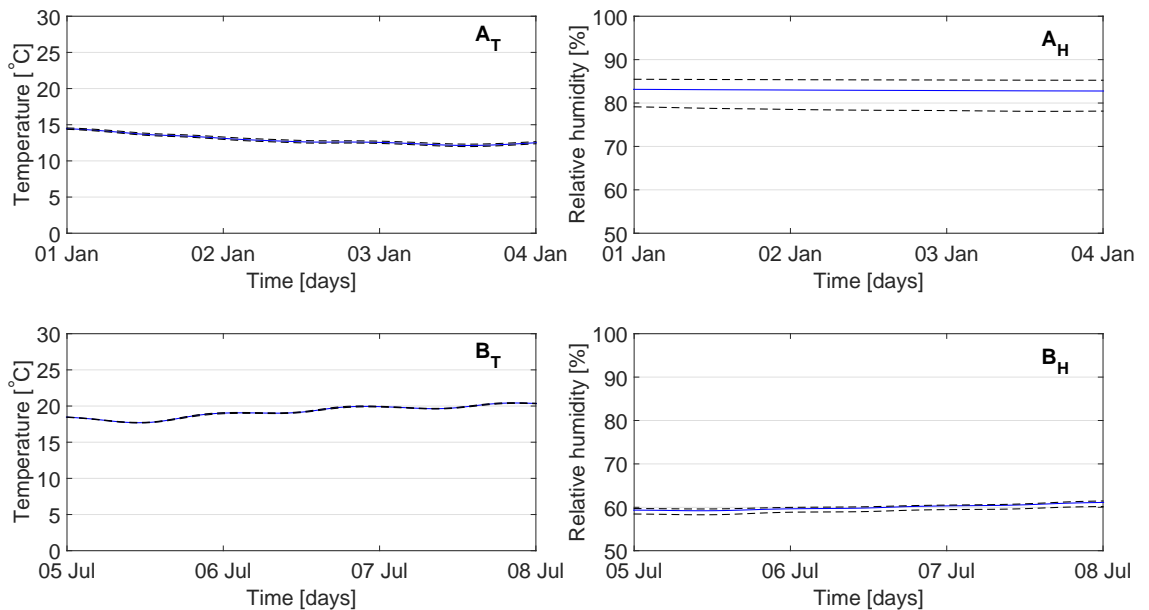


**Fig. 50:** Graphical result of sensitivity analysis in form of temperature ( $X_T$ ) and relative humidity ( $X_H$ ) fields of potential simulation outputs of time courses at monitoring position within AAC wall (0.195 m) during winter time - A (January) and summer time - B (July) simulated by WUFI<sup>®</sup> Pro software (blue line)

Tabs. 9 and 10 show standard deviations of sensitivity errors  $\sigma$  calculated according to equation (41) for each presented profile and time course. It represents 68.3<sup>th</sup> percentile of all recorded sensitivity deviations (errors) from mean simulation profile (time course) caused by uncertainty of material input data (see 4.3.3). In other words 68.3 % of sensitivity

analysis outputs are assumed to be within interval of  $1 \sigma$  from simulated mean profile (time course) represented by initial simulation output (original material input data).

The numerical results confirm all the previously mentioned observations. Standard deviation of sensitivity error  $\sigma$  of thermal simulation seldom exceeded  $0.1 \text{ }^\circ\text{C}$ , giving the thermal simulation high relevancy.  $\sigma$  of hygric simulations varies, as expected, substantially ( $1.4 \text{ \%} - 4.1 \text{ \% RH}$ ). An interesting phenomenon can be seen in Tab. 10. While  $\sigma$  of monitoring position within outside render is rather low ( $1.8 \text{ \% RH}$ ),  $\sigma$  of monitoring position within AAC shows much higher deviation ( $4.1 \text{ \% RH}$ ). This suggests that RH sensitivity error multiplies with longer distance from simulated boundary conditions.

Overall can be stated that hygric simulations performed by WUFI<sup>®</sup> Pro are more sensitive than thermal simulations. Standard deviations of sensitivity errors  $\sigma$  up to around  $4 \text{ \% RH}$  might not be already precise enough for certain desired applications. Uncertainty of especially hygric decisive parameters (*A-value*,  *$\mu$ -factor*, and *moisture storage function*  $w(\varphi)$ ) plays in hygrothermal simulations crucial role and should be kept down to its possible minimum.

**Tab. 9:** Standard deviation of potential simulation error caused by uncertainty of input material data for profiles at selected times

Profile (date)	Standard deviation $\sigma$	
	Temperature [ $^\circ\text{C}$ ]	Relative humidity [%]
A (24.2.)	0.12	4.0
B (16.4.)	0.09	3.3
C (31.7.)	0.05	1.4
D (16.10.)	0.09	1.4

**Tab. 10:** Standard deviation of potential simulation error caused by uncertainty of input material data for time courses at selected monitoring positions

Monitoring position	[m]	Standard deviation $\sigma$	
		Temperature [ $^\circ\text{C}$ ]	Relative humidity [%]
Outside render	0.005	0.06	1.8
AAC	0.195	0.13	4.1

## 5.3 Hygrothermal performance of wall systems under theoretical conditions

### 5.3.1 Sudden change in outside temperature

Fig. 51 shows heat flux through inside surface of each of studied wall components during 8 days after exposure to thermal shock (described in section 4.4.1). Solid lines stand for

wall systems made of RNBM, while dashed lines for conventional wall systems. Negative values of heat flux represent direction of flux from inside to outside.

It can be observed that eventual (permanent) heat flux through all components reaches value of about  $4.74 \text{ W/m}^2$ , which is given by the same U-value of all components ( $0.237 \text{ W}/(\text{m}^2 \text{ K})$ ). Time elapsed between the thermal shock and stabilized permanent heat flux through component, on the other hand, differs very much for individual wall systems. While heat flux through component (I) reaches its permanent value within hours, it takes more than a week in case of component (B). The newly defined parameter  $t_{s-s}$  (time to reach permanent heat transfer) addresses this phenomenon and its values for the simulated wall systems are summarized in Fig. 52.

The longest time to reach permanent heat flux  $t_{s-s}$  was obtained for component (B) (182 hrs) followed by component (E), (A) and (H). It should be noted that three out of these four components are representatives of the thickest considered components, which gives them more space for heat diffusion through them. Component (A) (holz100 panel) represents in this regard the best  $t_{s-s}$  to thickness ratio.

As expected, the two lightweight wall components (C and I) show the shortest  $t_{s-s}$ , when it takes only 8 hour for component (I) to reach permanent heat transfer through it. Components made of both types of concrete (regular (G) and aerated autoclaved (F)) together with component (D) did not reach times of the firstly mentioned components but performed considerably better than lightweight wall components.

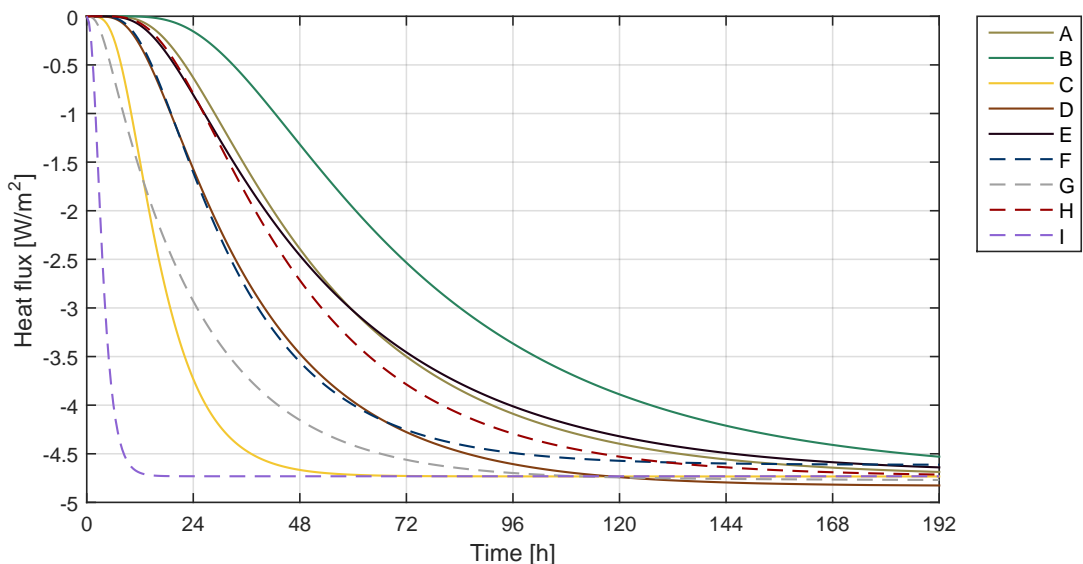


**Fig. 51:** Development of heat flux through inside surface of the wall systems during 8 days after imposed thermal shock

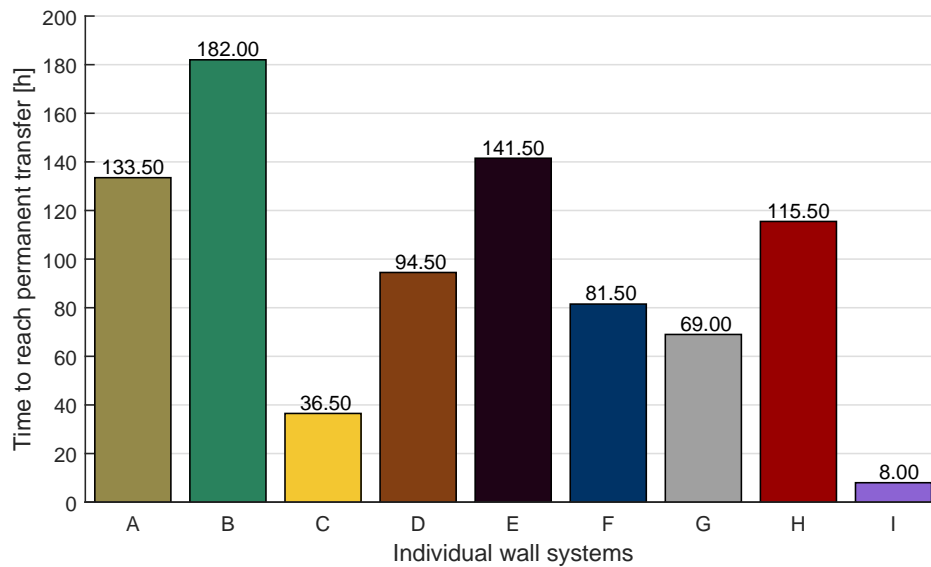


**Fig. 52:** Time to reach permanent transfer  $t_{s-s}$  after imposed thermal shock

Development of cumulative heat transferred through inside surface of components within first 24 hours after the thermal shock is shown in Fig. 53. As Evrard (2008) states, performance of wall systems shortly after thermal shock is an important quality, which should be taken into consideration when assessing thermal behaviour of the systems. Time interval of 24 hours was chosen for obvious reason of diurnal temperature fluctuation. Another interesting comparison can be made when focused on time 12 hours after the imposed thermal shock, which reflects potential of individual wall systems to buffer temperature difference between day and night time.

Simulation results presented in Fig. 53 were interpreted using only parameter  $Q_{24h}$ , which compares (in form of ratio) simulated heat loss through components within first 24 hours after the thermal shock to the theoretical steady-state heat loss (permanent heat transfer through components, see 4.4.1). Evaluation of this parameter for studied wall systems is shown in Fig. 54.

Close link between  $Q_{24h}$  and  $t_{s-s}$  can be observed, when low  $t_{s-s}$  of wall component projects into its high  $Q_{24h}$ . Components (B), (E), (A) and (H), thereafter transfer within first 24 hours after the thermal shock only few percent of heat of steady-state calculations. Components (D) and (F) follow with  $Q_{24h}$  of approximately 10 %. An interesting observation is given by comparison of components (C) (straw) and (G) (concrete). While it takes almost twice as long to reach permanent heat flux through component (G) than through component (C) (Fig. 52), heat transferred through the components within first 24 hours after the thermal shock is almost the same. When focusing only on first 12 hours component (C) transfers only 2/3 of heat transferred through component (G) (Fig. 53). Finally, component (I) transfers within first 24 hours after the thermal shock more than 80 % of heat assumed by steady-state calculation, which is given by its very fast reach of permanent heat transfer after the imposed thermal shock.

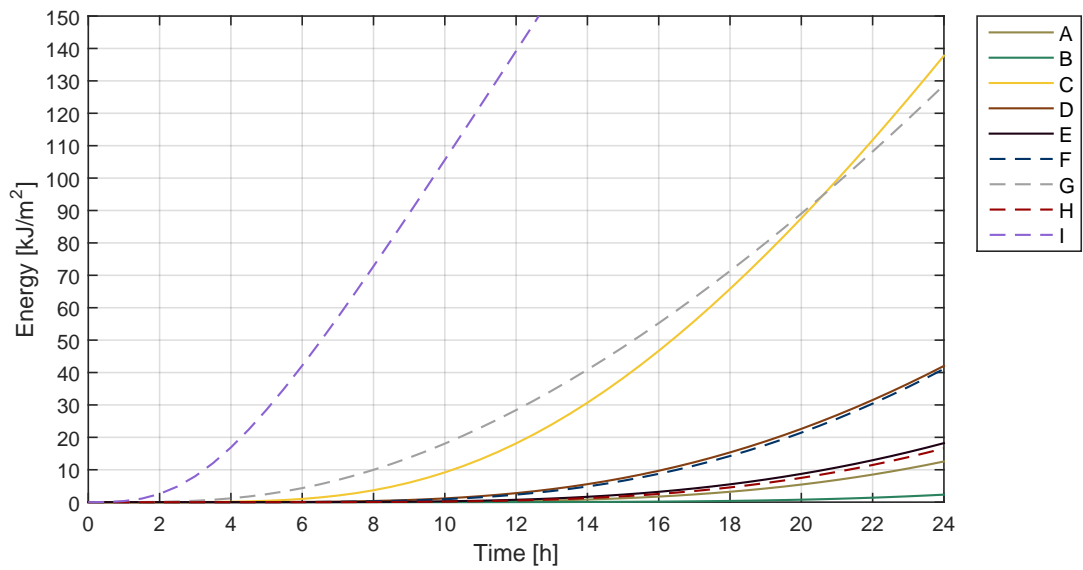


**Fig. 53:** Amount of heat (cumulative) transferred through inside surface of wall systems during first 24 hours after the imposed thermal shock

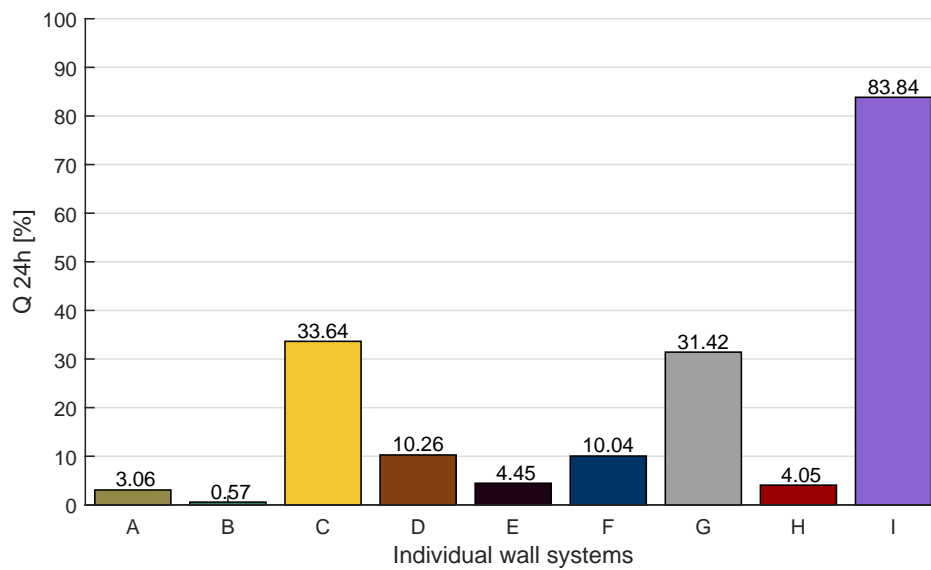


**Fig. 54:** Ratio of heat transferred through inside surface during first 24 hours after the imposed thermal shock to heat transferred when permanent transfer is assumed,  $Q_{24h}$

The simulation was also performed for outside temperature drop from 20 °C to 10 °C to assess influence of thermal shock magnitude upon resulting parameters. It was found out that the magnitude of imposed thermal shock does not influence either of the output parameters of this theoretical scenario.

### 5.3.2 Thermal cycles in outside environment

Fig. 55 shows course of heat flux through inside surface of the studied wall components when exposed to thermal cycles as described in section 4.4.2. Solid lines stand for wall systems made of RNBM, while dashed lines for conventional wall systems. The dot-and-dash line represents theoretical heat flux, which would be obtained by steady state calculations (permanent heat transfer). Limits of x-axis are set in the beginning of third week of simulation as it takes almost two weeks before the course of heat flux occurs in regular pattern.

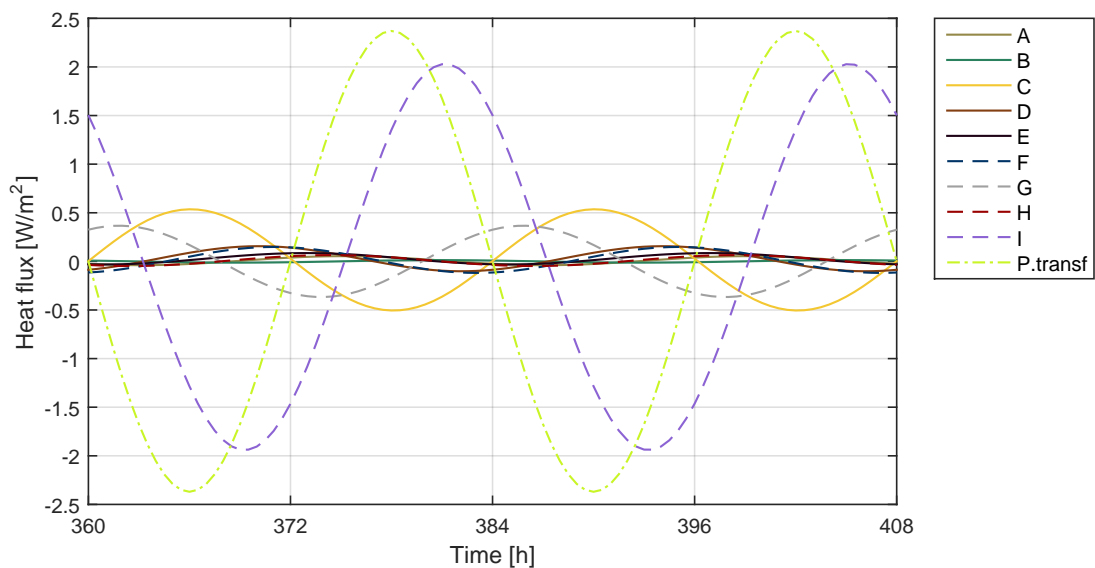


**Fig. 55:** Course of heat flux through inside surface of wall systems during two days of stabilized cycles

It can be observed that for most wall systems is U-value of  $0.237 \text{ W}/(\text{m}^2 \text{ K})$  already low enough to nearly eliminate effect of outside temperature fluctuation (provided that overall heat flux through wall component equals to zero). The only wall components, which are significantly influenced by the outside thermal cycles, are components (I), (C) and (G). It is due to their lower thermal inertia, which is in this simulation setting projected into shorter phase shift - *phs* (Fig. 56) and lower thermal damping - *dmp* (Fig. 57) with respect to theoretical steady-state heat transfer (dot-and-dash line).

As can be seen in Fig. 56, the phase shift parameter is again most distinct for wall component (B), followed by components (A), (E) and (H). These wall components are composed of materials with low thermal diffusivity and effusivity and, as stated above, they are thicker than the rest of the components. They have thus the highest thermal inertia, which is projected into all the thermal parameters introduced in this chapter. Phase shift of wall component made of straw (C) (12 hrs) is greater than phase shift of wall component made of concrete (G) (8 hrs), which gives this lightweight wall component potential for better thermal buffering of diurnal temperature fluctuations (when compared to component (G)).

Phase shift of component (I) was simulated to be only 3 hours, confirming its low potential for thermal buffering of diurnal temperature fluctuations.

The resulting thermal damping parameter  $dmp$  is superior for majority of studied wall components (more than 90 %) with the exception of components (I), (C) and (G). While wall components (C) and (G) dampen the outside thermal cycles still at satisfactory level ( $dmp$  around 80 %), component (I) was simulated to provide far the worst damping of the outside thermal cycles, when transferring around 85 % of theoretical permanent (steady-state) heat transfer ( $dmp \sim 15$  %) (Fig. 57).

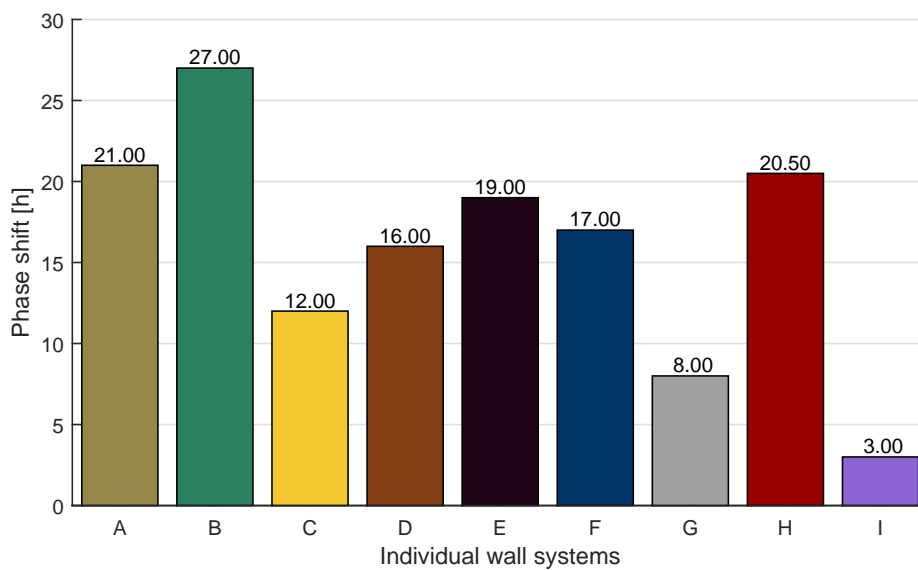


**Fig. 56:** Thermal phase shift of wall systems under cyclic outside temperature fluctuation -  $phs$  (delay of outside peak temperature)

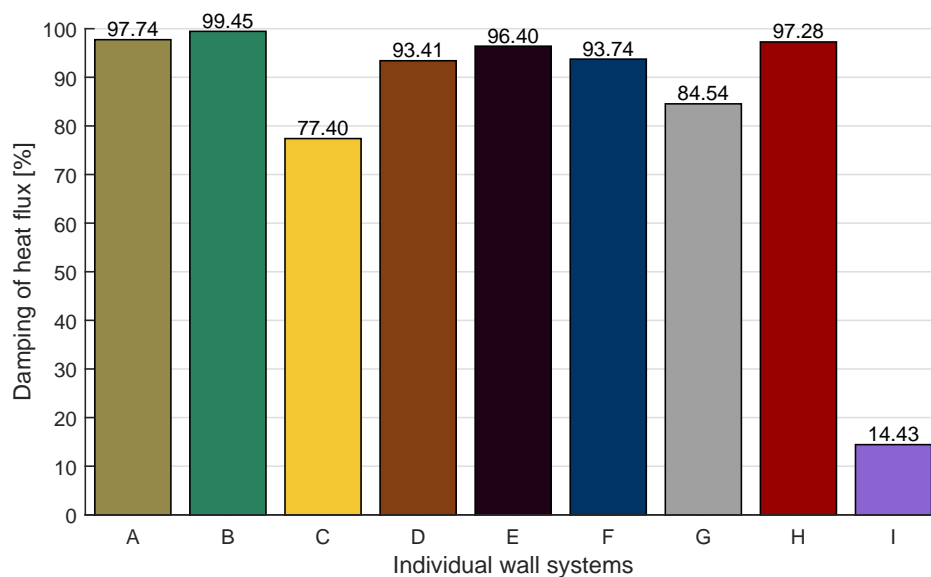


**Fig. 57:** Thermal damping of wall systems under cyclic outside temperature fluctuation -  $dmp$  (percentage saved by the wall system due to thermal inertia effect)

### 5.3.3 Inside moisture buffering

Fig. 58 shows interaction of studied wall systems with inside hygric fluctuations (described in section 4.4.3) in terms of cumulative amount of transferred moisture through inside surfaces of these systems (integration of moisture flux). The resulting chart is offset along y-axis due to initial moisture absorption of wall components. As 16 hour low RH indoor cycle phase occurs, not all the moisture absorbed during the high RH phase (negative chart values) is released back into indoor environment (positive chart values). It partially continues to travel further into the wall. This process repeats itself until moisture flux through inside surfaces stabilises. The final offset of mean values of displayed curves thus represents amount of moisture absorbed within wall components due to their hygric inertia. Fig. 58 shows courses of cumulative amount of transferred moisture at the end of first simulation month, which already represent values of stabilised moisture flux cycles. To assess moisture-buffering potential of other potential surface RNBM, two additional wall components were defined (see 4.4.3). Components (B-) and (D-) are displayed in Fig. 58 with dot-and-dash line.

$MBV_{simul}$  resulting from Fig. 58 is summarised for all studied components in Fig. 59. It can be observed that the highest values of  $MBV_{simul}$  were obtained for components (F), (G) and (H), which are all plastered with cement-lime plaster MVR Uni. It was already stated that MVR Uni plaster was designed to have high moisture buffering capability. This simulation therefore confirms this material quality.

The three conventional components (F, G and H) were also simulated with regular cement-lime plaster (from Fraunhofer IBP database) in order to compare  $MBV_{simul}$  of common cement-lime plaster with MVR Uni. It was found out that  $MBV_{simul}$  is approximately 30 % lower for common cement-lime plaster in all simulated cases ( $\sim 1.75 \text{ g}/(\text{m}^2 \%_{\text{RH}})$ ). This value is interestingly still comparable to  $MBV_{simul}$  of unplastered loam-based components (E and D-) ( $\sim 1.90 \text{ g}/(\text{m}^2 \%_{\text{RH}})$ ) and it is even higher than  $MBV_{simul}$  of wall components internally finished with loam plaster (C and D) ( $\sim 1.47 \text{ g}/(\text{m}^2 \%_{\text{RH}})$ ). High moisture buffering potential of loam-based materials discussed in section 2.2.1.3 is thus not supported by this theoretical simulation experiment.

High moisture buffering potential was, on the other hand, confirmed for wall systems made of hempcrete (B and B-,  $\sim 2.40 \text{ g}/(\text{m}^2 \%_{\text{RH}})$ ).  $MBV_{simul}$  is almost the same for both unplastered component and component plastered with lime plaster. This supports the claim that hempcrete (and hemp in general) possesses similar hygroscopic qualities as lime, which makes hemp and lime function in hygroscopic symbiosis.

Components (A) and (I) do not show considerably high  $MBV_{simul}$ , similarly like in case of  $MBV_{ideal}$  (see 5.1.2). It is due to very high  $\mu$ -factor of spruce wood in radial direction (component (A)) and low hygroscopicity of gypsum board (component (I)).

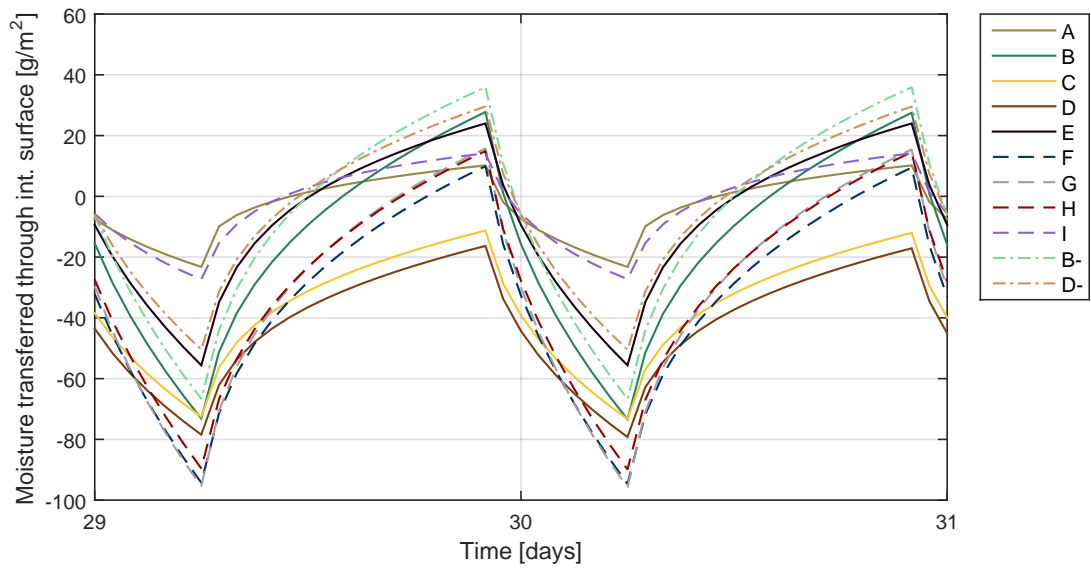


**Fig. 58:** Amount of moisture (cumulative) transferred through inside surface of wall systems as result of indoor moisture cycles

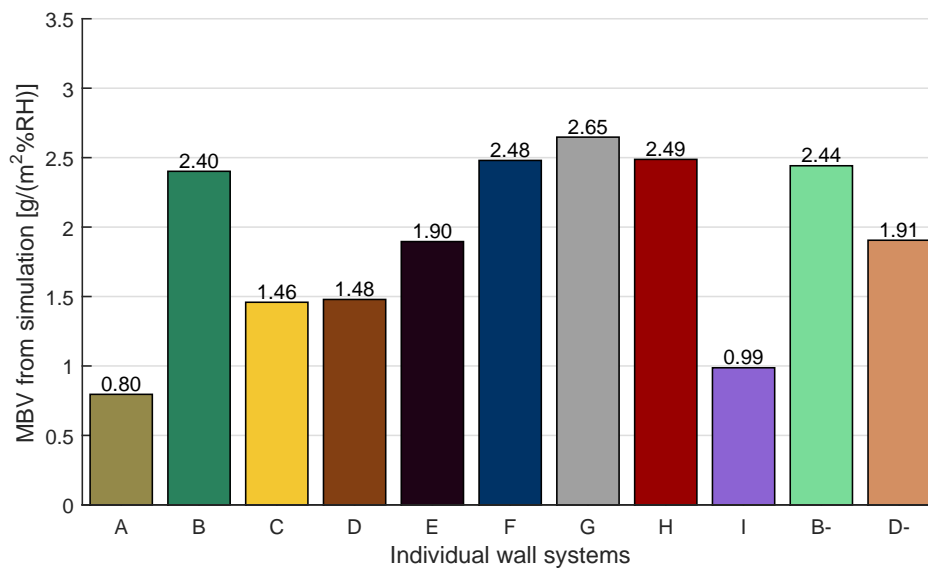


**Fig. 59:** Simulated inside moisture buffer value of studied wall systems -  $MBV_{simul}$

Concept of MBV was developed to assess potential of materials to buffer RH variation throughout diurnal RH cycles. Its absolute values are not considered relevant as they depend on assumed boundary conditions. Rode *et al.* (2005) consider relative comparison between materials more valuable and define for this purpose five classes of  $MBV_{practical}$  (negligible to excellent, see Appendix A). As this work uses concept of  $MBV_{simul}$ , which simulates  $MBV_{practical}$ , only relative comparison between materials is considered important.

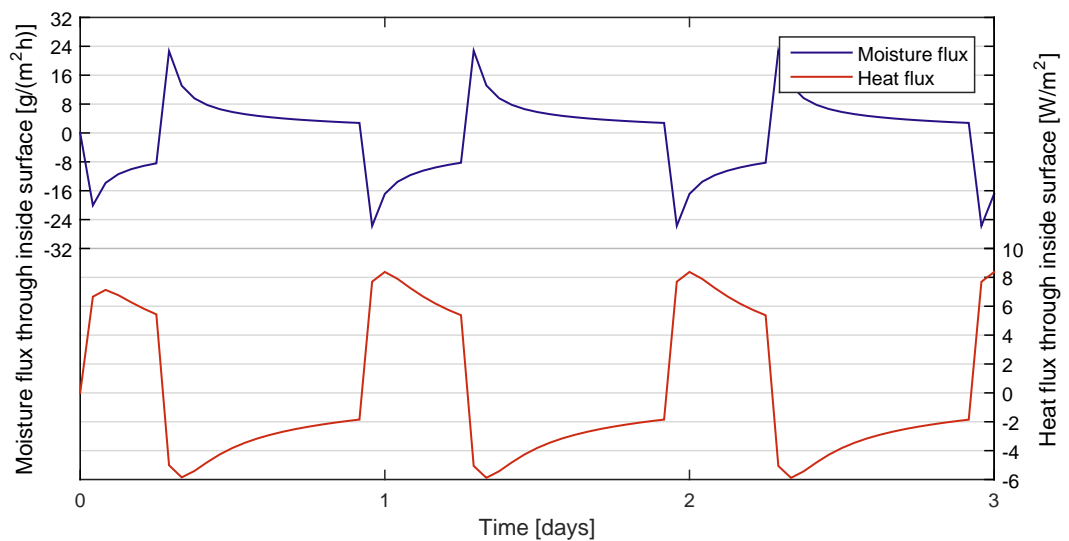
Tab. 11 shows both absolute and relative comparison of analytically computed  $MBV_{ideal}$  and simulated  $MBV_{simul}$ . As it was discussed in section 2.1.2.6,  $MBV_{ideal}$  reaches higher

values than  $MBV_{simul}$ . Relative comparison seems to be in good agreement with exception of components finished with cement-lime plaster. Those components have much lower  $MBV_{ideal}$  than lime plaster and hempcrete finishes, but their  $MBV_{simul}$  is higher. This is most likely caused by different shape of moisture storage functions of these materials, which is not taken into consideration in case of  $MBV_{ideal}$ . Also,  $MBV_{ideal}$  does not take into consideration additional wall layers which might still be within hygric penetration depth and thus influence  $MBV_{simul}$  (e.g. different  $MBV_{simul}$  between components (F) and (G)). Values in Tab. 11, however, suggest that  $MBV_{ideal}$  is useful parameter giving considerably reliable picture of relative moisture-buffering potential within studied set of materials.

**Tab. 11:** Comparison of absolute and relative values of ideal and simulated MBV

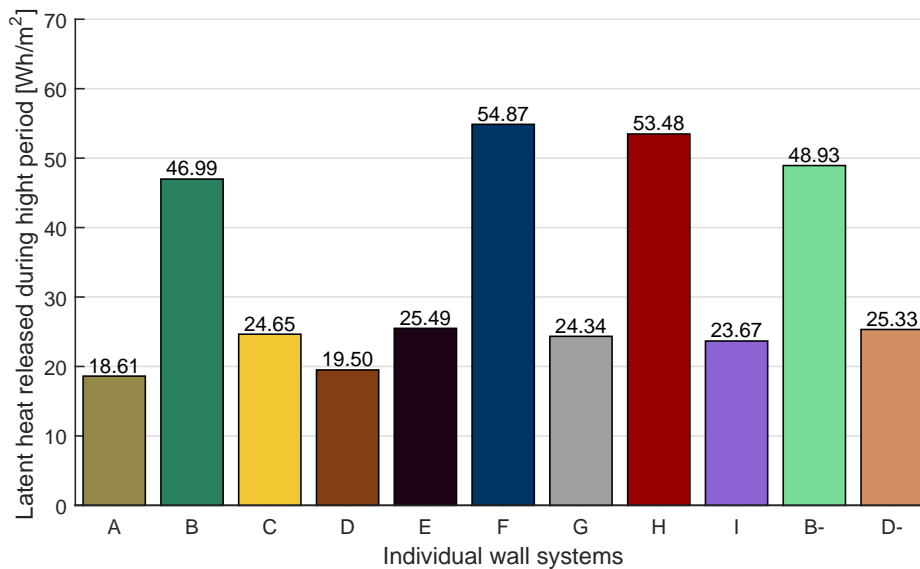
	A	B	C	D	E	F	G	H	I	B-	D-
<i>Absolute</i> [ $g/(m^2\%RH)$ ]											
$MVB_{ideal}$	1.01	3.43	1.86	1.86	2.63	2.88	2.88	2.88	1.26	3.60	2.61
$MBV_{simul}$	0.80	2.40	1.46	1.48	1.90	2.48	2.65	2.49	0.99	2.44	1.91
<i>Relative</i> [%]											
$MVB_{ideal}$	28	95	52	52	73	80	80	80	35	100	73
$MBV_{simul}$	30	91	55	56	72	94	100	94	37	92	72

Fig. 60 shows relation between moisture and heat flux through inside surface of reference component (F). It can be seen that as moisture adsorbs inside the pores of component's surface material it releases heat, which fluxes through inside surface of the component. This heat flux represents latent heat generated by adsorption of water molecules (see section 2.1.2.3).



**Fig. 60:** Relation between moisture and heat flux transferred through inside surface of component (F)

Latent heat released through inside surface during high RH period is for all components illustrated in Fig. 61. Interestingly, its value is not dependent only on  $MBV_{simul}$  as expected. It is high for components with high  $MBV_{simul}$  and lower thermal conductivity principal material layer (B, F, H and B-). The explanation is apparent. While components with high generation of latent heat and high thermal conductivity principal material layer conduct generated latent heat inside the wall, the previously mentioned components release generated latent heat through inside wall surface as it is not easily conducted within the wall. Spaces adjacent to wall components (B), (F), (H) and (B-) thus can be expected to have considerably higher thermal regulation caused by latent heat affect. However, heat release of about  $50 \text{ Wh/m}^2$  is not likely to be reached in reality due to extreme boundary conditions of this simulation scenario.



**Fig. 61:** Latent heat released through inside surface of wall systems during night period (8 hours) of the moisture cycle

Maximal increase of inside surface temperature of components during high RH phase of the moisture cycle (absorption) is shown in Fig. 62. It can be observed that components with high latent heat release (Fig. 61) present also high inside surface temperature variation. This confirms the discussed potential of hygroscopic materials with distinct latent heat effect to contribute to higher thermal comfort feeling (see section 2.1.2.3).

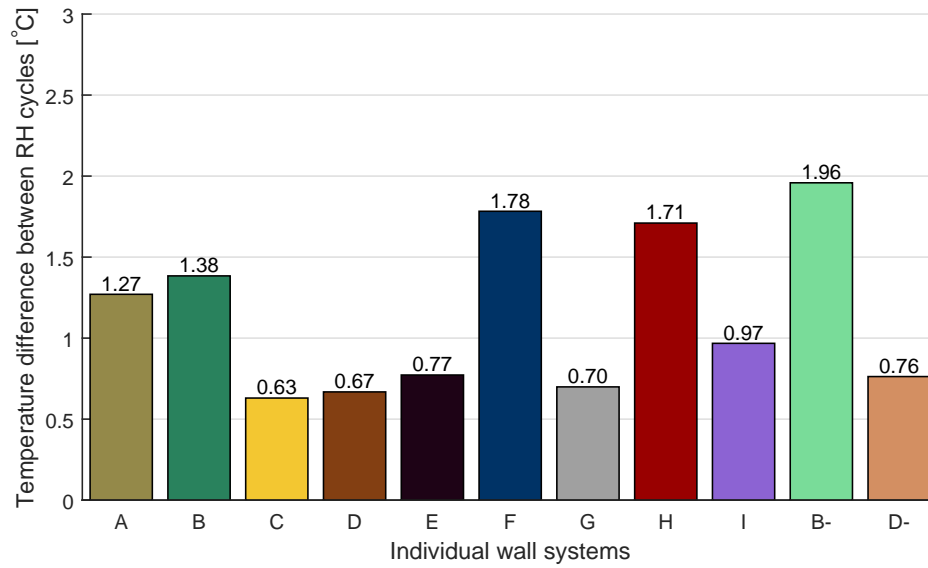


**Fig. 62:** Maximal temperature change of inside surfaces of wall systems during one RH cycle

### 5.3.4 Summary of results (theoretical simulations)

Tab. 12 shows summary of previously discussed theoretical simulations. The best thermal potential was achieved for wall systems (A), (B), (E) and (H) (light background of all four studied thermal parameters). Light wall system (I) (and partly light wall system (C) and low thermal inertia wall system (G)) is on the other hand expected to perform poorly in transient thermal environment (darkest background of all four studied parameters).

**Tab. 12:** Summary of theoretical simulation results (grey scale from light background (favourable values) to dark background (unfavourable values))

Component	thickness [m]	$t_{s-s}$ [h]	$Q_{24h}$ [%]	$phs$ [h]	$dmp$ [%]	$MBV_{simul}$ [g/(m <sup>2</sup> %RH)]	Latent heat release [Wh/m <sup>2</sup> ]	Inside surface temperature change [°C]
A	0.364	133.5	3.06	21.0	97.74	0.80	18.61	1.27
B	0.518	182.0	0.57	27.0	99.45	2.40	46.99	1.38
C	0.340	36.5	33.64	12.0	77.40	1.46	24.65	0.63
D	0.415	94.5	10.26	16.0	93.41	1.48	19.50	0.67
E	0.459	141.5	4.45	19.0	96.40	1.90	25.49	0.77
F	0.390	81.5	10.04	17.0	93.74	2.48	54.87	1.78
G	0.365	69.0	31.42	8.0	84.54	2.65	24.34	0.70
H	0.480	115.5	4.05	20.5	97.28	2.49	53.48	1.71
I	0.195	8.0	83.84	3.0	14.43	0.99	23.67	0.97
B-						2.44	48.93	1.96
D-						1.91	25.33	0.76

As discussed in section 5.2, hygric simulation results show increased sensitivity to quality of material input data. It is therefore important to take this into consideration when drawing hygric simulation conclusions. Inside moisture buffering theoretical simulation,

however, primarily relies on hygric simulation within surface layer of component, which was evaluated to have standard deviation of sensitivity error  $\sigma$  of 1.8 % RH (see Tab. 10). The previously presented results of  $MBV_{simul}$  are therefore considered relevant.

The main conclusion of theoretical hygric simulations is poor moisture-buffering potential of loam-based materials when compared with conventional finishing materials. The best combination of high  $MBV_{simul}$  and generated latent heat (inside surface temperature change) was simulated for wall components (F, H, B and B-).

When considering both thermal and hygric simulation results, components (H) and (B) present the highest resistance towards outside transient hygrothermal environment. Those two components are, on the other hand, the thickest wall components considered in this work.

## 5.4 Hygrothermal performance of wall systems under reference year

### 5.4.1 Thermal performance

Cumulative amount of heat transferred through one square meter of the studied wall components (inside surface) during reference years of different climates is shown in Fig. 63. It can be observed that majority of the wall components transfer heat in similar amounts regardless of reference climate or wall orientation. Considerably different amount of transferred heat can only be observed for wall system (I) and in certain cases for wall systems (F) and (H).

As expected, heat transfer through wall system (I), which has minimal thermal mass and presented the worst results in simulation under theoretical thermal conditions, does not deviate from the steady-state heat transfer calculation significantly (green dot-and-dash line in Fig. 63, Prague and Serak). This consequently results in higher annual heat loss when compared to higher thermal mass wall components. The only exception to this are wall systems (F) and (H), which, despite their higher thermal mass, transfer in certain cases (windward wall orientation in high precipitation climates) even more heat than wall system (I). It is due to combination of high *liquid transfer coefficients*  $D_{ws}$ ,  $D_{ww}$  and high dependency of *thermal conductivity*  $\lambda$  upon *moisture content*  $w$ , which are characteristic for AAC and perforated brick materials (see Appendix C). When material with such parameters is exposed to liquid water supply (e.g. wind driven rain), it swiftly transports this water deeper into the material, which causes local rise of  $w/c$  and subsequent degradation of insulating capabilities of the material. The *actual thermal conductivity*  $\lambda$  of such materials can thus often be higher than *design thermal conductivity*  $\lambda_d$ , which may lead to substantially higher annual heat losses than predicted by steady-state calculation (see Fig. 63, Vienna W and Serak W).

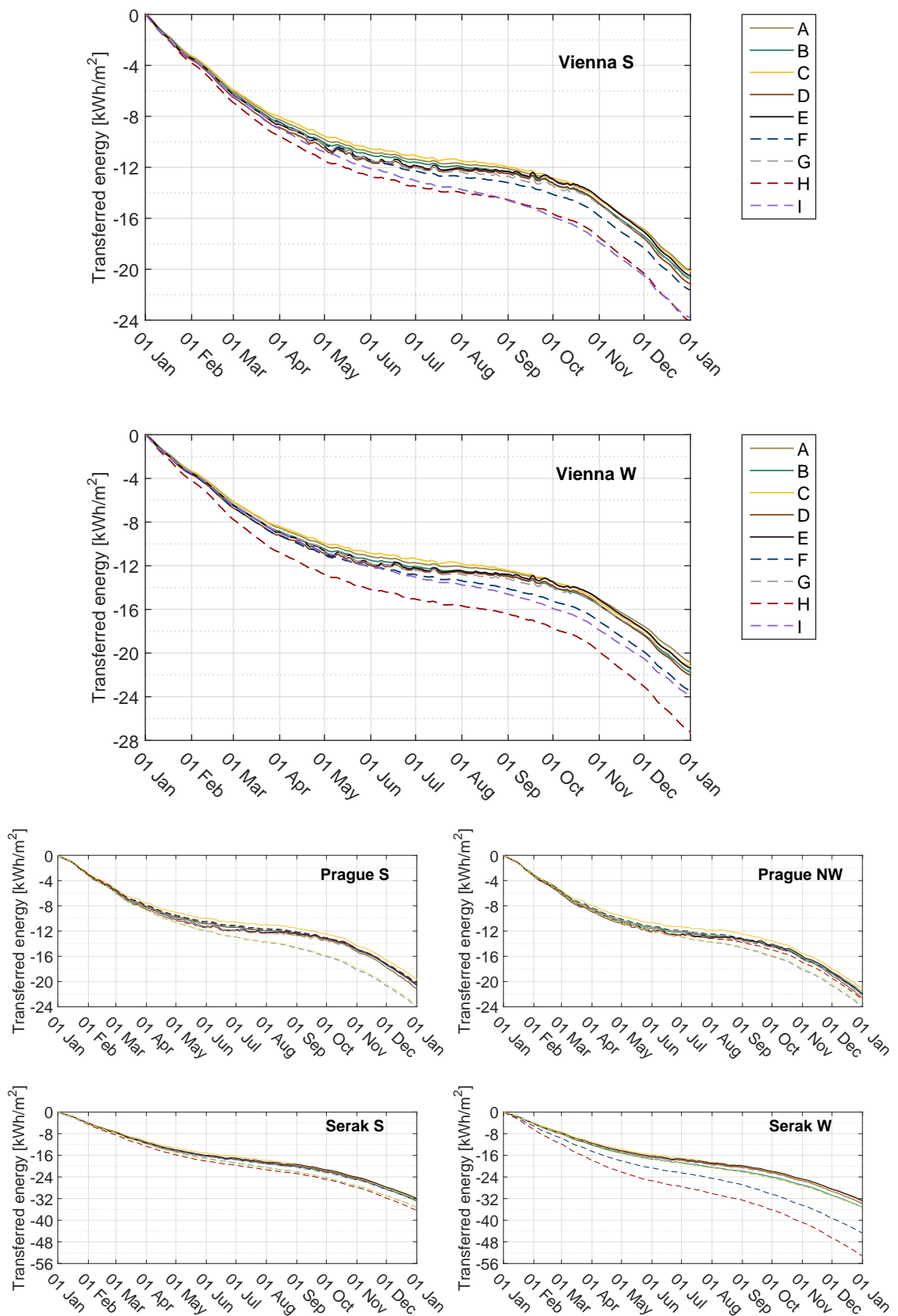


**Fig. 63:** Cumulative amount of heat transferred through inside surface of studied wall systems during 10<sup>th</sup> year of simulation for different locations and wall orientations (together with theoretically transferred heat when permanent (steady-state) heat transfer assumed: green dot-and-dash line)

Absolute [ $kWh/(m^2a)$ ] and relative [%] (with respect to heat loss of permanent (steady-state) heat transfer scenario (Prague, Serak) / heat loss through wall component (I) (Vienna)) values of annual heat losses through the wall components simulated under different climates and orientations are listed in Tab. 13.

**Tab. 13:** Overall annual heat losses (together with heat losses/gains during heating/cooling season) through inside surface of studied wall systems of different orientation and location. Relative values represent percentage of transferred heat with respect to permanent (steady-state) heat transfer scenario - P.t. (heat transferred through wall component (I) in case of Vienna climate). Grey scale - light background (favourable values) to dark background (unfavourable values).

	A	B	C	D	E	F	G	H	I	P. t.
<i>Annual heat losses</i>										
<b>Prague</b>										
S [ $kWh/m^2$ ]	20.3	20.6	19.6	21.2	20.6	20.2	20.9	20.3	24.0	23.7
S [%]	85.7	86.9	82.7	89.5	86.9	85.2	88.2	85.7	101.3	
NW [ $kWh/m^2$ ]	21.6	22.0	21.1	22.6	21.9	21.9	22.2	22.8	24.0	23.8
NW [%]	90.8	92.4	88.7	95.0	92.0	92.0	93.3	95.8	100.8	
<b>Serak</b>										
S [ $kWh/m^2$ ]	31.8	32.6	31.6	33.0	32.0	32.8	32.8	36.4	35.2	35.2
S [%]	90.3	92.6	89.8	93.8	90.9	93.2	93.2	103.4	100.0	
W [ $kWh/m^2$ ]	32.5	35.2	32.9	33.8	32.8	44.7	33.6	53.2	35.2	35.3
W [%]	92.1	99.7	93.2	95.8	92.9	126.6	95.2	150.7	99.7	
<b>Vienna</b>										
S [ $kWh/m^2$ ]	20.1	20.8	20.2	21.2	20.5	21.7	20.8	24.1	23.8	-
S [%]	84.5	87.4	84.9	89.1	86.1	91.2	87.4	101.3	100.0	
W [ $kWh/m^2$ ]	20.8	21.8	21.2	22.0	21.4	23.5	21.6	27.2	23.8	-
W [%]	87.4	91.6	89.1	92.4	89.9	98.7	90.8	114.3	100.0	
<i>Heat losses during heating season (Out. <math>T \leq 16^\circ C</math>)</i>										
<b>Prague</b>										
S [ $kWh/m^2$ ]	17.6	17.9	16.9	18.3	17.6	17.5	17.5	17.5	20.4	20.3
S [%]	86.7	88.2	83.3	90.1	86.7	86.2	86.2	86.2	100.5	
NW [ $kWh/m^2$ ]	18.5	18.9	18.0	19.3	18.6	18.7	18.5	19.5	20.4	20.3
NW [%]	91.1	93.1	88.7	95.1	91.6	92.1	91.1	96.1	100.5	
<b>Serak</b>										
S [ $kWh/m^2$ ]	27.7	28.5	27.3	29.3	28.3	28.4	28.6	31.6	30.1	30.2
S [%]	91.7	94.4	90.4	97.0	93.7	94.0	94.7	104.6	99.7	
W [ $kWh/m^2$ ]	28.4	30.6	28.4	30.0	29.1	38.2	29.3	45.7	30.1	30.2
W [%]	94.0	101.3	94.0	99.3	96.4	126.5	97.0	151.3	99.7	
<i>Heat gains during cooling season (Out. <math>T &gt; 25^\circ C</math>)</i>										
<b>Prague</b>										
S [ $kWh/m^2$ ]	0.20	0.22	0.07	0.28	0.36	0.15	0.33	0.18	-0.19	-0.20
S [%]	-100.0	-110.0	-35.0	-140.0	-180.0	-75.0	-165.0	-90.0	95.0	
NW [ $kWh/m^2$ ]	0.24	0.26	0.13	0.31	0.38	0.18	0.39	0.24	-0.19	-0.20
NW [%]	-120.0	-130.0	-65.0	-155.0	-190.0	-90.0	-195.0	-120.0	95.0	

Effect of thermal mass (diffusivity) can be most distinctively observed in case of wall components oriented to south and simulated under Prague reference year (minimum amount of received wind driven rain, see Fig. 64 A).

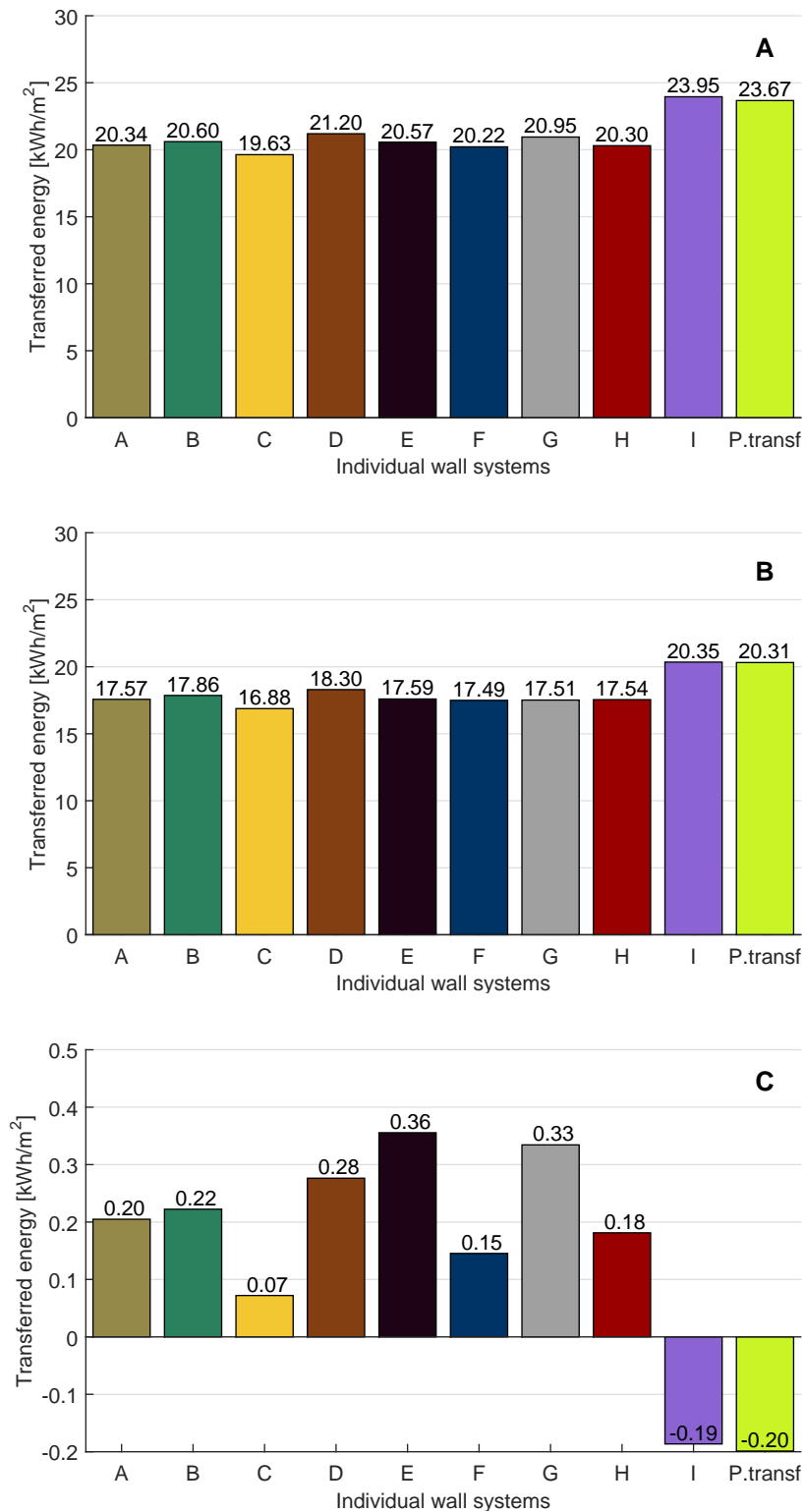


**Fig. 64:** Overall heat losses through inside surfaces of studied wall systems during reference year (A), winter (heating) days (B) and summer (cooling) days (C) in Prague (South orientation)

As already mentioned the difference in annual heat losses through components (A-H) is not very significant. The highest encountered deviation was observed between wall systems (C) and (D) -  $1.6 \text{ kWh}/(\text{m}^2\text{a})$ , being less than 7 % of the permanent (steady-state) heat transfer scenario. The difference between components (C) and (I) was about  $4.3 \text{ kWh}/(\text{m}^2\text{a})$ , corresponding to more than 18 % of the permanent (steady-state) heat transfer scenario. Similar results can be observed for southward oriented wall components simulated under Vienna and Serak climates (with exception of component (H), which is affected by higher precipitation rate). Those results suggest that effect of thermal mass (diffusivity), which was previously found to affect amount of heat transferred through walls in transient thermal environment (5.3.1), does not play a very significant role, when considering low U-value wall systems in Central European climate. The only exception is wall system (I) with no thermal accumulation layer. This is most likely due to character of the studied climate (non-continental climate with low diurnal temperature variations) in combination with high insulation quality of the walls (outside temperature variations does not penetrate all the way through the walls (see section 5.3.2, Fig. 55)). Fig. 55 also should explain higher annual heat loss through wall component (I).

Effect of the above discussed hygric parameters influencing overall annual heat transfer through the components is most distinct in case of westward oriented walls simulated under Viennese and Serak climate (substantial amount of received wind driven rain). The difference in heat transferred through components (F) and (H) and other considered wall systems is respectively up to  $2.7 \text{ kWh}/(\text{m}^2\text{a})$  (11.3 %) and  $6.4 \text{ kWh}/(\text{m}^2\text{a})$  (26.9 %) in Viennese climate and up to  $12.2 \text{ kWh}/(\text{m}^2\text{a})$  (34.5 %) and  $20.7 \text{ kWh}/(\text{m}^2\text{a})$  (58.6 %) in extreme climate of Serak. These differences are already substantial and those wall systems should be installed in such locations with roof overhangs or cladding systems to prevent this degradation of insulating quality of the walls.

Tab. 13 also lists heat losses/gains through the wall components during heating and cooling season (defined in section 4.5.1.1). Relative values of heat losses during heating season resemble previously discussed relative values of annual heat losses. This shows that heat transferred through wall components during non-heating season does not significantly influence the overall character of annual heat transfer. Amount of heat transferred through wall components during cooling season is thus marginal when compared to amount of heat transferred through components during heating season (Central European climate has high number of heating degree days and low number of cooling degree days).

In addition it was found out that majority of the wall systems transfer heat during cooling season mostly in outward direction (see Fig. 64 C), despite the fact of outside temperature being higher than inside temperature. This is due to effect of thermal inertia, which reduces overall heat transfer during cooling season. Fig. 64 C thus shows how well perform the individual wall systems in terms of thermal comfort feeling.

Influence of wind driven rain and direct sun radiation upon heat transfer through the wall systems in Viennese climate (southward orientation) is shown in Figs. 65 and 66.

Those figures show evolution of cumulative difference in heat transfer between reference simulation case and respective cases where no absorption of wind driven rain and no short/long wave absorptivity are assumed (e.g. wall construction with outside cladding). As discussed, wind driven rain causes higher heat transfer through components. The maximal difference between reference and new case can be observed in case of wall systems (F) –  $1.7 \text{ kWh}/(\text{m}^2\text{a})$  and (H) –  $4 \text{ kWh}/(\text{m}^2\text{a})$ , which accounts respectively for about 8 % and 17 % of the overall annual heat transfer. Heat transfer through the other wall components is influenced marginally. When assessing effect of direct sun radiation (Fig. 66), it can be observed that the direct sun radiation prevents annual heat loss of  $3 - 3.3 \text{ kWh}/(\text{m}^2\text{a})$  for most of the wall systems. In case of wall system (H) makes direct sun radiation even more significant difference ( $4.2 \text{ kWh}/(\text{m}^2\text{a})$ ), as it causes higher evaporation of absorbed rain water and consequent better insulation quality of the wall. Wall system (I) receives no sun radiation due to its outside cladding layer.

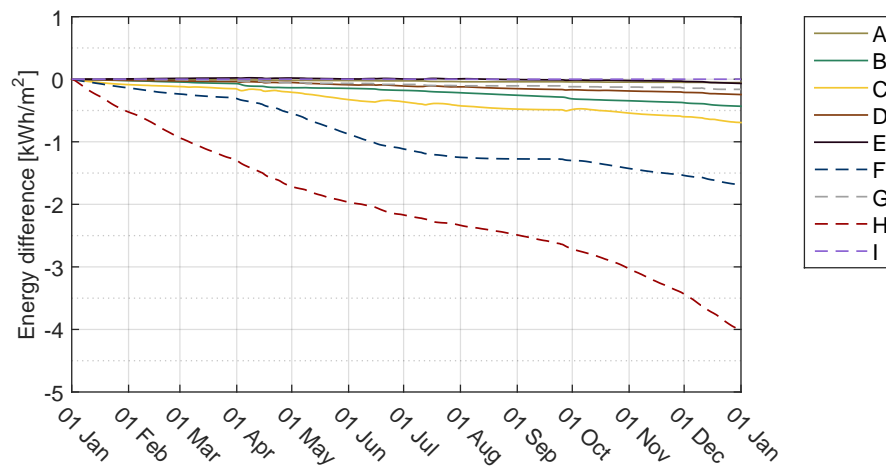


**Fig. 65:** Difference (cumulative) in heat transferred through inside surfaces of studied wall systems between reference case and case when no absorption of driving rain is assumed. Simulation case - Vienna South

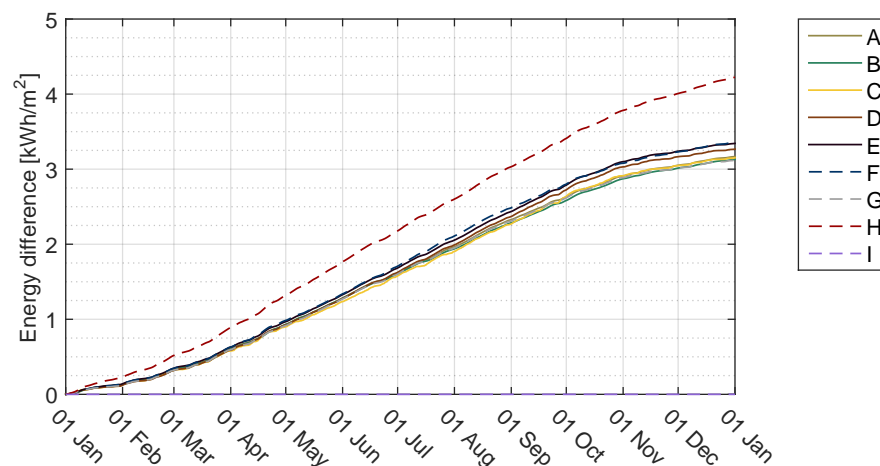


**Fig. 66:** Difference (cumulative) in heat transferred through inside surfaces of studied wall systems between reference case and case when no short/long wave radiation absorptivity is assumed. Simulation case - Vienna South

Heat flux through inside surface of studied components during selected two-week periods (winter, spring and summer) together with interior and exterior temperature is displayed in Fig. 67. Transient thermal effects discussed in (5.3.2) (damping and phase-shift) are clearly apparent in figures. The overall character of the heat flux, however, follows very irregular patterns due to complexity of combined hygrothermal phenomena. Conclusions are thus harder to draw and are restricted to clearly visible patterns.

Based on the character of heat flux can be studied wall systems divided into three groups:

1. lightweight wall systems (C and I)
2. wall systems composed of only one layer (excluding finishing layers) having both insulation and thermal mass (A, B, F and H)
3. wall systems with both insulation and accumulation layers (D, E and G)

When focusing on regular patterns in Fig. 67 (irregularities are mostly caused by events like rain, sudden change in outside temperature or their combination), heat flux through inside surface of wall systems (C) and (I) clearly shows diurnal fluctuations caused by day/night outside temperature variations. This can be also observed during wintertime in case of wall system (G). These results directly correlate with theoretical results displayed in Fig. 55, which confirms the concept of this theoretical simulation (thermal cycles in outside environment) to be useful. Thermal phase shift also seems to correlate with this theoretical simulation ( $\sim 12$  hrs (C),  $\sim 8$  hrs (G),  $\sim 3$  hrs (I)). The ideal thermal phase shift ( $\sim 12$  hrs) of component (C) is believed to be the main reason for its excellent overall thermal performance. Fig. 67 C also shows that evolution of heat flux through component (C) counteracts evolution of outside temperature, which shows a good potential for thermal buffering of interior climate during summer time (better thermal comfort).

Similarly like in Fig. 55, thermal phase shift and damping of non-lightweight wall components (group 2 and 3) is too high to be distinguished in Fig. 67. The difference between wall components of group 2 and 3 is mostly in reaction of heat flux to irregular evolution of inside temperature. While heat flux through inside surface of components with insulation layer (group 3) reacts to changes in inside temperature rather sensitively (instant high values after the change), heat flux through the other set of components (group 2) shows smaller reaction to these changes (lower values after the change). This can be explained by difference in thermal conductivities between high density accumulation inside wall layers of group 3 and medium density wall layers of group 2 (having both insulation and accumulation function). When indoor temperature decreases, the accumulated heat flows inwards in higher amounts through layers with higher thermal conductivity (group 3). Wall components (D, E and G) thus provide more stable indoor temperature conditions than the other studied wall systems (better comfort feeling).

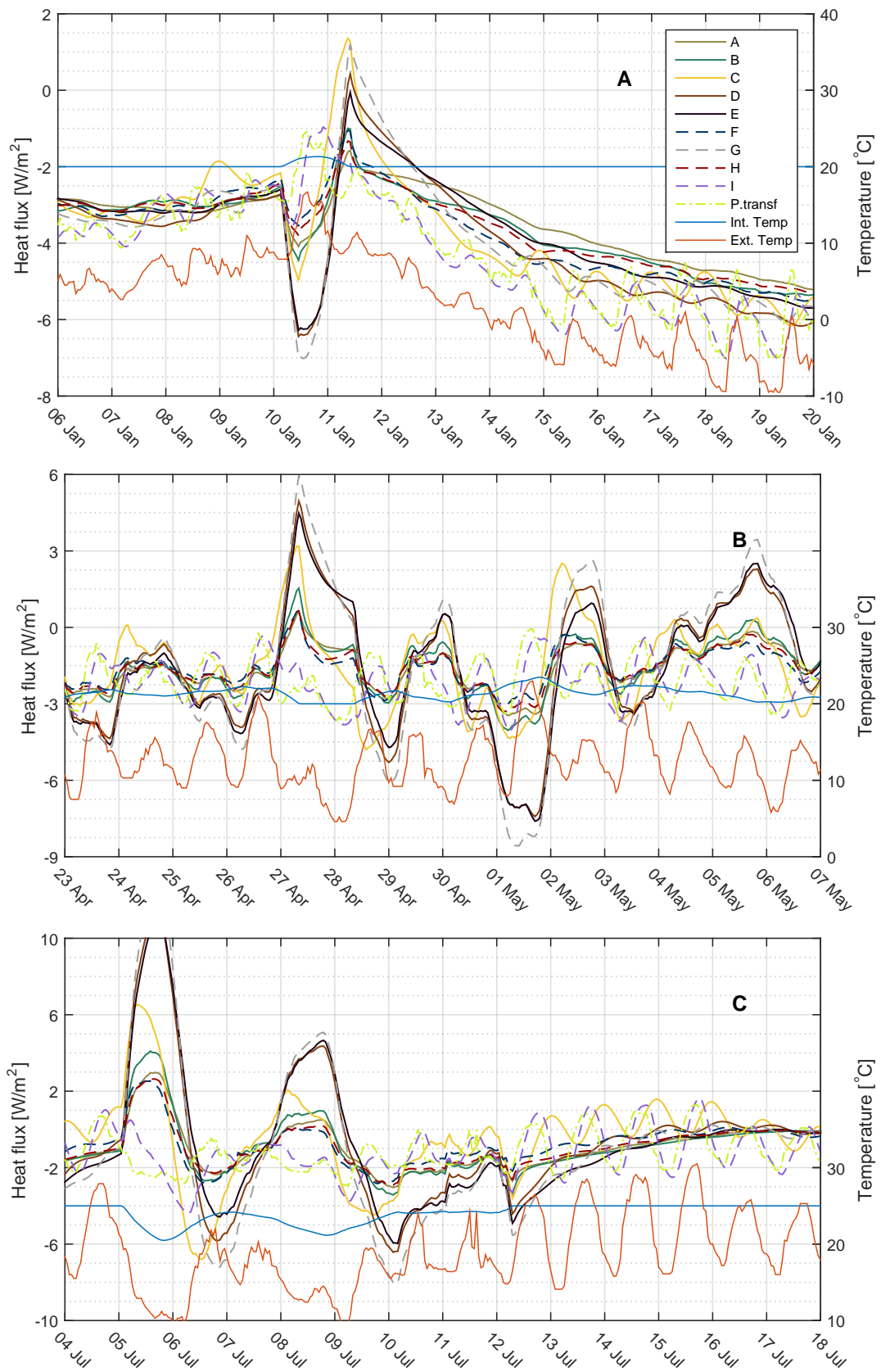


**Fig. 67:** Heat flux through inside surfaces of studied wall systems situated in Prague (south orientation) together with their external and internal ambient air temperature during selected winter (A), spring (B) and summer (C) two week periods (negative values represent heat flow from in to out).

## 5.4.2 Hygic performance

### 5.4.2.1 Existence of annual moisture accumulation phenomenon inside walls

As described in section 4.5.1.2, annual moisture balance was assessed for all the performed combinations of simulation (studied wall systems under different outside/inside climates and wall orientations). It was found out that none of the performed simulations showed residual condensation at the end of simulation year. None of the studied wall systems thus gradually accumulates moisture in transient hygrothermal environment of the selected locations, which proves those wall systems to have been suitably designed for these locations.

### 5.4.2.2 Moisture-buffering effect (MBE)

Cumulative amount of moisture transferred through inside surface of studied wall systems during 10<sup>th</sup> year of simulation is displayed in Fig. 68 for two extreme hygic simulation cases (southward orientation in Prague – driest case, and westward orientation in Serak – wettest case).

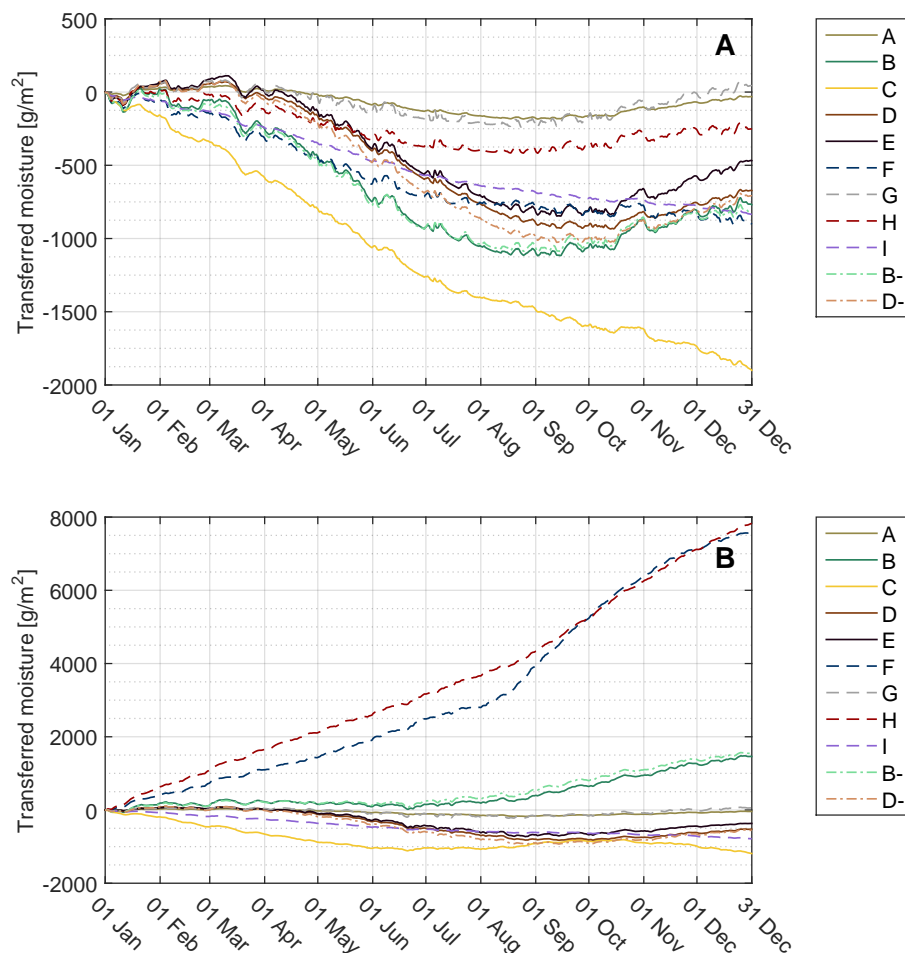


**Fig. 68:** Cumulative amount of moisture transferred through inside surfaces of studied wall systems during 10<sup>th</sup> year of simulation for Prague - south orientation (A) and Serak - west orientation (B) (negative values represent moisture flow from inside to outside).

It can be observed that in Prague climate (south orientation) flows moisture through most of the wall systems in principal outward direction during spring and summertime (March - August) and in principal inward direction during the rest of year. This directly relates to evolution of mean outside RH in Prague reference year, which gradually decreases from February to June and increases from July to January. The only exceptions to this are lightweight wall systems (C) and (I), which show outward principal direction of moisture flux throughout the simulation year. Short-term fluctuations in moisture flux are also clearly visible for all the wall components with exception of components (A) and (I) (Fig. 68 A). This is an expected phenomenon as components (A) and (I) have the lowest  $MBV_{simul}$  out of the studied wall systems (see 5.3.3).

Situation in Serak climate (west) is diametrically different due to high amount of incident rain upon outside wall surfaces. Wall systems, which are affected by this phenomenon and transfer high amount of moisture in inward direction are respectively wall systems (H) and (F) and partly wall systems (B) and (B-).

Overall amount of moisture transferred through inside surface of wall systems (in both directions) for different locations and orientations is summed up in Fig. 69. It is important to note that this sum of transferred moisture includes both short-term reactions of inside surface layer to indoor RH fluctuations and long-term moisture transfer caused by gradient between indoor and outdoor RH. Those phenomena happen simultaneously and cannot be separated one from another in case of real climate simulations.

When we compare Figs. 68 (A) and 69 (Prague S), which both represent the same simulation, we can see certain parallels. E.g. components (C) and (I) transfer much more moisture in outward direction or component (A) performs the lowest overall moisture transfer. On the other hand components (G) and (H), which show low annual cumulative moisture transfer in Fig. 68 A, show very high overall annual moisture transfer in Fig. 69 (Prague S) (relatively to other wall components). This suggests that short-term moisture flux fluctuations represent (when existent) higher share of overall moisture transfer through inside surface of walls (Fig. 69) than long-term moisture flux fluctuation.

MBE was thus decided to be assessed through comparison of lesser value of sum of annual moisture transfer through inside surface of the wall systems (non-principal moisture transfer direction, which is influenced less by long-term moisture flux fluctuations). Those final values are summed up for all simulated cases in Tab. 14.

When we compare relative performance of wall components in Tab. 14 (Prague), we can see that components with high MBV (see Tab. 11) transfer higher amount of moisture (higher MBE), which confirms usefulness of MBV parameter. It is, however, shown that MBV fails to predict MBE in case of exposure of components with high *liquid transfer coefficients*  $D_{ws}$ ,  $D_{ww}$  to high amount of incident rain (westward oriented wall components (F) and (H) under climate of Serak). In such case is MBE overcome by inward moisture flux caused by high amounts of liquid water transferred into material from outside surface by capillary forces.

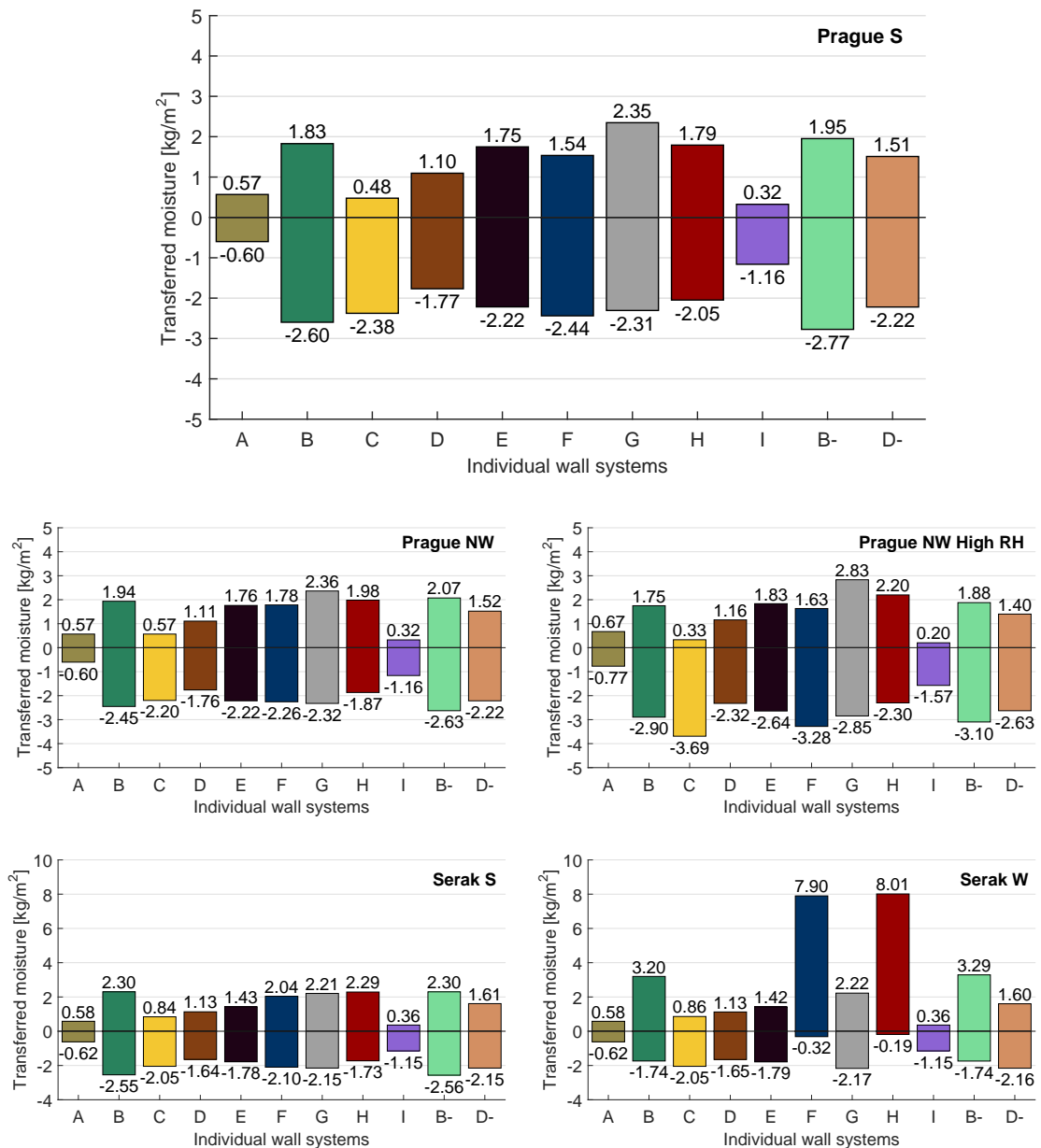


**Fig. 69:** Sum of annual moisture transferred through inside surfaces of studied wall systems for both directions of moisture flux (negative: outward moisture flow, positive: inward moisture flow) for different simulation set-ups

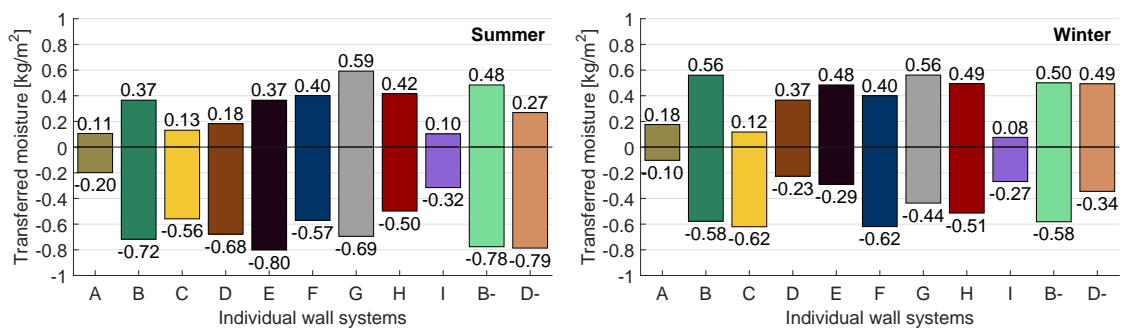


**Fig. 70:** Sum of moisture transferred through inside surfaces of studied wall systems for both directions of moisture flux during summertime (1.6. - 31.8.) and wintertime (1.12. - 28.2.) (Prague - south orientation)

Tab. 14 also shows comparison of MBE of walls exposed to high and medium inside moisture load (Prague NW vs. Prague NW - high RH) and comparison of MBE during summer (1.6. – 31.8.) and winter (1.12 – 28.2.) time (southward oriented Prague simulation case). Relative MBE of wall components remains similar for all those cases.

**Tab. 14:** Annual (seasonal) amount of moisture transferred through inside surfaces of studied wall systems in non-principal moisture flux direction representing MBE (different locations, wall orientations and time of year)

Transferred moisture [kg/m <sup>2</sup> ]	Prague			Serak		Prague - South	
	S	NW	NW - High RH	S	W	Summer	Winter
G	2.31	2.32	2.83	2.15	2.17	0.59	0.44
B-	1.95	2.07	1.88	2.30	1.74	0.48	0.50
B	1.83	1.94	1.75	2.30	1.74	0.37	0.56
H	1.79	1.87	2.20	1.73	0.19	0.42	0.49
E	1.75	1.76	1.83	1.43	1.42	0.37	0.29
F	1.54	1.78	1.63	2.04	0.32	0.40	0.40
D-	1.51	1.52	1.40	1.61	1.60	0.27	0.34
D	1.10	1.11	1.16	1.13	1.13	0.18	0.23
A	0.57	0.57	0.67	0.58	0.58	0.11	0.10
C	0.48	0.57	0.33	0.84	0.86	0.13	0.12
I	0.32	0.32	0.20	0.36	0.36	0.10	0.08

Detailed reaction of moisture flux through inside surface of wall components upon fluctuation of indoor RH is shown in form of charts (selected summer and winter periods) in Fig. 71. The previously discussed results (Tab. 14) can be verified by those charts as they show only short-term moisture flux fluctuations. Wall component (G) shows again the highest indoor moisture buffering, despite the fact that it has the same finishing layer like components (F) and (G). It is believed that this difference is caused by different  $\mu$ -factor of materials under finishing layer. While components (F) and (G) are composed of diffusion-open materials (AAC and perforated brick), which transport moisture absorbed by surface layer deeper into the component, component (G) is composed of concrete with high  $\mu$ -factor, which prevents moisture absorbed by surface layer from further diffusion into the component. Surface layer of component (G) thus holds all the absorbed moisture within itself and when indoor RH drops, it gives it back in higher amounts.

Among wall systems with high MBE can be further counted systems (B), (B-), (E) and partly (D-). Those systems show similar amplitude of heat flux fluctuation like wall systems (F) and (H). On the other hand wall systems with inside loam plaster (D and C) show much lower MBE, when compared to previously discussed group of wall systems. Wall systems (A) and (I) were confirmed to have negligible MBE, due to very high  $\mu$ -factor of spruce wood in radial direction and low  $MBV_{ideal}$  of gypsum board (see 5.1.2).

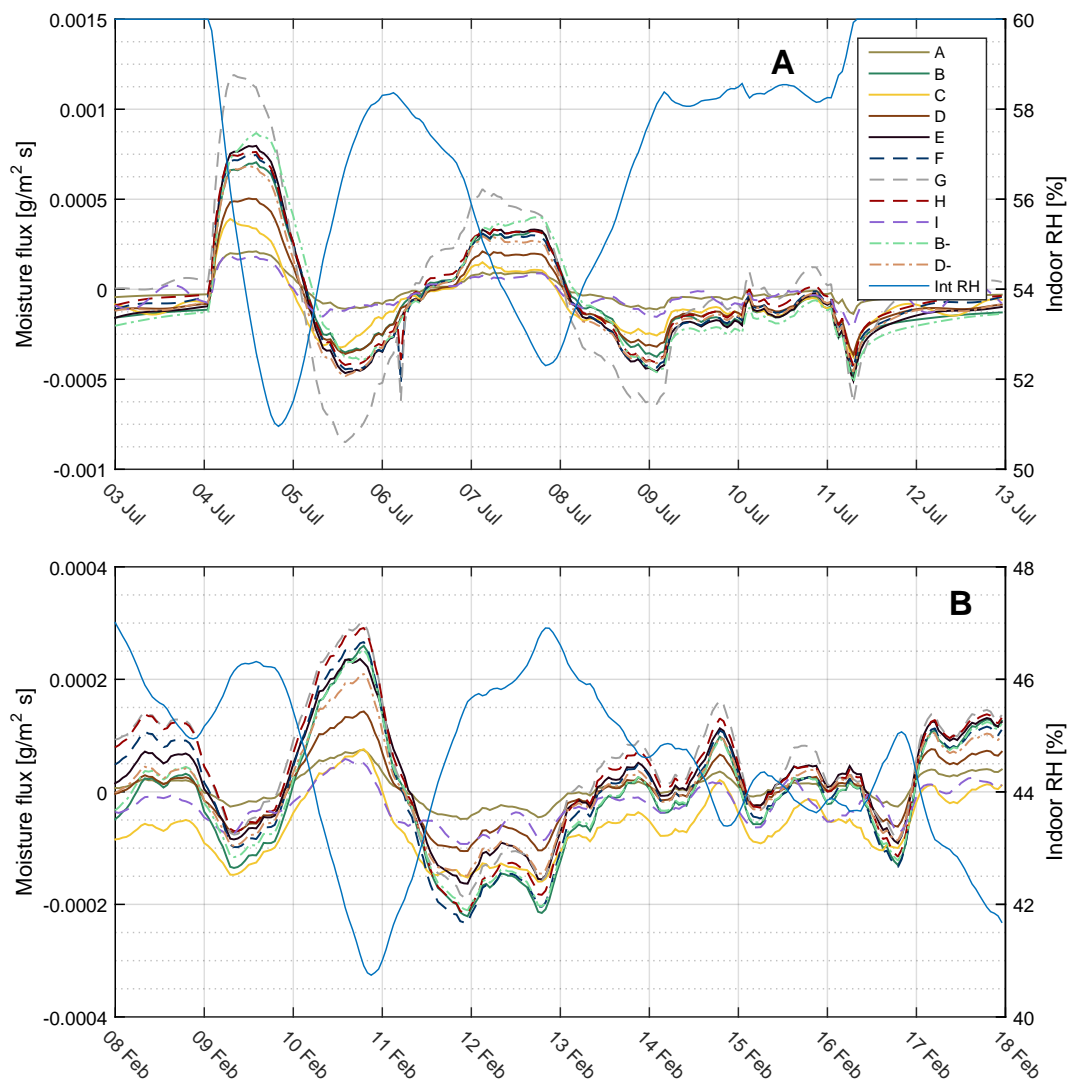


**Fig. 71:** Moisture flux through inside surfaces of studied wall systems situated in Prague (south orientation) together with indoor RH during selected summer (A) and winter (B) periods

#### 5.4.2.3 Time-of-wetness (TOW)

TOW function was computed for grid of monitoring positions (1 cm interval) throughout cross-section of studied wall systems. The resulting charts (see Fig. 72) show wall profiles of frequency of critical hygrothermal conditions (defined in section 4.5.1.2) throughout the simulation year for windward orientations of all studied locations.

The effect of different climates can be clearly seen. TOW of walls simulated under Prague climate counts for only few hundred hours per year, while TOW of walls simulated under Serak climate reaches up to 8760 hrs/year. This means that certain parts of wall systems (B), (F) and (H) are (in Serak location) exposed to critical hygrothermal conditions all year long, which makes those wall systems unsuitable for such climates. Fig. 72 also shows that, wall systems (F), (H) and (B) have considerably high range of non-zero values of TOW throughout their cross-section (when compared to the other studied wall systems), which indicates occurrence of critical hygrothermal conditions deep within the wall systems. On

the other hand, wall systems (A), (D), (E) and (G) were computed to have non-zero TOW value only in regions close to outside surface.

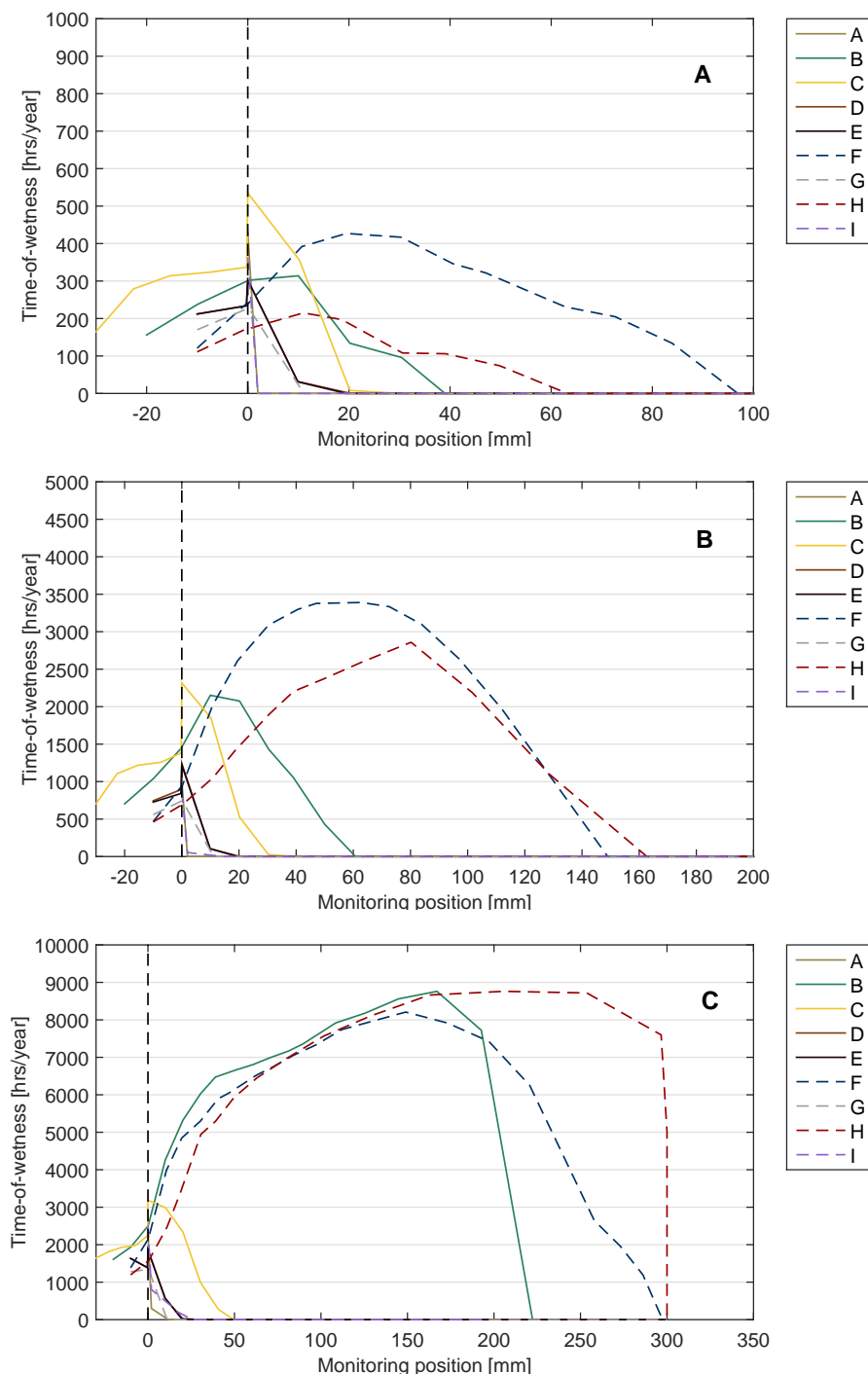


**Fig. 72:** Simulated TOW profiles: (A) Prague - NW, (B) Vienna - W, (C) Serak - W (negative monitoring position represents outside finishing layer (render) of simulated wall systems)

Outside surface of wall systems and interface of outside render and insulation layer is, however, believed to be the most vulnerable area towards atmospheric corrosion. TOW function was primarily designed for assessment of material surfaces, as those have higher oxygen supply than inside of materials. It is therefore much easier for microorganisms to

propagate on material surfaces rather than inside of materials, which rises biodegradation potential at surface region considerably. Vulnerability to potential moisture/frost straining is also higher at this region due to higher probability of freezing temperatures.

Surface TOW of individual wall systems was thus computed for monitoring position between outside render and insulation layer in case of wall systems (B-H) and for monitoring position 2 mm under outside surface in case of wall systems with no outside finishing layer (A and I). Final comparison of surface TOW of all simulated climates is shown in Fig. 73.

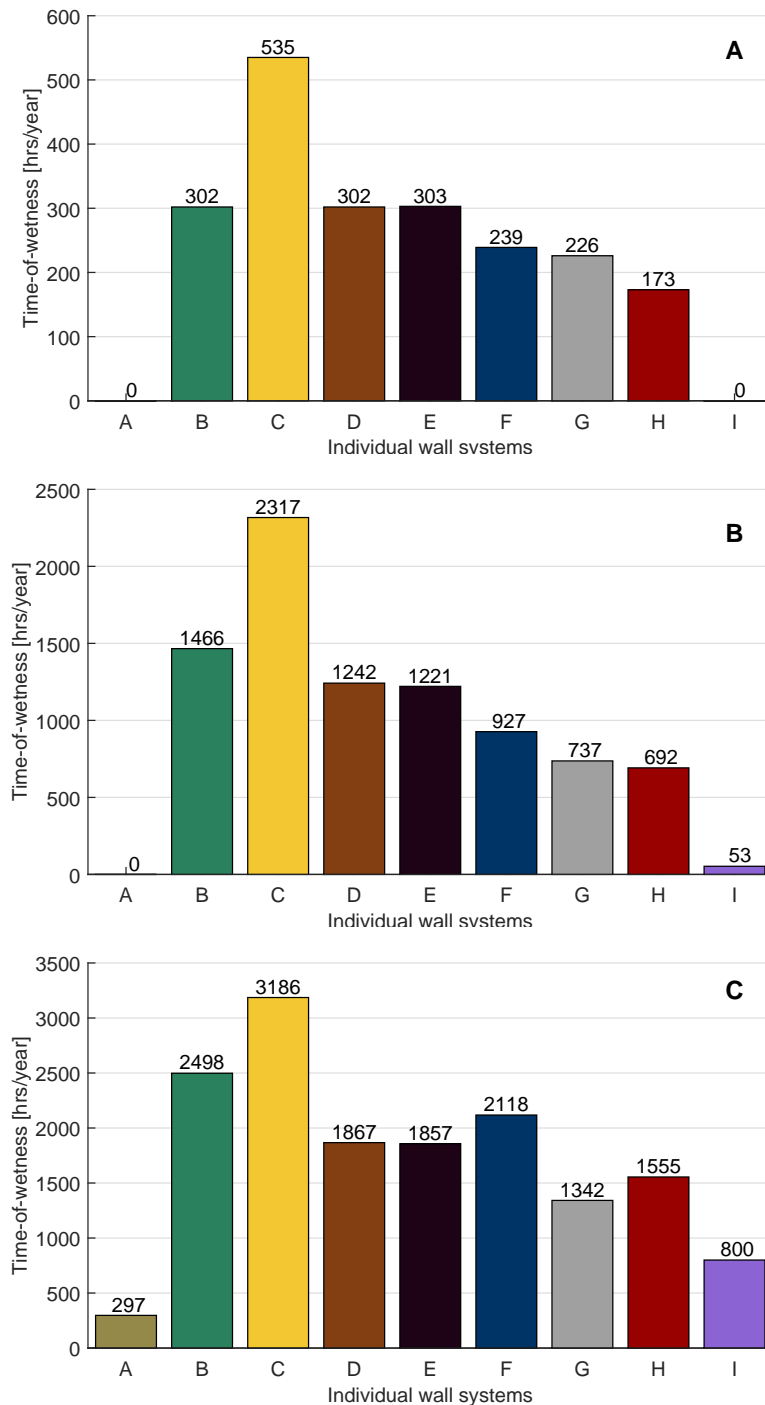


**Fig. 73:** TOW surface values (region 1 - 2 mm behind outside render layer): (A) Prague - NW, (B) Vienna - W, (C) Serak - W

It can be observed that situation closer to outside surface of wall components is very different to situation inside the components. Wall components (F) and (H) were computed to have lower surface TOW than components (B-E) under Prague and Viennese climate, despite having higher inside TOW (see Fig. 72). It is most likely again due to ability of those materials to swiftly transport liquid moisture from outside layers deeper into the material.

The worst surface TOW was encountered for wall component (C), which was computed to have by far the highest count of TOW for all simulated cases. Wall component (C) should thus be always protected from windward side by roof overhang or wall cladding to lower TOW count and prevent surface decay of straw. Another poorly performing wall component was component (B), which was, despite its higher RH threshold value of 95 % (in comparison with 90 % of other RNBM wall components), computed to have second highest surface TOW and third highest inside TOW (depending on climate, see Fig. 72).

The other RNBM wall components were computed to have mostly higher TOW counts than wall components of conventional materials, which confirms the general fact that RNBM require more precise detailing during design stage of project. An exception is wall component (A), which was (together with wall component (I)) computed to have lowest TOW (both surface and inside) out of all simulated wall components. This is most likely due to very high  $\mu$ -factor and low *liquid transfer coefficients*  $D_{ws}$ ,  $D_{ww}$  of spruce wood in radial direction. For tabular summary of surface TOW of all simulated cases, see Tab. 15.

**Tab. 15:** *Time-of-wetness damage function for different locations and wall orientations (measured at interface of outside render and insulation layer or 2 mm below outside surface in case of wall systems without outside render)*

Time-of-wetness [hrs/year]	Prague			Vienna		Serak	
	S	NW	NW - High RH	S	W	S	W
A	0	0	0	0	0	25	297
I	0	0	0	53	53	800	800
G	24	226	226	413	737	1090	1342
H	7	173	174	409	692	709	1555
E	52	303	305	745	1221	1668	1857
D	58	302	305	737	1242	1657	1867
F	17	239	240	547	927	1068	2118
B	0	302	308	792	1466	1326	2498
C	0	535	562	1300	2317	2273	3186

As discussed in section 5.2, hygric simulation results show increased sensitivity to quality of material input data. Also, it was concluded that Künzel's mathematical model gets very sensitive in situations with high moisture content and moisture flux within simulated walls, which suggests that hygric simulation results of wall systems under Serak climate may have lower accuracy than simulation results of Prague (Vienna) climate. The final discussion was therefore focused on non-marginal differences, which are less likely to be caused by uncertainties of input material data.

## 6 CONCLUSION

---

This thesis aimed to investigate hygrothermal behaviour of wall systems composed of RNBM and compare this with nowadays conventionally used wall systems. Effect of hygrothermal storage parameters (thermal/hygric mass) upon hygrothermal fluxes in BE under transient hygrothermal conditions was the main subject of this comparison.

Transient hygrothermal parameters of individual materials were firstly assessed analytically using concept of hygrothermal diffusivity and effusivity. Effect of these parameters was further analysed by means of computer-aided hygrothermal simulations under theoretical and real climatic conditions.

The results presented in this work are not calibrated with real measurements due to limited budget and time frame of this work. They, however, allow relative comparison of different cases, which brings new perspective upon hygrothermal behaviour of the selected materials and wall systems under simulated climates.

It was found out that hygrothermal transient parameters (diffusivity and effusivity) do not provide sufficient information about the actual hygrothermal performance of selected wall systems. Transient hygrothermal behaviour of wall systems, which are composed of several layers, cannot be predicted by these parameters, as there are too many other influencing factors. The most useful transient parameter was found to be hygric effusivity, based on which is calculated  $MBV_{ideal}$ . Concept of  $MBV_{ideal}$  was found to provide useful information about material's moisture buffering potential.

Similarly,  $MBV_{simul}$  was found to be the most useful parameter obtained from hygrothermal simulations under theoretical conditions. With regard to transient thermal parameters, thermal phase shift  $phs$  and damping  $dmp$  were concluded to be more relevant parameters than  $t_{s-s}$  and  $Q_{24h}$ , as they predicted the character of heat flux of real climate simulation satisfactorily. Parameters  $t_{s-s}$  and  $Q_{24h}$  were, on the other hand, found not useful as they did not reflect the actual amount of transferred heat of real climate simulation. It is believed that  $t_{s-s}$  and  $Q_{24h}$  can be useful for assessment of transient thermal behaviour of wall systems under climate with high diurnal temperature variation (e.g. continental climate). Neither of the studied thermal parameters, however, addresses dependency of *thermal conductivity*  $\lambda$  upon *moisture content*  $w$ , which turned out to have high influence upon the actual heat transfer.

The real climate simulations considered heat transfer by combined conduction and radiation. The simulations showed that wall systems, which were designed with the same U-value, transfer in most cases similar amounts of heat, whereby differences between the lowest and highest deviations of the dynamically simulated values from the theoretical steady-state calculation were up to 7 % (for wall systems A, B, C, D, E and G). The influence of thermal mass upon heat transfer in real climate is apparent from the comparison of simulated annual heat losses with annual heat losses obtained by theoretical steady-state

calculation (based on steady-state heat transfer given by immediate temperature difference between indoor and outdoor environment, considering hourly temperature values of real climate, see section 4.5.1.1). Wall systems (A, B, C, D, E and G) were simulated to have up to 17 % lower heat losses (depending on location and assumed wall orientation) when compared with theoretical steady-state calculation.

Wall system (I), which is composed of low thermal mass material layers, was simulated to have similar annual heat losses to the theoretical steady-state calculation. Wall system (I) transferred up to 18 % more heat than wall systems (A, B, C, D, E and G).

Considerably higher deviation from predicted annual heat transfer was found to be caused by high *liquid transfer coefficients*  $D_{ws}$ ,  $D_{ww}$ , in combination with high dependency of *thermal conductivity*  $\lambda$  upon moisture content  $w$ , which were encountered for AAC and perforated brick materials (wall systems (F and H)). These wall systems transferred in cold humid environment of Serak up to 50 % more heat than predicted by U-value calculation.

The heat flux through inside surface of components was found to be dependent on the wall layer composition. While wall systems composed of high thermal mass layer and separate insulation layer (D, E and G) reacted to changes in inside temperatures sensitively (instant high values of heat flux after the change), wall systems composed of one main layer having both insulation and accumulation function showed poorer reaction to these changes (lower values of heat flux after the change). Wall systems (D, E and G) were thus concluded to provide more stable indoor temperature conditions than the other studied wall systems. The least stable indoor temperature conditions were provided by wall system (I).

The main conclusion of hygric simulations is poor indoor moisture buffering potential of loam-based products in comparison with other simulated finishing materials. Both lime render and cement-lime render were simulated to have considerably higher MBV than loam render. SRE and adobe bricks showed better results, yet they did not reach MBV of the two conventional renders. High hygroscopicity of clay particles is not necessarily a guarantee for exceptional moisture performance. Loam-based materials require research and development to be able to fully exploit hygroscopic potential of clay particles.

The only low embodied energy material with high indoor moisture buffering potential was concluded to be hempcrete (wall system (B-)), which showed similar MBV as wall systems with lime/cement-lime render (B, F, G and H).

Final hygric comparison of wall systems, conducted with use of TOW damage function, showed that wall system (C) suffers from highest amount of hours with overcritical surface hygrothermal conditions (see 4.5.1.2), which makes it the most vulnerable out of the studied wall systems. This wall system should thus not be used in humid locations (especially in case of windward oriented walls) without appropriate rain protection (roof overhang, wall cladding etc.). Wall system (A) showed on the other hand the highest resistance towards outside humid environment, as its simulated surface TOW was zero hours for most of the simulation cases.

In general, surface TOW function was higher for RNBM, as they are not capable of withstanding higher levels of RH without significant deterioration. It is, however, important to note that TOW does not address, whether material is exposed to negative hygrothermal conditions continuously over longer period or discretely with only short durations of those conditions. This can make a difference in the final interpretation of the TOW results, but it was considered outside of the scope of this work and could be subject of further research.

To conclude, this thesis presented hygrothermal comparisons of selected wall systems conducted in 1D hygrothermal simulation tool WUFI<sup>®</sup> Pro. The presented results are considered relevant especially when the relative differences between the wall systems are studied. Further understanding of the hygrothermal behaviour of the selected wall systems and its effect on indoor environment (hygrothermal comfort) could be developed by coupling of indoor conditions with effects of hygrothermal processes inside the simulated wall systems in relevant simulation software (e.g. WUFI<sup>®</sup> Plus).

# List of Figures

1	Amount of necessary resources for top world's economies (when recomputed to entire world's population) expressed in planet Earth equivalent (Global Footprint Network, 2016) . . . . .	2
2	Hygrothermal fluxes and their alternating diurnal or seasonal directions acting upon building envelope according to ASHRAE (2009) . . . . .	5
3	Relationship of thermal gradient caused by different potentials to direction of induced heat flux (Bošová and Kulhánek, 2014) . . . . .	7
4	Scheme of distribution of radiation incident on a surface of a wall (Bošová and Kulhánek, 2014) . . . . .	9
5	Combination of all heat transfer mechanisms on an example of external wall (Moss, 2007) . . . . .	11
6	Heat transfer mechanisms within granular material – microscale (Hall and Allinson, 2009) . . . . .	11
7	Distribution of temperature through a multi-layered composite wall in steady state temperature environment (Hall and Allinson, 2010) . . . . .	13
8	Visual explanation of effect of high thermal mass wall on moderation of external temperature fluctuations (Hall and Allinson, 2008) . . . . .	15
9	Blocks of high thermal diffusivity (effusivity) material (a) and low thermal diffusivity (effusivity) material (b) heated at the same rate ((Ahmed and Sturges, 2014)). . . . .	16
10	An example of psychrometric chart (Earle, 1983) . . . . .	18
11	Schematic representation of physical adsorption phenomena in a pore (Moevus <i>et al.</i> , 2013) . . . . .	19
12	A typical sorption isotherm of porous material (wetting and drying curves) with corresponding moisture storage regions (Hall and Allinson, 2009) . . . . .	20
13	Surface temperature of hemp-lime composite samples subjected to RH variation cycles (determined by real measurement and two simulation software tools) (Dubois <i>et al.</i> , 2013) . . . . .	22
14	Mechanisms of vapour diffusion in porous materials (Hall and Allinson, 2009) . . . . .	24
15	Moisture transfer in porous BE wall element and the phenomena resulting from it (Heitz <i>et al.</i> , 2015) . . . . .	26
16	Thermal (left) and hygric (right) transient evolution of hemp-lime wall component after thermal and hygric shock respectively (simulated in WUFI® Pro computer simulation tool) (Evrard, 2008) . . . . .	29
17	Course of the RH step cycles during Nordtest experiment and their relation to mass of the tested samples together with graphical representation of moisture uptake $\Delta m$ during one RH cycle (Rode <i>et al.</i> , 2007) . . . . .	31
18	RH related effects on health and indoor air quality (Simonson <i>et al.</i> , 2001) . . . . .	32

19	Four raw building materials analysed in this paper; earth (loam) (Stockscape, n.d.), straw (Flamingo, n.d.), hemp (Gettyimages, n.d.) and wood (Wrrnetwork, n.d.) . . . . .	33
20	Examples of use of earth for building purposes; City of Shibam in Yemen (Günter, n.d.), Martin Rauch’s personal house in Austria (Rauch, n.d.) . . .	34
21	Electroskan microscope image of flat kaolinite clay vs. granular silt (Couvreur, 2015) . . . . .	35
22	Different loam construction techniques: a) rammed earth (left) b) adobe bricks and cob (right) (Rieger-Jandl, 2015) . . . . .	35
23	Relative sizes of adsorbed water layers (surface potential) of montmorillonite and kaolinite clay particles (Holtz and Kovacs, 1981) . . . . .	36
24	Illustration of single fibre cell (cell walls surrounding the lumen; right) together with complex structure of the cell wall (left). Note the difference in cellulose micro fibre orientation in the primary and secondary cell walls (Hopkins <i>et al.</i> , 1999) . . . . .	37
25	Cross-section of cellular composition of wheat straw (a) miscanthus straw (b) and hemp straw (c) scanned by electron microscope (Wihan, 2007). The dense cellular structure with higher pore surface area and higher lignification level of hemp makes it considerably better moisture buffering material. . . .	39
26	Hierarchical organization of wood: (a) cross-section of a log, (b) longitudinal section showing horizontal fibres (rays) going through vertical ones, (c) transverse section through softwood, (d) transverse section through hardwood, (e) section of cell wall showing the cell wall layers ( $S_1$ , $S_2$ ), (f) fibrous structure of the cell wall, (g) chemical structure of lignin, (h) chemical structure of cellulose (Eitelberger, 2011). . . . .	40
27	Structural systems of straw bale construction: Nebraska style system (left) and timber frame system (right) (Márton, 2014) . . . . .	42
28	The Burke house in Nebraska built in 1903 (left) (Márton, 2014) and spiral house built by Barbara Jones in Ireland in 2003 (right) (Jones, n.d.) . . . .	43
29	Most common binders for hempcrete mix, Tradical <sup>®</sup> , VICAT and Batichanvre <sup>®</sup> (left) and loose hemp shiv (right) (Stanwix and Sparrow, 2014) . . . . .	45
30	Examples of houses constructed of hempcrete; classical (left) and modern (right) design (Stanwix and Sparrow, 2014) . . . . .	46
31	Example of one level of wall formwork filled with hempcrete (left) and cast hempcrete variations of construction elements; roof, wall and floor (right) (Stanwix and Sparrow, 2014) . . . . .	46
32	Low embodied energy wall systems (based on RNBM) considered in this work; (A) spruce panel Holz100, (B) hempcrete wall component, (C) straw bale wall component, (D) insulated adobe brick wall component, (E) insulated SRE wall component . . . . .	51

33	Conventional wall systems considered in this work; (F) AAC wall component, (G) insulated concrete wall component, (H) perforated brick wall component, (I) lightweight wall component . . . . .	52
34	User interface of WUFI <sup>®</sup> Pro 6.0 simulation tool . . . . .	55
35	User interface of HeMoT simulation tool . . . . .	55
36	Flow chart for hygrothermal simulations from former version of EN 15026 (2004) (Künzel and Karagiozis, 2010) . . . . .	56
37	Reference indoor climate in Prague together with its defining functions (medium moisture load according to EN 15026) . . . . .	61
38	Graphical representation of numerical grid through wall element in WUFI <sup>®</sup> Pro . . . . .	61
39	Analysis of climates used in this work: (A) Prague (B) Vienna (C) Serak . . . . .	68
40	Sorption isotherm of straw together with regions of different rates of decomposition (84 % RH - start of decomposition process at marginal rates, 98 % RH - critical boundary (high rate of decomposition)) (Wihan, 2007) . . . . .	73
41	Thermal diffusivity of principal wall materials considered in this work . . . . .	74
42	Thermal effusivity of principal wall materials considered in this work . . . . .	75
43	Hygric diffusivity of principal wall materials (above) and potential finishing materials (below) . . . . .	76
44	Hygric effusivity of principal wall materials (above) and potential finishing materials (below) . . . . .	77
45	Comparison of temperature ( $X_T$ ) and relative humidity ( $X_H$ ) fields of profiles at selected times simulated by HeMoT (red line) and WUFI <sup>®</sup> Pro (blue line) software. A - 24.2. (10:00), B - 16.4. (16:00), C - 31.7. (15:00), D -16.10. (7.00) . . . . .	79
46	Comparison of temperature ( $X_T$ ) and relative humidity ( $X_H$ ) time courses at monitoring position within the outside render (0.005 m) during selected winter month - A (January) and summer month - B (July) - HeMoT (red line), WUFI <sup>®</sup> Pro (blue line) . . . . .	80
47	Comparison of temperature ( $X_T$ ) and relative humidity ( $X_H$ ) time courses at monitoring position within AAC wall (0.195 m) during selected winter month - A (January) and summer month - B (July) - HeMoT (red line), WUFI <sup>®</sup> Pro (blue line) . . . . .	81
48	Graphical result of sensitivity analysis in form of temperature ( $X_T$ ) and relative humidity ( $X_H$ ) fields of potential simulation outputs of profiles at selected times simulated by WUFI <sup>®</sup> Pro software (blue line). A - 24.2. (10:00), B - 16.4. (16:00), C - 31.7. (15:00), D -16.10. (7.00) . . . . .	83
49	Graphical result of sensitivity analysis in form of temperature ( $X_T$ ) and relative humidity ( $X_H$ ) fields of potential simulation outputs of time courses at monitoring position within the outside render (0.005 m) during winter time - A (January) and summer time - B (July) simulated by WUFI <sup>®</sup> Pro software (blue line) . . . . .	84

50	Graphical result of sensitivity analysis in form of temperature ( $X_T$ ) and relative humidity ( $X_H$ ) fields of potential simulation outputs of time courses at monitoring position within AAC wall (0.195 m) during winter time - A (January) and summer time - B (July) simulated by WUFI® Pro software (blue line) . . . . .	84
51	Development of heat flux through inside surface of the wall systems during 8 days after imposed thermal shock . . . . .	86
52	Time to reach permanent transfer $t_{s-s}$ after imposed thermal shock . . . . .	87
53	Amount of heat (cumulative) transferred through inside surface of wall systems during first 24 hours after the imposed thermal shock . . . . .	88
54	Ratio of heat transferred through inside surface during first 24 hours after the imposed thermal shock to heat transferred when permanent transfer is assumed, $Q_{24h}$ . . . . .	88
55	Course of heat flux through inside surface of wall systems during two days of stabilized cycles . . . . .	89
56	Thermal phase shift of wall systems under cyclic outside temperature fluctuation - phs (delay of outside peak temperature) . . . . .	90
57	Thermal damping of wall systems under cyclic outside temperature fluctuation - dmp (percentage saved by the wall system due to thermal inertia effect) . . . . .	90
58	Amount of moisture (cumulative) transferred through inside surface of wall systems as result of indoor moisture cycles . . . . .	92
59	Simulated inside moisture buffer value of studied wall systems - $MBV_{simul}$ . . . . .	92
60	Relation between moisture and heat flux transferred through inside surface of component (F) . . . . .	93
61	Latent heat released through inside surface of wall systems during night period (8 hours) of the moisture cycle . . . . .	94
62	Maximal temperature change of inside surfaces of wall systems during one RH cycle . . . . .	95
63	Cumulative amount of heat transferred through inside surface of studied wall systems during 10 <sup>th</sup> year of simulation for different locations and wall orientations (together with theoretically transferred heat when permanent (steady-state) heat transfer assumed: green dot-and-dash line) . . . . .	97
64	Overall heat losses through inside surfaces of studied wall systems during reference year (A), winter (heating) days (B) and summer (cooling) days (C) in Prague (South orientation) . . . . .	99
65	Difference (cumulative) in heat transferred through inside surfaces of studied wall systems between reference case and case when no absorption of driving rain is assumed. Simulation case - Vienna South . . . . .	101
66	Difference (cumulative) in heat transferred through inside surfaces of studied wall systems between reference case and case when no short/long wave radiation absorptivity is assumed. Simulation case - Vienna South . . . . .	101

67	Heat flux through inside surfaces of studied wall systems situated in Prague (south orientation) together with their external and internal ambient air temperature during selected winter (A), spring (B) and summer (C) two week periods (negative values represent heat flow from in to out). . . . .	103
68	Cumulative amount of moisture transferred through inside surfaces of studied wall systems during 10 <sup>th</sup> year of simulation for Prague - south orientation (A) and Serak - west orientation (B) (negative values represent moisture flow from inside to outside). . . . .	104
69	Sum of annual moisture transferred through inside surfaces of studied wall systems for both directions of moisture flux (negative: outward moisture flow, positive: inward moisture flow) for different simulation set-ups . . . . .	106
70	Sum of moisture transferred through inside surfaces of studied wall systems for both directions of moisture flux during summertime (1.6. - 31.8.) and wintertime (1.12. - 28.2.) (Prague - south orientation) . . . . .	106
71	Moisture flux through inside surfaces of studied wall systems situated in Prague (south orientation) together with indoor RH during selected summer (A) and winter (B) periods . . . . .	108
72	Simulated TOW profiles: (A) Prague - NW, (B) Vienna - W, (C) Serak - W (negative monitoring position represents outside finishing layer (render) of simulated wall systems) . . . . .	109
73	TOW surface values (region 1 - 2 mm behind outside render layer): (A) Prague - NW, (B) Vienna - W, (C) Serak - W . . . . .	110
A.1	Glaser diagram showing distribution of saturation pressure $P_s$ (solid line) and partial water vapour pressure P (dashed line) through a multi-layered composite wall in steady state RH environment: By depicting single layers in terms of equivalent air layer thickness $s_d$ , it can be assumed that the propagation of water vapour and thus distribution of partial water vapour pressure of diffused air through the newly defined component thickness is linear (dashed line). When the solid line (representing saturation pressure of air at computed temperature) gets at any point of the diagram under the dashed line, interstitial condensation inevitably occurs. . . . .	133
A.2	Chemical composition of different bast fibres (hemp, flax and jute), wood fibres (Norway spruce) and straw fibres (barley straw and corn stover) (Thygesen, 2001) . . . . .	133
A.3	Absolute humidity [g/m <sup>3</sup> ] of air of different temperatures at different RH states (atmospheric pressure of 101 kPa) . . . . .	134
A.4	MBV classification according to Rode <i>et al.</i> (2005) . . . . .	134

# List of Tables

1	Basic parameters of materials used in this work (together with their sources)	58
2	Remaining main input data required for successful simulation . . . . .	60
3	Simulation input material properties and their uncertainties (Holm and Künzel, 2002) . . . . .	63
4	Boundary condition data considered for real climate simulations . . . . .	67
5	Simulated orientations for different locations . . . . .	69
6	Limiting amounts of moisture (RH) for RNBM for different types of damages	72
7	Analytically determined parameters describing material properties in transient hygrothermal environment from most favourable (light background) to least favourable values (dark background) (values of thermal and hygric diffusivity and effusivity are displayed for materials in dry state) . . . . .	78
8	Classification of sensitivity of WUFI <sup>®</sup> Pro mathematical model to uncertainties of input material parameters . . . . .	82
9	Standard deviation of potential simulation error caused by uncertainty of input material data for profiles at selected times . . . . .	85
10	Standard deviation of potential simulation error caused by uncertainty of input material data for time courses at selected monitoring positions . . . . .	85
11	Comparison of absolute and relative values of ideal and simulated MBV . . . . .	93
12	Summary of theoretical simulation results (grey scale from light background (favourable values) to dark background (unfavourable values)) . . . . .	95
13	Overall annual heat losses (together with heat losses/gains during heating/cooling season) through inside surface of studied wall systems of different orientation and location. Relative values represent percentage of transferred heat with respect to permanent (steady-state) heat transfer scenario - P.t. (heat transferred through wall component (I) in case of Vienna climate). Grey scale - light background (favourable values) to dark background (unfavourable values). . . . .	98
14	Annual (seasonal) amount of moisture transferred through inside surfaces of studied wall systems in non-principal moisture flux direction representing MBE (different locations, wall orientations and time of year) . . . . .	107
15	Time-of-wetness damage function for different locations and wall orientations (measured at interface of outside render and insulation layer or 2 mm below outside surface in case of wall systems without outside render) . . . . .	111
B.1	Composition of SRE wall mix (Allinson and Hall, 2010) . . . . .	135
B.2	Composition of Hempcrete wall mix (Evrard, 2008) . . . . .	135

# List of Equations

1	Fourier's first law: one-dimensional, (Bošová and Kulhánek, 2014)	6
2	Fourier's first law: three-dimensional, (Bošová and Kulhánek, 2014)	7
3	Fourier's second law: one-dimensional, (Bošová and Kulhánek, 2014)	7
4	Fourier's second law: three-dimensional, (Bošová and Kulhánek, 2014)	7
5	Calculation of thermal diffusivity $\alpha$ , (Bošová and Kulhánek, 2014)	8
6	Newton's law of cooling, (Vaverka <i>et al.</i> , 2000)	8
7	Relationship between surface absorptivity $\alpha$ , reflectivity $\rho$ and transmissivity $\tau$ , (Vaverka <i>et al.</i> , 2000)	10
8	Stefan-Boltzmann law, (Vaverka <i>et al.</i> , 2000)	10
9	Calculation of emittance $M$ of "grey" body, (Vaverka <i>et al.</i> , 2000)	10
10	Calculation of component's total thermal resistance $R_T$ , (ISO, 2007c)	12
11	Calculation of thermal resistance of $j^{th}$ layer of component, (ISO, 2007c)	12
12	Calculation of thermal resistances of interior and exterior stagnant air layers $R_{si,se}$ adjacent to wall surfaces, (ISO, 2007c)	13
13	Calculation of distribution of temperature through a multi-layer composite wall in steady state, (ISO, 2007c)	13
14	Calculation of thermal transmittance $U$ , (ISO, 2007c)	14
15	Calculation of steady state 1D heat flux density through a building component, (ISO, 2007c)	14
16	Calculation of heat capacity, (Hens, 2008)	14
17	Calculation of thermal diffusivity $\alpha$ , (Evrard, 2008)	15
18	Calculation of thermal effusivity $b$ , (Evrard, 2008)	16
19	Calculation of relative humidity $\varphi$ , (ISO, 2012)	17
20	Calculation of specific hygric capacity $\xi$ , (Hall and Allinson, 2010)	21
21	Fick's first law of diffusion, (Moss, 2007)	23
22	Calculation of water vapour diffusion coefficient $D$ , (Moss, 2007)	23
23	Fick's first law of diffusion expressed by water vapour partial pressure gradient, (Moss, 2007)	24
24	Calculation of capillary liquid water flux density, (Moss, 2007)	25
25	Darcy's law of fluid, (Moss, 2007)	25
26	Calculation of liquid water flux density $q_w$ , (Hens, 2008)	25
27	Calculation of component's total water vapour resistance $Z_{pT}$ , (ISO, 2007d)	26
28	Calculation of water vapour resistance of $j^{th}$ layer of component, (ISO, 2007d)	26
29	Calculation of water vapour resistances of interior and exterior stagnant air layers $Z_{pi,pe}$ adjacent to wall surfaces, (ISO, 2007d)	27

---

30	Calculation of convective water vapour transfer coefficient $\beta_{pi,pe}$ , (ISO, 2007d) . . .	27
31	Calculation of steady state 1D water vapour diffusive flux density through a building component, (ISO, 2007d) . . . . .	27
32	Condition for occurrence of interstitial condensation within a component, (ISO, 2007d) . . . . .	27
33	Calculation of sd-value, (ISO, 2007d) . . . . .	27
34	Calculation of hygric diffusivity $\alpha_h$ , (Evrard, 2008) . . . . .	29
35	Calculation of hygric effusivity $b_h$ , (Evrard, 2008) . . . . .	29
36	Calculation of practical moisture buffer value $MBV_{practical}$ , (Rode <i>et al.</i> , 2005) .	30
37	Calculation of ideal moisture buffer value $MBV_{ideal}$ , (Rode <i>et al.</i> , 2005) . . . . .	30
38	Calculation of moisture dependent thermal conductivity $\lambda^*$ , (Evrard, 2008) . . .	50
39	Calculation of moisture dependent specific heat capacity $c^*$ , (Jerman and Černý, 2012) . . . . .	50
40	Calculation of moisture dependent bulk density $\rho^*$ , (Jerman and Černý, 2012) . .	51
41	Calculation of standard deviation $\sigma$ , (Lee and Peters, 2015) . . . . .	64

## References

- Ahmed, Arshad, and Sturges, John. 2014. *Materials Science in Construction: An Introduction*. Routledge.
- Allin, Steve. 2012. *Building with hemp*. 2nd edn. SEED PRESS.
- Allinson, David, and Hall, Matthew. 2010. Hygrothermal analysis of a stabilised rammed earth test building in the UK. *Energy and Buildings*, **42**(6), 845–852.
- Antretter, Florian, Mitterer, Christoph, and Young, Seoung-Moon. 2012. Use of moisture-buffering tiles for indoor climate stability under different climatic requirements. *HVA-CandR Research*, **18**(1-2), 275–282.
- ASHRAE, ANSI. 2009. Standard 160-2009, Criteria for Moisture-Control Design Analysis in Buildings. *Atlanta, GA: American Society of Heating, Refrigerating and Air-conditioning Engineers, Inc.*
- Asif, M, Muneer, T, and Kelley, R. 2007. Life cycle assessment: a case study of a dwelling home in Scotland. *Building and environment*, **42**(3), 1391–1394.
- Auracher, H. 1974. Water vapor diffusion and frost formation in porous materials. *VDI Forschungsheft*, **566**.
- Babbitt, JD. 1942. On the adsorption of water vapour by cellulose. *Canadian Journal of Research*, **20**(9), 143–172.
- Bear, Jacob. 2013. *Dynamics of fluids in porous media*. Courier Corporation.
- Berthold, Jesper, Olsson, Ralf JO, and Salmén, Lennart. 1998. Water sorption to hydroxyl and carboxylic acid groups in carboxymethylcellulose (CMC) studied with NIR-spectroscopy. *Cellulose*, **5**(4), 281–298.
- Bevan, Rachel, Woolley, Tom, Pritchett, I, Carpenter, R, Walker, Peter, and Duckett, M. 2008. *Hemp lime construction: a guide to building with hemp lime composites*. BRE Press.
- Bošová, Daniela, and Kulhánek, František. 2014. *Stavební fyzika II*. 6. edn. V Praze: České vysoké učení technické.
- Bronsema, Nicholas Rangco. 2010. Moisture movement and mould management in straw bale walls for a cold climate.
- Bui, Quoc-Bao, Morel, Jean-Claude, Hans, Stéphane, and Walker, Peter. 2014. Effect of moisture content on the mechanical characteristics of rammed earth. *Construction and Building materials*, **54**, 163–169.

- Cagnon, H, Aubert, JE, Coutand, M, and Magniont, C. 2014. Hygrothermal properties of earth bricks. *Energy and Buildings*, **80**, 208–217.
- Céline, Amandine, Fréour, Sylvain, Jacquemin, Frédéric, and Casari, Pascal. 2013. The hygroscopic behavior of plant fibers: A review. *Frontiers in chemistry*, **1**.
- Christian, Jeffrey E., Desjarlais, Andre O., and Stovall, Therese K. 1998. Straw Bale Wall Hot Box Test Results and Analysis. In: *Thermal Performance of the Exterior Envelopes of Buildings VII*.
- Couvreur, Lucile. 2015. Building with earth: From matter to architecture. Amáco.
- CSN, EN. 2005. 73 0540-3. *Thermal protection of buildings—Part 3: Design value quantities*, **2**.
- Cunningham, MJ. 1996. Controlling dust mites psychrometrically—a review for building scientists and engineers. *Indoor air*, **6**(4), 249–258.
- Danielewicz, I, Fitz, C, Hofbauer, W, Klátecki, M, Krick, B, Krueger, N, Krus, M, Minke, G, Otto, F, Scharmer, D, *et al.* 2008. Grundlagen zur bauaufsichtlichen Anerkennung der Strohballenbauweise-Weiterentwicklung der lasttragenden Konstruktionsart und Optimierung der bauphysikalischen Performance. *DBU, Az*, **22430**.
- de Bruijn, Paulien Brigitte, Jeppsson, Knut-Håkan, Sandin, Kenneth, and Nilsson, Christer. 2009. Mechanical properties of lime–hemp concrete containing shives and fibres. *Biosystems Engineering*, **103**(4), 474–479.
- Desch, Harold Ernest, Dinwoodie, John M, *et al.* 1996. *Timber structure, properties, conversion and use*. MacMillan Press Ltd.
- Dubois, Samuel, Evrard, Arnaud, and Lebeau, Frédéric. 2013. Modeling the hygrothermal behavior of biobased construction materials. *Journal of Building Physics*, **38**(3), 191–213.
- Dubois, Samuel, McGregor, Fionn, Evrard, Arnaud, Heath, Andrew, and Lebeau, Frédéric. 2014. An inverse modelling approach to estimate the hygric parameters of clay-based masonry during a Moisture Buffer Value test. *Building and Environment*, **81**, 192–203.
- Dutton, Frederic B. 1961. Dalton’s law of partial pressures. *J. Chem. Educ*, **38**(8), A545.
- Earle, R. L. 1983. *Psychometry*. [online]. [cit. 2017-04-11] Available from: <http://www.nzifst.org.nz/unitoperations/drying3.htm#psychometric>.
- Eitelberger, Johannes. 2011. *A multiscale material description for wood below the fiber saturation point with particular emphasis on wood-water interactions*. October, TU Wien.
- Elfordy, S, Lucas, F, Tancret, F, Scudeller, Y, and Goudet, L. 2008. Mechanical and thermal properties of lime and hemp concrete (“hempcrete”) manufactured by a projection process. *Construction and Building Materials*, **22**(10), 2116–2123.

- 
- EnergyPlus. 2017. *version 8.7.0*. National Renewable Energy Laboratory (NREL). Available from: <https://energyplus.net/>.
- Evrard, A, De Herde, A, and Minet, J. 2006. Dynamical interactions between heat and mass flows in Lime-Hemp Concrete. *Pages 27–31 of: 3rd International Building Physics Conference*.
- Evrard, A, Flory-Celini, C, Claeys-Bruno, M, and De Herde, A. 2014. Influence of liquid absorption coefficient on hygrothermal behaviour of an existing brick wall with Lime-Hemp plaster. *Building and environment*, **79**, 90–100.
- Evrard, Arnaud. 2008. Transient hygrothermal behaviour of lime-hemp materials. *PhD, Université Catholique De Louvain*.
- Evrard, Arnaud, and De Herde, André. 2005. Bioclimatic envelopes made of lime and hemp concrete. *Proceeding of CISBAT*, 1–6.
- Evrard, Arnaud, Louis, Arnaud, Biot, Benjamin, and Dubois, Samuel. 2012. Moisture equilibrium in straw bale walls. *In: Opportunities, Limits and Needs Towards an environmentally responsible architecture*.
- Fernández-Cabo, José L. 2009. A timber cantilevered view walkway in Vitoria, Spain. *Proceedings of the Institution of Civil Engineers-Construction Materials*, **162**(4), 167–174.
- Fix, Stuard, and Richman, Russell. 2009 (May). *Viability of Rammed Earth Building Construction in Cold Climates*.
- Flamingo. [online]. [cit. 2017-02-12] Available from: <http://www.flamingo-shipping.com/public/uploads/files/Square-Straw-Bales-4.jpg>.
- Gaur, RC, and Bansal, NK. 2002. Effect of moisture transfer across building components on room temperature. *Building and Environment*, **37**(1), 11–17.
- Gettyimages. [online]. [cit. 2017-02-12] Available from: <http://www.gettyimages.com/detail/photo/cannabis-stem-royalty-free-image/480560893>.
- Ghrici, M, Kenai, S, and Said-Mansour, M. 2007. Mechanical properties and durability of mortar and concrete containing natural pozzolana and limestone blended cements. *Cement and Concrete Composites*, **29**(7), 542–549.
- Gibson, Lorna J. 2012. The hierarchical structure and mechanics of plant materials. *Journal of the Royal Society Interface*, rsif20120341.
- Global Footprint Network. 2016. The National Footprint Accounts, 2016 Edition. *Oakland, CA*. <http://www.footprintnetwork.org/our-work/ecological-footprint/#worldfootprint>.
- Gram-Hanssen, Kirsten. 2010. Residential heat comfort practices: understanding users. *Building Research and Information*, **38**(2), 175–186.

- Gregory, Katherine, Moghtaderi, Behdad, Sugo, Heber, and Page, Adrian. 2008. Effect of thermal mass on the thermal performance of various Australian residential constructions systems. *Energy and Buildings*, **40**(4), 459–465.
- Grunewald, John, Nicolai, Andreas, Ruisinger, Ulrich, and Fechner, Heiko. 2015. *DELPHIN*. Dresden, Germany: Technische Universität Dresden. Available from: <http://bauklimatik-dresden.de/delphin/index.php>.
- Günter. [online]. [cit. 2017-04-12] Available from: <http://www.panoramio.com/photo/115724679>.
- Hall, Matthew, and Allinson, David. 2008. Assessing the moisture-content-dependent parameters of stabilised earth materials using the cyclic-response admittance method. *Energy and Buildings*, **40**(11), 2044–2051.
- Hall, Matthew, and Allinson, David. 2009. Analysis of the hygrothermal functional properties of stabilised rammed earth materials. *Building and Environment*, **44**(9), 1935–1942.
- Hall, Matthew R. 2010. *Materials for energy efficiency and thermal comfort in buildings*. Elsevier.
- Hall, MR, and Allinson, D. 2010. Heat and Mass Transport Processes in Building Materials. *Pages 3–53 of: Materials for Energy Efficiency and Thermal Comfort in Buildings*. Woodhead Publishing Cambridge.
- Heitz, Philippe, Morel, Jean-Claude, Fabbri, Antonin, Soudani, Lucile, Champiré, Florient, and Meunier, Nicolas. 2015. Construction terre l’isolation du pisé: Pertinence et principes. *LGCB-LTDS (ENTPE-CNRS)*.
- Hens, Hugo SLC. 2008. *Building physics-heat, air and moisture: fundamentals and engineering methods with examples and exercises*. John Wiley and Sons.
- Hofer, Susanne. 2014. *Raw natural building materials*. Tech. rept. University of Technology Delft.
- Holm, Andreas H, and Künzel, Hartwig M. 2002. Practical application of an uncertainty approach for hygrothermal building simulations—drying of an AAC flat roof. *Building and environment*, **37**(8), 883–889.
- Holtz, Robert D, and Kovacs, William D. 1981. *An introduction to geotechnical engineering*.
- Hopkins, William G, et al. 1999. *Introduction to plant physiology*. John Wiley and Sons.
- Huovila, Pekka, Ala-Juusela, M, Melchert, L, Pouffary, S, Cheng, CC, Urge-Vorsatz, D, et al. 2009. Buildings and Climate Change: Summary for Decision-Makers. *Paris: United Nations Environment Programme-Sustainable Buildings and Climate Change Initiative (UNEP-SBCI)*.
- ISO, EN. 2001. 12572: 2001. *Hygrothermal performance of building materials and products. Determination of water vapor transmission properties*.

- 
- ISO, EN. 2007a. 10456: 2007. *Building materials and products – Hygrothermal properties – Tabulated design values and procedures for determining declared and design thermal values.*
- ISO, EN. 2007b. 15026: 2007. *Hygrothermal performance of building components and building elements. Assessment of moisture transfer by numerical simulation.*
- ISO, EN. 2007c. 6946: 2007. *Building components and building elements–Thermal resistance and thermal transmittance–Calculation method.*
- ISO, EN. 2007d. 9346: 2007. *Hygrothermal performance of buildings and building materials – Physical quantities for mass transfer – Vocabulary.*
- ISO, EN. 2012. 13788: 2012. *Hygrothermal performance of building components and building elements – Internal surface temperature to avoid critical surface humidity and interstitial condensation – Calculation methods.*
- ISO, INTERNATIONAL STANDARD. 1992. 9223. *Corrosion of Metals and Alloys: Corrosivity of Atmospheres: Classification.*
- Jerman, M, Kočí, V, Maděra, J, Vybourný, J, and Černý, R. 2010. Water and heat transport parameters of materials involved in AAC-based building envelopes. *Pages 39–45 of: 1st Central European symposium on building physics.*
- Jerman, Miloš, and Černý, Robert. 2012. Effect of moisture content on heat and moisture transport and storage properties of thermal insulation materials. *Energy and Buildings*, **53**, 39–46.
- Jerman, Miloš, Keppert, Martin, Vybourný, Jaroslav, and Černý, Robert. 2013. Hygric, thermal and durability properties of autoclaved aerated concrete. *Construction and building materials*, **41**, 352–359.
- Jones, Barbara. *The Natural Building, Homestead and Natural Living World*. [online]. [cit. 2017-02-13] Available from: <http://naturalhomes.org/timeline/spiralstrawbaleir>.
- Joule, James Prescott. 2011. *The Scientific Papers of James Prescott Joule*. Vol. 1. Cambridge University Press.
- Karlsson, Jonathan, Wadsö, Lars, and Öberg, Mats. 2013. A conceptual model that simulates the influence of thermal inertia in building structures. *Energy and Buildings*, **60**, 146–151.
- Kettunen, P. O. 2006. *Wood structure and properties*. Enfield, N.H.: Trans Tech Publications Ltd.
- Kočí, J, Pavlík, Z, Pavlíková, M, and Černý, R. 2010a. Validation of computer simulation tool for modeling heat transport in multi-layered systems of building materials. *The Ninth Asian Thermophysical Properties Conference*, 21–27.

- Kočí, Jan, Maděra, Jiří, and Černý, Robert. 2014a. Generation of a critical weather year for hygrothermal simulations using partial weather data sets. *Building and Environment*, **76**, 54–61.
- Kočí, V, Maděra, J, Černý, R, and Rovnaníková, P. 2009. Application of a combined computational–experimental approach for service life estimate of exterior plasters of historical buildings. *Structural Studies, Repairs and Maintenance of Heritage Architecture XI, WIT Press, Southampton*, 303–314.
- Kočí, V, Kočí, J, Maděra, J, and Černý, R. 2010b. Computer code HEMOT for hygrothermal assessment of thermal insulation systems. *Thermophysics 2010*, 133–140.
- Kočí, Václav, Maděra, Jiří, Fořt, Jan, Žumár, Jaromír, Pavlíková, Milena, Pavlík, Zbyšek, and Černý, Robert. 2014b. Service life assessment of historical building envelopes constructed using different types of sandstone: a computational analysis based on experimental input data. *The Scientific World Journal*, **2014**.
- Kočí, Václav, Maděra, Jiří, Jerman, Miloš, Žumár, Jaromír, Koňáková, Dana, Čáchová, Monika, Vejmelková, Eva, Reiterman, Pavel, and Černý, Robert. 2016. Application of waste ceramic dust as a ready-to-use replacement of cement in lime-cement plasters: an environmental-friendly and energy-efficient solution. *Clean Technologies and Environmental Policy*, **18**(6), 1725–1733.
- Korecký, Tomáš, Jerman, Miloš, and Vejmelková, Eva. 2013. Homogenizace fyzikálních parametru vyplněného děrovaného cihelného bloku. *STAVEBNÍ OBZOR*, 44–47.
- Künzel, H. M., and Karagiozis, A. 2010. *Materials for energy efficiency and thermal comfort in buildings*. CRC Press. Hygrothermal behaviour and simulation in buildings.
- Künzel, Hartwig M. 1995. Simultaneous heat and moisture transport in building components. *One-and two-dimensional calculation using simple parameters*. IRB-Verlag Stuttgart.
- Künzel, HM, Schmidt, T, and Holm, A. 2006. WUFI Pro 4.1: Programm zur instationären berechnung des eindimensionalen Wärme und Feuchtetransports in Bauteilen. *Fraunhofer Institut für Bauphysik, Holzkirchen*.
- Le, AD Tran, Maalouf, Chadi, Mai, Ton Hoang, Wurtz, Etienne, and Collet, Florence. 2010. Transient hygrothermal behaviour of a hemp concrete building envelope. *Energy and buildings*, **42**(10), 1797–1806.
- Lee, Nick, and Peters, Mike. 2015. *Business statistics using EXCEL and SPSS*. Sage.
- Liuzzi, S, Hall, MR, Stefanizzi, P, and Casey, SP. 2013. Hygrothermal behaviour and relative humidity buffering of unfired and hydrated lime-stabilised clay composites in a Mediterranean climate. *Building and Environment*, **61**, 82–92.
- Lucas, Franck, Adelard, Laetitia, Garde, Francois, and Boyer, Harry. 2002. Study of moisture in buildings for hot humid climates. *Energy and Buildings*, **34**(4), 345–355.

- Márton, Jan. 2014. *Stavby ze slaměných balíků*. Liberec: J. Márton.
- MATLAB. 2010. *version 7.10.0 (R2010a)*. Natick, Massachusetts: The MathWorks Inc. Available from: <https://www.mathworks.com/products/matlab.html>.
- Mayo, Joseph. 2015. *Solid Wood: Case Studies in Mass Timber Architecture, Technology and Design*. Routledge.
- McGregor, Fionn, Heath, Andrew, Fodde, Enrico, and Shea, Andy. 2014. Conditions affecting the moisture buffering measurement performed on compressed earth blocks. *Building and Environment*, **75**, 11–18.
- Minke, Gernot. 2012. *Building with earth: design and technology of a sustainable architecture*. Walter de Gruyter.
- Minke, Gernot., and Mahlke, Friedemann. 2005. *Building with straw*. 1st edition edn. Boston: Birkhäuser.
- Moevus, Mariette, Fontaine, Laetitia, Anger, Romain, and Doat, Patrice. 2013. Projet: Béton d'Argile Environnemental (BAE).
- Morton, Tom, Stevenson, Fionn, Taylor, Bruce, and Charlton Smith, N. 2005. Low cost earth brick construction. *Arc Chartered Architects, Fife*.
- Moss, Keith. 2007. *Heat and mass transfer in buildings*. 2nd ed. edn. New York: Taylor.
- Mrlík, František. 1985. *Vlhkostné problémy stavebných materiálů a konstrukcií*. ALFA-vydavatel'stvo technickej a ekonomickej.
- Mundt Petersen, Solof, and Harderup, Lars-Erik. 2013. Validation of a 1D transient heat and moisture calculation tool under real conditions. *In: Thermal Performance of the Exterior Envelopes of Whole Buildings XII*.
- Newport Partners. 2004. Building moisture and durability: Past, present and future work. *U.S. Department of Housing and Urban Development*. Available from: <https://www.huduser.gov/Publications/pdf/BuildingMoistureandDurability.pdf>.
- Nguyen, Tai-Thu, Picandet, Vincent, Amziane, Sofiane, and Baley, Christophe. 2009. Influence of compactness and hemp hurd characteristics on the mechanical properties of lime and hemp concrete. *European Journal of Environmental and Civil Engineering*, **13**(9), 1039–1050.
- Nordby, Anne Sigrid, and Shea, Andrew David. 2013. Building materials in the operational phase. *Journal of Industrial Ecology*, **17**(5), 763–776.
- Nytsch-Geusen, Christoph, Nouidui, Thierry, Holm, Andreas, and Haupt, Wolfram. 2005. A hygrothermal building model based on the object-oriented modeling language Modelica. *Pages 867–876 of: Proceedings of the Ninth International IBPSA Conference*, vol. 1.

- Pickover, Clifford. 2008. *Archimedes to Hawking: laws of science and the great minds behind them*. Oxford University Press.
- Pumpelly, Raphael. 1908. *Explorations in Turkestan*.
- Rani, Manviri, Shim, Won Joon, Han, Gi Myung, Jang, Mi, Song, Young Kyoung, and Hong, Sang Hee. 2014. Hexabromocyclododecane in polystyrene based consumer products: an evidence of unregulated use. *Chemosphere*, **110**, 111–119.
- Rauch, Martin. [online]. [cit. 2017-04-12] Available from: <http://www.lehmtonerde.at/en/projects/project.php?pID=7>.
- Rieger-Jandl, Andrea. 2015. Experimenteller Lehm-bau im Waldökozentrum Sopron. TU Wien.
- Rode, Carsten, and Clorius, Christian Odin. 2004. Modeling of moisture transport in wood with hysteresis and temperature dependent sorption characteristics.
- Rode, Carsten, Peuhkuri, Ruut Hannele, Mortensen, Lone Hedegaard, Hansen, Kurt Kielsgaard, Time, Berit, Gustavsen, Arild, Ojanen, Tuomo, Ahonen, Jarkko, Svennberg, Kaisa, Arfvidsson, Jesper, *et al.* 2005. *Moisture buffering of building materials*. Tech. rept. Technical University of Denmark, Department of Civil Engineering.
- Rode, Carsten, Peuhkuri, Ruut, Time, Berit, Svennberg, Kaisa, and Ojanen, Tuomo. 2007. Moisture buffer value of building materials. *Journal of ASTM International*, **4**(5), 1–12.
- Rozumek, Jakub. 2013. *Experimental determination of component ratio for new hemp-lime based blocks*. M.Phil. thesis, Czech Technical University in Prague.
- Samuel, Dubois, Arnaud, Evrard, Christophe, Blecker, and Frédéric, Lebeau. 2016. Temperature and moisture storage in crop-based materials: Modelling a straw bale wall subject to a thermal shock. *Journal of Building Physics*, **39**(5), 421–439.
- Schmidt, Olaf. 2007. Indoor wood-decay basidiomycetes: damage, causal fungi, physiology, identification and characterization, prevention and control. *Mycological Progress*, **6**(4), 261–279.
- Shea, Andy, Lawrence, Mike, and Walker, Pete. 2012. Hygrothermal performance of an experimental hemp–lime building. *Construction and Building Materials*, **36**, 270–275.
- Simonson, Carey J., Salonvaara, Mikael, and Ojanen, Tuomo. 2001. *Improving indoor climate and comfort with wooden structures*. Technical Research Centre of Finland.
- Ståhl, Fredrik. 2009. *Influence of thermal mass on the heating and cooling demands of a building unit*. Chalmers University of Technology.
- Stanwix, William, and Sparrow, Alex. 2014. *The HempcHemp Book: Design and building with hemp-lime*. Green Books.

- Stockscape. [online]. [cit. 2017-02-12] Available from: <http://www.stockscape.co.uk/wp-content/uploads/2013/10/Clay.jpg>.
- Stone, Clayton, and Katunsky, Dusan. 2015. Dynamic thermal properties of uninsulated rammed earth envelopes. *Pollack Periodica*, **10**(1), 103–112.
- Straube, J. 2006. *Moisture, materials, and straw bales. V: Design of straw bale building-The state of the artpages*, B. King ed.
- Summers, Matthew D, Blunk, Sherry L, and Jenkins, Bryan M. 2003. How straw decomposes: Implications for straw bale construction. *Ecological Building Network, San Rafael, CA, USA*.
- Svoboda, Zbyněk. 2015. *Teplo*. Prague, Czechia: K-CAD. Available from: <http://kcad.cz/cz/stavebni-fyzika/tepelna-technika/teplo/>.
- Szász, Bianka. 2013 (December). *Comparison between a brick building and straw-bale building in terms of energy efficiency*. M.Phil. thesis, TU Wien, Vienna.
- Taylor, P, and Luther, MB. 2004. Evaluating rammed earth walls: a case study. *Solar Energy*, **76**(1), 79–84.
- Thygesen, Anders. 2001. *Properties of hemp fibre polymer composites-An optimisation*. Vol. 5.
- Van den Bulcke, Jan, Van Acker, Joris, and De Smet, Jordi. 2009. An experimental set-up for real-time continuous moisture measurements of plywood exposed to outdoor climate. *Building and Environment*, **44**(12), 2368–2377.
- Vaverka, Jiří, Chybík, Josef, and Mrlík, František. 2000. *Stavební fyzika 2: stavební tepelná technika*. Vutium.
- Wihan, Jakub. 2007. Humidity in straw bale walls and its effect on the decomposition of straw. *University of East London*.
- Winkler, Matthias, Nore, Kristine, and Antretter, Florian. 2014. Impact of the moisture buffering effect of wooden materials on energy demand and comfort conditions. 10th Nordic Symposium on Building Physics. Available from: <https://wufi.de/literatur/Winkler,%20Nore%20et%20al%202014%20-%20Impact%20of%20the%20moisture%20buffering.pdf>.
- Wrrnetwork. [online]. [cit. 2017-02-12] Available from: <http://wrrnetwork.com/wp-content/uploads/2015/06/timbewr.jpg>.
- WUFI. 2016. *version 6.1*. Munich, Germany: Fraunhofer Institut für Bauphysik. Available from: <https://wufi.de/en/>.
- Yates, T. 2002. Final report on the construction of the hemp houses at Haverhill, Suffolk. *Building Research Establishment, Watford, report*, 209–717.

Zillig, Wolfgang. 2009 (May). *Moisture transport in wood using a multiscale approach*.  
Ph.D. thesis, University of Leuven, Kasteelpark Arenberg 40, B-3001 Leuven.

## Appendix A Tables and Figures

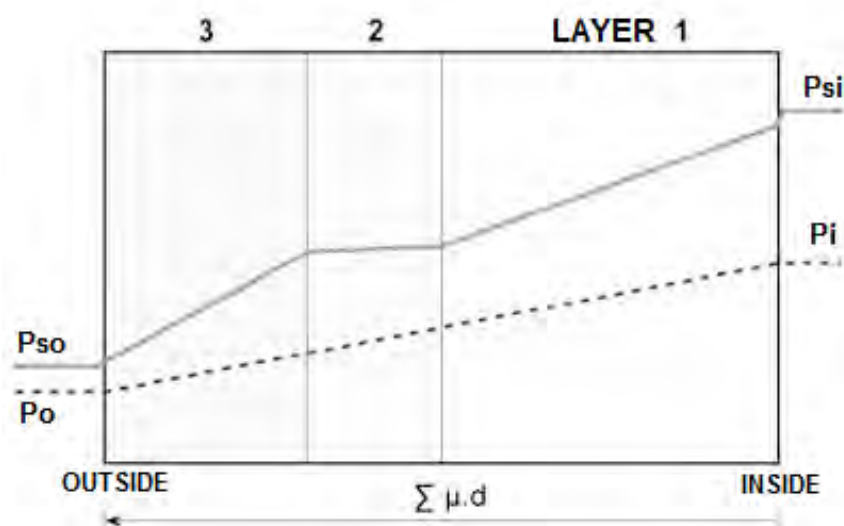


**Fig. A.1:** Glaser diagram showing distribution of saturation pressure  $P_s$  (solid line) and partial water vapour pressure  $P$  (dashed line) through a multi-layered composite wall in steady state RH environment:

By depicting single layers in terms of equivalent air layer thickness  $s_a$ , it can be assumed that the propagation of water vapour and thus distribution of partial water vapour pressure of diffused air through the newly defined component thickness is linear (dashed line). When the solid line (representing saturation pressure of air at computed temperature) gets at any point of the diagram under the dashed line, interstitial condensation inevitably occurs.

Fibre composition (g/100 g DM)	Cellulose	Hemi- cellulose	Lignin	Pectin	Wax	Water extractives	Minerals
<b>Hemp fibres from different cultivars</b>							
Futura 77	54	14	13	●	15 <sup>1</sup>	●	4
Fedora 19 (stems)	61	10	12	●	12 <sup>1</sup>	●	4
Fedora 19 (shives)	47-48	21-25	16-19	●	8-9 <sup>1</sup>	●	1-2
<b>Fibres from other plants</b>							
Flax	64	16	2	2	n.a. <sup>2</sup>	n.a. <sup>2</sup>	n.a. <sup>2</sup>
Jute	58-60	14-16	12	0-2	n.a. <sup>2</sup>	n.a. <sup>2</sup>	8
Norway spruce	49	20	29	1	0	1	0
Barley straw	43	38	9	0	0	5	5
Corn stover	33	33	14	1	3	10	7

1: Measured "non cell wall material" including pectin, wax and water

2: n.a. = Not available

**Fig. A.2:** Chemical composition of different bast fibres (hemp, flax and jute), wood fibres (Norway spruce) and straw fibres (barley straw and corn stover) (Thygesen, 2001)

Air Temperature	Relative Humidity					
	100 %	90 %	80 %	70 %	60 %	50 %
20 °C	17,29	15,56	13,83	12,10	10,37	8,65
18 °C	15,37	13,84	12,30	10,76	9,22	7,69
16 °C	13,63	12,27	10,90	9,54	8,18	6,82
14 °C	12,07	10,87	9,66	8,45	7,24	6,04
12 °C	10,67	9,60	8,53	7,47	6,40	5,33
10 °C	9,41	8,46	7,52	6,58	5,64	4,70
8 °C	8,28	7,45	6,62	5,80	4,97	4,14
6 °C	7,26	6,54	5,81	5,08	4,36	3,63
4 °C	6,36	5,73	5,09	4,46	3,82	3,18
2 °C	5,56	5,00	4,45	3,89	3,34	2,78
0 °C	4,85	4,36	3,88	3,39	2,91	2,42
-2 °C	4,14	3,72	3,31	2,90	2,48	2,07
-4 °C	3,52	3,17	2,82	2,47	2,11	1,76
-6 °C	2,99	2,69	2,39	2,09	1,79	1,49
-8 °C	2,53	2,28	2,02	1,77	1,52	1,27
-10 °C	2,14	1,93	1,71	1,50	1,29	1,07
-12 °C	1,80	1,62	1,44	1,26	1,08	0,90
-14 °C	1,52	1,37	1,21	1,06	0,91	0,76
-16 °C	1,27	1,14	1,02	0,89	0,76	0,64
-18 °C	1,07	0,96	0,85	0,75	0,64	0,53
-20 °C	0,88	0,79	0,70	0,62	0,53	0,44

*Fig. A.3: Absolute humidity [g/m<sup>3</sup>] of air of different temperatures at different RH states (atmospheric pressure of 101 kPa)*

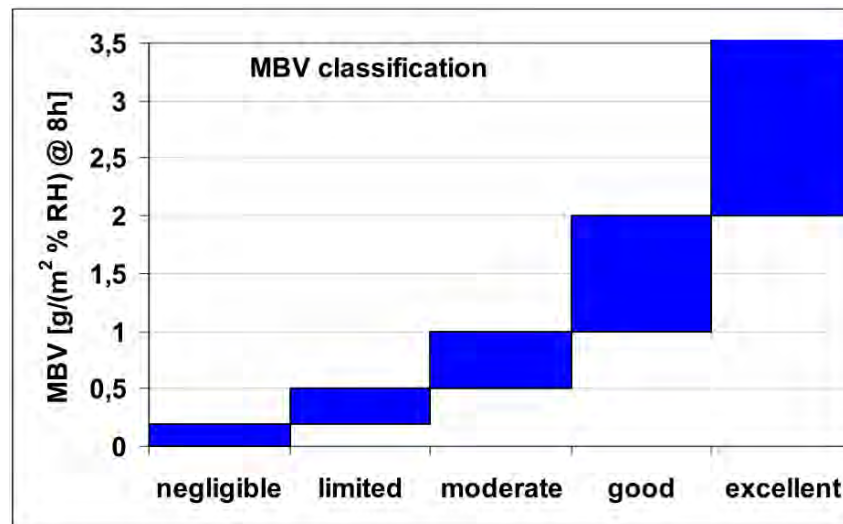


*Fig. A.4: MBV classification according to Rode et al. (2005)*

## Appendix B Composition of simulated RNBM

**Tab. B.1:** *Composition of SRE wall mix (Allinson and Hall, 2010)*

Constituents	Earth mix [by volume]	SRE [wt%]
Ironstone quarry waste	2/3	83
Grit sand	1/3	
Portland cement (white) with hydrophobic chemical admixture		7

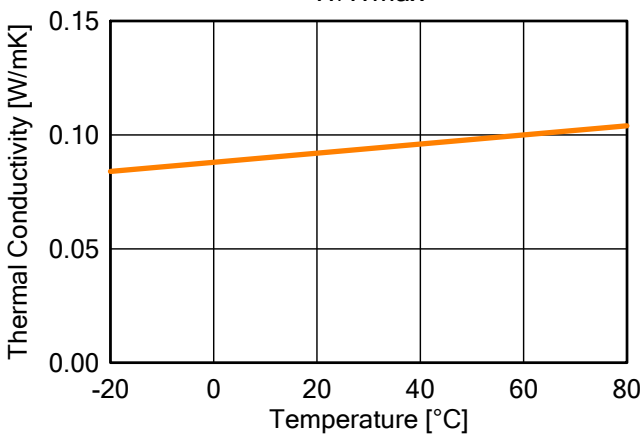
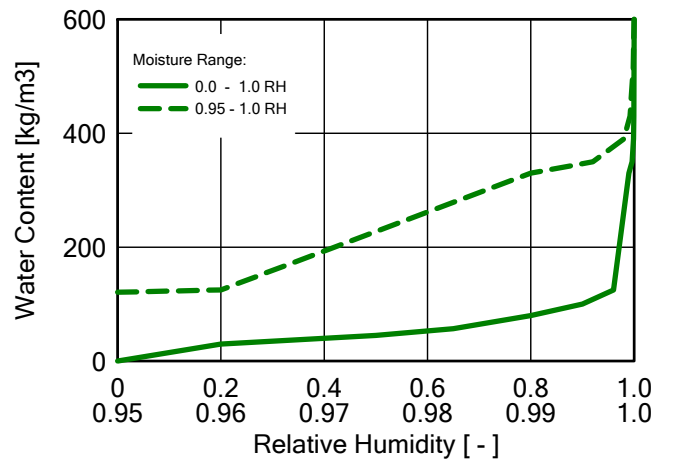
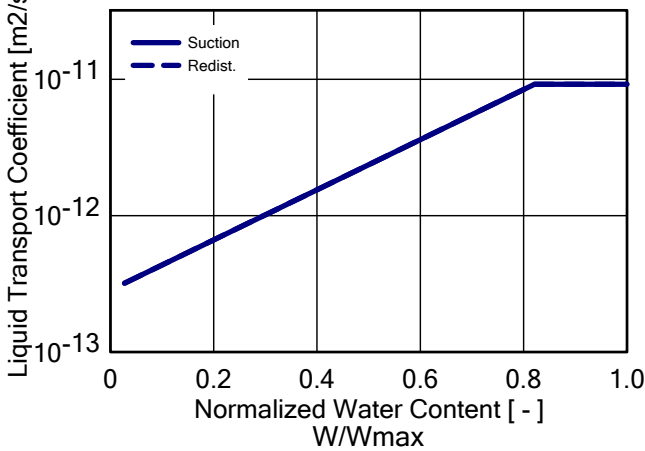
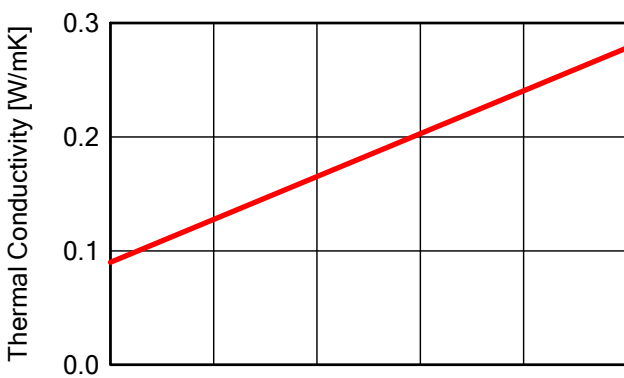
**Tab. B.2:** *Composition of Hempcrete wall mix (Evrard, 2008)*

Constituents	Mass [kg]	Volume [l]
Hemp shiv (Chanvribat)	20	1010
Lime binder (Tradical pf 70)	40	410
Water	60	400

## Appendix C Simulation input material data

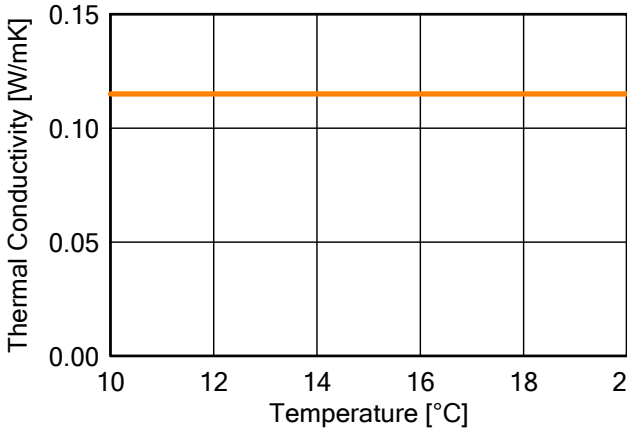
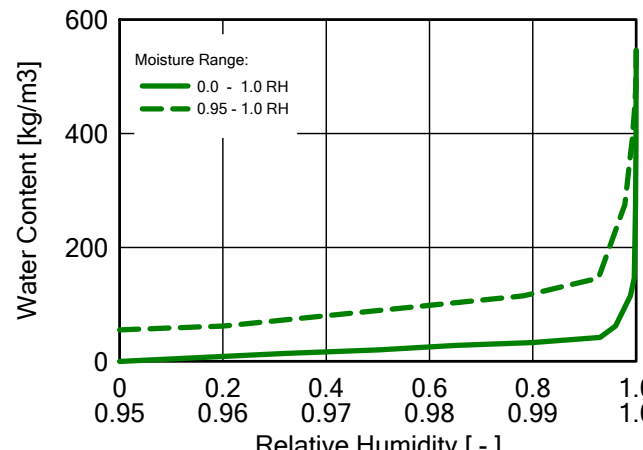
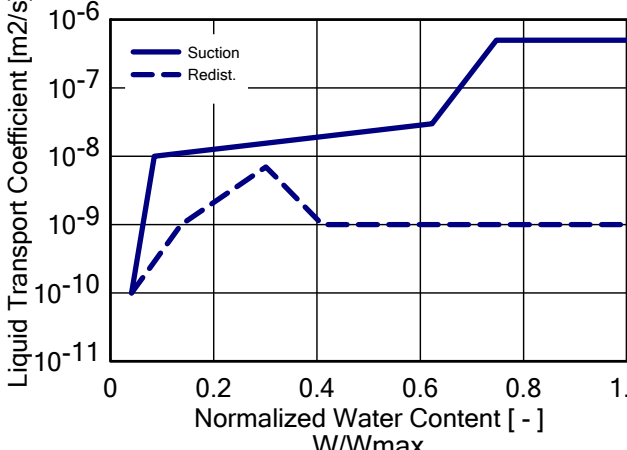
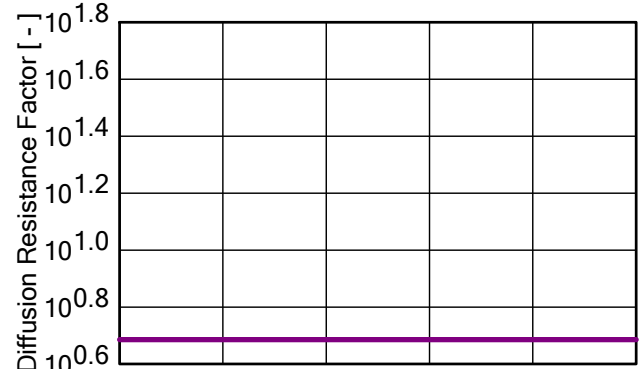
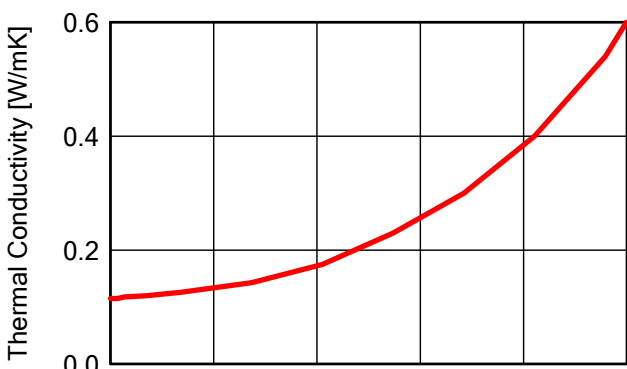
Material: Spruce, radial (Holz 100)

Property	Unit	Value
Bulk density	[kg/m <sup>3</sup> ]	455.0
Porosity	[m <sup>3</sup> /m <sup>3</sup> ]	0.73
Specific Heat Capacity, Dry	[J/kgK]	1500.0
Thermal Conductivity, Dry, 10°C	[W/mK]	0.09
Water Vapour Diffusion Resistance Factor	[-]	130.0
Moisture-dep. Thermal Cond. Supplement	[%/M.-%]	1.3
Temp-dep. Thermal Cond. Supplement	[W/mK <sup>2</sup> ]	0.0002
Thermal Conductivity, Design Value	[W/mK]	0.1066



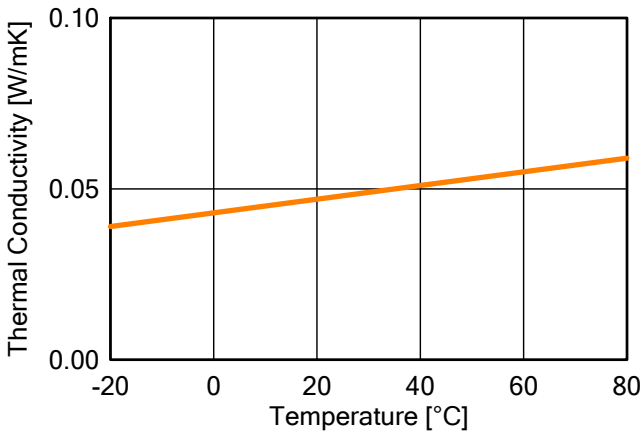
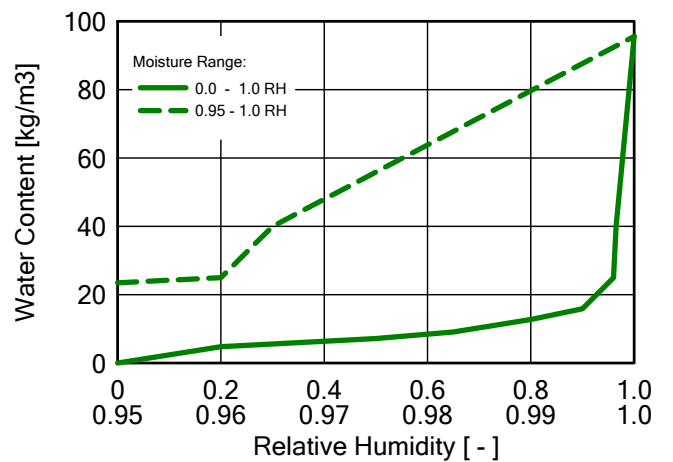
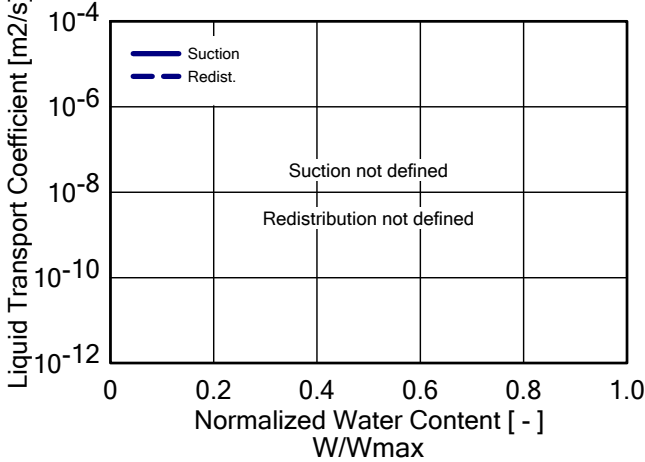
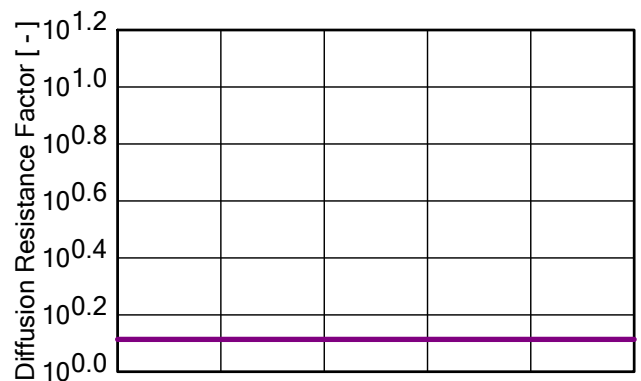
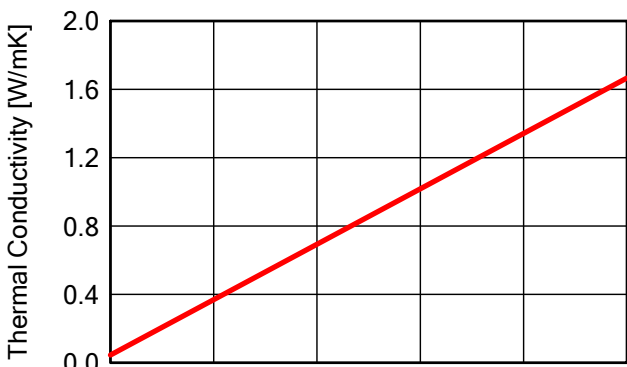
Material: Hempcrete

Property	Unit	Value
Bulk density	[kg/m <sup>3</sup> ]	440.0
Porosity	[m <sup>3</sup> /m <sup>3</sup> ]	0.73
Specific Heat Capacity, Dry	[J/kgK]	1560.0
Thermal Conductivity, Dry, 10°C	[W/mK]	0.115
Water Vapour Diffusion Resistance Factor	[ - ]	4.85
Thermal Conductivity, Design Value	[W/mK]	0.119



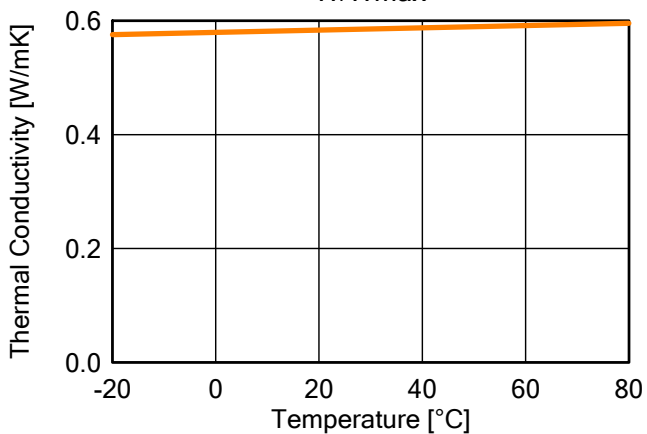
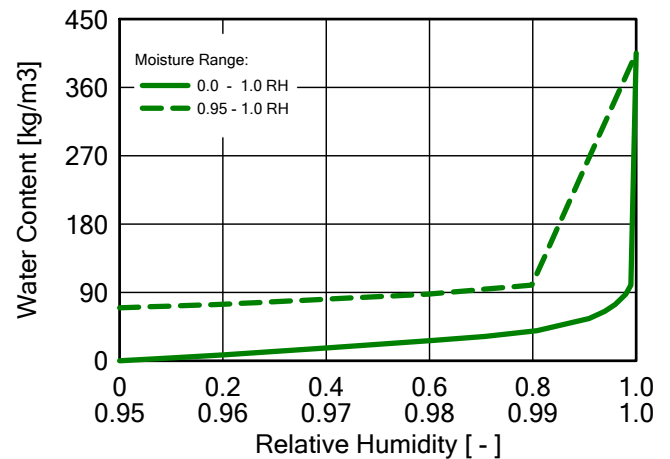
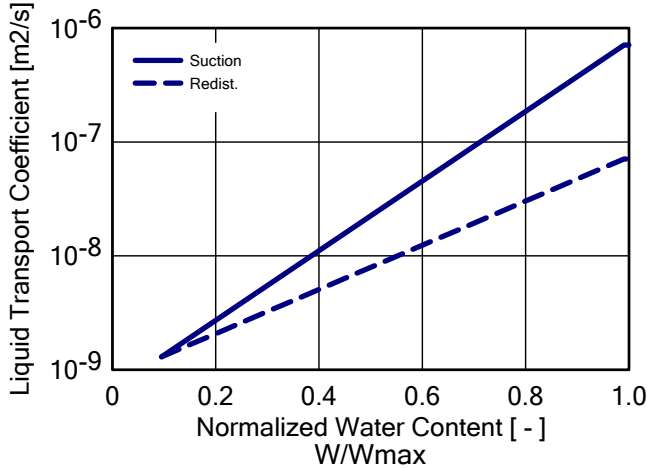
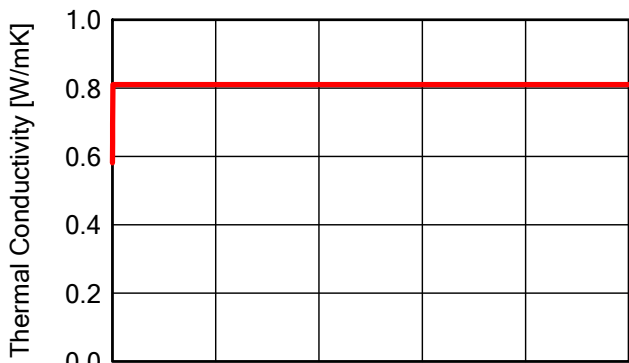
Material: Straw bale

Property	Unit	Value
Bulk density	[kg/m <sup>3</sup> ]	100.0
Porosity	[m <sup>3</sup> /m <sup>3</sup> ]	0.9
Specific Heat Capacity, Dry	[J/kgK]	2000.0
Thermal Conductivity, Dry, 10°C	[W/mK]	0.045
Water Vapour Diffusion Resistance Factor	[ - ]	1.3
Moisture-dep. Thermal Cond. Supplement	[%/M.-%]	4.0
Temp-dep. Thermal Cond. Supplement	[W/mK <sup>2</sup> ]	0.0002
Thermal Conductivity, Design Value	[W/mK]	0.0636



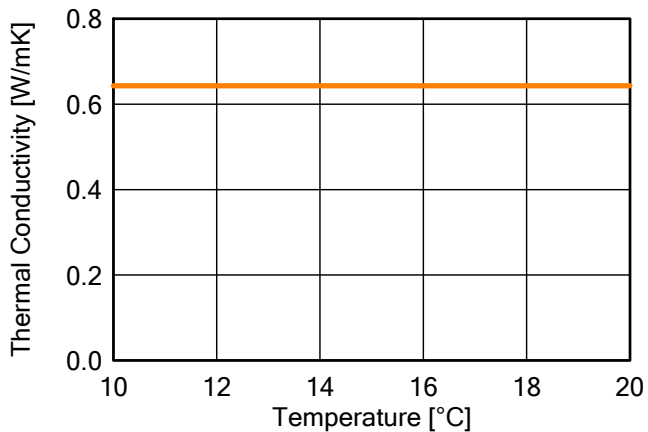
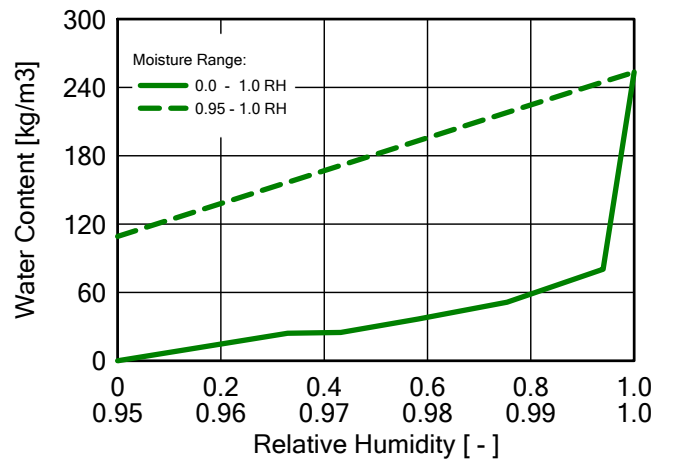
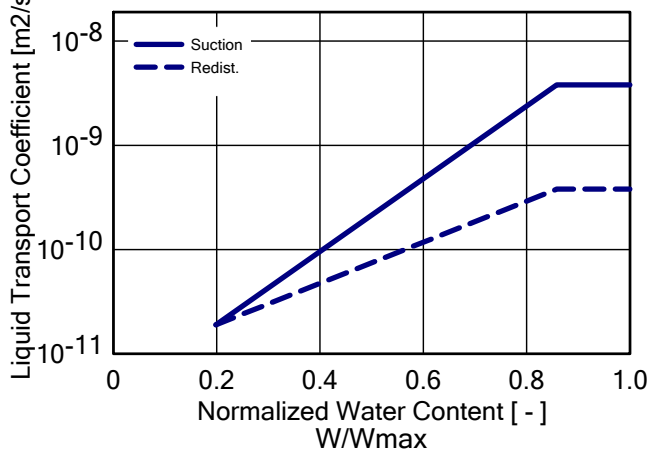
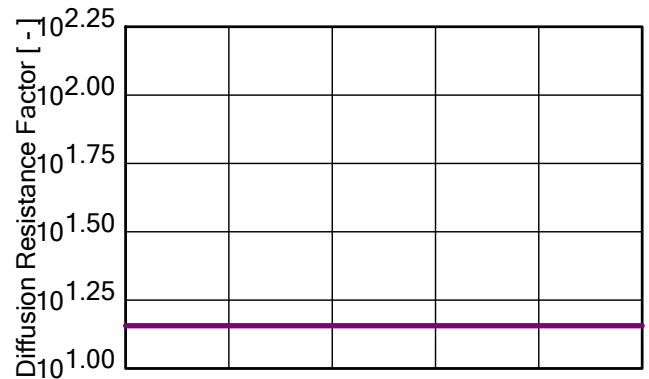
Material: Loam Brick (adobe)

Property	Unit	Value
Bulk density	[kg/m <sup>3</sup> ]	1567.77
Porosity	[m <sup>3</sup> /m <sup>3</sup> ]	0.408387
Specific Heat Capacity, Dry	[J/kgK]	880.389
Thermal Conductivity, Dry, 10°C	[W/mK]	0.5815
Water Vapour Diffusion Resistance Factor	[ - ]	11.3684
Reference Water Content	[kg/m <sup>3</sup> ]	38.9
Free Water Saturation	[kg/m <sup>3</sup> ]	405.0
Water Absorption Coefficient	[kg/m <sup>2</sup> s <sup>0.5</sup> ]	0.175662
Temp-dep. Thermal Cond. Supplement	[W/mK <sup>2</sup> ]	0.0002
Thermal Conductivity, Design Value	[W/mK]	0.599



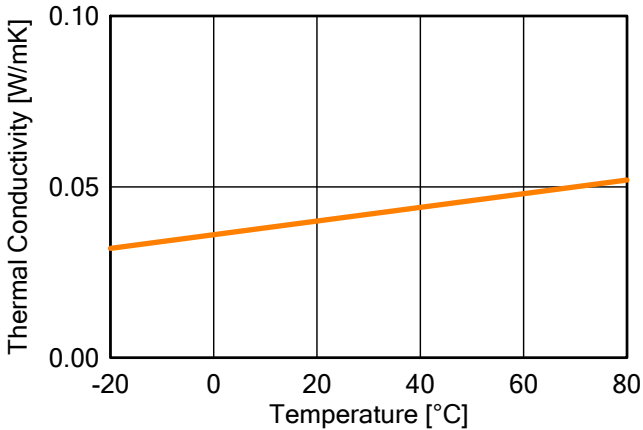
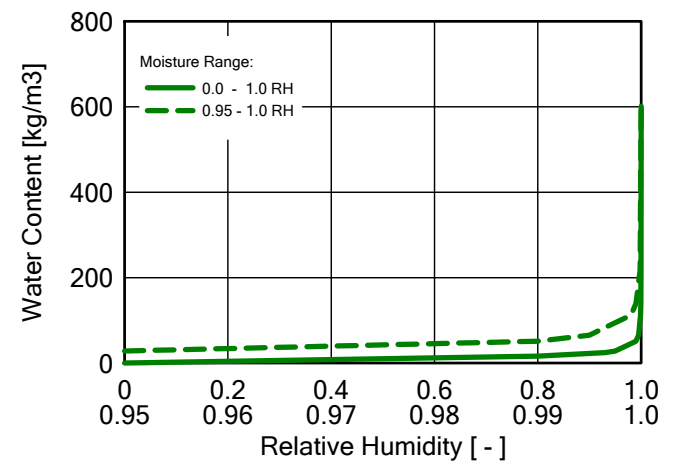
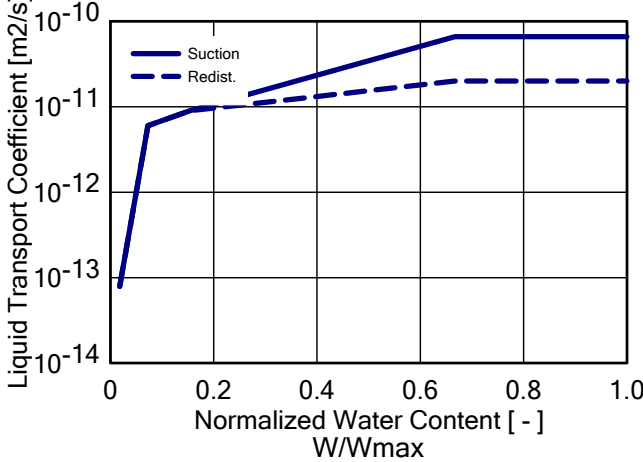
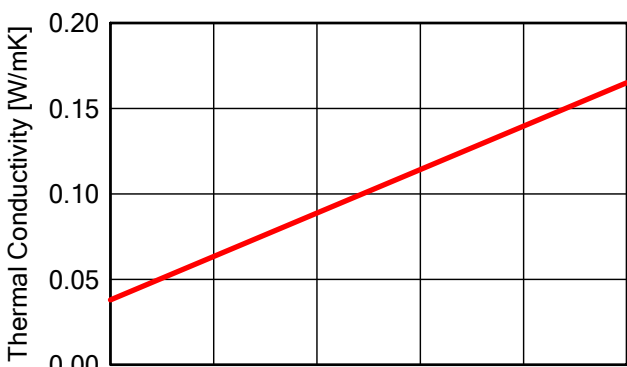
Material: Stabilised rammed earth (SRE)

Property	Unit	Value
Bulk density	[kg/m <sup>3</sup> ]	1900.0
Porosity	[m <sup>3</sup> /m <sup>3</sup> ]	0.295
Specific Heat Capacity, Dry	[J/kgK]	868.0
Thermal Conductivity, Dry, 10°C	[W/mK]	0.643
Water Vapour Diffusion Resistance Factor	[ - ]	14.34
Reference Water Content	[kg/m <sup>3</sup> ]	58.5873
Free Water Saturation	[kg/m <sup>3</sup> ]	253.47
Water Absorption Coefficient	[kg/m <sup>2</sup> s <sup>0.5</sup> ]	0.008
Moisture-dep. Thermal Cond. Supplement	[%/M.-%]	4.39
Thermal Conductivity, Design Value	[W/mK]	0.713



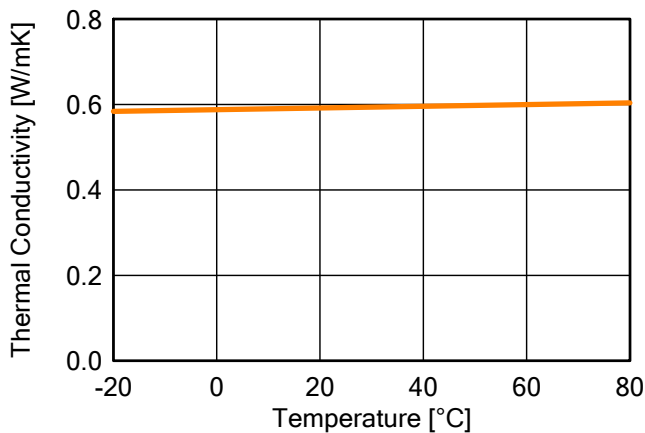
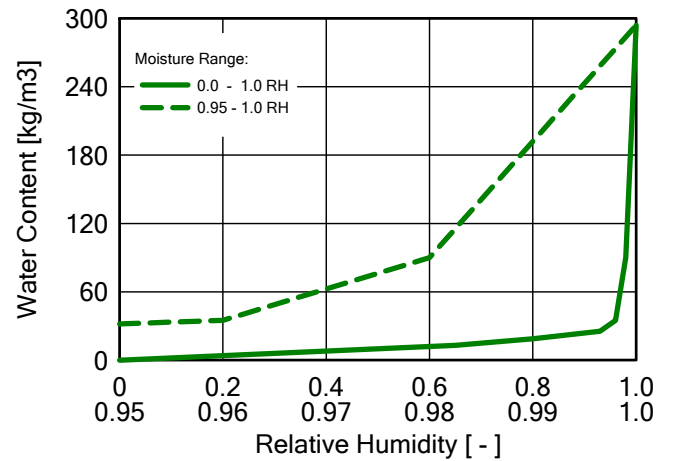
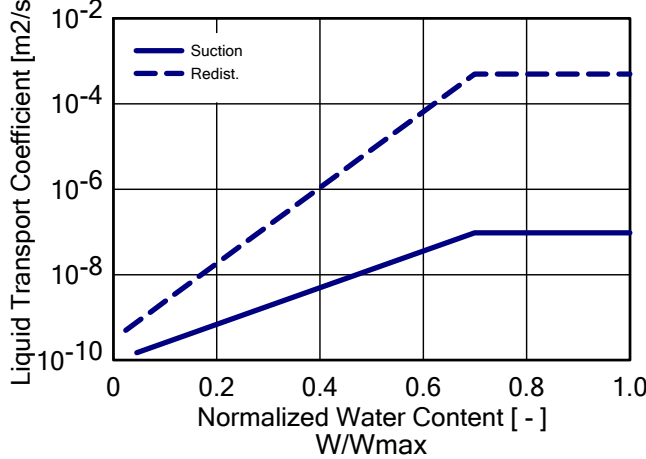
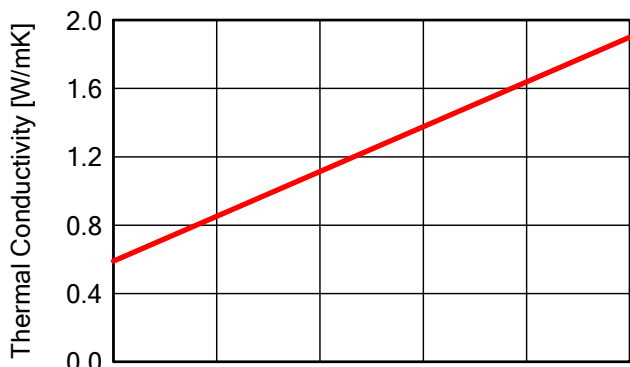
Material: HOMATHERM EnergiePlus massive (wood fibre insulation)

Property	Unit	Value
Bulk density	[kg/m <sup>3</sup> ]	135.0
Porosity	[m <sup>3</sup> /m <sup>3</sup> ]	0.9
Specific Heat Capacity, Dry	[J/kgK]	2100.0
Thermal Conductivity, Dry, 10°C	[W/mK]	0.038
Water Vapour Diffusion Resistance Factor	[-]	2.1
Moisture-dep. Thermal Cond. Supplement	[%/M.-%]	0.5
Temp-dep. Thermal Cond. Supplement	[W/mK <sup>2</sup> ]	0.0002
Thermal Conductivity, Design Value	[W/mK]	0.04



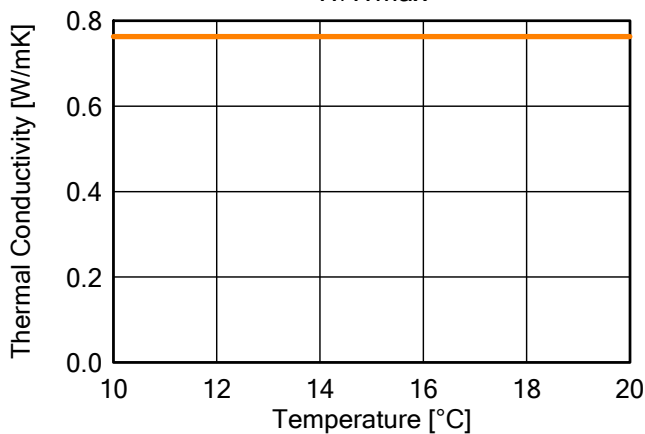
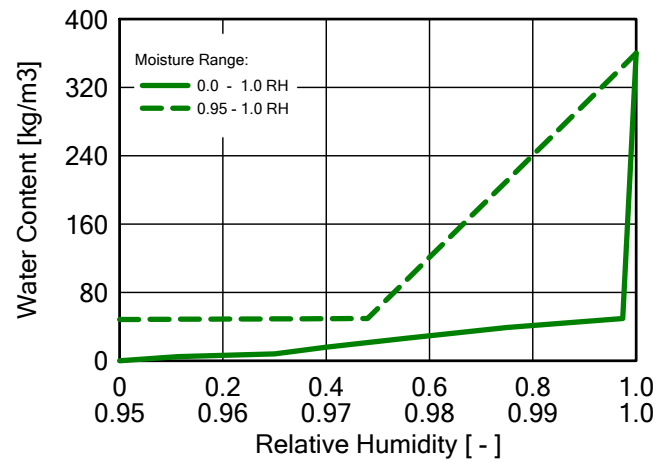
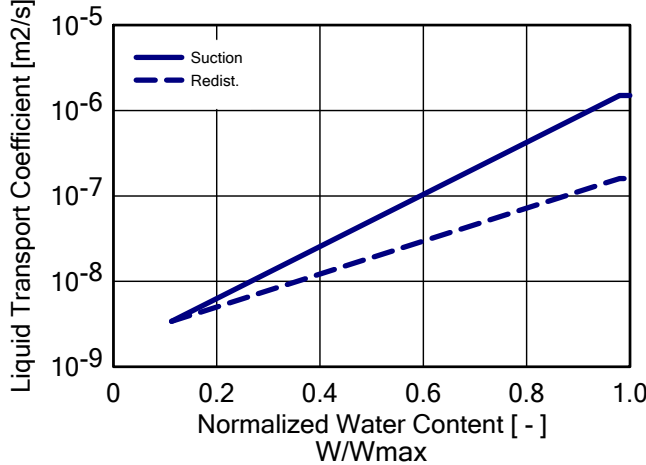
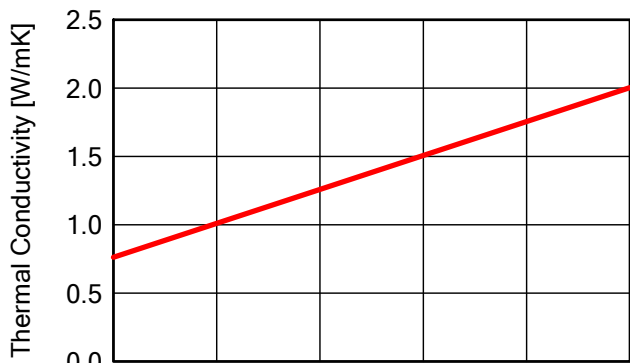
Material: Loam Plaster

Property	Unit	Value
Bulk density	[kg/m <sup>3</sup> ]	1514.0
Porosity	[m <sup>3</sup> /m <sup>3</sup> ]	0.42
Specific Heat Capacity, Dry	[J/kgK]	1000.0
Thermal Conductivity, Dry, 10°C	[W/mK]	0.59
Water Vapour Diffusion Resistance Factor	[ - ]	11.0
Reference Water Content	[kg/m <sup>3</sup> ]	19.0
Free Water Saturation	[kg/m <sup>3</sup> ]	294.0
Water Absorption Coefficient	[kg/m <sup>2</sup> s <sup>0.5</sup> ]	0.0467
Moisture-dep. Thermal Cond. Supplement	[%/M.-%]	8.0
Temp-dep. Thermal Cond. Supplement	[W/mK <sup>2</sup> ]	0.0002
Thermal Conductivity, Design Value	[W/mK]	0.637



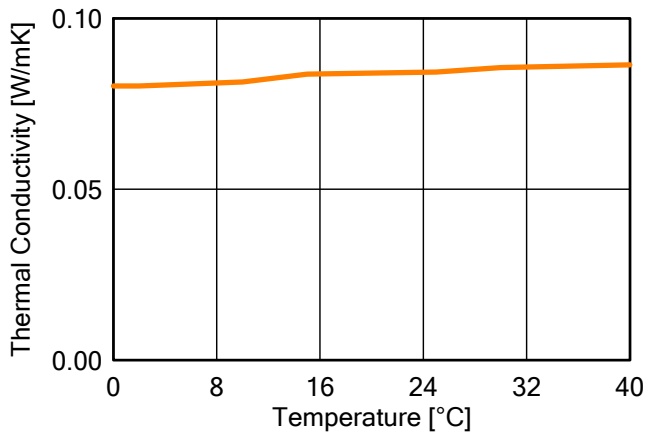
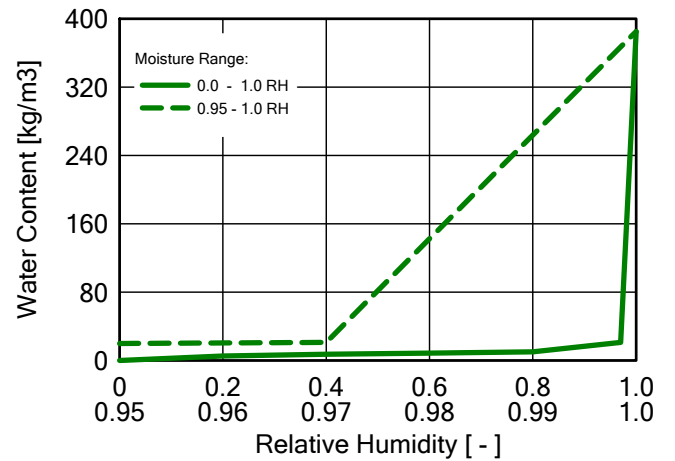
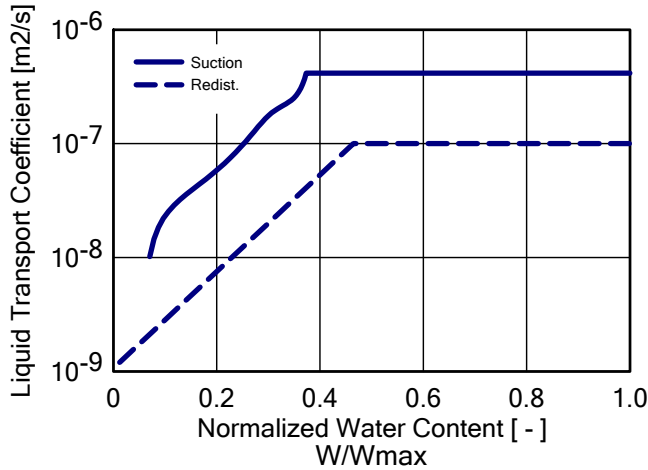
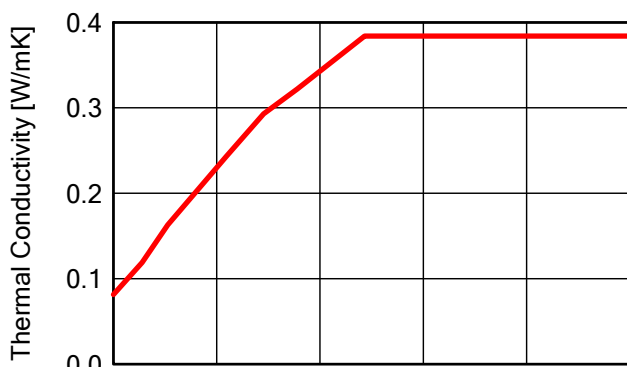
Material: Lime render

Property	Unit	Value
Bulk density	[kg/m <sup>3</sup> ]	1650.0
Porosity	[m <sup>3</sup> /m <sup>3</sup> ]	0.367
Specific Heat Capacity, Dry	[J/kgK]	910.0
Thermal Conductivity, Dry, 10°C	[W/mK]	0.763
Water Vapour Diffusion Resistance Factor	[ - ]	9.0
Reference Water Content	[kg/m <sup>3</sup> ]	41.3438
Free Water Saturation	[kg/m <sup>3</sup> ]	360.0
Water Absorption Coefficient	[kg/m <sup>2</sup> s <sup>0.5</sup> ]	0.23
Moisture-dep. Thermal Cond. Supplement	[%/M.-%]	7.3
Thermal Conductivity, Design Value	[W/mK]	0.884



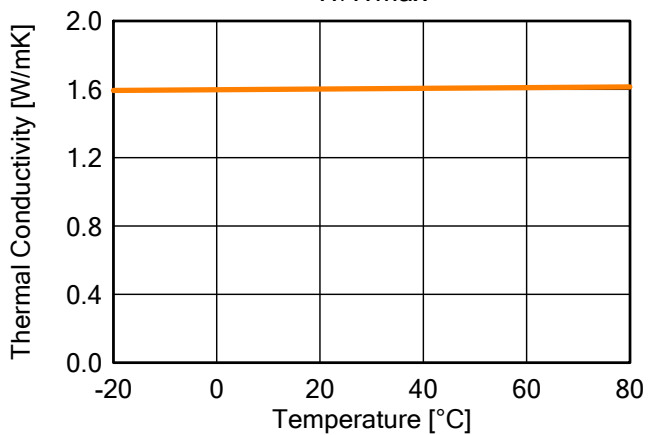
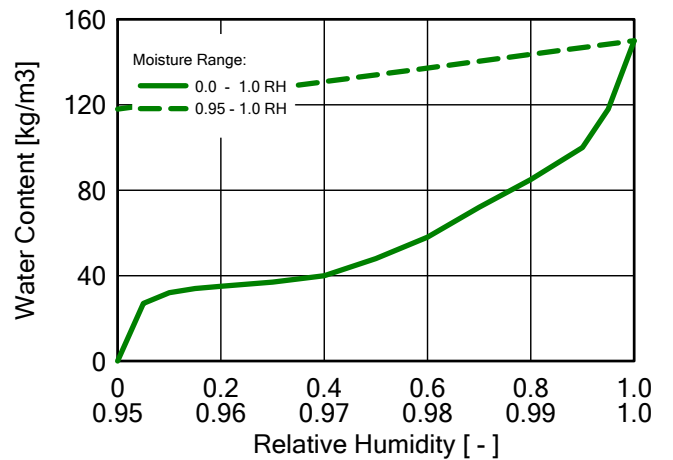
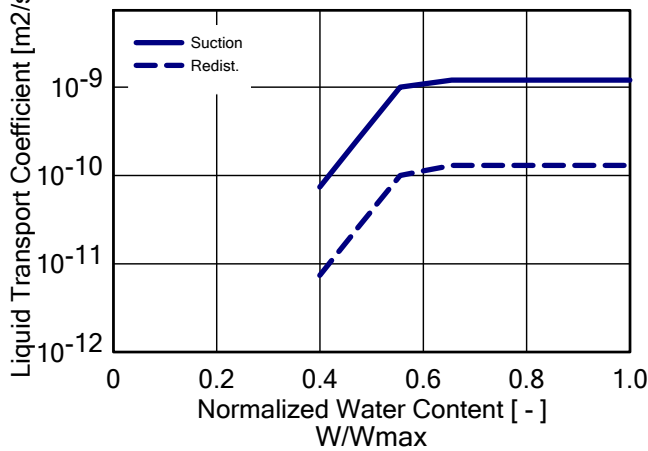
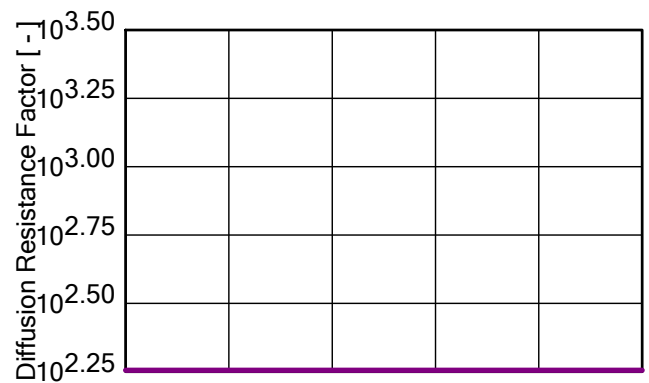
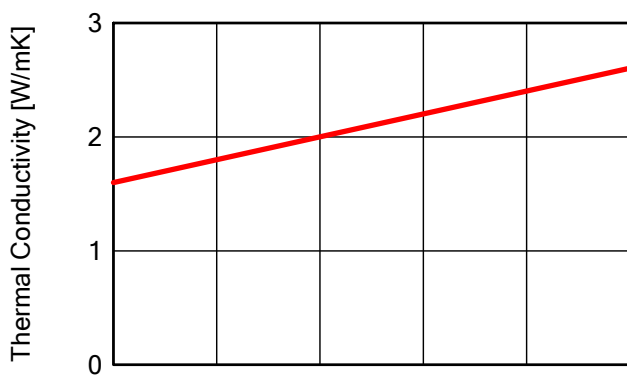
Material: AAC\_P2-350

Property	Unit	Value
Bulk density	[kg/m <sup>3</sup> ]	363.0
Porosity	[m <sup>3</sup> /m <sup>3</sup> ]	0.828
Specific Heat Capacity, Dry	[J/kgK]	1160.0
Thermal Conductivity, Dry, 10°C	[W/mK]	0.0814
Water Vapour Diffusion Resistance Factor	[ - ]	12.0
Reference Water Content	[kg/m <sup>3</sup> ]	10.02
Free Water Saturation	[kg/m <sup>3</sup> ]	385.0
Water Absorption Coefficient	[kg/m <sup>2</sup> s <sup>0.5</sup> ]	0.2
Thermal Conductivity, Design Value	[W/mK]	0.092



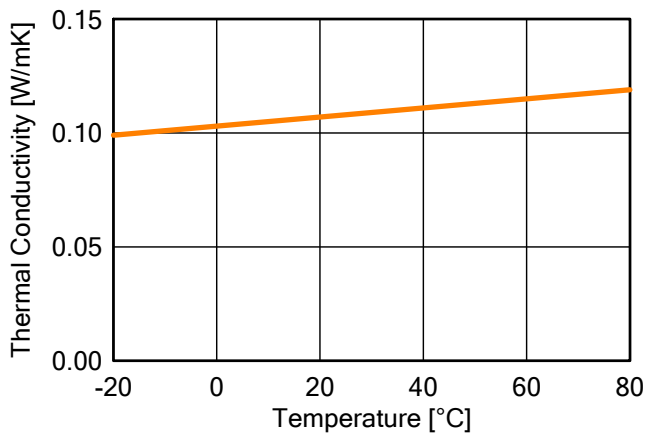
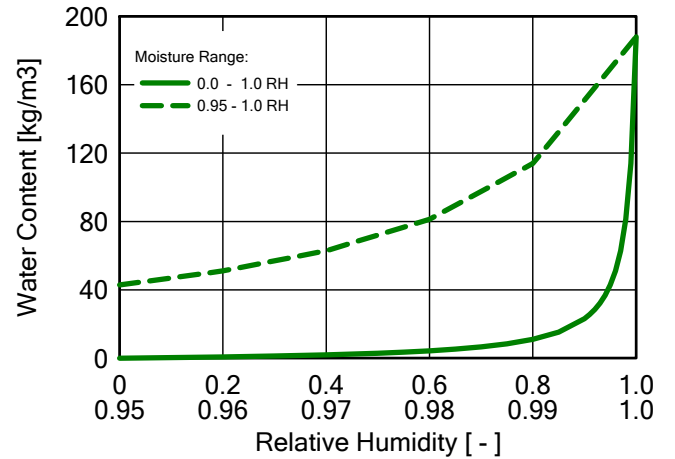
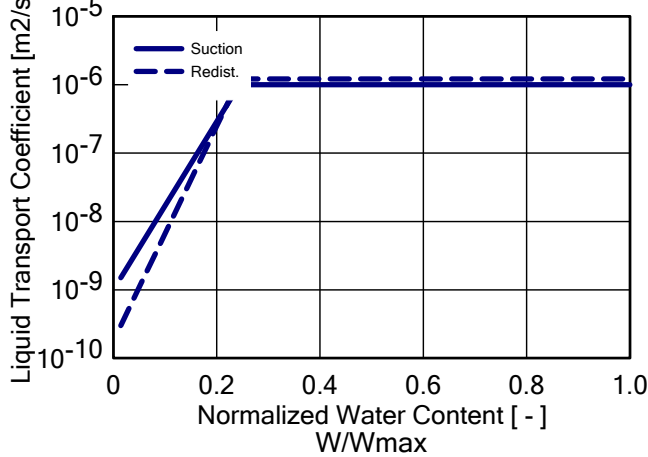
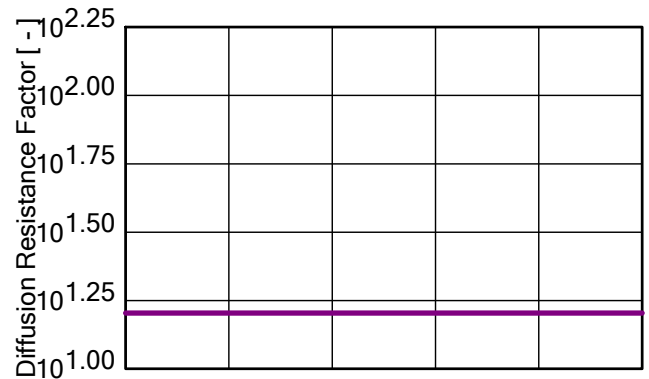
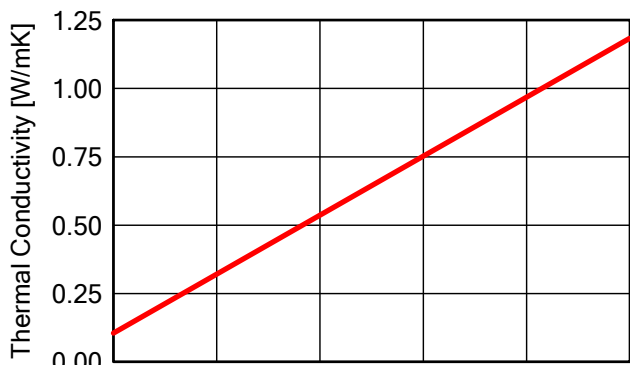
Material: Concrete, w/c=0.5

Property	Unit	Value
Bulk density	[kg/m <sup>3</sup> ]	2300.0
Porosity	[m <sup>3</sup> /m <sup>3</sup> ]	0.18
Specific Heat Capacity, Dry	[J/kgK]	850.0
Thermal Conductivity, Dry, 10°C	[W/mK]	1.6
Water Vapour Diffusion Resistance Factor	[-]	180.0
Moisture-dep. Thermal Cond. Supplement	[%/M.-%]	8.0
Temp-dep. Thermal Cond. Supplement	[W/mK <sup>2</sup> ]	0.0002
Thermal Conductivity, Design Value	[W/mK]	2.001



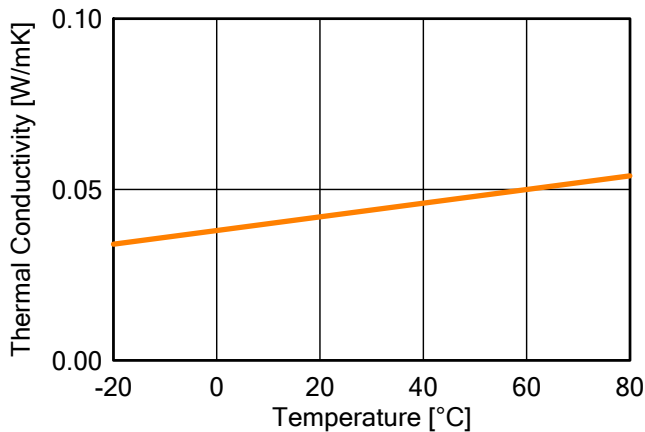
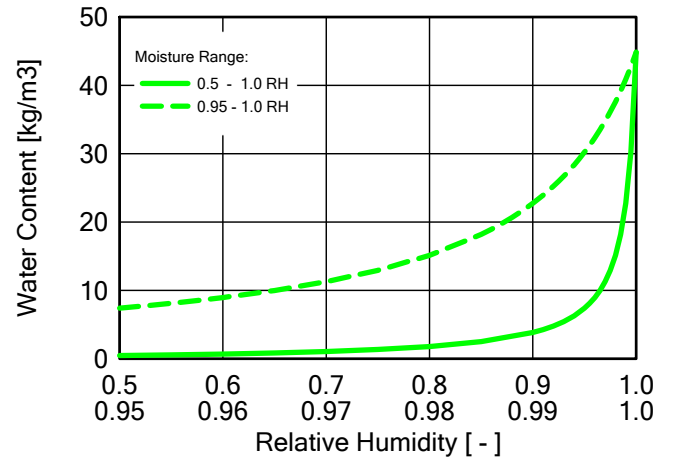
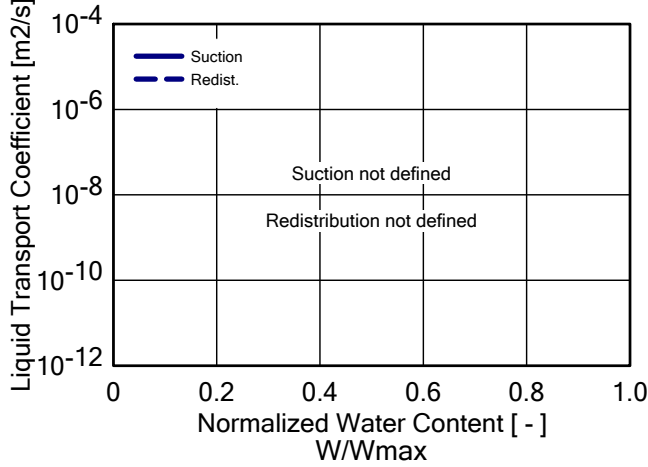
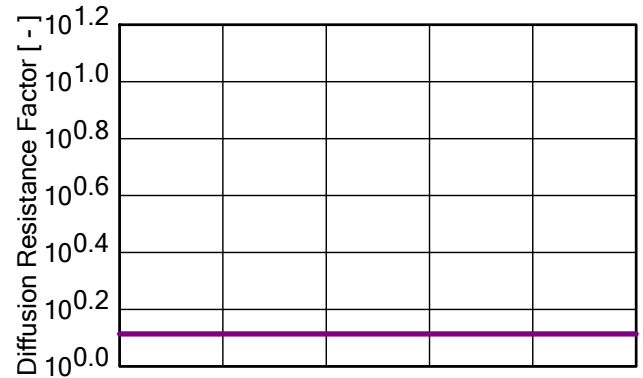
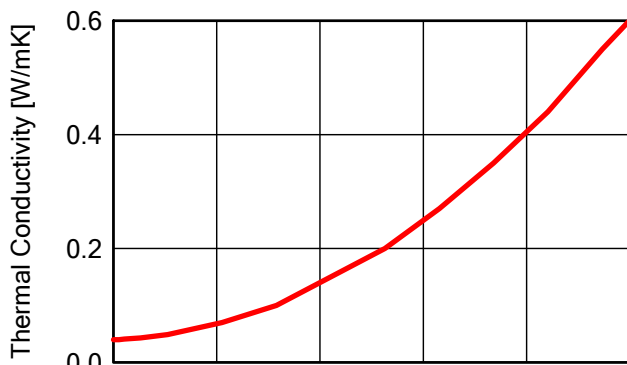
Material: Perforated brick

Property	Unit	Value
Bulk density	[kg/m <sup>3</sup> ]	600.0
Porosity	[m <sup>3</sup> /m <sup>3</sup> ]	0.77
Specific Heat Capacity, Dry	[J/kgK]	850.0
Thermal Conductivity, Dry, 10°C	[W/mK]	0.105
Water Vapour Diffusion Resistance Factor	[ - ]	16.0
Reference Water Content	[kg/m <sup>3</sup> ]	11.0
Free Water Saturation	[kg/m <sup>3</sup> ]	188.0
Water Absorption Coefficient	[kg/m <sup>2</sup> s <sup>0.5</sup> ]	0.0983
Moisture-dep. Thermal Cond. Supplement	[%/M.-%]	8.0
Temp-dep. Thermal Cond. Supplement	[W/mK <sup>2</sup> ]	0.0002
Thermal Conductivity, Design Value	[W/mK]	0.1142



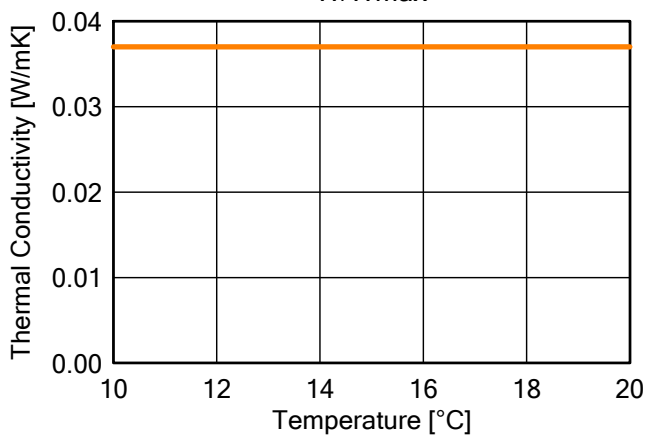
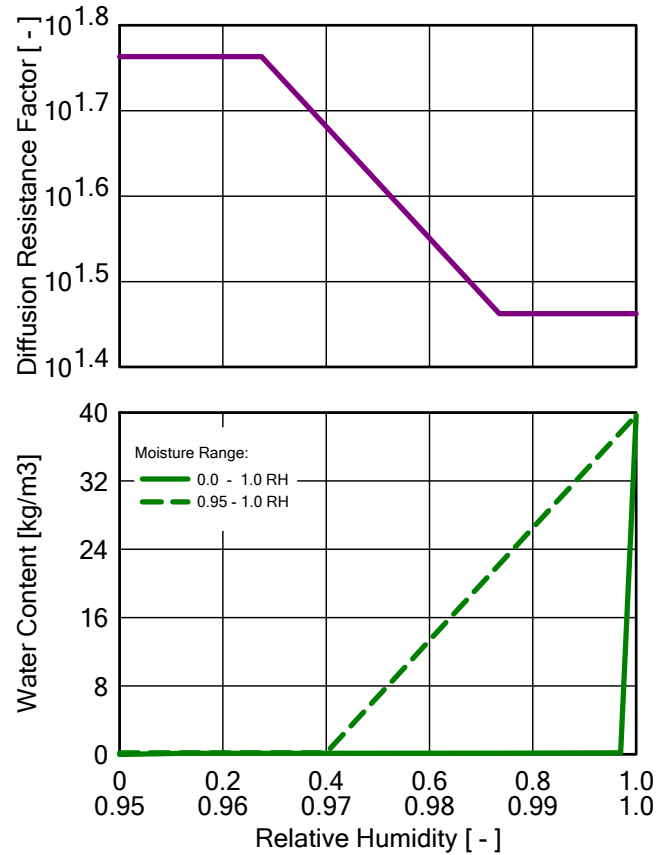
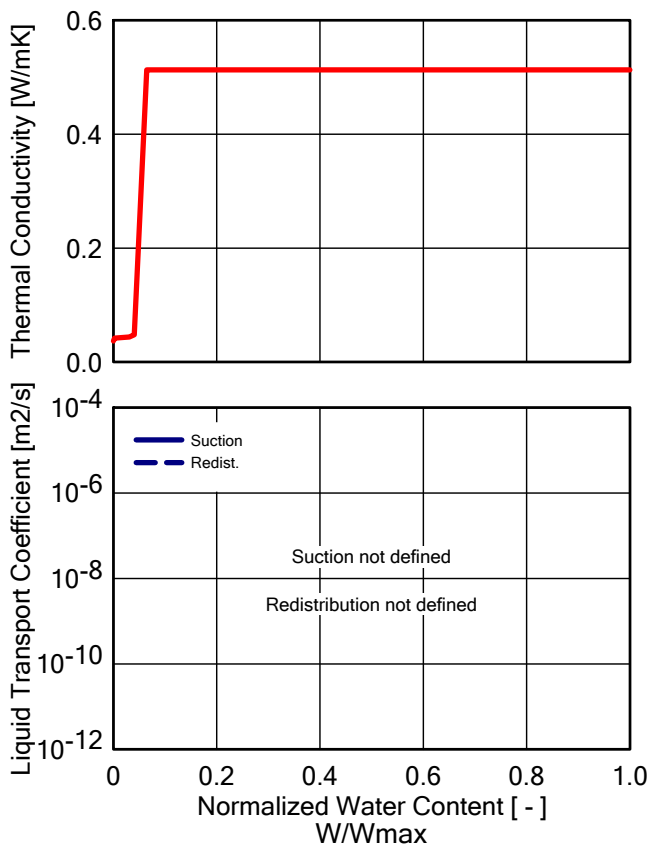
Material: Mineral Wool

Property	Unit	Value
Bulk density	[kg/m <sup>3</sup> ]	60.0
Porosity	[m <sup>3</sup> /m <sup>3</sup> ]	0.95
Specific Heat Capacity, Dry	[J/kgK]	850.0
Thermal Conductivity, Dry, 10°C	[W/mK]	0.04
Water Vapour Diffusion Resistance Factor	[ - ]	1.3
Temp-dep. Thermal Cond. Supplement	[W/mK <sup>2</sup> ]	0.0002
Thermal Conductivity, Design Value	[W/mK]	0.04



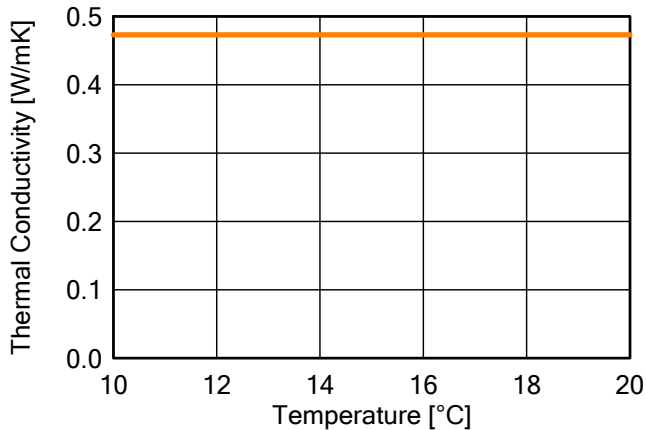
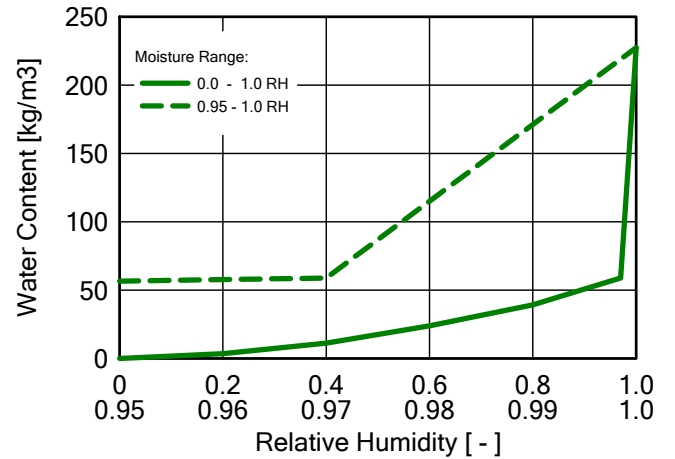
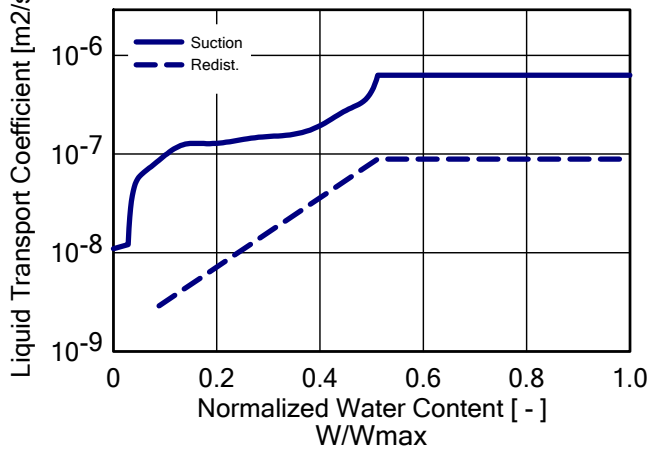
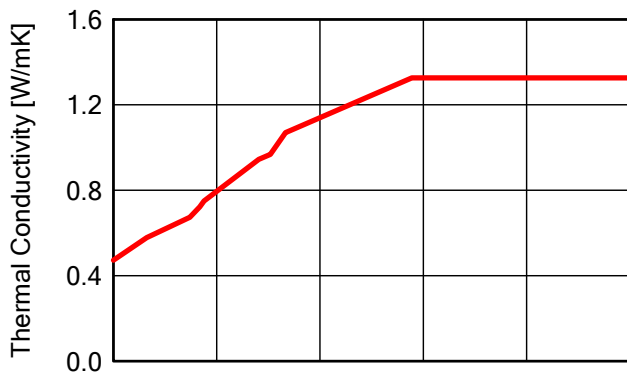
Material: EPS

Property	Unit	Value
Bulk density	[kg/m <sup>3</sup> ]	16.5
Porosity	[m <sup>3</sup> /m <sup>3</sup> ]	0.984
Specific Heat Capacity, Dry	[J/kgK]	1570.0
Thermal Conductivity, Dry, 10°C	[W/mK]	0.037
Water Vapour Diffusion Resistance Factor	[ - ]	58.0
Thermal Conductivity, Design Value	[W/mK]	0.037



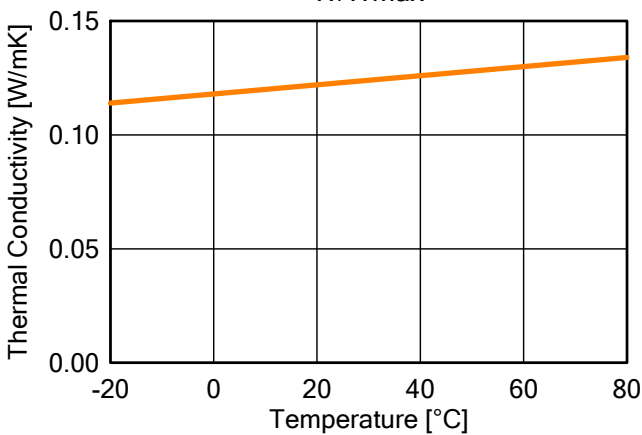
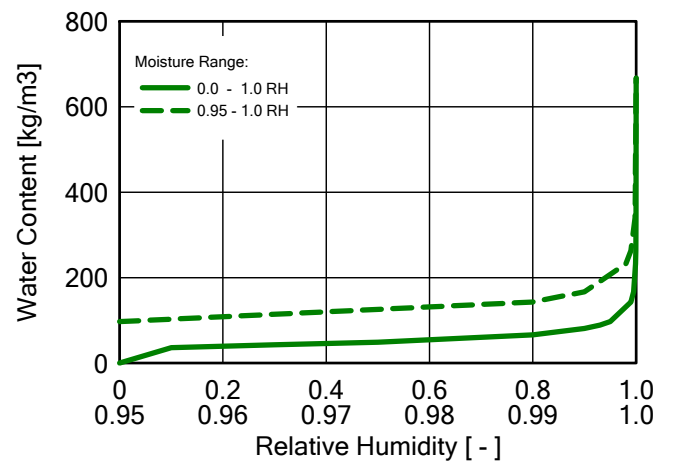
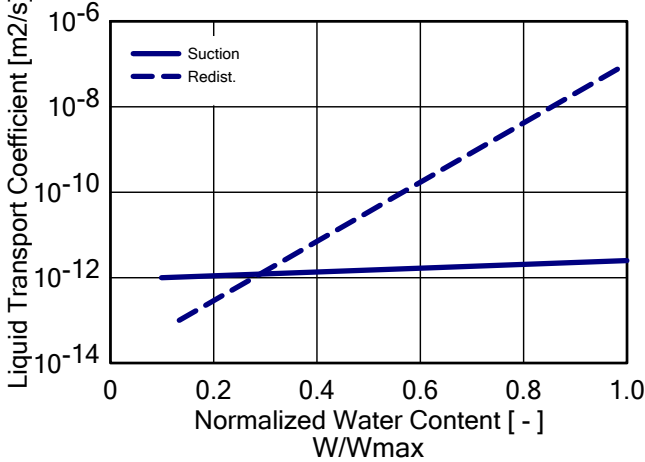
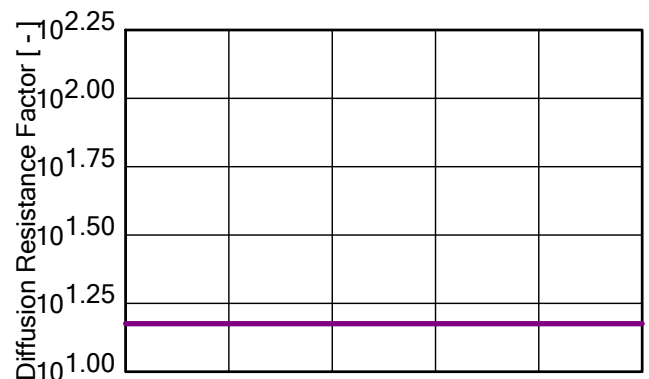
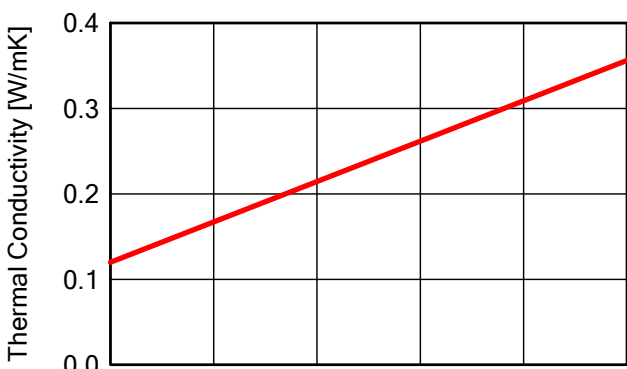
Material: Baumit MVR Uni

Property	Unit	Value
Bulk density	[kg/m <sup>3</sup> ]	1402.0
Porosity	[m <sup>3</sup> /m <sup>3</sup> ]	0.444
Specific Heat Capacity, Dry	[J/kgK]	1276.41
Thermal Conductivity, Dry, 10°C	[W/mK]	0.473
Water Vapour Diffusion Resistance Factor	[ - ]	12.0
Reference Water Content	[kg/m <sup>3</sup> ]	39.23
Free Water Saturation	[kg/m <sup>3</sup> ]	227.4
Water Absorption Coefficient	[kg/m <sup>2</sup> s <sup>0.5</sup> ]	0.11
Thermal Conductivity, Design Value	[W/mK]	0.585



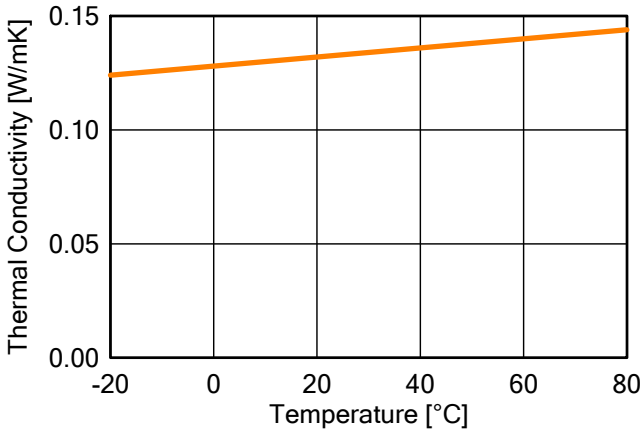
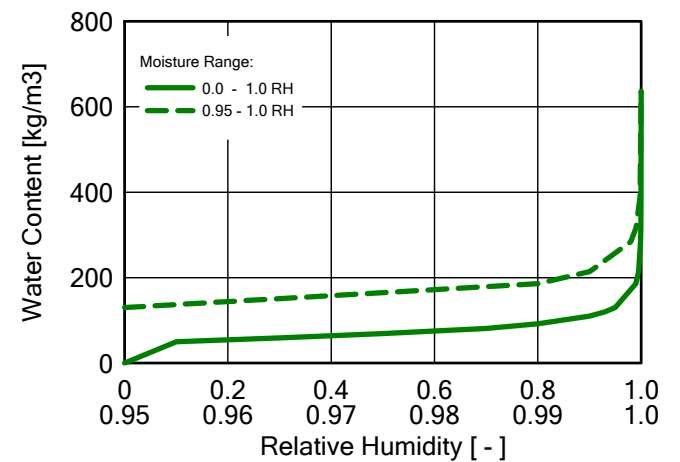
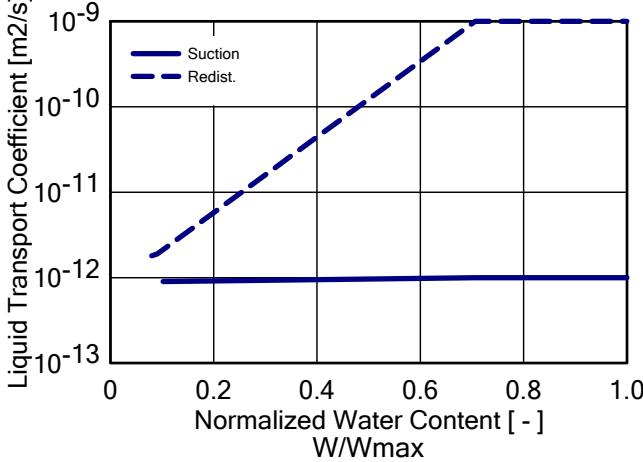
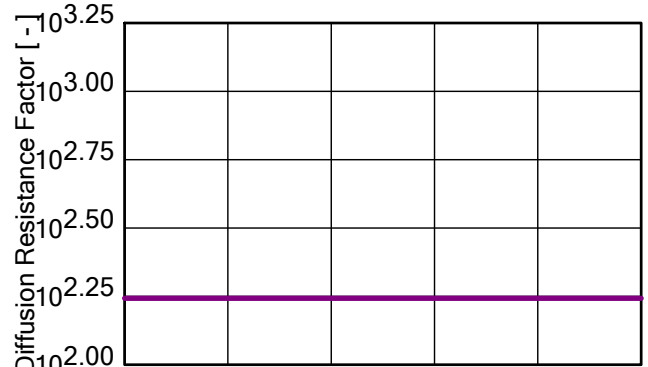
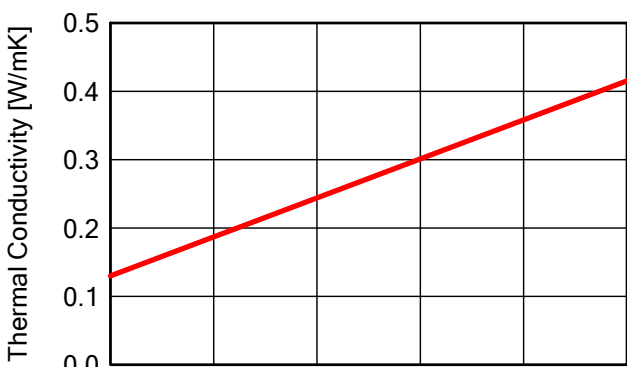
Material: Medium density fibreboard

Property	Unit	Value
Bulk density	[kg/m <sup>3</sup> ]	508.0
Porosity	[m <sup>3</sup> /m <sup>3</sup> ]	0.667
Specific Heat Capacity, Dry	[J/kgK]	1400.0
Thermal Conductivity, Dry, 10°C	[W/mK]	0.12
Water Vapour Diffusion Resistance Factor	[-]	15.0
Moisture-dep. Thermal Cond. Supplement	[%/M.-%]	1.5
Temp-dep. Thermal Cond. Supplement	[W/mK <sup>2</sup> ]	0.0002
Thermal Conductivity, Design Value	[W/mK]	0.141



Material: Oriented Strand Board (OSB)

Property	Unit	Value
Bulk density	[kg/m <sup>3</sup> ]	615.0
Porosity	[m <sup>3</sup> /m <sup>3</sup> ]	0.9
Specific Heat Capacity, Dry	[J/kgK]	1400.0
Thermal Conductivity, Dry, 10°C	[W/mK]	0.13
Water Vapour Diffusion Resistance Factor	[-]	175.0
Moisture-dep. Thermal Cond. Supplement	[%/M.-%]	1.5
Temp-dep. Thermal Cond. Supplement	[W/mK <sup>2</sup> ]	0.0002
Thermal Conductivity, Design Value	[W/mK]	0.156



Material: Gypsum Board

Property	Unit	Value
Bulk density	[kg/m <sup>3</sup> ]	850.0
Porosity	[m <sup>3</sup> /m <sup>3</sup> ]	0.65
Specific Heat Capacity, Dry	[J/kgK]	850.0
Thermal Conductivity, Dry, 10°C	[W/mK]	0.2
Water Vapour Diffusion Resistance Factor	[-]	8.3
Moisture-dep. Thermal Cond. Supplement	[%/M.-%]	8.0
Temp-dep. Thermal Cond. Supplement	[W/mK <sup>2</sup> ]	0.0002
Thermal Conductivity, Design Value	[W/mK]	0.21

